

University of Southampton Research Repository ePrints Soton

Copyright © and Moral Rights for this thesis are retained by the author and/or other copyright owners. A copy can be downloaded for personal non-commercial research or study, without prior permission or charge. This thesis cannot be reproduced or quoted extensively from without first obtaining permission in writing from the copyright holder/s. The content must not be changed in any way or sold commercially in any format or medium without the formal permission of the copyright holders.

When referring to this work, full bibliographic details including the author, title, awarding institution and date of the thesis must be given e.g.

AUTHOR (year of submission) "Full thesis title", University of Southampton, name of the University School or Department, PhD Thesis, pagination

University of Southampton

IMPROVING SOLAR CELL PERFORMANCE
THROUGH SURFACE MODIFICATION OF
SILICON

By

Nicholas Alderman

A thesis for the degree of

Doctor of Philosophy

Faculty of Engineering and the Environment

March 2013

Declaration of Authorship

I, Nicholas Alderman, declare that the thesis entitled “Improving Solar Cell Performance through Surface Modification of Silicon” and the work presented in this thesis is my own, generated by me as the result of my own original research.

Portions of the work have been published in the following journals (as indicated in the relevant chapters):

- N. Alderman, L. Danos, M. Grossel and T. Markvart, ‘Effect of surface roughness on the recombination lifetime of hydrogen fluoride etched crystalline silicon’, *Proceedings of Photovoltaic Science Application and Technology (PVSAT)-6 conference*, 2010, 59-62.
- N. Alderman, L. Danos, M. C. Grossel and T. Markvart, ‘Large surface photovoltages observed at methyl-terminated silicon surfaces synthesised through a two-step chlorination-alkylation method’, *RSC Advances*, 2012, **2**, 7669-7672.
(doi:10.1039/C2RA20465G)
- N. Alderman, L. Danos, M. Grossel and T. Markvart, ‘Passivation of n-type silicon (111) surfaces by the attachment of charged molecules’, *Proceedings of the 38th IEEE photovoltaics specialists conference (PVSC)*, 2012, 000992.
(doi:10.1109/PVSC.2012.6317769)
- T. Markvart, L. Danos, N. Alderman, L. Fang and T. Parel, ‘Harvesting sunshine: Solar cells, photosynthesis and the thermodynamics of light’, *Proceedings of the 27th European Photovoltaic Solar Energy Conference (PVSEC)*, 2012.

Signed:

Date:

Declaration of Authorship

Abstract

This project sets out to improve the efficiency of thin crystalline silicon solar cells by enhancing the photoexcitation through light harvesting, and by developing a novel surface passivation technique via the covalent attachment of organic molecules to the surface. To aid the characterisation of these novel structures, we have developed a new measurement technique for surface recombination using the Kelvin probe.

A passivation method through the attachment of alkyl monolayers to the silicon surface has been developed. These layers were shown to have good passivation properties whilst retaining excellent resilience to oxidation. The passivation effect was determined to be caused by the generation of surface charge, as measured by the Kelvin probe. Further functionalisation of the organic monolayers was undertaken to attach fluorescent chromophores.

A novel method for measurement of the surface recombination velocity was developed utilising the Kelvin probe. Changing the incident photon flux, and thus the photogenerated current, allows measurement of the surface recombination current through the change in surface photovoltage. This dependence can then be used to extract the value of the surface recombination velocity. Furthermore, we have shown that this method can be developed further into a mapping technique for surface recombination lifetime, of potentially significant industrial interest.

The effect of the silicon surface charge on the passivation observed has been investigated through the attachment of charged monolayers. It was found that

through the attachment of a positive charge, the observed recombination lifetime in n-type silicon decreased whilst a negative charge (through the attachment of carboxylic acid groups to the surface) was found to improve the surface passivation. The carboxylic acid functional groups were charged through immersion in triethylamine (base) and returned to the neutral, starting state through immersion in acetic acid. We have found that the recombination lifetime decreases linearly with decreasing charge-surface distance. This technique allows an in-depth study of surface passivation to be carried out by separating the two principal causes for passivation – the removal of surface states and charge attachment to the surface.

Fluorescent chromophores were attached to the silicon surface by two different techniques – through the reaction of an alcohol-terminated monolayer with an acyl chloride porphyrin and by palladium-catalysed cross-coupling of an allyl-terminated surface with a cyanine dye. The fluorescence quenching was investigated at various chromophore-silicon distances by varying the length of the alkyl chain spacer. We find that the fluorescence lifetime decreases with decreasing chromophore-silicon distance, and follows a logarithmic trend. Further work is required, however, to combine sensitisation with surface passivation as incorporation of a sensitisation layer by the palladium cross coupling of an allyl-terminated surface results in metal contamination to the surface, reducing recombination lifetime.

Acknowledgements

After 7 years at the University of Southampton, my time as a student is coming to an end. During my time here I have been lucky enough to meet and work with some great people.

First and foremost, I wish to thank my supervisors Professor Tom Markvart and Doctor Martin Grossel for their support and advice during my PhD studies. I especially wish to thank Professor Tom Markvart for his encouragement and explanations in semiconductor theory. It has been a pleasure working in the group of Doctor Martin Grossel, and I wish to thank him for all the guidance with the project.

I wish to thank the numerous members of my groups in both engineering (Lefteris, Liping, Thomas, Bob, Adib and Nazila) and chemistry (Dom, Andrew, Adam, Darren, Nancy, Gavin, Richard, Hassan, Gareth, Francesco, Alan and Jon) for all of their help, understanding, coffee and chats. Special mention should go to Lefteris Danos for all of your help with the project and papers.

Thank you to all of the members of the stores team (Keith, Carl and Clive). Without you and your understanding things would take so much more time! I also wish to thank Dr Colin Flowers and Professor Philippa Reed for their advice and demonstrating chances, and for allowing me to gain teaching experience.

Finally I wish to thank my family for all of their help and support, both during my undergraduate degree and PhD.

Acknowledgements

Table of Contents

Declaration of Authorship.....	i
Abstract.....	iii
Acknowledgements.....	v
Abbreviations and Symbols.....	xi
1. Introduction.....	1
1.1 Aims and Objectives	1
1.2 Motivation	2
2. Silicon Surface Chemistry.....	11
2.1 Absorption in Silicon	11
2.2 Silicon Surface Structure.....	13
2.3 Passivation Methods.....	18
2.3.1 Reduction of Surface States	18
2.3.2 Passivation by Charge	26
2.5 Functionalisation of Silicon.....	32
2.5.1 Alkylation of Silicon Surfaces	32
2.5.2 Secondary / Other Functionalisation of Silicon Surfaces	38
2.6 Conclusions	43
3. Semiconductors: Junctions and Surfaces	45
3.1 Carrier Concentrations and Carrier Flow	45
3.2 The p-n and one sided junction	47
3.2.3 Equilibrium case.....	47
3.2.4 Non-equilibrium case	50
3.3 Carrier Generation	53
3.4 Recombination: General	53
3.5 Recombination: Statistics	58
3.5 Conclusions	62

4. Etching and Bulk Lifetime.....	65
4.1 Introduction	65
4.2 Etching of Silicon Substrates	66
4.3 Estimation of the Bulk Lifetime.....	70
4.4 Conclusions	74
5. Organic Passivation of Silicon Substrates.....	75
5.1 Introduction	75
5.2 Characterisation of Samples.....	78
5.2.1 Chlorine-terminated Surfaces	78
5.2.2 Alkylated Surfaces	81
5.3 Recombination Lifetime Studies.....	87
5.4 Electronic Characterisation of Samples	91
5.5 Conclusions	98
6. Determination of the Surface.....	99
6.1 Introduction	99
6.2 Development of Theory	99
6.3 Calibration of Photon Source	103
6.4 Surface Recombination Velocity Measurements	104
6.5 2D Surface Lifetime Mapping.....	108
6.6 Conclusions	111
7. Passivation by Charge Anchorage	113
7.1 Introduction	113
7.2 Attachment of a Positive Charge to n-type Silicon.....	114
7.3 Attachment of a Negative Charge to n-type Silicon	117
7.4 Comparison of Surface Photovoltages	130
7.5 Conclusions	132
8. Attachment of Dyes to Silicon.....	135

8.1	Introduction	135
8.2	Protoporphyrin IX Functionalised Surfaces	137
8.3	Attachment of 3,3'-di(4-bromobenzyl)thiadibenzocarbocyanine bromide	150
8.4	Conclusions	155
9.	Conclusions and Further Work.....	157
9.1	Conclusions	157
9.2	Future Work	161
10.	Experimental.....	165
10.1	Etching and Bulk Lifetime	165
10.1.1	Etching Experiments	165
10.1.2	Bulk Lifetime Measurements	165
10.2	Alkylation of Silicon Wafers.....	166
10.3	Passivation by Charge Anchorage.....	168
10.3.1	Choline Iodide Terminated Surfaces.....	168
10.3.2	Carboxylic Acid Terminated Surfaces	168
10.4	Attachment of Dyes to Silicon	169
10.4.1	Attachment of 3,3'-di(4-bromobenzyl)thiadibenzocarbocyanine bromide	169
10.4.1	Synthesis of Acyl Chloride Protoporphyrin IX.....	171
10.4.2	Attachment of Protoporphyrin IX	172
10.5	Characterisation Techniques	173
10.5.1	Ellipsometry	173
10.5.2	Infra-red Spectroscopy	173
10.5.3	Recombination Lifetime Measurements	175
10.5.4	X-ray Photoelectron Spectroscopy (XPS).....	176
10.5.5	Contact Angle Goniometry	177
10.5.6	Nuclear Magnetic Resonance (NMR).....	177
10.5.7	Mass Spectroscopy.....	178
10.5.8	Kelvin Probe (Surface Photovoltage) Measurements	178
10.5.9	Fluorescence Spectra.....	179

Table of Contents

10.5.10 Fluorescence Lifetime Measurements180

11. References.....181

Abbreviations and Symbols

α	absorption coefficient
ϵ	permittivity
Θ	tilt angle
λ	wavelength
μ_n	electron mobility
μ_p	hole mobility
σ_n	electron capture cross section
σ_p	hole capture cross section
τ_b	bulk recombination lifetime
τ_{eff}	effective recombination lifetime
τ_s	surface recombination lifetime
ϕ	photon flux
ϕ_s	surface potential
AFM	atomic force microscopy
D	diffusion coefficient
DCM	dichloromethane
E	electric field
E_{fn}	electron Fermi-level
E_{fp}	hole Fermi-level
E_i	intrinsic Fermi-level
eV	electron volt
G	generation rate
HF	hydrofluoric acid
J	current density
J_0	dark current density
J_L	photogenerated current density
J_s	surface recombination current

k_B	Boltzmann constant
L	diffusion length
N	surface charge atom density
n_0	equilibrium electron concentration
N_A	acceptor concentration
N_D	donor concentration
n_i	intrinsic carrier concentration
n_s	electron surface concentration
N_t	density of traps
NMR	nuclear magnetic resonance
p_0	equilibrium hole concentration
p_s	hole surface concentration
Q	surface charge
q	charge of an electron
QSS	quasi-steady state
R	reflection
S	surface recombination velocity
SPV	surface photovoltage
SRV	surface recombination velocity
THF	tetrahydrofuran
U	recombination rate
V_{bi}	built-in voltage
V_{th}	thermal voltage
W	sample thickness
W_n	n-type depletion width
W_p	p-type depletion width
XPS	x-ray photoelectron spectroscopy

1. Introduction

1.1 Aims and Objectives

The aim of this project is to improve the efficiency of thin crystalline silicon solar cells by attachment of organic molecules to the surface, to reduce surface recombination and enhance photoexcitation via light harvesting. To achieve this goal, the following objectives will need to be met:

- Synthesis of organic thin-film passivation layers covalently bound to silicon
- Characterisation and understanding of the electronic properties of the resulting structures, in particular, surface charge and surface recombination
- Secondary functionalisation of the thin-film passivation layers to incorporate chromophores
- Characterisation of the dipole-dipole interaction between the chromophore and silicon, with the aim of detecting energy transfer

To achieve the aims and objects listed above, infrared spectroscopy, x-ray photoelectron spectroscopy, contact angle goniometry, ellipsometry, Kelvin probe and fluorescence lifetime will be used.

1.2 Motivation

In 2007, the European Council reached an agreement of a 20% target for renewable energy generation by 2020¹. Since this point, photovoltaics (and other renewable energy sources) have received a great deal of interest and investment.

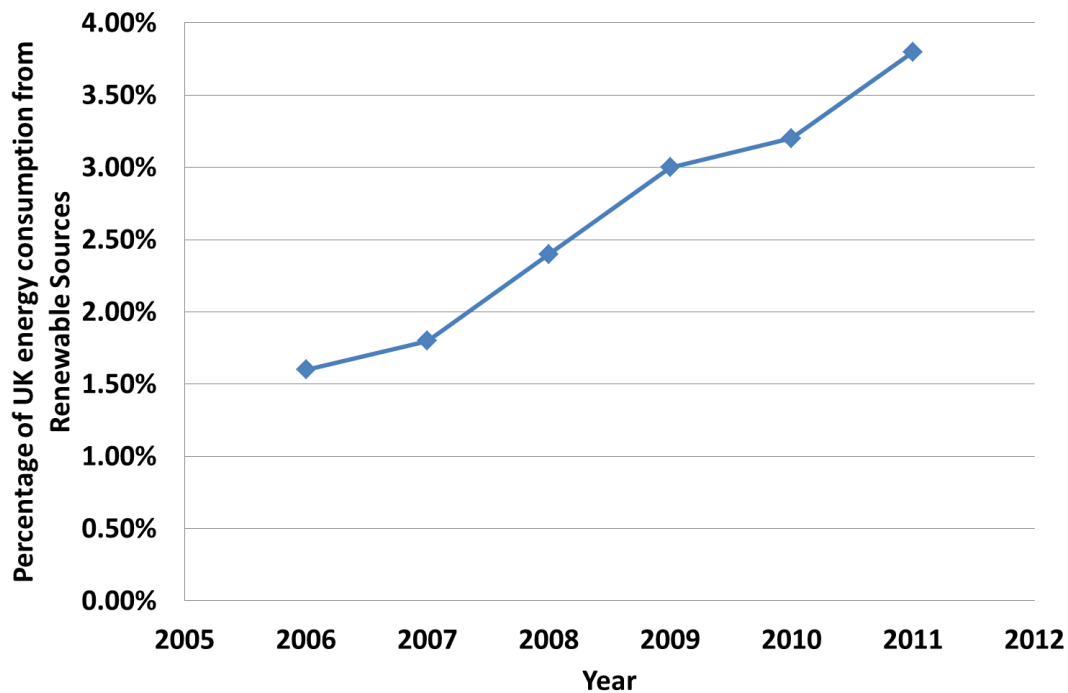


Fig. 1.0 - Percentage of the UK energy consumption from renewable sources¹

In the UK, the percentage of energy from renewable sources has increased in recent years but currently stands at a mere 3.75% (Fig. 1.0), a great deal away from the target of 20% set by the European Council. Currently the cost of photovoltaic electricity is around 20-30 p/kWh², significantly higher than the cost of electricity generated by conventional means³. Clearly, substantial cost reductions are needed to allow photovoltaics to take a sizable share of UK electricity supply.

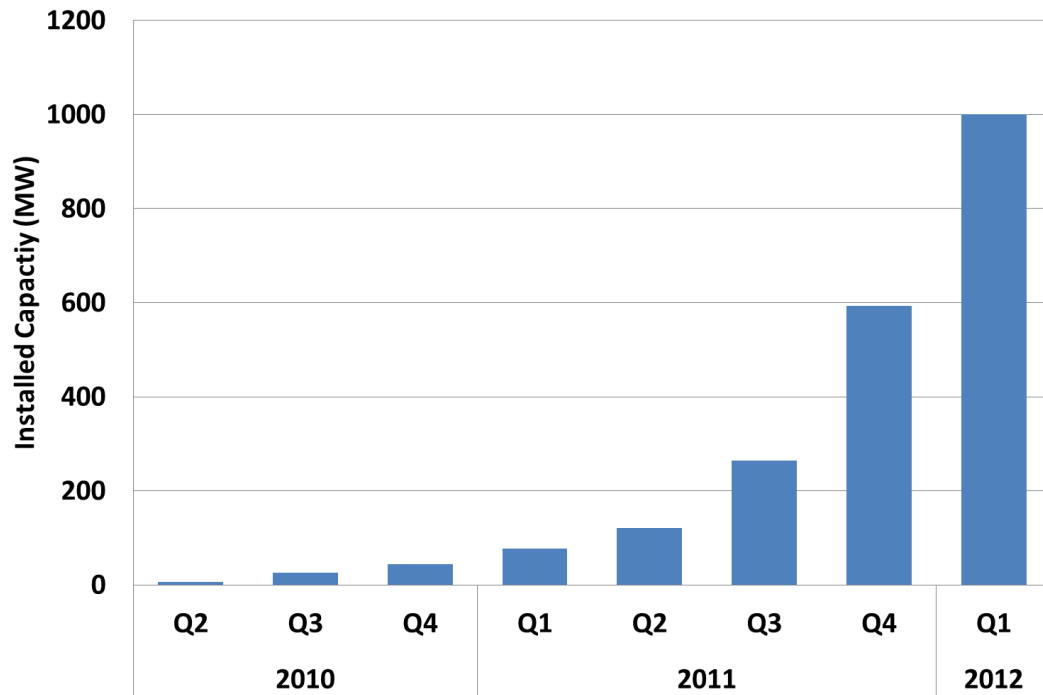


Fig. 1. 1 – The installed capacity of photovoltaics in the United Kingdom since 2010¹

Fig 1.1 shows the installed capacity of photovoltaics since April 2010. In 2012, the installed capacity of photovoltaics hit the 1000 MW, after year on year growth at an exponential rate. With such a high growth in the photovoltaic market, research into next generation photovoltaic concepts becomes increasingly important as the market demands even greater efficiency improvements.

The first modern silicon solar cell was produced in 1954 by Pearson, Chapin and Fuller with a conversion efficiency of close to 6%⁴. The current record efficiency for a solar cell is 43.5%, held by a multi-junction solar cell produced by Solar Junction Corporation⁵. For a crystalline silicon solar cell, the record currently stands at 25.0%, achieved by the University of New South Wales, Australia⁶.

There are 3 main categories of solar cells; crystalline silicon solar cells, thin film solar cells such as amorphous silicon, CdTe and CIGS, and “excitonic” solar cells

comprising of dye-sensitised and organic/plastic solar cells. The dominant technology in commercial production is mono- or multi-crystalline silicon (Fig. 1.2).

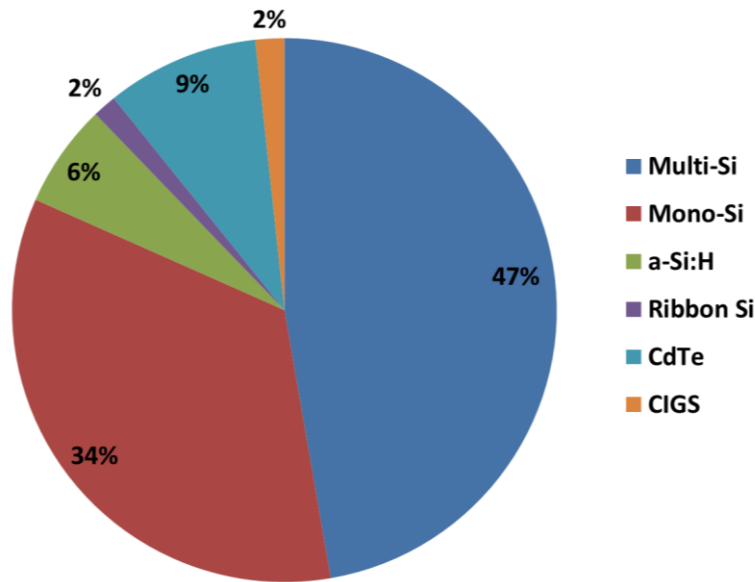


Fig. 1. 2 - Solar cell production in 2009⁷

Crystalline silicon solar cells performance is affected by several different loss mechanisms. This thesis focuses on two principle loss mechanisms: surface recombination and incomplete absorption of photons on account of the indirect bandgap of silicon.

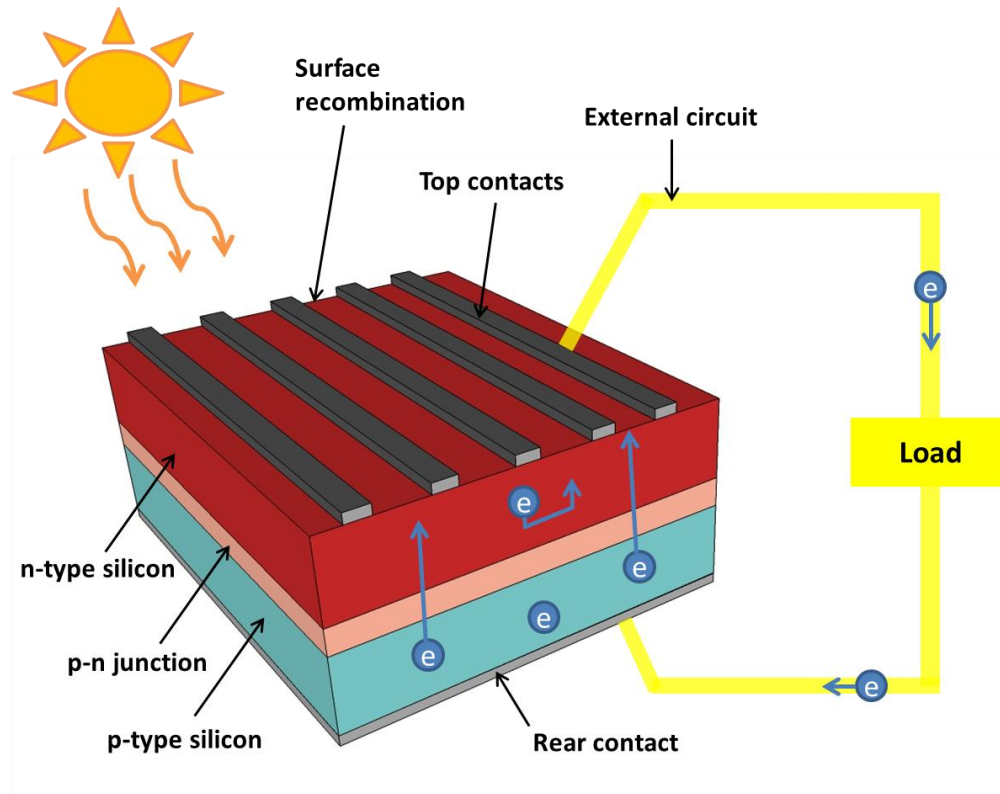


Fig. 1.3 – Diagram of a solar cell, highlighting surface recombination

A diagram of a crystalline silicon solar cell is shown in Fig. 1.3. Electron-hole pairs are generated through irradiation, before being separated by the p-n junction and collected at the contacts. The diagram highlights surface recombination which, in production cells, is normally reduced by the deposition or growth of a silicon nitride or silicon oxide film, which also acts as an anti-reflection coating.

Crystalline silicon is an indirect bandgap semiconductor⁸: to absorb a photon, a lattice vibration (phonon) is required to conserve simultaneously both energy and momentum. Due to the two-step absorption process, silicon does not absorb light efficiently requiring hundreds of micrometers of material to achieve a good efficiency⁹. For comparison, direct bandgap semiconductors such as CdTe solar cells require a few micrometers of material to absorb the majority of solar radiation¹⁰. The

absorption coefficient of silicon at different wavelength incident photons is shown in Chapter 2 (Fig. 2.1).

The low absorption coefficient of silicon is arguably the single most important reason for the high costs of photovoltaics today. Large amounts of expensive semiconductor material are used which contributes a significant cost to the final device comprising some 40% of the cost of the finished solar cell¹¹. Therefore any reduction in the thickness of the semiconductor layer would be a welcome improvement, potentially lowering the cost of PV to below that of fossil fuel electricity generation.

Thin film crystalline silicon solar cells have been produced in our laboratory at Southampton which have a device thickness in the order of 200 nm¹². The substantial reduction in the quantity of silicon, however, brings with it a low efficiency due to poor light absorption, and defines a fundamental challenge which represents one of the aims of this work: improving photoexcitation by 'light harvesting'^{13,14,15,16}. Well known in photosynthesis, this process involves the sensitisation of solar cells by the near-field interaction of dyes with silicon, and by analogy with Förster energy transfer between molecules, stimulating energy transfer^{17,18,14} and generating electron-hole pairs in the silicon¹⁹.

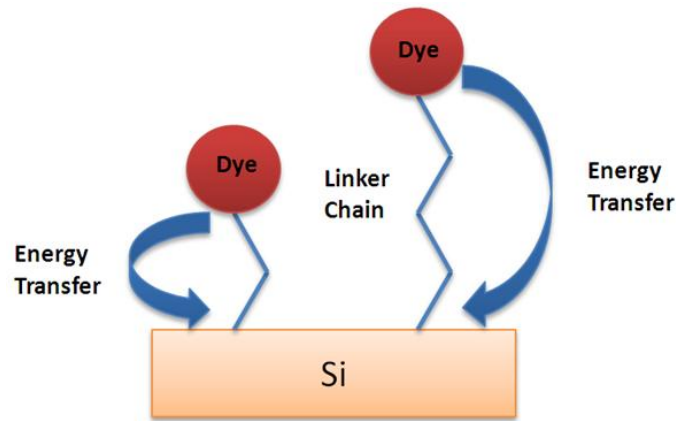


Fig. 1. 4 - The attachment of dyes to silicon at distances close enough for energy transfer

The working hypothesis in this thesis is that a careful selection of the dye and a close proximity between the dye and silicon surface (<1 nm) will result in a high degree of energy transfer and a substantial improvement in electron-hole pair generation²⁰. Further efficiency gains can be made by depositing Langmuir-Blodgett films on the initial silicon-dye bond layer and by tailoring these layers to absorb the full spectrum of incident radiation. Other high efficiency concepts such as down-conversion^{21,22} and up-conversion^{23,24} could then potentially be incorporated into the sensitisation layer, increasing the solar cell efficiency above the Shockley-Queisser limit of around 33%²⁵.

Light harvesting and energy transfer concepts have been around for many years, with the first observation of the transfer of energy from one excited ion to another with the emission of a photon by Varsanyi and Dieke in 1961²⁶. A similar effect has been used for many years in photographic films, where the silver bromide pigment sensitivity is extended from the UV region through to the visible region.

The electron-hole pairs generated in such a device will be generated close to the semiconductor surface, at a distance of the order of 1 nm¹⁹. Not only would this result in a saving of expensive silicon material, but lower quality material can be

used with a lower diffusion length as the electron hole pairs will not need to diffuse as far through the silicon material. The use of lower quality semiconductor with a much reduced thickness will result in substantial reductions in the solar cell manufacturing cost and introduce a greater flexibility in the tailoring of the absorbing layer to the light source and semiconductor.

The short dye-silicon interaction distance, however, defines a further challenge to be overcome, as traditional passivation layers are much thicker than is needed for good energy transfer^{27,28}. Therefore, a new method of surface passivation requires much thinner layers, and defines a second principal objective to be investigated in this thesis.

Organic monolayers formed through a two-step chlorination-alkylation technique are ideal for this purpose – they have shown excellent surface passivation properties and can be further functionalised to incorporate the fluorescent chromophore^{29,30}. These layers are typically in the range 0.2 – 1 nm from the surface, and allow the distance dependency of the dye to silicon to be investigated.

By combining the passivation layer with the dye sensitisation layer, improvements to thin silicon devices can be made, with the ultimate goal of lower cost photovoltaics. At the same time, the research direction followed in this thesis allows a fundamentally new approach to photovoltaics by separating the two main principals of solar cell operation – photon absorption and charge separation – into separate parts of the device (the dye layer and silicon material).

In this thesis, Chapter 2 details the silicon surface, with a discussion of the band structure, surface structure and surface functionalisation. Chapter 3 outlines the semiconductor statistics and describes the principal elements of surface

recombination. Chapters 4-8 contain the etching and bulk lifetime measurements (Chapter 4), organic passivation through monolayer attachments (Chapter 5), a novel method for determining recombination through the use of the Kelvin probe (Chapter 6), passivation through the attachment of charged organic layers (Chapter 7) and studies on the attachment of fluorescent chromophores to silicon (Chapter 8). The conclusions and future work are discussed in Chapter 9, whilst Chapter 10 contains the experimental details of all experiments performed in this thesis.

2. Silicon Surface Chemistry

In this chapter, the silicon surface will be discussed. The differences between <111> and <100> silicon are shown with regards to the surface bonding, and how the surface states arise from ‘dangling bonds’. The band structure surface before and after passivation is shown. The density of surface states is shown throughout the band-gap and how this relates to the electronic structure of the bands. Different methods of passivating the ‘dangling bonds’ are shown; through chemically removing the surface states or through surface charging. Both methods of passivation are discussed, with current literature discussions on the topic shown.

The two-step chlorination-alkylation technique is shown in detail, and will be discussed later in this thesis in Chapter 5. Other methods for the functionalisation and secondary functionalisation of silicon are shown, along with a brief overview of the spectroscopic methods used throughout this thesis for characterisation of silicon monolayers.

2.1 Absorption in Silicon

The band structure of silicon is shown below³¹.

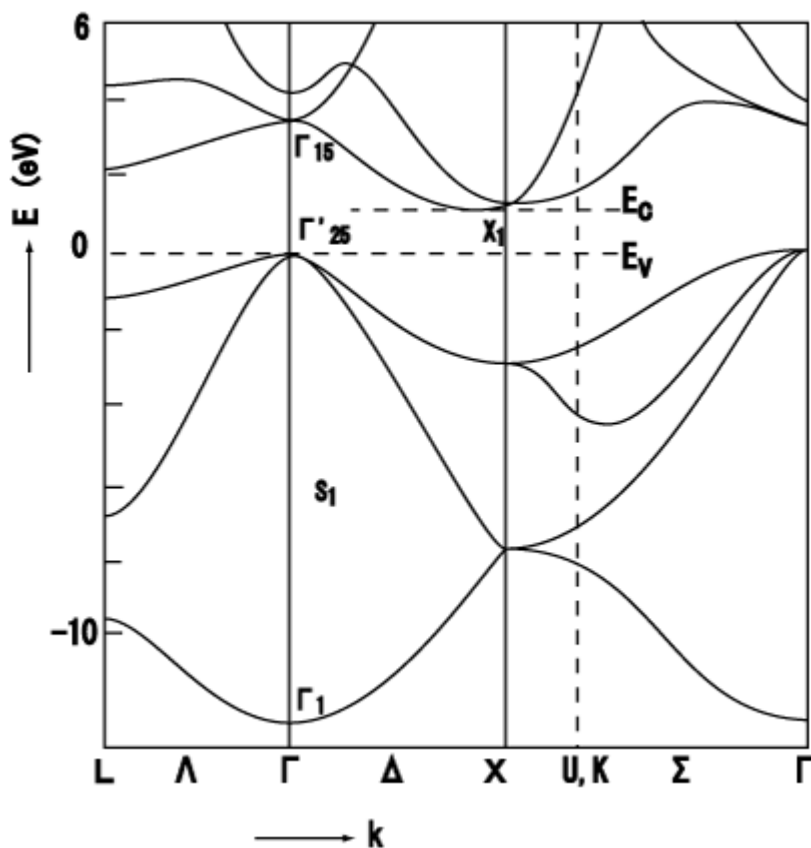


Fig. 2.0 –The electronic band structure of silicon at different wavevectors

Semiconductors can have band gaps that are either aligned (direct band gaps) or not aligned in k -space (indirect band gaps). Direct band gap semiconductors can promote an electron from the valence to conduction band without change in momentum, whereas in indirect band gap semiconductors the band edges are not aligned in k -space and momentum must change. A phonon (or lattice vibration) must also be involved for absorption to occur.

The first band gap in silicon is Γ'_{25} to X_1 , and is shown in Fig. 2.0. This transition of 1.12 eV is an indirect band gap, as a change in momentum must occur. The first direct band gap (from Γ'_{25} to Γ_{15}) occurs at 3.4 eV, far above the indirect band gap.

The absorption coefficient of silicon at different wavelength incident photons is shown below³².

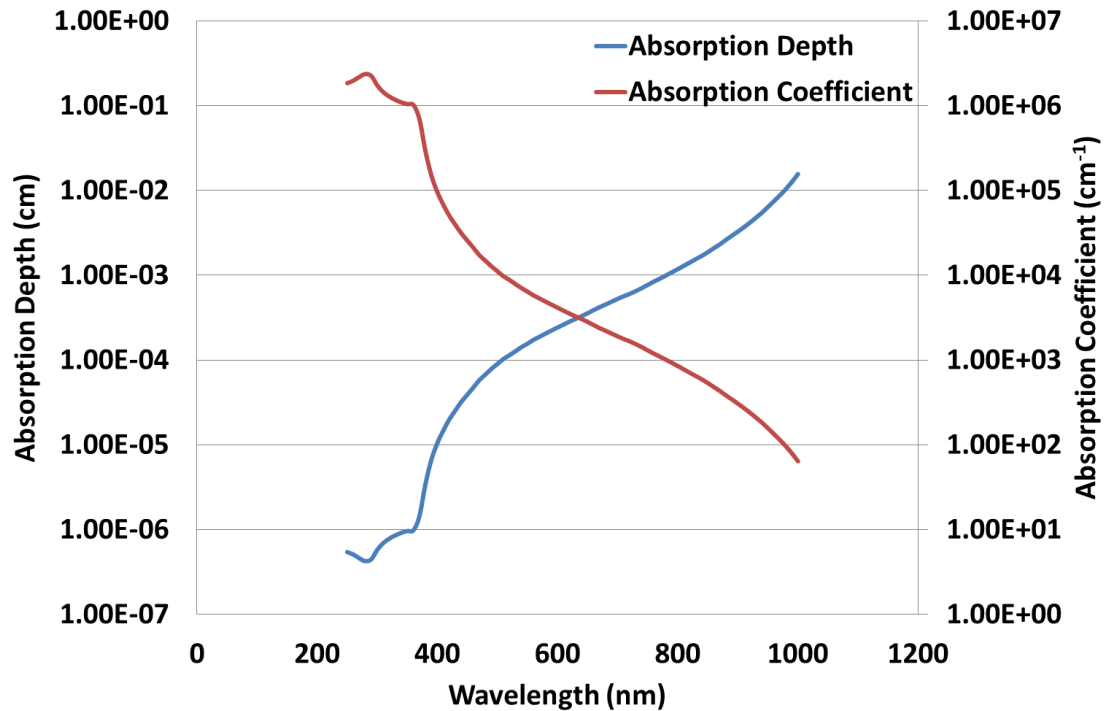


Fig. 2.1 - The absorption depth (to reduce intensity to $1/e$) and absorption coefficient of photons in silicon (where the silicon indirect bandgap is at around 1100 nm)

Above 1.12 eV (approximately 1100 nm) the absorption of photons in silicon is minimal because this is the first (indirect) transition. In Fig. 2.1 two distinct bumps can be observed in the absorption depth and absorption coefficient, which correspond to the first and second direct transitions in silicon (with the first direct transition occurring at 365 nm)³³.

2.2 Silicon Surface Structure

The silicon crystal structure is based upon the diamond lattice, with the structure of the silicon (111) surface is shown in Fig. 2.2. Silicon (111) surfaces have a single unfilled valency, allowing monohydride surfaces to be formed by immersion in hydrofluoric acid or ammonium fluoride^{34,35,36,37}. Silicon (100) on the other hand has 2 unfilled valencies on the surface atoms, such that dihydride species would preferably form on the surface³⁸. For the experiments included in this thesis, silicon

(111) was chosen as the semiconductor material. This was chosen as it should allow larger alkyl groups, such as methyl groups, to fill more of the silicon surface atom valencies than on silicon (100) (Fig. 2.3).

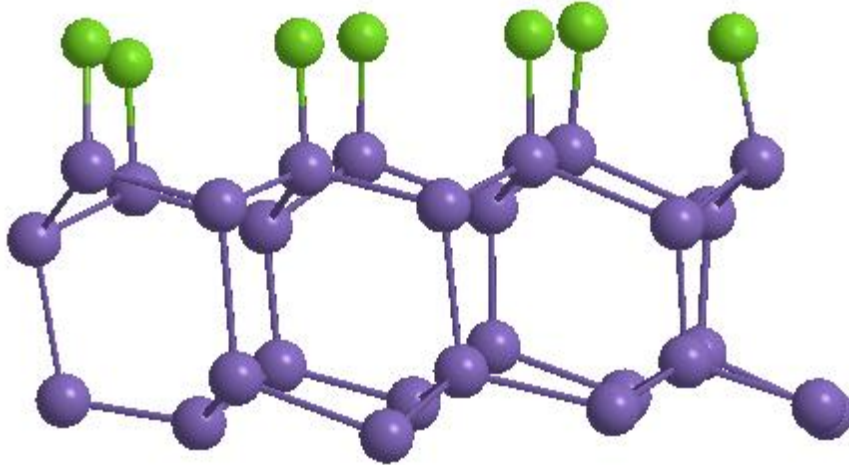


Fig. 2.2 - Silicon (111) surface showing the single silicon atom bonding site

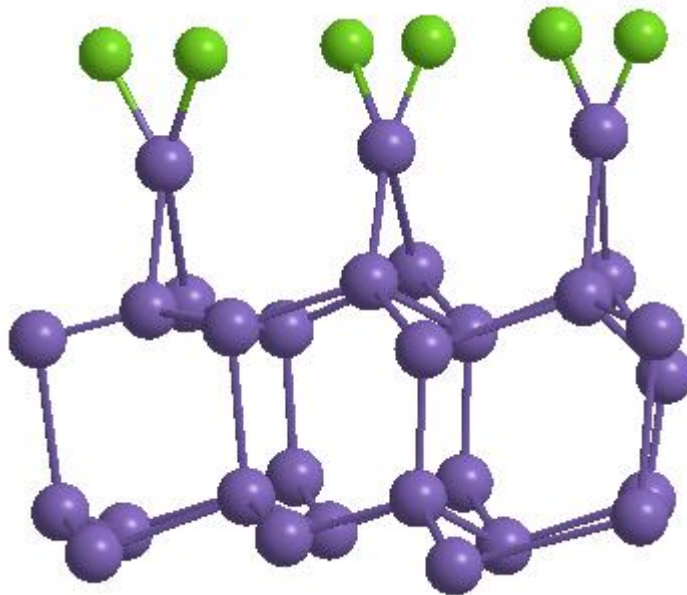


Fig. 2.3 - Silicon (100) surface showing the two silicon atom bonding sites

These unfilled silicon surface valencies are created as a result of the sudden termination of the crystalline bulk. The unfilled silicon surface valencies (also known as surface states) promote electron-hole recombination by the incorporation

of energy levels between the valence and conduction bands^{39,40,41}. Therefore to have high efficiency devices the surface states must be minimised. Native oxide terminated surfaces have a trap density of approximately $10^{12} \text{ cm}^{-2} \text{ eV}^{-1}$ ⁴².

Upon etching and hydrogen termination, the number of electrically active surface states can be reduced to around $10^{10} \text{ cm}^{-2} \text{ eV}^{-1}$. The hydrogen-terminated surface can be oxidised by water or oxygen, resulting in the formation of a silicon oxide layer and dangling bonds at the semiconductor surface (Fig. 2.4). As the number of electrically active surface states will increase, the recombination lifetime decreases towards that of the native oxide value.

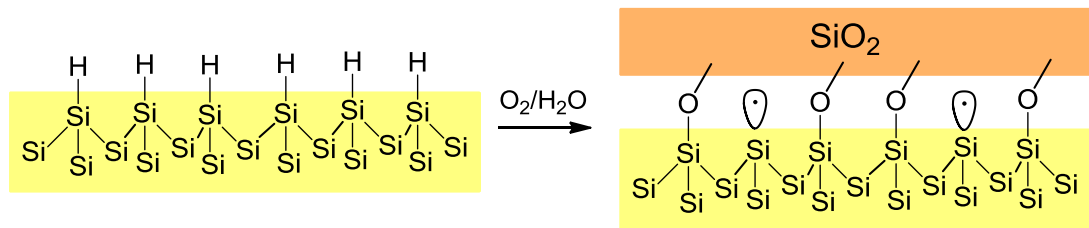


Fig. 2.4 - Generation of electrical active traps (dangling bonds) at a hydrogen terminated silicon 111 surface by oxygen / water⁴³

Before surface passivation, the dangling bonds produce 2 electrically active energy levels at approximately 0.25 eV above the valence band, and 0.35 eV below the conduction band⁴². Both of the electrically active energy levels arise from the same silicon orbital, and result from electron-electron interactions. For samples with a Fermi-level below 0.77 eV, the dangling bond orbital will be singly occupied.

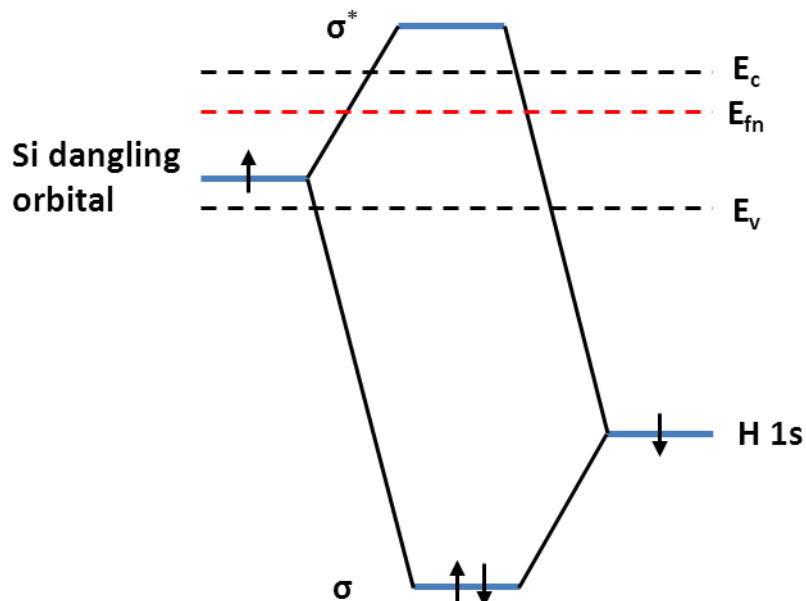


Fig. 2.5 - The orbital diagram of a silicon dangling bond interacting with a hydrogen atom, showing the bonding and antibonding orbitals with respect to the silicon conduction and valence bands

Upon hydrogen-termination of the silicon surface the hydrogen and silicon orbitals mix, forming bonding and antibonding orbitals (Fig 2.5). These two orbitals repel one another, reducing the energy of the bonding state to below the atomic hydrogen state. Similarly the antibonding state increases in energy to above the conduction band. As both states (bonding and antibonding) are not present in the energy gap between the valence and conduction band, the electrical activity of the state is removed. The surface is therefore ‘passivated’, reducing the surface recombination.

Current methods of removal of surface states (also known as surface passivation) are shown in Section 2.3. The density of surface states at the Si/SiO₂ (native oxide) interface has been investigated widely in the literature for the silicon surface and is shown in Fig. 2.6⁴⁴. From the figure, it can be seen that the number of surface states drops to almost zero at the mid-gap, with maximum values at approximately half way between the intrinsic Fermi-level and the valence and conduction bands.

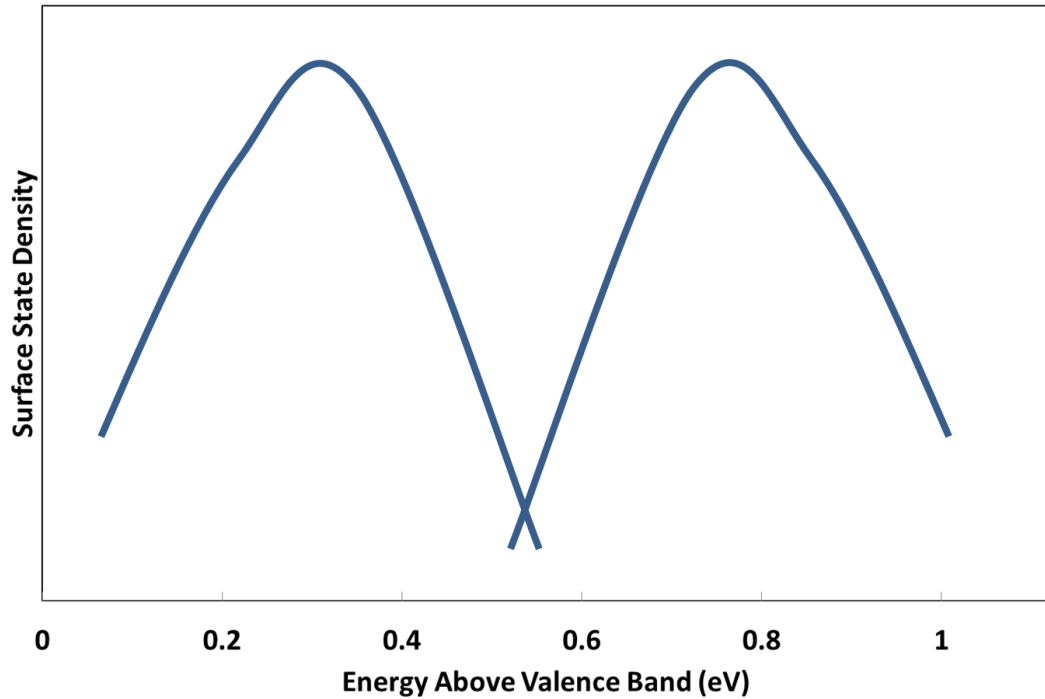


Fig. 2.6 – A schematic of the number of surface states with respect to energy above the valence band

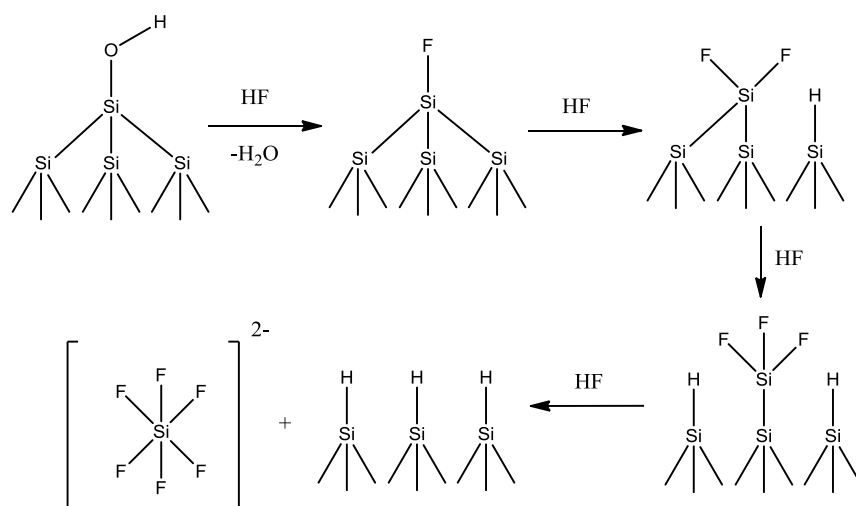
The semiconductor surface before passivation contains a high density of surface states between the valence and conduction band. For n-type silicon, the Fermi-level will be above the intrinsic Fermi-level (at around 0.56 eV). Therefore the surface states will be filled up to the Fermi-level of the sample. This high concentration of electrons on the surface has the effect of charging the surface when compared to the bulk; n-type silicon surfaces become negatively charged whilst p-type surfaces become positively charged. The surface charge can affect the surface chemistry that can be undertaken as well as inducing an opposite charge within the surface depletion region of silicon, uncovering the dopant charge.

2.3 Passivation Methods

2.3.1 Reduction of Surface States

There are currently two main surface passivation techniques: removal of the surface states by the formation of surface bonds^{45,46,47}; and repulsion of minority carriers from the surface by charging^{48,49,50}. A common way of removing the surface states is the formation of hydrogen^{36,51} or alkyl monolayers on the surface^{52,53}, whilst charging of the surface can be obtained by corona discharge⁵⁰, deposition of silicon nitride⁴⁹ and aluminium oxide⁴⁸ or the growth of a thick thermal oxide layer⁵⁴.

Removal of the surface states is often achieved by immersion in hydrofluoric acid; in fact this method was used to achieve the lowest surface recombination velocity ever reported (0.25 cm s^{-1})⁵¹. The hydrofluoric acid removes the native oxide layer from the silicon wafer, leaving the surface hydrogen terminated. The mechanism is shown in Scheme 2.0⁵⁵.

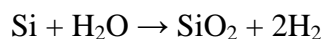
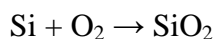


Scheme 2.0 - The mechanism of etching silicon surfaces with hydrofluoric acid

It has also been reported that this method leaves up to 0.3% of the surface fluorine terminated, which could influence further reactivity⁵⁶. Another downside of this

method is that it does not form atomically flat surfaces. With longer etching times the crystalline silicon can be etched away, leading to surface roughness and pitting^{57,58}. This also results in different hydrogen termination of the silicon surface, for example the presence of dihydride and trihydride silicon species^{59,37}. Other methods of hydrogen terminated silicon surface preparation are covered in Section 4.2.

The hydrogen-terminated surface is not stable in ambient conditions, and re-oxidises upon storage in air^{59,60,61}. Re-oxidation occurs through the insertion of oxygen into the silicon back bonds⁶². Over the first few days, oxygen uptake is slow, followed by more rapid oxidation of the surface. It has also been suggested that the first layer of oxide is formed by water vapour⁵⁹. The reactions for oxidation of the silicon for both oxygen and water are as follows⁶³:



The hydrogen terminated surfaces oxidise slowly in air for the first 60 minutes, losing only 10% hydrogen coverage⁶⁰. After 4 hours in air, this increases to approximately a 60% loss, as shown in Fig. 2.7⁶⁴.

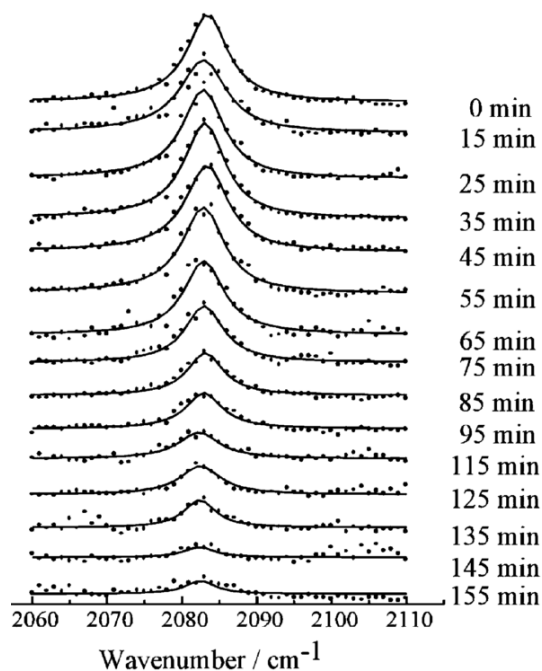
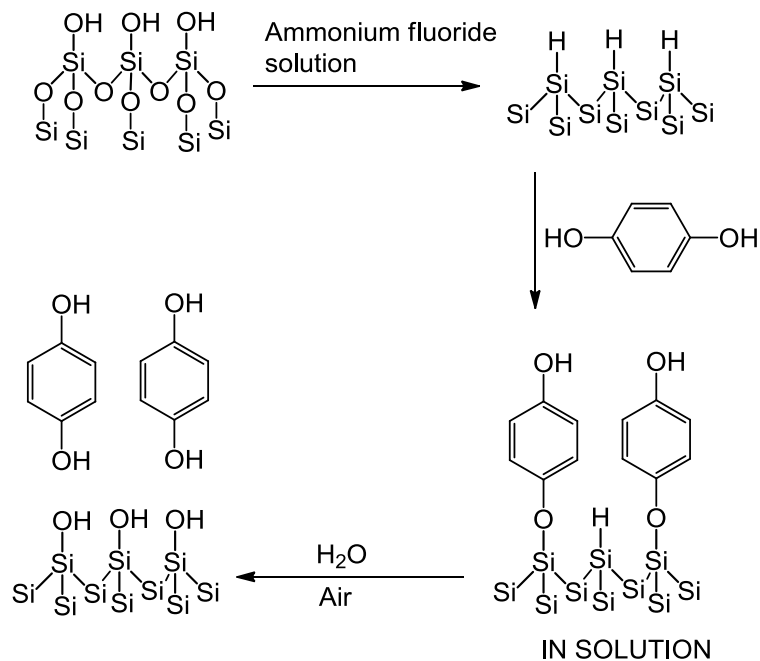


Fig. 2.7 - Infra-red studies of hydrogen terminated silicon stored in air⁶⁰

Initial oxidation is observed through insertion of oxygen into the silicon backbond, retaining the hydrogen termination. This was shown by an asymmetric Si-O-Si stretch and a shift in the Si-H stretch when studied by high-resolution electron energy loss spectroscopy (HREELS)⁶⁵. As oxygen was observed in both the surface and bulk bridge bonding sites, it was suggested that oxide formation does not occur in a layer-by-layer manner.

Another method of removing the surface states is by immersion of a hydrogen terminated surface in a solution of quinhydrone in methanol⁶⁶. The surface also retains some passivation effects after removal of the sample from the solution⁶⁷. This process involves the formation of silicon-oxygen bonds between the surface and quinhydrone, removing the surface states (Scheme 2.1).



Scheme 2.1 - Schematic showing the bonds formed at the hydrogen terminated surface when immersed in a quinhydrone in methanol solution⁶⁶

Once the sample is removed from the solution, the unstable silicon-quinhydrone bond is broken, leaving behind a hydroxyl-terminated surface with free quinhydrone. Therefore to achieve high lifetimes, the silicon must be immersed in the solution limiting the potential applications to bulk lifetime determination.

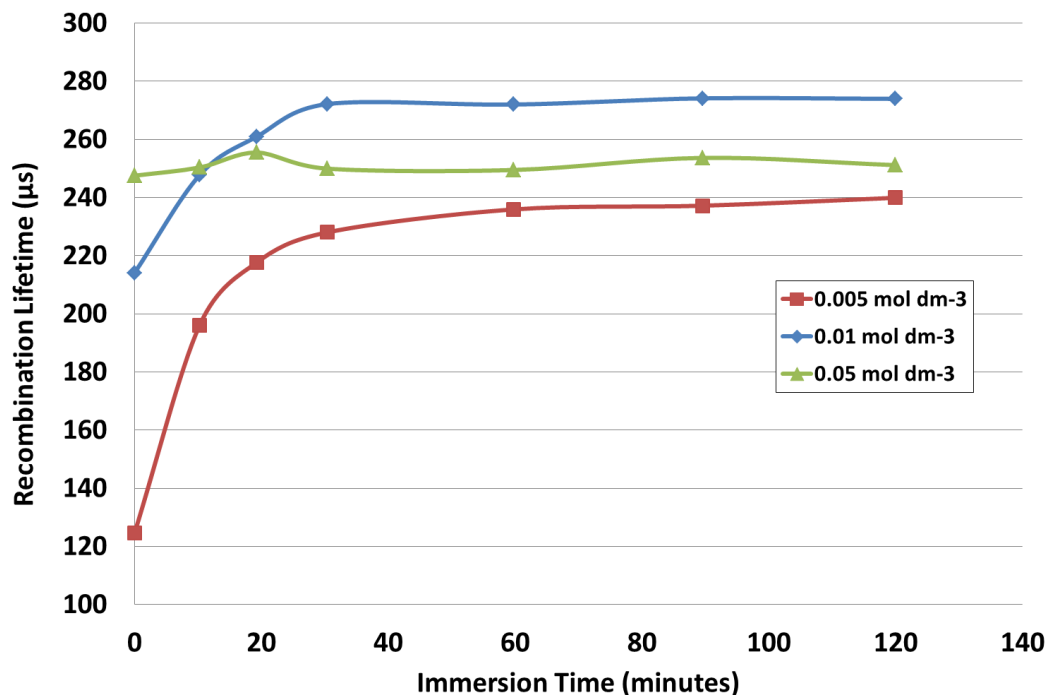
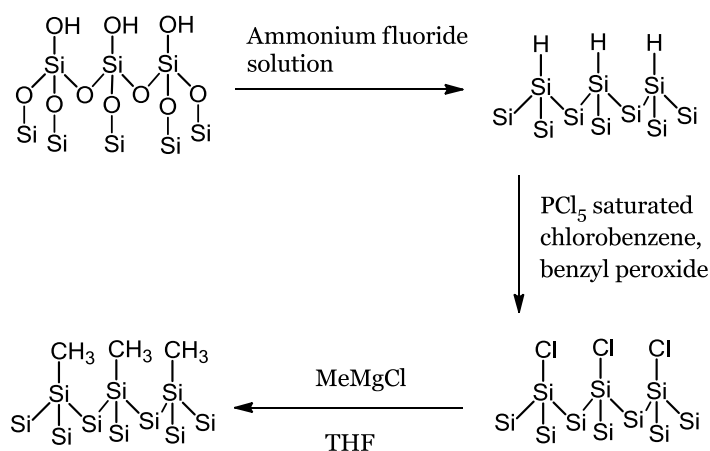


Fig. 2.8 - The recombination lifetime of an n-type silicon wafer after immersion in a quinhydrone in methanol solution at various concentrations⁶⁸

The highest recombination lifetimes were found to be achieved at a concentration of around 0.01 mol dm^{-3} of quinhydrone in methanol (Fig. 2.8). This technique has also been reported to be very sensitive to low concentrations of contaminants in solution. Therefore care must be taken when preparing the passivating solution to avoid contamination. However very high lifetimes are achievable, allowing an estimate of the bulk lifetime to be obtained⁶⁸. This has also been shown to retain greater passivation out of solution than immersion in an iodine-in-ethanol solution, which is also another common literature technique for the determination of the bulk lifetime (which will be discussed later in this chapter).

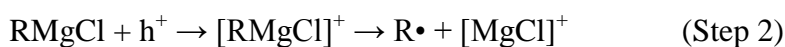
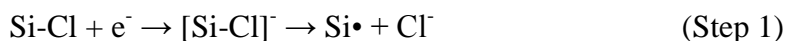
The formation of alkyl monolayers through a two-step chlorination-alkylation reaction has been shown to produce well-passivated surfaces^{46,29,38}. This is achieved through etching of the silicon oxide layer with ammonium fluoride, leaving an

atomically flat hydrogen terminated surface^{37,57}. The hydrogen terminated surface can then be chlorine terminated either by chlorine gas⁶⁹ or phosphorus pentachloride in chlorobenzene⁶⁹. The chlorine gas method has been shown to produce a silicon surface with less surface oxide, but the phosphorus pentachloride in chlorobenzene allows easy transfer to subsequent reactions. Once the chlorine-terminated surface has been produced, alkylation of the surface can be achieved by the use of a Grignard reagent (Scheme 2.2).



Scheme 2.2 - Reaction scheme for the synthesis of passivating alkyl monolayers on silicon

The mechanism of alkylation has been proposed by Nemanick *et al.*²⁹.



Any silicon sites which cannot be alkylated would then pick up a hydrogen atom from the solvent, hydrogen terminating any part of the surface which was not alkylated. This fits in with other literature examples where the Si-Cl infrared peak is not visible after alkylation^{70,29}.

The alkylated silicon surface has been shown to be air stable for over 1000 hours, whilst retaining excellent passivation²⁹. Such surfaces have the advantage of being very thin layers (<1nm) whilst being air-stable. Therefore other concepts such as light harvesting can be incorporated into these passivating layers.

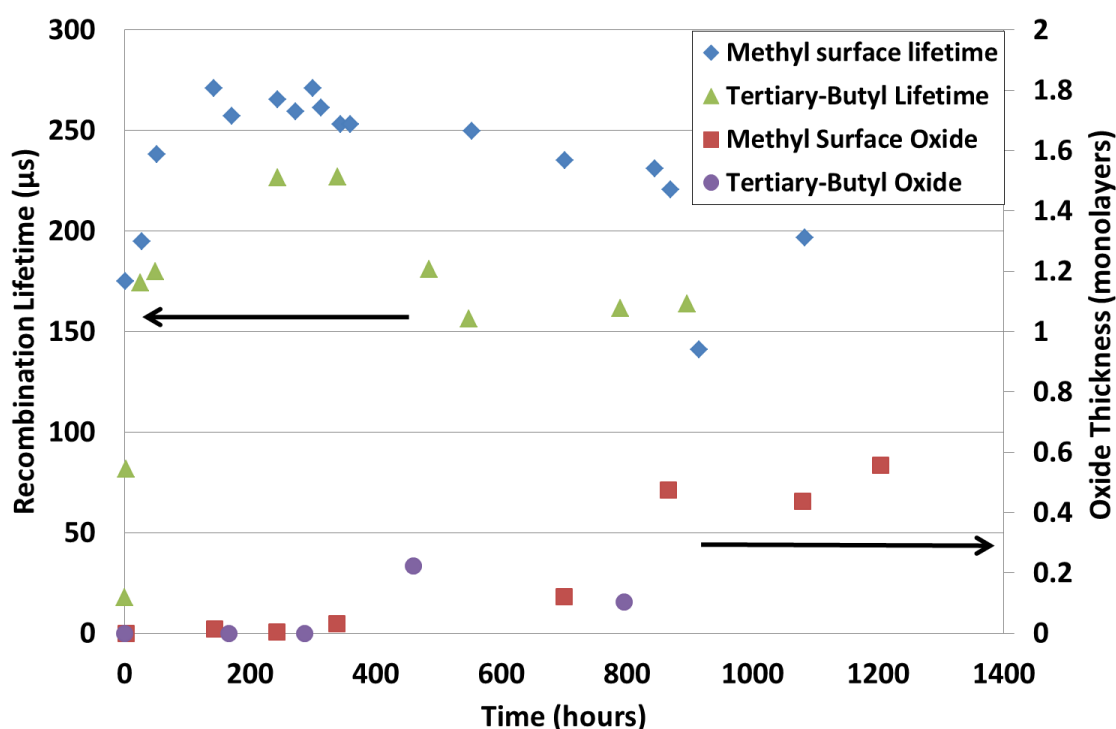


Fig. 2.9 - The recombination lifetime and oxide growth on a methyl and tertiary-butyl terminated silicon (111, n-type) surface²⁹

As the storage time in air increases, the recombination lifetime slowly decreases because of oxide growth (Fig. 2.9). It was also found that as the chain length of the alkyl group increased, the surface coverage decreased due to steric hindrance. As bulkier groups such as phenyl, isopropyl or tertiary butyl groups were attached to the surface the alkyl coverage also decreased, again because of steric factors. As higher surface coverage leads to fewer surface states, the smaller alkyl chains give a higher recombination lifetime (Table 2.0).

	Ratio C _{Si} /Si	% of methyl coverage	Recombination Lifetime (μs)
Methyl	0.16 ± 0.02		230 ± 40
Ethyl	0.14 ± 0.02	90 ± 20	180 ± 50
Iso-propyl	0.06 ± 0.02	40 ± 20	200 ± 50
Tert-Butyl	0.061 ± 0.008	40 ± 20	160 ± 60
Phenyl	0.08 ± 0.02	50 ± 20	200 ± 90
Octyl	0.092 ± 0.008	60 ± 10	
Hydrogen			<10

Table 2.0 - Literature values of the surface coverage of various alkyl-terminated silicon (n type, 111 orientation) surfaces as measured by X-ray Photoelectron Spectroscopy (XPS) with the recombination lifetime. The coverage was calculated from the ratios of the carbon bonded to silicon peak, normalised by dividing by the silicon 2p peaks for the sample, with the coverage for each sample reported as a percentage of the methyl coverage²⁹

As can be seen in the above Table, the highest recombination lifetimes were achieved with a methyl-terminated surface. It has been shown by Rivillon *et al.* that the surface coverage when using the older Grignard solution was around 30% less than a freshly opened bottle⁶⁹. Lewis *et al.* suggest that this could be due to trace concentrations of water in the glovebox, which through long term exposure could result in the hydrolysis of the organometallic reagent. This decreases the concentration of the active Grignard and allows oxidation of the chlorine-terminated surface to compete with alkylation⁶⁹. Therefore, to obtain the highest surface coverage of the alkyl substituent and maximise the lifetime, fresh bottles of the Grignard reagent should be used.

The two-step chlorination-alkylation technique is the only surface alkylation technique that can methylate the silicon surface (see Chapter 2.5 for further methods of alkylation), as well as imparting excellent passivation properties. It has been shown by high-resolution synchrotron photoelectron spectroscopy that the alkylated surfaces synthesised by this route are in an almost flat-band state, corresponding to a large reduction in the number of surface states.

2.3.2 Passivation by Charge

There are 4 main methods of passivation by charge: corona discharge⁵⁰; immersion in an iodine in ethanol solution⁷¹; deposition of silicon nitride⁷² or aluminium oxide⁷³; and the growth of a thick thermal oxide⁵⁴.

For field effect passivation (by corona discharge), the corona charge is deposited on an insulating layer such as native oxide⁵⁰. This builds up a space-charge region below the silicon surface, imparting passivation. However this method of passivation has no importance in device manufacturing, because of the instability of the charge in ambient conditions. A potential use of this technique is to investigate the bulk properties of the silicon by reducing the surface recombination. By corona discharging, it is possible to passivate n-type silicon with either a positive or negative charge⁷⁴. This is either the result of an inversion layer forming because of a positively charged surface (reducing the hole concentration close to zero) or an accumulation layer (where the majority carrier concentration is reduced to around zero). As the minority carrier concentration is orders of magnitude lower than the majority carrier concentration, it is preferable to have an inversion layer to keep the minority carriers as far from the recombination centres as possible.

A method of surface charging suitable of measuring the bulk lifetime of the silicon is immersion of the sample in an iodine-in-ethanol solution.

After etching the surface in hydrofluoric acid to remove the native oxide layer, the sample is immersed in a 0.08 molar iodine-in-ethanol solution⁷¹. This imparts an improvement in the recombination lifetime of the sample, allowing a value closer to the bulk lifetime to be obtained (Table 2.1).

Wafer resistivity ($\Omega \text{ cm}^{-1}$)	Dopant Type	Thickness (μm)	Recombination Lifetime (μs)	Surface Recombination Velocity (cm s^{-1})
0.5	P	16	20	40.4
0.5	P	50	60	41.6
1.0	P	290	293	49.5
2.5	P	194	555	17.5
10	P	298	1550	9.6
100	P	279	1700	8.2
1000	P	280	2500	5.6
100	N	430	2720	7.9

Table 2.1 - The recombination lifetime and surface recombination velocity of various silicon samples during immersion in a 0.08 molar iodine in ethanol solution⁷¹

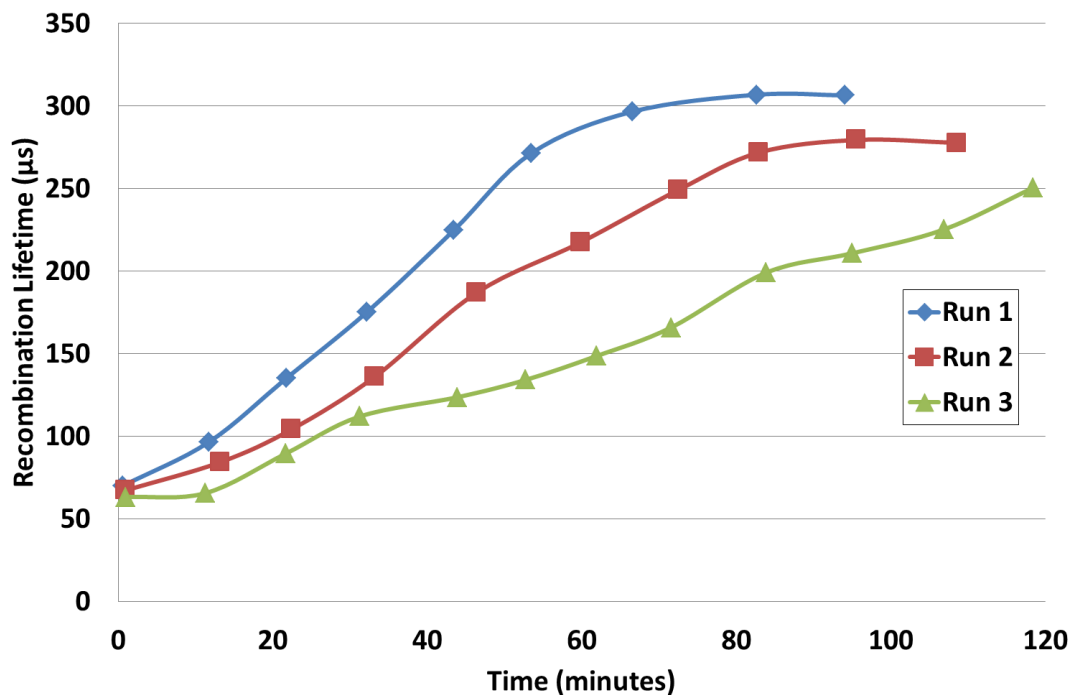


Fig. 2.10 - Time dependence of the silicon sample recombination lifetime when immersed in an iodine in ethanol solution

From Table 2.1, it can be seen that the iodine-in-ethanol solution is suitable for passivating different dopant concentrations and silicon types. Therefore it is a very useful technique allowing different types of silicon to be compared. However this passivation is lost once the sample is removed from solution, so is therefore useful only in determining the bulk properties of silicon.

Fig 2.10 shows the time dependency of the recombination lifetime for the samples⁷⁵. An almost linear increase is observed for the first hour, after which the recombination lifetime plateaus giving a lifetime close to that of the bulk lifetime. Therefore the measurements should be undertaken once the sample reaches the maximum lifetime.

Iodine-in-ethanol passivates the silicon surface by band-bending (charging of the surface). There are two possible mechanisms from which band-bending can arise;

exclusively because of the difference in the chemical potential between the solution and the sample, or as a result of the ionic charges in solution (I^-) becoming attached to the surface inducing band-bending. Both of these could reduce recombination by repelling one type of carrier from the surface, although further literature suggests the band bending is more likely due to I^- ions producing the surface field (Fig 2.11)⁷¹.

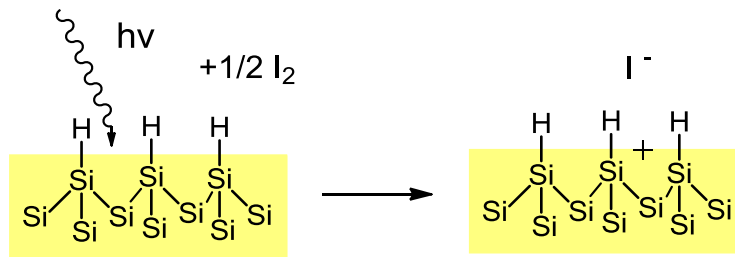


Fig. 2. 11 – The method of passivation for iodine in ethanol solutions

Experimental determination of the surface recombination lifetime with varying surface potential has been investigated by Glunz *et al.*. They found that the maximum rate of recombination occurs when the ratio of the electrons to holes at the surface is equal to the ratio of hole to electron capture cross section, and can be expressed for p-type silicon by⁷⁶:

$$\frac{n_s}{p_s} = \frac{\sigma_p}{\sigma_n} \approx \frac{1}{100} \quad (\text{eqn 2.0})$$

where n_s is the surface electron concentration, p_s is the surface hole concentration, σ_p is the hole capture cross section and σ_n is the electron capture cross section.

Therefore changing the concentration of electron and holes at the silicon surface by band-bending (charging) can impact the recombination lifetime. This has been investigated for the applied surface potential by Glunz *et al.*⁷⁶ and is shown in Fig 2.12.

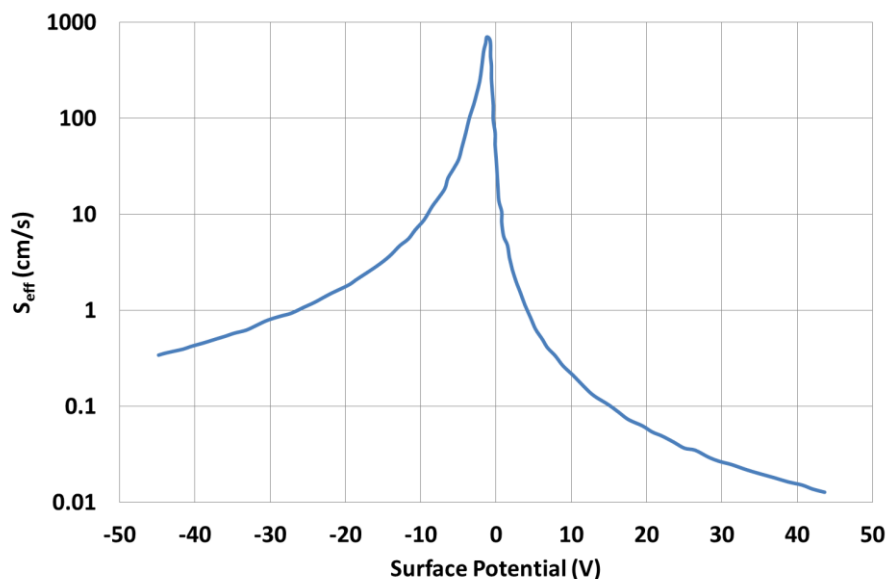


Fig. 2.12 - The change in surface recombination velocity with applied surface potential for a p-type silicon sample⁷⁶

As can be seen in Fig 2.12, the surface recombination velocity initially increases as a negative potential is applied (from a zero surface potential). Once the maximum value of the SRV is obtained, the value decreases with further charging as a result of a decrease in minority carrier concentration. This behaviour is not observed upon application of a positive charge in the p-type silicon, with the SRV decreasing with charging due to a reduction in the hole (majority) carrier concentration.

The applied surface potential (through corona discharge in this case) allows much larger charging of the surface than chemical method, and the methods used within this thesis. A clear maximum in surface recombination velocity is observed at a surface potential of approximately -1.5 V. Upon application of a positive potential, a rapid decrease in surface recombination velocity is observed, reaching that of the bulk at around 10 V. A positive potential will decrease the majority carrier concentration (holes in this case) in the p-type semiconductor material.

Addition of a negative surface potential initially increases the surface recombination velocity, probably as a result of the surface electron and hole concentration approaching the value given in equation 2.0. Increasing the surface potential further leads to a slower decrease in the surface recombination velocity when compared to the application of a positive potential, with the lifetime approaching that of the bulk at a surface potential of -40 V. The increase in lifetime can be attributed to a reduction of the minority carrier (electron) concentration at the surface.

As can be seen in this section, there are numerous different passivation techniques for reducing surface recombination. Immersion techniques such as quinhydrone in methanol and iodine in ethanol are suitable for measuring lifetimes close to the bulk lifetime; however these are not stable in ambient conditions so are unsuitable for our application^{66,77,75}.

The alkylated silicon surfaces produced through the two-step chlorination-alkylation technique have shown excellent surface passivation which is maintained for times longer than 1000 hours²⁹. The versatility of the Grignard solutions available allows different functionalities such as allyl groups to be easily incorporated onto the surface, resulting in secondary functionalisation^{30,78}. This will allow concepts such as light harvesting to be explored. As these are monolayers, the alkylated surfaces also have the advantage of being very thin, with the consequence that chromophores can be brought into close proximity with the silicon surface. Therefore this passivation method was chosen to be investigated further.

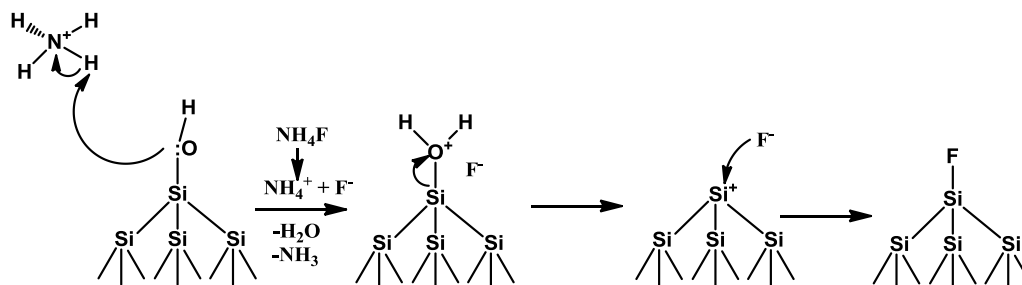
2.5 Functionalisation of Silicon

2.5.1 Alkylation of Silicon Surfaces

Numerous literature methods exist for the formation of alkyl monolayers on silicon; a two-step chlorination-alkylation technique covered earlier (Section 2.3.1)⁴⁷; an ultra-violet attachment technique⁷⁹; thermal grafting⁸⁰; and electrochemical grafting³⁸.

All of these methods require a smooth, oxide free, hydrogen-terminated surface before subsequent reactions can be undertaken. The hydrofluoric acid route previously mentioned is not suitable for this, because of roughening of the surface and a range of different hydrogen species being present on the surface³⁷.

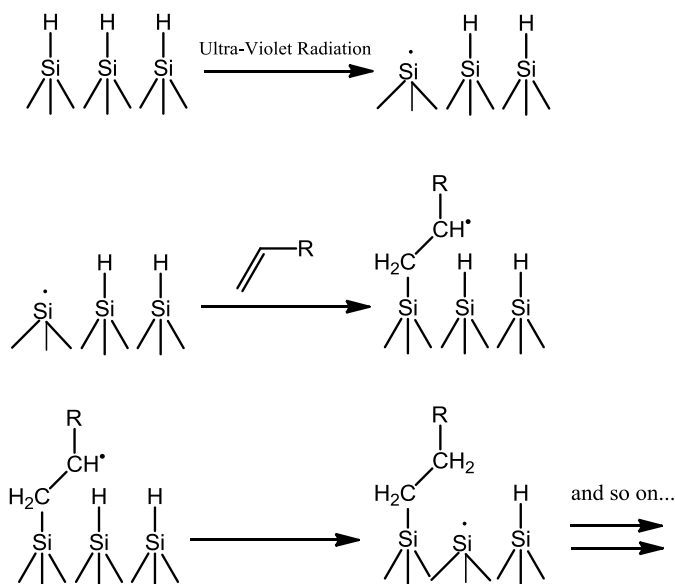
Ammonium fluoride is another commonly used etchant that, with etching times greater than 6.5 minutes, has been shown to remove the native oxide layer (~1.5 nm of oxide). It was also found that a solution of ammonium fluoride in water should be degassed with nitrogen or argon prior to immersion of the wafer to reduce the pitting caused by oxygen attack⁸¹. This results in an atomically flat, hydrogen-terminated surface which can undergo further alkylation steps. The most atomically flat surfaces have been reported using low doped silicon, with higher doping leading to rougher surfaces³⁷.



Scheme 2.3 - The method of oxide removal and hydrogen termination of silicon by ammonium fluoride

The mechanism for oxide removal and hydrogen-terminated by ammonium fluoride is shown in Scheme 2.3. Further attack of the fluorine-terminated surface as in Scheme 2.0 results in the hydrogen-terminated silicon surface³⁵. Once again, these surfaces are not stable under ambient conditions and re-oxidise as explained in Section 2.3.1.

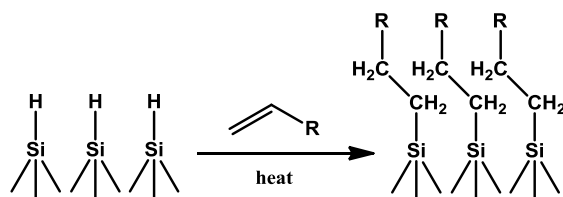
The ultra-violet method of alkyl attachment uses UV radiation to generate radicals on the hydrogen-terminated silicon surface. These then react with an alkene to produce the alkyl substituent directly bonded to the surface. The radical which remains on the alkyl substituent then picks up a hydrogen atom from the surface, forming another radical. This process can continue across the surface, until full coverage occurs (Scheme 2.4)⁸².



Scheme 2.4 - The mechanism for attachment of alkyl groups by the ultra-violet method

This method of attachment has the advantage of only being a two-step method – etching followed by alkylation. It produces very similar surface coverage to the other two alkylation methods, but does not result in an increased recombination lifetime. A disadvantage of this technique is that, to simplify the procedure, the alkene used must be liquid at room temperature. Therefore short chain alkenes are not suitable for this approach.

The thermal method of attaching alkyl substituents to the silicon is one of the simplest methods available. Upon refluxing of the alkene with the hydrogen-terminated surface, the alkene double bond reacts with the surface, forming a silicon-carbon bond and attaching the alkyl substituent to the surface (Scheme 2.5)⁷⁹. After the reaction has completed, the samples need to be sonicated in a mixture of methanol / acetic acid to remove any physisorbed alkene.



Scheme 2.5 - The attachment of alkyl groups through the thermal scheme

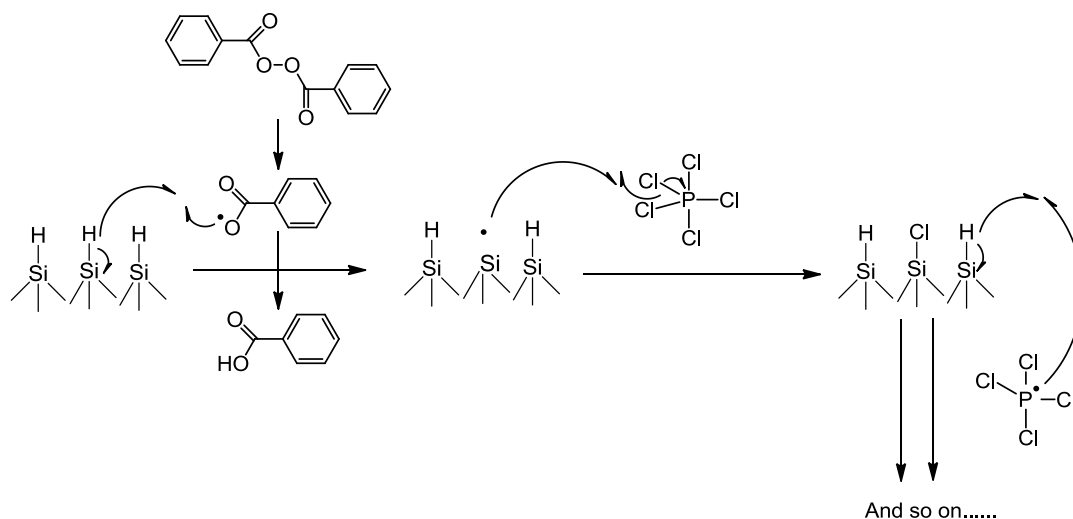
Like the UV method, this has the disadvantage of having to use long chain lengths, as the boiling point of the alkene has to be above the activation energy of the reaction, otherwise no reaction will occur. With longer chains though there is less surface coverage, since the bulk of the chains restricts the area over which other units can bond to the surface.

Through the use of a two-step chlorination-alkylation technique, a Grignard reagent can alkylate the silicon surface as previously shown. This has the advantage of allowing attachment of short chain alkyl groups which the thermal and UV method cannot achieve (in fact this is the only silicon alkylation technique that can methylate silicon surfaces).

The first step towards alkyl attachment is chlorination of the hydrogen-terminated surface. Two methods for surface chlorination have been described in the literature: a ‘wet chemistry’ route that uses phosphorus pentachloride in chlorobenzene⁶⁹; and an alternative route uses chlorine gas⁸³.

The wet chemical chlorination uses a method developed by Lewis *et al*⁸⁴. The hydrogen-terminated sample is first chlorinated using a mixture of phosphorus pentachloride, benzyl peroxide, and chlorobenzene. This is a radical-based process, where the reaction mixture is heated to ~100°C for 1 hour. The peroxide bond in benzyl peroxide splits homolytically, forming 2 radicals. The benzyl radical species

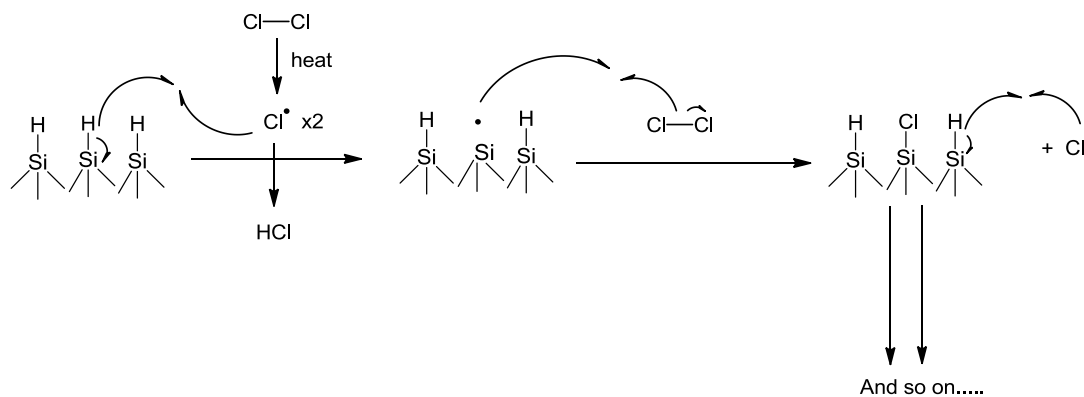
then reacts with the hydrogen-terminated surfaces, forming a radical on the surface. By reaction with a phosphorus pentachloride molecule, the surface is chlorinated, forming a phosphorus tetrachloride radical in the process. This radical can extract a hydrogen atom from the surface, forming a new radical centre on the surface and repeating the cycle (Scheme 2.6).



Scheme 2.6 - Chlorination mechanism for the wet-chemistry route

With this method of chlorination, up to 98% surface coverage has been reported⁸⁵. Therefore this step should have a negligible limit the surface coverage for methylation of the surface, which has a maximum theoretical coverage of a complete monolayer coverage on silicon (111)^{29,86}.

To chlorinate samples by the chlorine gas method, a mixture of nitrogen and chlorine gas (~0.3% chlorine) is passed over the sample inside a stainless steel reactor. The reactor is heated to 95°C for 1 hour after which the system is purged with nitrogen for 20 minutes. The sample is then chlorine terminated and ready to be used in subsequent reactions.



Scheme 2.7 - The mechanism of chlorination for the gaseous chlorination method

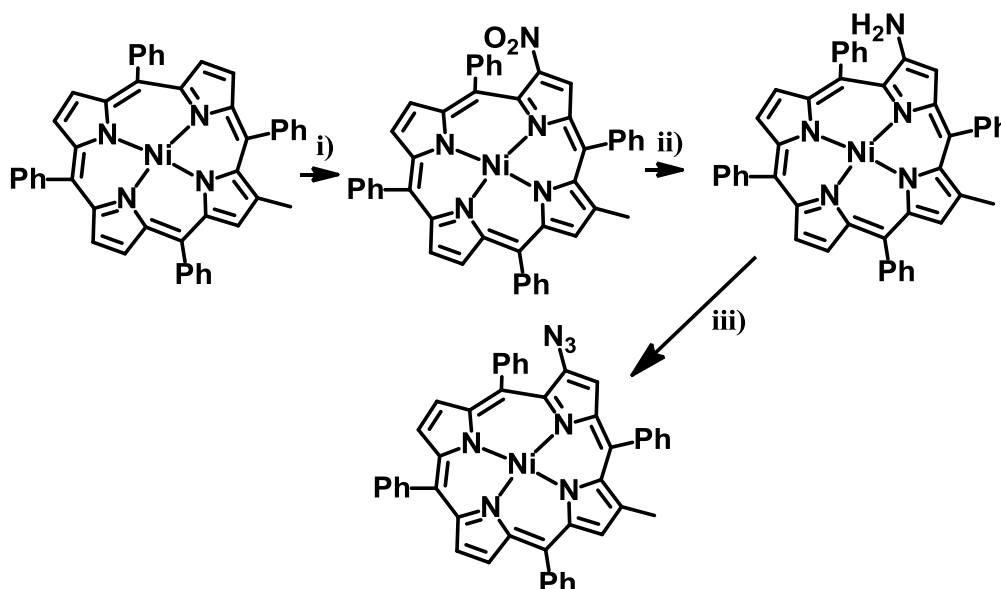
This is another radical-based process. The chlorine-chlorine bond is broken homolytically upon heating, producing two chlorine radicals. These can then react with the hydrogen-terminated surface producing silicon radicals and hydrochloric acid gas. Subsequently, the silicon radical can react with another molecule of chlorine gas to produce a chlorine-terminated surface and a further chlorine radical. The mechanism can then repeat until the surface is completely chlorine-terminated (Scheme 2.7)⁸⁷.

Rivillon *et al.* discovered that this method could lead to a relatively small amount of surface contamination when compared with the wet chemistry method, as they determined that ~3% of a monolayer of Si-O-Si had been incorporated into the silicon surface via the chlorine gas method. For comparison, the Si-O-Si incorporated by the wet chlorination method was larger, at around 15% incorporation⁸⁵.

Once the surface has been chlorinated, a Grignard reagent can be used to alkylate the sample. The passivating properties of these surfaces have been discussed in detail in Section 2.3.1.

2.5.2 Secondary / Other Functionalisation of Silicon Surfaces

Many different routes exist to secondary functionalise alkylated silicon surfaces. One of the most interesting reactions involves attaching a porphyrin onto an acetylene-terminated surface⁸⁸. Firstly, a diazide functionalised porphyrin is produced by mono-nitration of the porphyrinic core, followed by a reduction of the amine group. The final product is then obtained in good yield (85%) after diazotisation. This can be reacted with the acetylene-terminated surface, resulting in the porphyrin substituent being covalently bonded to the monolayer. The synthesis method for the diazide porphyrin synthesis is shown in Scheme 2.8.



Scheme 2.8 - Formation of the porphyrin for attachment to the acetylene terminated silicon
 where (i) $\text{Cu}(\text{NO}_3)_2 \cdot 3\text{H}_2\text{O}$, $(\text{CH}_3\text{CO})_2\text{O}$, rt, 3 h; (ii) Sn/HCl , CHCl_3 , rt, 2 h; (iii) (a) NaNO_2 , H_2SO_4 , $\text{THF}-\text{H}_2\text{O}$, rt, 30 min; (b) NaN , H_2O , rt, 30 min

Carboxylic acid terminated silicon surfaces can be produced by heating⁸⁹ or UV irradiation⁹⁰ of a hydrogen-terminated silicon surface with a terminal alkene carboxylic acid. Further functionalisation of the carboxylic-acid terminated monolayer can then be undertaken, such as immersion in base to generate the ester

between two adjacent carboxylic acid groups⁸⁹. By reacting the carboxylic acid-functionalised surface with an appropriate amine, secondary functionalisation is possible⁸⁹. Another route similar to this is to react the carboxylic acid-terminated surface with *n*-hydroxysuccinimide (NHS), which can then undergo nucleophilic substitution with an appropriate amine⁹⁰.

The methyl-terminated surfaces produced by the two-step chlorination-alkylation technique previously discussed can also be further functionalised^{91,92,93}. By using a photoactive aryldiazirine such as commercially available 4'-[3-Trifluoromethyl-3H-diazirin-3-yl]-benzoic acid *n*-hydroxysuccinimide ester (TDBA-OSu) and irradiating with UV light (at 365 nm), the TDBA-OSu inserts into the terminal C-H bond of a methyl substituent⁹². Interesting the surface retained passivation effects after the secondary functionalisation of the surface, with very little oxide growth on the surface after 2 months exposure to ambient conditions. By changing the alkyl chain lengths bonded to the silicon surface, the distance between the surface and the TDBA-OSu can be modified for studying the effects of silicon-chromophore distance on fluorescence quenching for example.

The synthesis of carbon-carbon bonds on monolayers attached to silicon has also been investigated in the literature. These have been achieved by cross metathesis between alkene-terminated silicon surfaces and 1-alkenes using a Grubbs catalyst^{94,82,30}. This was achieved through either the thermal grafting of an alkene chain onto the surface of silicon⁹⁴ or through the two-step chlorination-alkylation technique previously discussed^{30,95}. The appropriate alkene was then added to the functionalised surface, along with the Grubbs catalyst and heated for 48 hours. This resulted in cross metathesis, forming a new C-C bond bound to silicon. This could be

suitable for the reaction of the alkene monolayer with a dye, as long as the passivating effect is retained.

The final noteworthy method of secondary functionalisation of an alkyl monolayer is thiol-ene click chemistry on allyl-functionalised surfaces⁹⁶. By heating a diene with a hydrogen-terminated surface, a terminal alkene was produced. The appropriate thiol was added after alkylation of the surface and irradiated with 365 nm UV light in the presence of a photoinitiator (2,2-dimethoxy-2-phenylacetophenone [DMPA]). This reaction requires irradiation for 1.5 hours, but can be carried out at room temperature and under ambient conditions⁹⁶. A downside of this method is that no passivation of the silicon surface is observed. Functionalisation of the silicon surface with allyl groups can also be achieved through the two-step chlorination-alkylation technique which does passivate the surface^{78,30}. Therefore a potential route to a passivation layer with chromophore attachment could be thiol-ene click chemistry on an allyl surface produced through the chlorination-alkylation technique.

A summary of routes to secondary functionalisation of silicon is shown in Fig. 2.13.

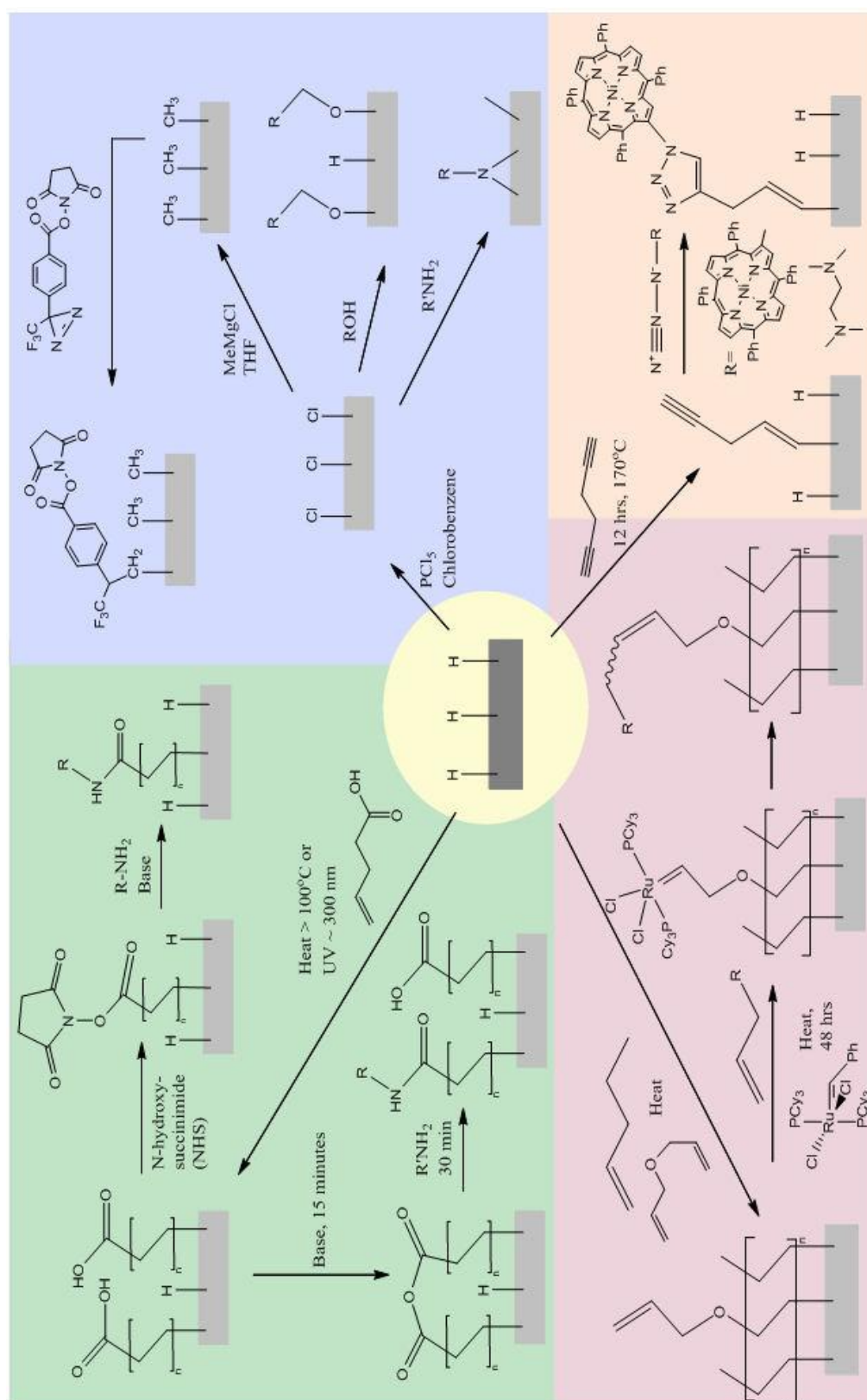
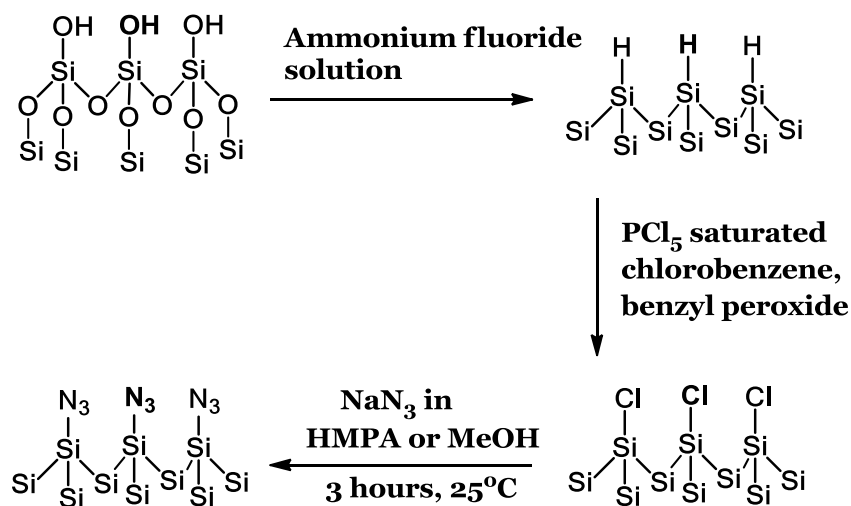


Fig. 2.13 - Some literature examples of previous functionalisation routes for silicon

120,185,69,98,88,186,90,187,89,94,92,91,93

Various other methods of functionalisation of silicon which do not involve formation of a Si-C bond have been widely investigated in the literature. Some of the more common functionalisation methods are azidation of the silicon surface or forming silicon-transition metal bonds⁹⁷.

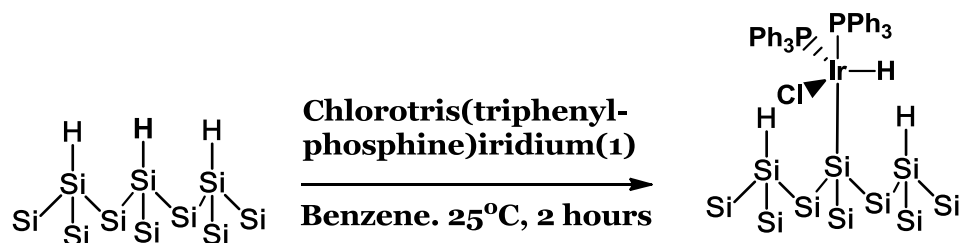


Scheme 2.9 - Reaction scheme for azidation of the silicon surface

To functionalise the surface with azide groups, a hydrogen-terminated surface is once again required. The hydrogen-terminated surface is chlorine-terminated (by either the wet chemical or chlorine gas method), followed by azidation with sodium azide (Scheme 2.9)⁹⁷. These surfaces are unstable with respect to oxidation, with 0.4 monolayers of oxygen forming in the first 60 hours in air. The maximum coverage achieved for these surfaces, however, was only 55%.

Another literature example of passivation uses transition metals (iridium in particular)⁹⁸. The first step in the reaction is once more to remove the oxide layer and form a hydrogen-terminated surface. The hydrogen-terminated surface is then reacted directly with chlorotris-(triphenylphosphine)iridium (Scheme 2.10). This forms a direct bond between the transition metal and the silicon surface, resulting in

partial coverage. From XPS studies, the coverage of iridium on the surface was deemed to be only 1.4%, because of the bulky transition metal and ligands sterically hindering further attachment.



Scheme 2.10 - Addition reaction of an iridium complex onto a hydrogen-terminated silicon surface

An advantage of this type of passivation is that the transition metal and ligands can be tuned to change the chemical and electrical properties of the silicon surface, for example through changing the wavelength of absorption of the transition metal complex. This would give a surface that can be adapted to give the most beneficial characteristics.

2.6 Conclusions

The motivation for this research project is to reduce the thickness (and therefore cost) of crystalline silicon solar cells by the incorporation of passivation / light harvesting layers. Many routes to passivation have been discussed, through removal of surface states and charging of the semiconductor surface. The technique most suited to our purpose was deemed as being the two-step chlorination-alkylation technique. This has been shown to have relatively good stability in ambient conditions, whilst affording excellent passivation properties with the ability to further functionalise the monolayers. The chemical structure of the silicon surface

has been discussed, including a discussion of the current understanding as to how the passivation effect arises.

Many routes for secondary functionalisation of alkyl monolayers have been shown from the literature, allowing the one most suited to our purpose to be used. A route for attaching a porphyrin chromophore has been shown, through the use of an azide linkage.

3. Semiconductors: Junctions and Surfaces

This chapter deals with the fundamental equations and theory that describe semiconductor surface and bulk. Expressions for the carrier concentrations both in equilibrium and under illumination are obtained. The p-n junction will also be discussed, with relevance to the silicon surface both in equilibrium and under illumination.

The generation and recombination of charge-carriers under illumination will be discussed and we shall consider a model that links the bias voltage to the surface recombination velocity.

3.1 Carrier Concentrations and Carrier Flow

The density of electrons in the conduction band is related to the position of the electron Fermi-level by the equation⁹⁹:

$$n = n_i \exp\left(\frac{E_{fn} - E_i}{k_B T}\right) \quad (\text{eqn 3.0})$$

for electron concentrations, and:

$$p = n_i \exp\left(\frac{E_i - E_{fp}}{k_B T}\right) \quad (\text{eqn 3.1})$$

for hole concentrations, where n and p are the electron and hole concentrations, E_{fn} and E_{fp} are the Fermi-levels for electrons and holes, E_i is the intrinsic Fermi-level, n_i is the intrinsic carrier concentration, k is the Boltzmann constant and T is the

temperature. We note that the concentration of electrons in the conduction band increases, the electron Fermi-level will move further away from the intrinsic Fermi-level. At equilibrium when electrons and holes are described by a single Fermi level, the charge carriers concentrations comply with the mass action law:

$$np = n_i^2 \quad (\text{eqn 3.2})$$

which holds for intrinsic as well as doped semiconductors. Illumination generates electron-hole pairs. Majority carrier concentration is usually high and does not change significantly under illumination. Concentration of minority carriers, however, is low and will change significantly. In this non-equilibrium situation the mass action law has to be generalised to:

$$np = n_i^2 \exp\left(\frac{E_{fn} - E_{fp}}{k_B T}\right) \quad (\text{eqn 3.3})$$

There are two principal mechanisms of conduction in semiconductors; drift and diffusion. Drift is caused by the presence of an electric field (E), whilst diffusion occurs due to a concentration gradient. The drift current density is given, in terms of the mobility (μ):

$$J_n = nqE\mu_n \quad (\text{eqn 3.4})$$

where q is the carrier charge. A similar equation is also obtainable for the drift current density due to hole flow. The rate at which carriers diffuse is proportional to the concentration gradient (Fick's law), which we can write as:

$$Flux = -D \frac{dn}{dx} \quad (\text{eqn 3.5})$$

where flux is the number of carriers crossing a unit area per second, D is the diffusion coefficient and dn/dx is the concentration gradient, giving an equation for the electrical current density due to diffusion:

$$J_n = qD_n \frac{dn}{dx} \quad (\text{eqn 3.6})$$

where a similar equation can be written for holes. As the total current is due to the flow of carriers by drift and diffusion, a simple addition of equations 3.4 and 3.6 leads us to an expression for total current density due to carrier flow.

$$J_n = q\mu_n nE + qD_n \frac{dn}{dx} \quad (\text{eqn 3.7})$$

with a similar expression for holes. The diffusion coefficient (D) can be linked to the carrier mobility (μ) by the Einstein relation:

$$D_n = \frac{\mu_n k_B T}{q} \quad (\text{eqn 3.8})$$

3.2 The p-n and one sided junction

The p-n junction forms the basis of operation of crystalline silicon solar cells, and is formed by diffusing a dopant (for example phosphorus) into the oppositely doped silicon wafer (in this case p-type). We will now cover the p-n junction in equilibrium (in darkness) and in non-equilibrium (under illumination), with both related to the silicon surface (equivalent of a one sided junction).

3.2.3 Equilibrium case

The band diagram of a p-n junction (Fig. 3.0) and a one sided junction (silicon surface) (Fig. 3.1) in equilibrium is shown below:

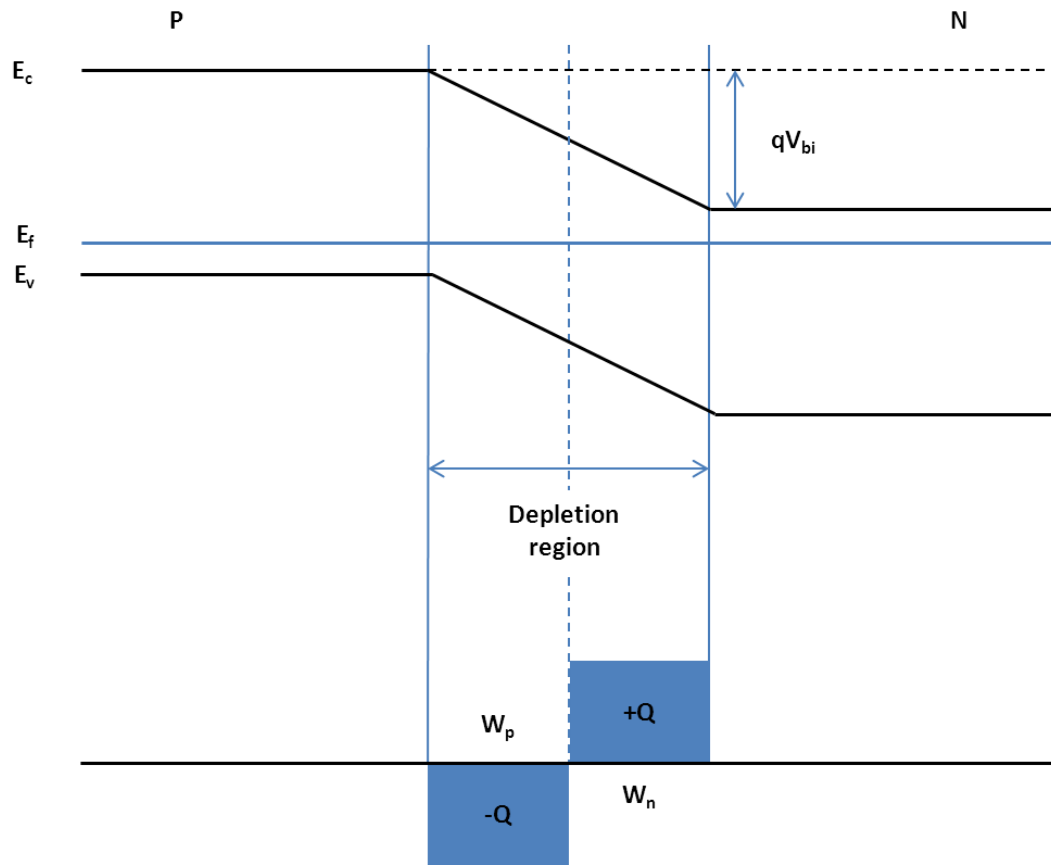


Fig. 3.0 - The band diagram of a p-n junction in equilibrium showing the Fermi-levels for electrons and holes (solid lines), the intrinsic Fermi-level (dashed line) and the charge distribution (not to scale)

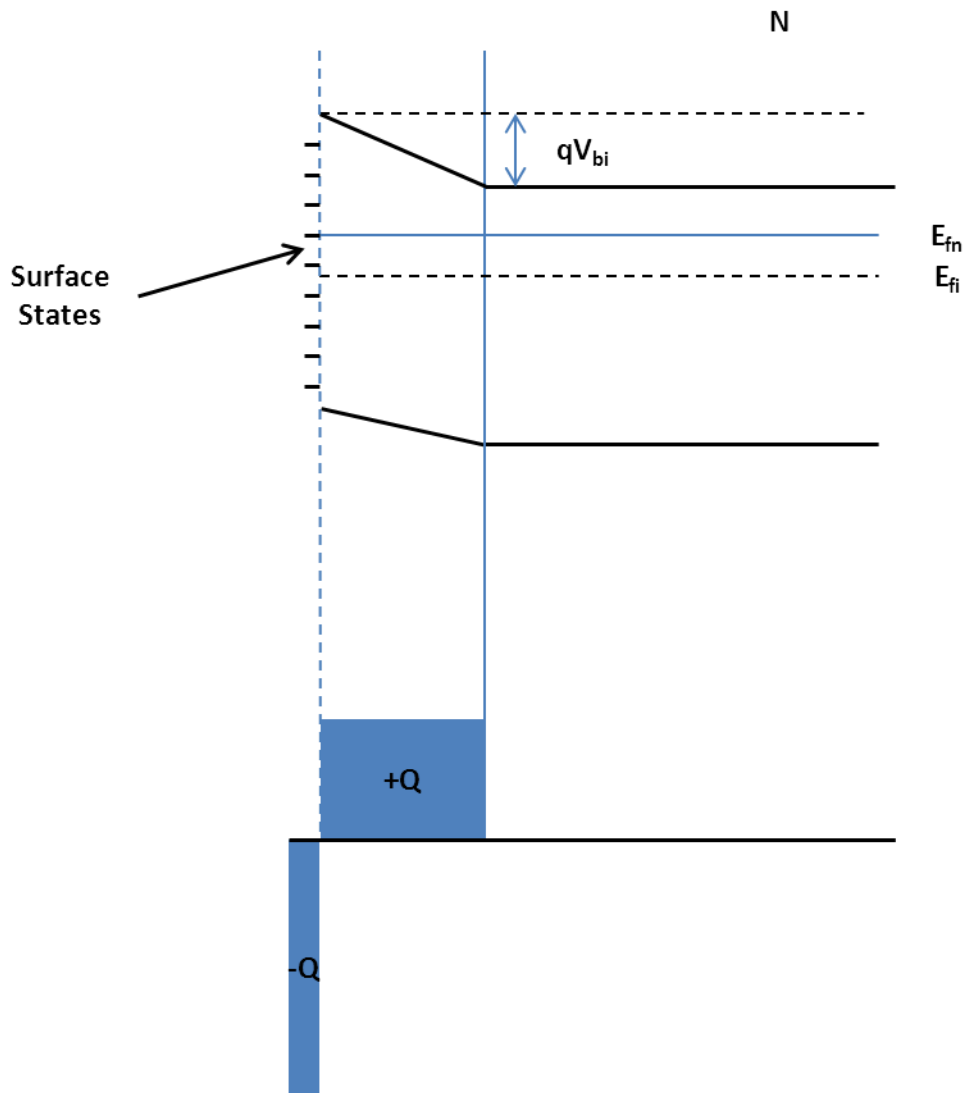


Fig. 3.1 - The band diagram of a one sided junction in equilibrium showing the Fermi-levels for electrons (solid lines), the intrinsic Fermi-level (dashed line) and the charge distribution (not to scale)¹⁰⁰

As can be seen in Fig. 3.0 and Fig. 3.1, the silicon surface bands can be treated as one side of a p-n junction with a thick depletion region in the silicon and a thin surface charge layer. In the equilibrium situation, the surface charge can be calculated from:

$$Q = qN_D W_n = qN_A W_p \quad (\text{eqn 3.9})$$

Where Q is the surface charge, N_D and N_A are the donor and acceptor concentrations and W_n and W_p are the depletion widths of the n and p side of the junction. The built-in voltage can be calculated from⁹⁹:

$$V_{bi} = \frac{Q}{2\epsilon} w \quad (\text{eqn 3.10})$$

By combination of equation 3.9 and 3.10 we can obtain the following expression:

$$qV_{bi} = \frac{Q^2}{2\epsilon} \left(\frac{1}{N_A} + \frac{1}{N_D} \right) \quad (\text{eqn 3.11})$$

for a p-n junction or for a one sided junction (or surface):

$$qV_{bi} = \frac{Q^2}{2\epsilon N_A} \quad (\text{eqn 3.12})$$

3.2.4 Non-equilibrium case

Upon illumination, the carriers are no longer in equilibrium. Away from equilibrium the electric field in the junction pulls minority carriers from each side through the depletion region, onto the other side of the junction. The majority carriers on the other hand are hindered from transport across the junction by the potential barrier qV . Thus, the p-n junction acts a semiconductor diode.

Close to the junction, the single electron and hole Fermi-level in equilibrium now splits into two quasi-Fermi-levels. The splitting of the Fermi-levels gives the open circuit voltage, one of the characteristic values of a solar cell. The band diagram of a p-n junction and one sided junction under illumination is shown below (Fig. 3.2 and Fig. 3.3):

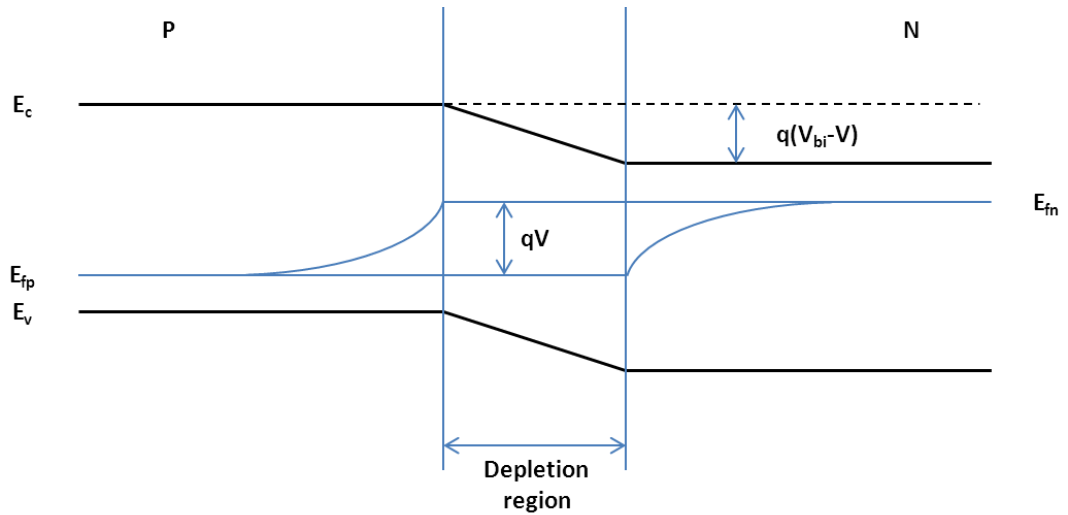


Fig. 3.2 - The band diagram of a p-n junction in non-equilibrium (not to scale)

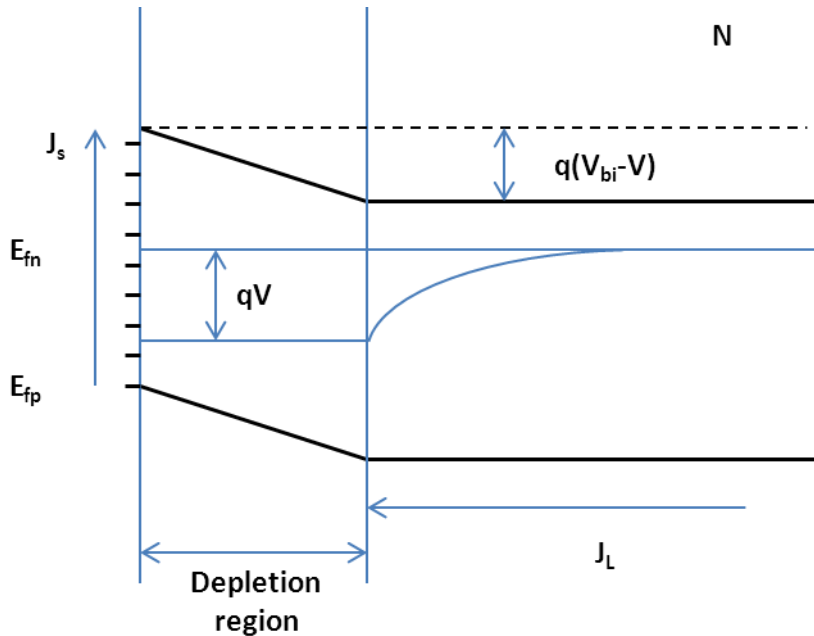


Fig. 3.3 - The band diagram of a one sided junction in non-equilibrium (not to scale)

As the surface states will be filled up to the Fermi-level of the sample, a high concentration of electrons on the surface has the effect of charging the surface when compared to the bulk. As can be seen in the diagram, the surface charge accelerates any holes (minority carriers) generated in the bulk of the sample towards the surface. Upon reaching the depletion region, the minority carriers are accelerated towards the surface by the electric field, where they can recombine with electrons (majority

carriers) at the surface states. In a solar cell, the minority carrier flow through the p-n junction gives a current, J , which can be calculated from:

$$J = J_L - J_0(e^{\frac{qV}{k_B T}} - 1) \quad (\text{eqn 3.13})$$

Where J_L is the photogenerated current density and J_0 is the dark current density. At photon energies above the semiconductor band gap, absorbed photons give rise to electron-hole pairs. If the diffusion length is sufficiently long (i.e. larger than the semiconductor thickness), the photogenerated current will be equivalent to the number of photons absorbed multiplied by the charge of an electron. Equations for the number of photons absorbed are shown in Chapter 3.3.

At the surface, a current (denoted J_s) exists due to surface recombination. The surface current is proportional to the minority carrier concentration, and is given by replacing J in equation 3.13 with J_s :

$$J_s = J_L - J_0(e^{\frac{qV}{k_B T}} - 1) \quad (\text{eqn 3.14})$$

where V is the internal voltage due to the splitting of the quasi-fermi-levels. Under highly illuminated samples (where $V = V_{bi}$) the surface bands flatten leading to the saturation voltage. The value of J_0 can be calculated from¹⁰¹:

$$J_0 = qp_0\left(\frac{D}{\tau}\right)^{0.5} \quad (\text{eqn 3.15})$$

The concentration of electrons in n-type silicon will not change significantly under illumination ($n_s = n_b$). The hole concentration will change substantially, and will be given by:

$$p_s = p_0 e^{\frac{qV}{k_B T}} \quad (\text{eqn 3.16})$$

where p_s is the concentration of holes at the surface and p_0 is the concentration of holes in the bulk.

3.3 Carrier Generation

It is also important to obtain an expression for the generation of electron-hole pairs in the semiconductor. When light of a wavelength λ is incident upon the surface, the electron-hole pair generation rate is given by:

$$G(\lambda) = \alpha(\lambda) \phi(\lambda) [1-R(\lambda)] \exp(-\alpha(\lambda)x) \quad (\text{eqn 3.17})$$

where $\phi(\lambda)$ is the incident number of photons per cm^2 per second, R is the number of photons reflected from the surface and α is the absorption coefficient of silicon. If there is no recombination in the bulk of the silicon, we integrate over the wavelengths considered and the silicon thickness is larger than the absorption depth, equation 3.17 can be simplified to:

$$G = \phi [1-R] \quad (\text{eqn 3.18})$$

allowing the generation rate of the electron-hole pairs to be calculated as long as the total average reflectivity of the sample and total photon flux are known. This links back to the photogenerated current (J_L) in Section 3.2.4, and is given by:

$$J_L = q\phi[1 - R] \quad (\text{eqn 3.19})$$

3.4 Recombination: General

There are three main types of charge-carrier recombination in semiconductors; recombination through defects, radiative recombination and Auger recombination (Fig. 3.4). Radiative recombination is band to band recombination, dominant in direct bandgap semiconductors. In indirect bandgap semiconductors, this mechanism

is usually negligible and can be ignored. Auger recombination involves high carrier densities and is not observed in situations concerned with in this thesis.

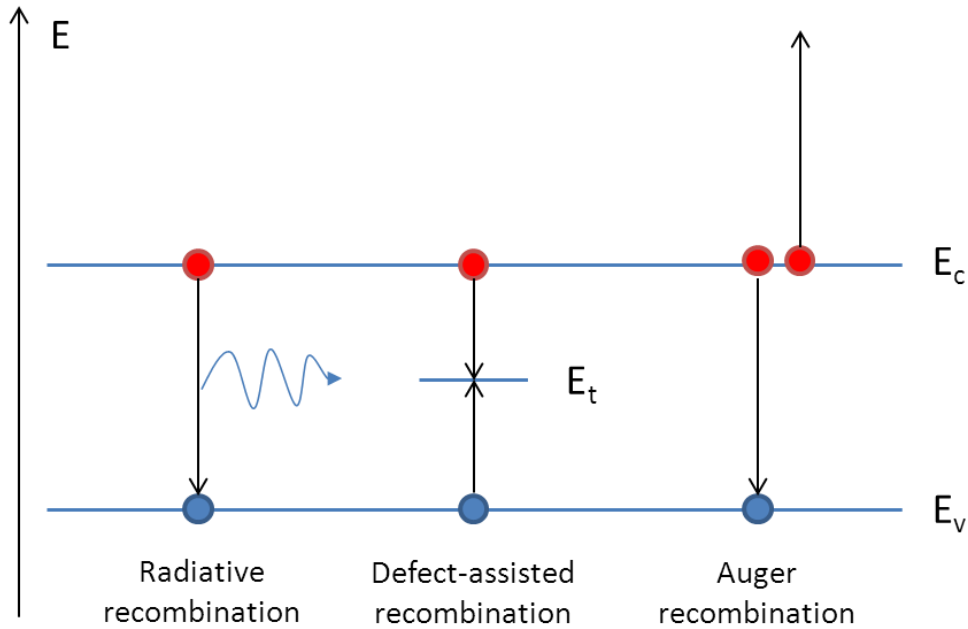


Fig. 3.4 - The three main types of recombination in semiconductors

Under low injection conditions which are generally applicable in the present work, recombination rate per unit volume can be expressed in terms of recombination lifetime:

$$U = k(p - p_0) \quad (\text{eqn 3.20})$$

Where k is proportional to $1/\tau$. The analogous quantity for surface recombination rate (per unit surface area) is the surface recombination velocity (SRV, denoted by S), which is a measure of the rate of minority carrier flow through surface states:

$$U_{surf} = S(p - p_0) \quad (\text{eqn 3.21})$$

The aim of surface passivation is to reduce the value of surface recombination velocity S . Equations 3.20 and 3.21 hold for n-type samples; analogous expressions (with hole concentrations replaced by electron concentrations) are valid of p type.

The recombination lifetime also depends upon minority carrier injection level, with an example shown in Fig. 3.5.

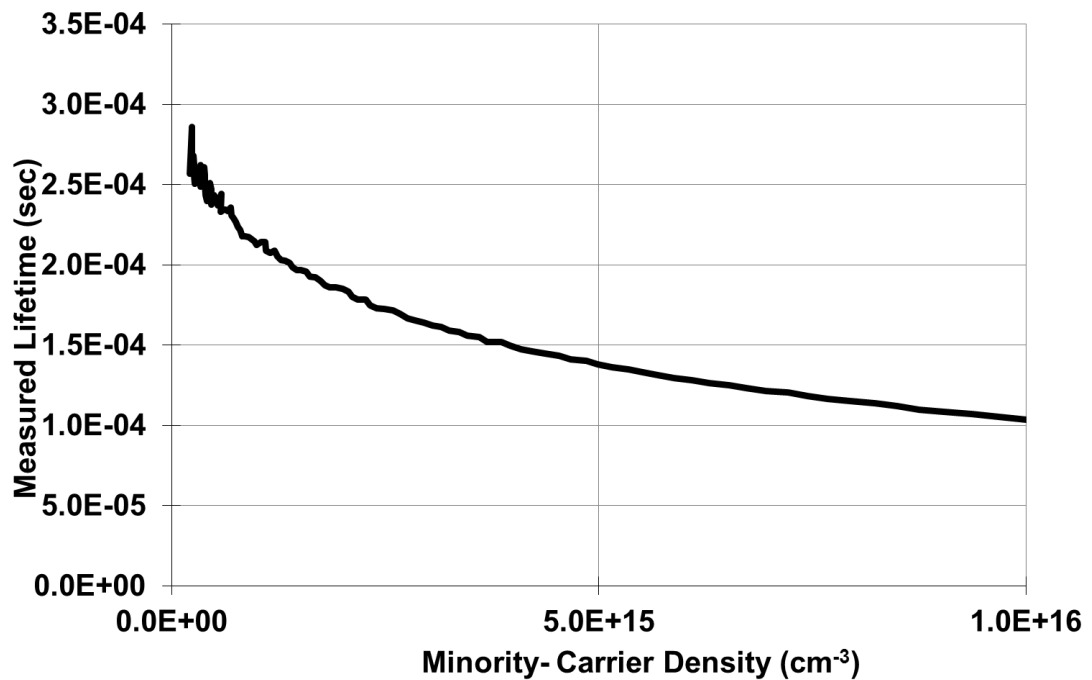


Fig. 3.5 - The change in recombination lifetime with minority carrier density as measured by a Sinton WCT-120

One way of measuring the lifetime is by monitoring the carrier density as a function of photogenerated excess carriers. This technique is used by the Sinton WCT wafer lifetime tool, which is used during recombination lifetime measurements in this thesis¹⁰². The Sinton WCT-120 measures the effective lifetime containing contributions from the surface and bulk which should be separated to get a true value of the surface recombination.

Carrier density can be determined from the transient decay of minority carriers after illumination or under varying light intensity in quasi-steady state (QSS). The appropriate mode to use depends upon the lifetime of the sample. The QSS mode is generally applicable if the lifetime of a sample is much lower than the decay constant of the xenon flash lamp (~2.3 ms) and the sample can be considered as being in steady-state at each different light intensity¹⁰³. The total (effective) lifetime can then be determined from the generation rate (G) of the excess carriers and excess carrier density (Δn):

$$\tau_{eff} \Delta n = \frac{\Delta n}{G} \quad (\text{eqn 3.22})$$

In transient mode, carrier lifetime is determined from the decay of carrier density following a short pulse of illumination. This mode is suited towards higher (>200 μs) lifetimes, and can be described by:

$$\tau_{eff} \Delta n = - \frac{\Delta n(t)}{d\Delta n(t)/dt} \quad (\text{eqn 3.23})$$

where $\Delta n(t)$ is the time dependent average excess carrier density.

The observed effective lifetime (τ_{eff}) contains contributions from recombination in the bulk and from the surface; in addition, we must consider the time constant due to diffusion to the surface. These three components will now be discussed to determine τ_{eff} under flat band conditions.

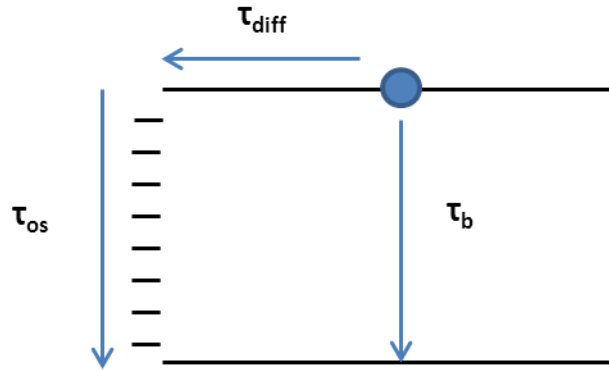


Fig. 3.6 - The recombination processes in the bulk and at the surface

Upon photon absorption in the silicon, an electron-hole pair is generated in the silicon bulk. The electron-hole pair can recombine at either the surface or in the bulk. For recombination to occur at the surface, the charge-carrier must diffuse to the surface (Fig. 3.6). As the diffusion and recombination processes are sequential, we can obtain the following expression:

$$\tau_s = \tau_{diff} + \tau_{os} \quad (\text{eqn 3.24})$$

where τ_s is the surface recombination lifetime, τ_{diff} is the time to diffuse to the surface and τ_{os} is the minority carrier lifetime due to lifetime of the recombination at the surface. τ_{os} can be determined from the lifetime when diffusion is very fast – in other words, under uniform concentration when $\tau_{os} = W/2S$, where S is the surface recombination velocity. The determination of τ_{diff} is less straightforward but an approximate value found to give an accurate answer is found to be¹⁰⁴:

$$\tau_{diff} = \frac{1}{D} \left(\frac{W}{\pi} \right)^2 \quad (\text{eqn 3.25})$$

where D is the diffusion constant. Combining the two results, we obtain:

$$\tau_s = \frac{W}{2S} + \frac{1}{D} \left(\frac{W}{\pi} \right)^2 \quad (\text{eqn 3.26})$$

which will be applied in Chapter 6. The second term dominates when the surface recombination is fast. For smaller values of S , recombination is not limited by diffusion to the surface and the second term can be neglected, giving:

$$\tau_s = \frac{w}{2S} \quad (\text{eqn 3.27})$$

The total effective lifetime for charge-carriers can be calculated through adding the rates of the two recombination processes:

$$\frac{1}{\tau_{eff}} = \frac{1}{\tau_b} + \frac{1}{\tau_s} \quad (\text{eqn 3.28})$$

where τ_b is the bulk lifetime. By replacing τ_s from equation 3.27 with equation 3.27, we obtained the required expression:

$$\frac{1}{\tau_{eff}} = \frac{1}{\tau_b} + \frac{2S}{w} \quad (\text{eqn 3.29})$$

which will be applied in Chapters 4,5 and 7. The distance over which a minority carrier diffuses on average before recombination is known as the diffusion length, and can be calculated from:

$$L = (D\tau_b)^{0.5} \quad (\text{eqn 3.30})$$

This will be applied in Chapter 6.

3.5 Recombination: Statistics

Recombination through defects, governed by Shockley-Read-Hall statistics¹⁰⁵, is a two-step process, where an electron is trapped at an energy state deep in the forbidden band. The rate of this process depends on the position of the level, with energy bands near the centre of the gap usually most effective for recombination^{106,40}.

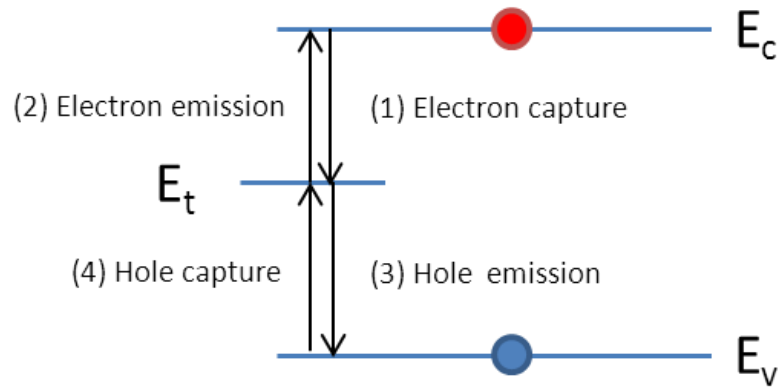


Fig. 3.7 - The relevant carrier capture and emission rates contributing to defect-assisted recombination under flat band conditions

The defect-assisted recombination process is shown schematically in Fig. 3.7 under flat band conditions. An electron is captured from the conduction band to the trap state. From here, the electron can either be emitted back to the conduction band, or a hole can be captured into the trap state which recombines with the electron. Likewise if a hole is first captured by the trap state, either electron capture or hole emission can occur. The rate of electron capture (1) can be expressed as:

$$k_n n (1 - f) \quad \text{eqn (3.31)}$$

where k_n is a proportionality constant, n is the electron concentration and f is the probability that the trap is occupied. A similar expression can be obtained for holes, where $(1-f)$ is replaced by f , as a hole can only be captured if the trap state is occupied by an electron. The electron emission rate is then simply:

$$k'_n f \quad \text{eqn (3.32)}$$

A similar expression is obtained for holes, with $(1-f)$ replacing f as a hole can only be emitted if there is no electron present.

In steady state, the rates of electron and hole capture must be equal and we can therefore write:

$$k_n n(1 - f) - k'_n f = k_p p f - k'_p (1 - f) \quad \text{eqn (3.33)}$$

In efficient recombination centres, the emission processes are generally negligible.

Equation 3.33 can therefore be simplified to:

$$k_n n(1 - f) = k_p p f \quad \text{(eqn 3.34)}$$

The probability that a trap is occupied (f) can be given by simple rearrangement of equation 3.34.

$$f = \frac{k_n n}{k_n n + k_p p} \quad \text{(eqn 3.35)}$$

The total recombination rate U per unit volume is equal to the left or right hand side of equation 3.34 multiplied by the density of traps (N_t):

$$U_{SRH} = N_t U = N_t k_n n \frac{k_p p}{k_n n + k_p p} \quad \text{(eqn 3.36)}$$

Since the capture rate k is a product of the carrier capture cross section and the thermal velocity:

$$k_p = \sigma_p v_{th} \quad \text{(eqn 3.37)}$$

we obtain the following expression for the Shockley-Read-Hall recombination rate at a single trap level (see, for example Olibet *et al.*¹⁰⁷):

$$U_{SRH} = \frac{n_s p_s}{\left(\frac{n_s}{\sigma_p}\right) + \left(\frac{p_s}{\sigma_n}\right)} v_{th} N_s \quad \text{(eqn 3.38)}$$

Equation 3.38 holds for a level in the bulk or at the surface, and will form a useful starting point for the discussion of surface recombination in Chapter 5. As previously discussed in this chapter, the surface bands under illumination causes band bending, with splitting of the quasi-fermi-levels (Fig. 3.8).

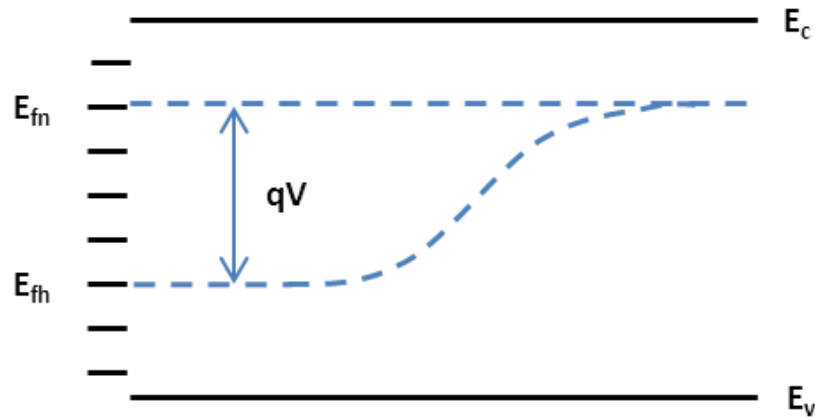


Fig. 3. 8 - The surface bands of silicon under strong illumination (When $V=V_{bi}$) showing the splitting of the Fermi-levels into quasi-Fermi-levels

In equation 3.16, it was shown that the hole concentration due to the internal voltage is given by:

$$p_s = p_0 e^{\frac{qV}{k_B T}} \quad (\text{eqn 3.16})$$

whilst the electron concentration will remain constant. As the Fermi-level splitting increases (qV), the hole concentration at the surface (p_s) increases. With a decrease in surface hole concentration, Shockley-Read-Hall recombination from equation 3.38 will also decrease. The effective surface recombination velocity can be calculated from the Shockley-Read-Hall single trap level recombination rate from equation 3.21 by neglecting the emission process, p_0 :

$$S_{eff} = \frac{U_{SRH}}{p} \quad (\text{eqn 3.39})$$

The effective surface recombination velocity with bias voltage obtained through these equations is shown in Fig. 3.9 and will be compared to experimental data in Chapter 7.

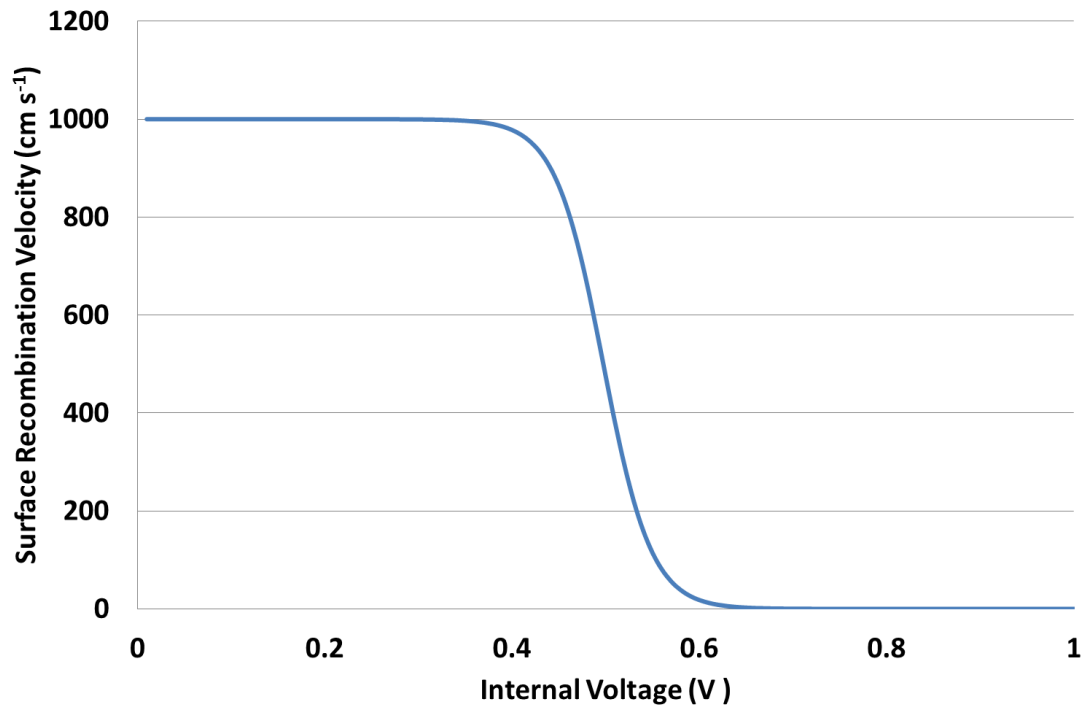


Fig. 3.9 - The change in surface recombination velocity with internal voltage

As shown in Fig. 3.9, the surface recombination velocity changes between an internal voltage of 0.4 and 0.6 V. After this value of internal voltage, the surface is depleted of electrons, reducing the surface recombination velocity.

3.5 Conclusions

In this chapter the carrier concentrations in silicon have been discussed and described, both in equilibrium and under illumination. The flow of current due to diffusion and drift have been discussed, and linked to the p-n junction. The electronic properties of the silicon surface has been discussed and related back to the p-n junction.

Different mechanisms of electron-hole pair recombination have been outlined. The focus in this thesis is on recombination via defects, described in terms of Shockley-Read-Hall statistics. We have constructed an approximate model that links the voltage with the surface recombination velocity, which will be used to discuss experimental data in Chapter 7.

Observed surface recombination lifetime contains several components due to carrier diffusion to the surface and recombination through surface levels. We have discussed a simple method as to how these effects can be combined in a quantitative manner.

4. Etching and Bulk Lifetime

This chapter has been published in part as:

N. Alderman, L. Danos, M. Grossel and T. Markvart, 'Effect of surface roughness on the recombination lifetime of hydrogen fluoride etched crystalline silicon', *Proceedings of Photovoltaic Science Application and Technology (PVSAT)-6 conference*, 2010, 59-62.

4.1 Introduction

The surface preparation of silicon wafers is an important step in semiconductor processing, because of the need to remove the native oxide layer, the cleaning of the sample and hydrogen termination of the surface^{34,108,109,55}. This leaves a clean, atomically flat, hydrogen-terminated surface that can be further functionalised by other chemical methods^{47,110,38}. Two main etching solutions are readily available for this purpose; hydrofluoric acid and ammonium fluoride. Ammonium fluoride has been shown to produce semiconductor surfaces with less pitting than hydrofluoric acid etched surfaces, although the recombination lifetime produced after processing is reduced when compared to hydrofluoric acid¹¹¹. This could be due to incorporation of charge during the etching step, as hydrofluoric acid has been shown to incorporate up to 0.3% fluorine⁵⁶.

The bulk lifetime is an important parameter in the manufacture of high efficiency solar cells. It is also important to understand this parameter for the calculation of the

surface recombination velocity, which is useful for comparing and observing the degree of surface passivation across different wafers.

4.2 Etching of Silicon Substrates

The hydrofluoric acid etched silicon samples were characterised by ellipsometry and recombination lifetime. It has been shown that ellipsometry measurements are not only sensitive towards oxide thickness, but also surface roughness^{58,112}. This can be seen in Fig. 4.0, where the measured layer thickness decreases as the native oxide is removed, and then increases with further etching time as surface roughness increases.

The recombination lifetime increases rapidly with etching time of up to 15 seconds, achieving a maximum recombination lifetime value of 32 μ s. This does not correspond to the minimum point in the ellipsometry oxide thickness (which is achieved after a 10 second etch) due to residual oxide remaining which is removed after a further 5 seconds of etching, giving the maximum recombination lifetime. After this point, the recombination lifetime decreases, and the ellipsometry readings increase. We interpret this decrease as being due to surface roughness, giving a larger surface area for recombination to occur.

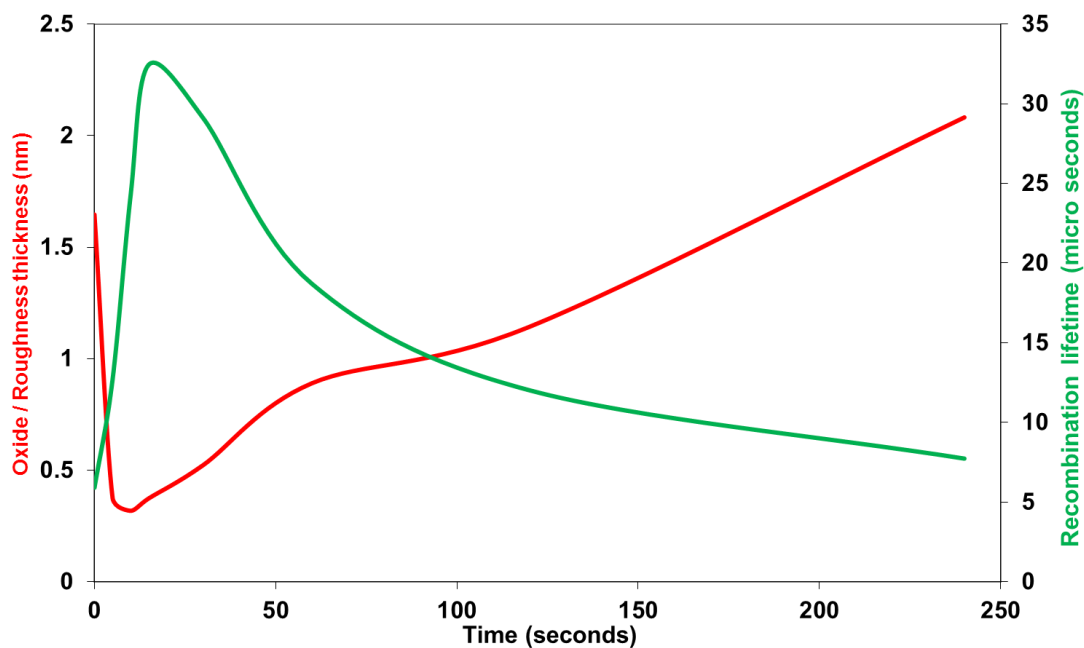


Fig. 4. 0 - Comparison of recombination lifetime and ellipsometry layer thickness for wafers etched in a 2% HF solution

To confirm that these were in fact hydrogen-terminated surfaces, infra-red spectroscopy and contact angle goniometry were undertaken on the samples. We observe a clear hydrogen peak in the infra-red spectrum as shown in Fig. 4.1. This was consistent with literature findings^{64,59}.

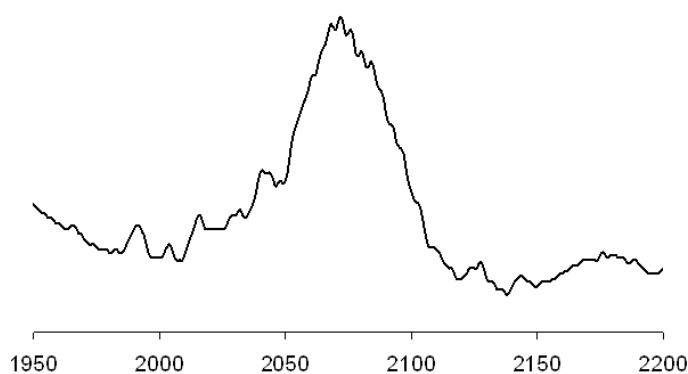


Fig. 4. 1 - Infrared spectrum of the hydrofluoric acid etched surface showing Si-H peak at 2072 cm^{-1}

Through measuring the water contact angle, it was shown that the native oxide samples were hydrophilic, reflecting the presence of surface hydroxyl groups hydrogen bonding to the water droplet. However, after etching there are no hydroxyl groups for the water droplet to hydrogen bond to, increasing the contact angle and making the surface hydrophobic.

After etching with hydrofluoric acid, the contact angle increased from $<10^\circ$ to 101.9° , showing the increase in hydrophobicity and confirming hydrogen termination of the surface (Fig. 4.2).

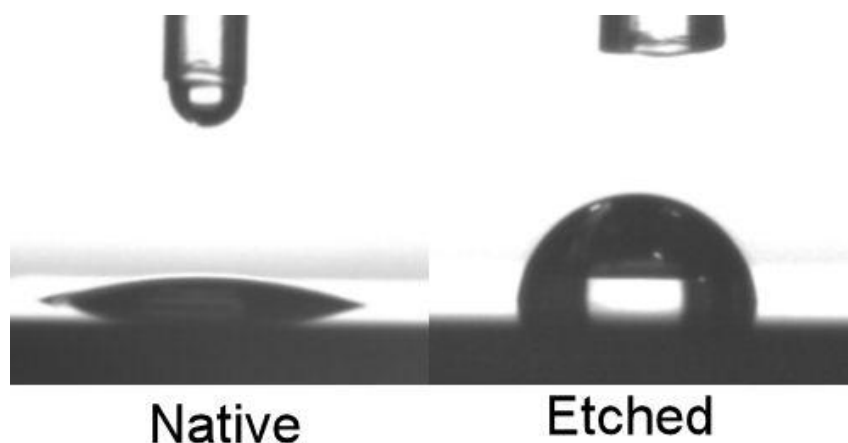


Fig. 4.2 - Comparison of water contact angles for native oxide silicon surfaces and hydrogen-terminated (etched) surfaces

Re-oxidation of the hydrogen-terminated sample was investigated by ellipsometry (Fig. 4.3). Although the sample readily oxidises in ambient conditions, this process is slower than one may have predicted with only 0.25 nm of oxide forming in the first 5 hours in air. The recombination lifetime also decreases back to the native oxide value (3.5 - 4.5 μs) during the first hour in air. To achieve high lifetime samples during the etching and subsequent chemical passivation steps, it is important to limit the surface oxide growth by storing the sample in an inert atmosphere as soon as possible after etching.

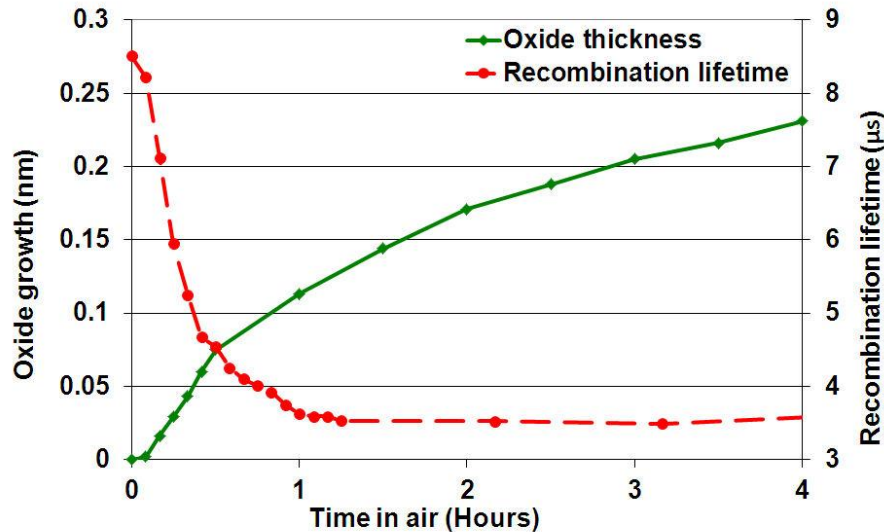


Fig. 4. 3 - Re-oxidation and recombination lifetimes of ammonium fluoride etched (hydrogen terminated) surfaces during storage in air over 4 hours

By controlling the wafer etching time in 2% hydrofluoric acid solutions, the surface recombination can be reduced considerably by a 15 second etch in the case of the wafers used in the experiments; at this point, the total lifetime is closer to the bulk lifetime of the sample. This etching time corresponds with the most atomically smooth surface that is free of oxide. Shorter etching times lead to residual oxide on the surface, which shortens the recombination lifetime. At etching times longer than this, surface roughness ensues. This is due to preferential etching at defects in the silicon, resulting in a larger surface area and a lower recombination lifetime. By increasing the roughness the recombination lifetime changes dramatically between 32 and 8 μ s.

Freshly etched samples have been shown to oxidise slowly in ambient conditions, averaging a growth rate of 0.05 nm of oxide per hour over the first five hours. Over this period of time, we find that the recombination lifetime also reduces from 32 μ s to 4.5 μ s during the first hour as the oxide layer re-grows. Therefore to be able to

measure high recombination lifetimes / bulk lifetime of the silicon, freshly etched samples have been used.

4.3 Estimation of the Bulk Lifetime

The bulk lifetime of silicon wafers was estimated by passivation of the surface by one of three literature techniques; involving immersion of wafers in either: (i) HF solutions^{55,51}; (ii) iodine in methanol solutions^{71,75}; or (iii) quinhydrone in methanol solutions^{66,68}. Each of these has been shown to give a value of recombination lifetime close to that of the bulk lifetime of the wafer. For each type of wafer (either 10.5 x 10.5mm squares, n type, 25 Ωcm^{-1} , 500 μm thickness or 10x10mm squares, n type, 2500 Ωcm^{-1} , 300 μm thickness) the three different passivation methods were attempted and the results are plotted in Fig. 4.4.

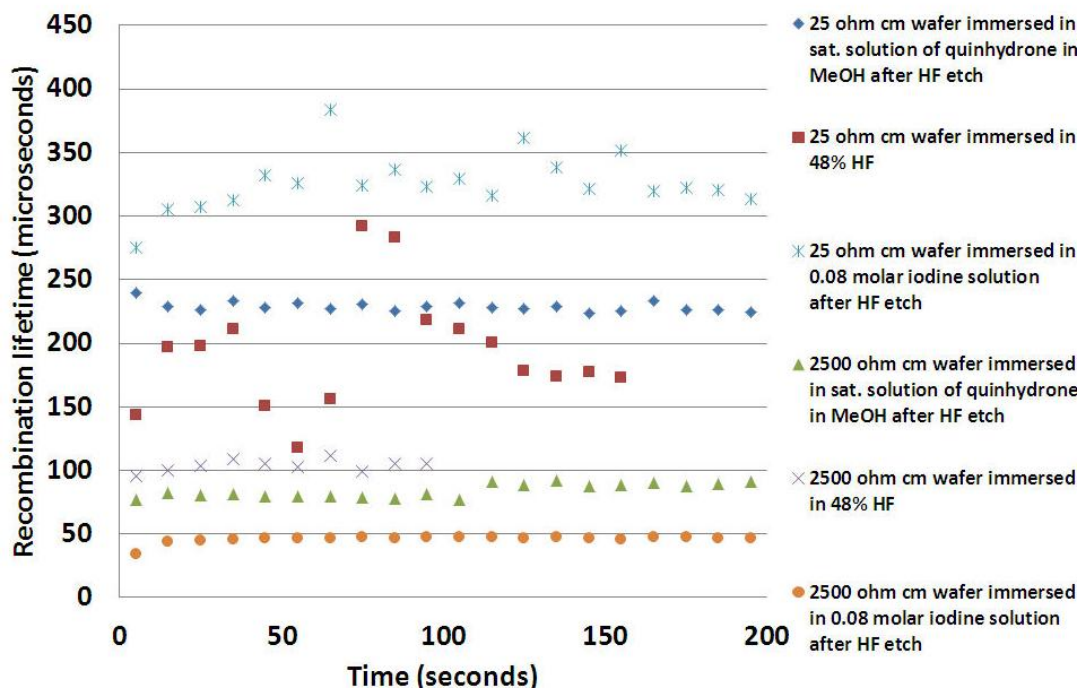


Fig. 4. 4 - Comparison of the different techniques to estimate the bulk lifetime for two different wafers

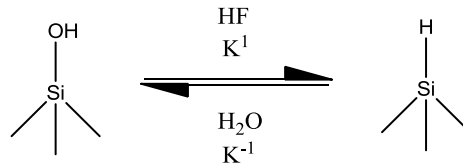
Although a large amount of the literature suggests using concentrated HF to measure the bulk lifetime of the samples^{51,113}, we have found that this method gives a very

variable value of recombination lifetime. A problem with using the iodine or quinhydrone method of passivation is that after the initial HF etch, oxide can re-grow whilst in solution.

For the higher ($2500 \Omega \text{ cm}^{-1}$) resistivity wafers, the bulk lifetime was found to be lower than that of the $25 \Omega \text{ cm}^{-1}$ wafer. However, the largest recombination lifetimes were achieved by immersing the wafers in either a 0.08 molar iodine solution or in 48% HF.

For the $25 \Omega \text{ cm}^{-1}$ wafer, the bulk lifetime was estimated to be around $325 \mu\text{s}$, whereas on the $2500 \Omega \text{ cm}^{-1}$ wafer the bulk lifetime was estimated to be around $100 \mu\text{s}$ through chemical passivation. However, both wafers had a guaranteed lifetime of over 1 ms showing that the chemical passivation methods did not show the true bulk lifetime. A likely reason for this is either due to surface oxide growth after the etching step^{114,115}, or trace amounts of contamination in the passivating solution which has been shown to have a large effect on the lifetime^{116,67}. Because of to this drawback, and the associated problems with immersion of wafers in concentrated (48%) HF, a new method of determining the bulk lifetime using kinetics was investigated.

At different immersion concentrations of HF, it was shown that the recombination lifetime stabilises at different values. It has been shown that the predominant cause of oxidation of the uppermost layer of the hydrogen-terminated surface was water¹¹⁴. Therefore the following equilibrium can be considered:



Scheme 4.0 - The equilibrium of surface oxide to hydrogen terminated surface in a HF / water mixture

The kinetics of the etching has been shown to be a second order reaction, which is affected by both the concentration of surface hydroxyl groups and hydrofluoric acid concentration¹¹⁷. The reverse oxidation reaction has been shown to be a first order reaction, depending only upon the concentration of hydrogen-terminated silicon⁶³.

The change in the hydrogen-terminated and oxidised silicon surface with time can be written as:

$$\frac{d[\text{Si} - \text{H}]}{dt} = k^1 \text{ T Si} - \text{OH} [\text{HF}]$$

$$\frac{d[\text{Si} - \text{OH}]}{dt} = k^{-1} \text{ T Si} - \text{H}$$

$$\text{At equilibrium} - \frac{d[\text{Si} - \text{H}]}{dt} = \frac{d[\text{Si} - \text{OH}]}{dt}$$

$$\text{Therefore } k^1 \text{ T Si} - \text{OH} [\text{HF}] = k^{-1} \text{ T Si} - \text{H}$$

$$\text{As } k_{\text{eq}} = \frac{k^1}{k^{-1}}$$

$$k_{\text{eq}} = \frac{\text{Si} - \text{H}}{\text{Si} - \text{OH} [\text{HF}]}$$

$$k^1 = 3.1428 \times 10^{-2} \text{ mol}^{-1} \text{ dm}^3 \text{ s}^{-1} \text{ }^{117}$$

$$k^{-1} = 2 \times 10^{-14} \text{ s}^{-1} \text{ }^{63}$$

$$\text{So } k_{\text{eq}} = 1.571 \times 10^{12} \text{ mol}^{-1} \text{ dm}^3$$

We also presume that [HF] does not change as the reaction rates are low and the amount of HF solution used is high.

$$As \frac{[Si - H]}{[Si - OH]} = k_{eq} HF$$

Therefore:

$$\frac{[Si - H]}{[Si - OH]} = 1.571 \times 10^{12} [HF]$$

This would show that as the concentration of HF changes, the ratio of Si-OH and Si-H also changes. A small change in surface oxide level will change the number of recombination centres, and thus will affect the recombination lifetime significantly.

By taking the inverse of the [Si-H] to [Si-OH], we can obtain the ratio of recombination centres to passivated area at each concentration of HF. By multiplication of this by the number of surface silicon atoms (7.83×10^{14} atoms cm^{-2} ¹⁸) the number of recombination centres per cm^2 can be calculated (Fig. 4.5).

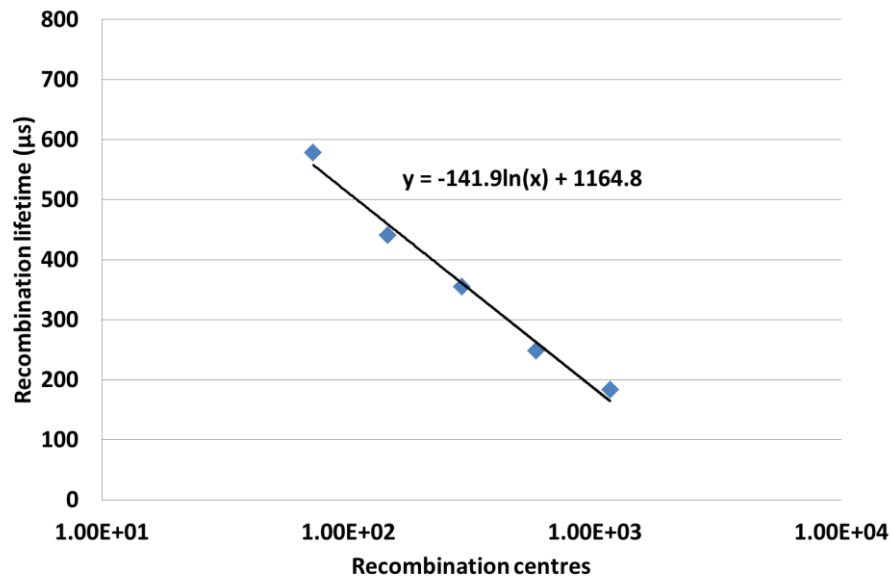


Fig. 4.5 - The recombination lifetime of the $25 \Omega \text{ cm}^{-1}$ at various concentrations (0.75-12%) of HF

By observing where the trendline crosses the 1 recombination centre point, the bulk lifetime can be estimated. In this case, the bulk lifetime was estimated to be 1165 μs , which fits in with the manufacturer's guarantee of over 1000 μs bulk lifetime.

Therefore we have developed a novel technique where the bulk lifetime of silicon can be reliably and accurately obtained without using high concentrations of HF.

4.4 Conclusions

The native oxide layer can be removed by etching in hydrofluoric acid. A 1.5 nm native oxide layer can be removed by a 15 second etch in a 2% HF solution. At longer etching times, the surface becomes roughened and pitted, reducing the recombination lifetime. The recombination lifetime of the hydrogen-terminated surfaces returns to the starting value after just one hour in air, although to achieve a similar oxide thickness (1.5 nm) takes considerably longer.

Both quinhydrone in methanol and iodine in ethanol have been shown to passivate silicon substrates successfully, allowing the bulk lifetimes of samples to be investigated. Neither of these have been shown to be a reliable method of passivation however, as the chemical passivation method that gave the highest lifetime depended upon the sample investigated. Not only was the lifetime achieved lower than the guaranteed bulk lifetime from the manufacturer, the method is also very sensitive to surface contamination requiring samples and solutions to be carefully prepared and stored.

By considering the equilibrium of hydrogen termination and re-oxidation of the surface by hydrofluoric acid in water, the number of recombination centres can be estimated and extrapolated to zero in order to estimate the bulk lifetime. The bulk lifetime was determined to be approximately 1165 μs by this method.

5. Organic Passivation of Silicon Substrates

This chapter has been published in part as:

N. Alderman, L. Danos, M. C. Grossel and T. Markvart, ‘Large surface photovoltages observed at methyl-terminated silicon surfaces synthesised through a two-step chlorination-alkylation method, *RSC Advances*, 2012, **2**, 7669-7672. (doi:10.1039/C2RA20465G)

5.1 Introduction

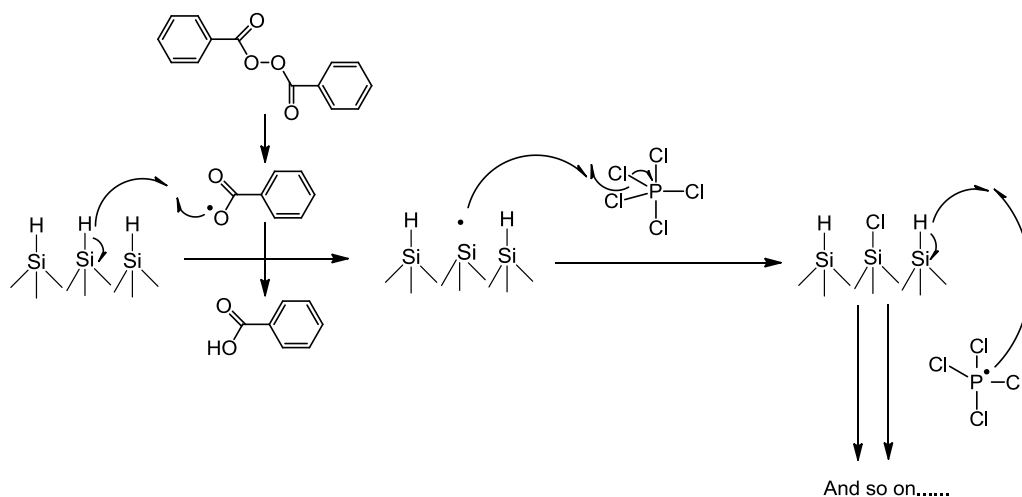
Surface properties of semiconductors are becoming increasingly important due to the reduced size of micro-electronics and the search for ever more efficient devices such as solar cells. Current generations of solar cells use high temperature (>500°C) passivation techniques, such as the growth of a thermal oxide layer¹¹⁹ or plasma-enhanced chemical vapour deposition (PECVD) of silicon nitride layers^{27,49,72}. Alkylation of silicon surfaces can lead to excellent passivation properties as well as being a lower-temperature technique than current passivation methods^{45,52}. A lower-temperature passivation method is advantageous because of the lower impact on the bulk silicon properties with the possibility of reduced costs^{120,121}.

Alkyl monolayers synthesised in this chapter also have the advantage of providing a suitable test-bed for other technologies, such as dye sensitisation. Facile alteration of the alkyl linker chain length allows the silicon-dye distance dependency to be investigated.

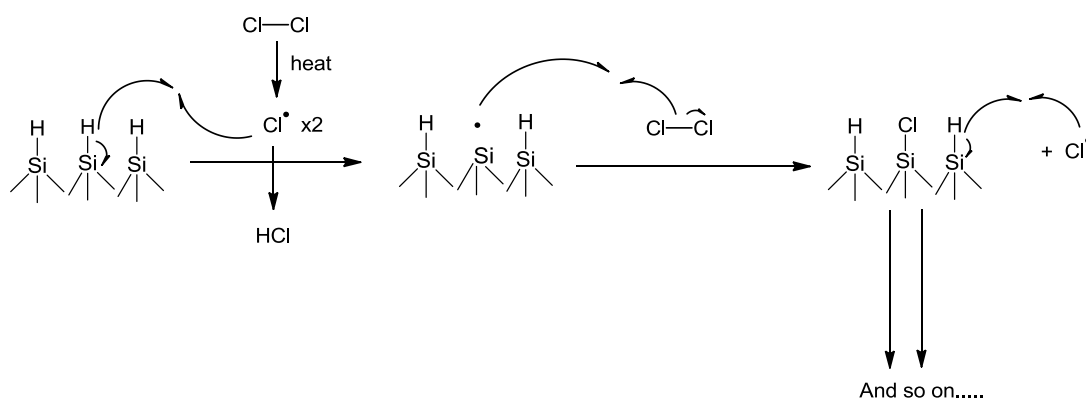
Organic modification of semiconductor surfaces would therefore be an attractive solution for reducing electron-hole recombination in these devices as well as providing a test-bed for further functionalisation. Recently a large amount of research has examined the possibility of secondary functionalisation of alkylated silicon surfaces. It is therefore of importance that we understand the electronic properties and the mechanism of passivation of these surfaces in detail.

In this study, we have chosen to use a two-step chlorination-alkylation technique developed by Lewis *et al.*¹²², which report a large increase in the recombination lifetime. As well as affording excellent passivation, this technique is also the only alkylation technique that has been reported to produce a methyl-terminated surface. Firstly, a hydrogen-terminated surface is produced through the etching of a silicon sample in ammonium fluoride.

Once a hydrogen-terminated surface has been produced, chlorination can be achieved by one of two literature methods; through a wet chemistry route involving phosphorus pentachloride in chlorobenzene and a gas-chlorination method involving chlorine gas in nitrogen. Both methods involve radical generation, which can remove a hydrogen atom from the silicon surface. This generates another radical on the silicon surface, which can then react further generating the chlorine-terminated surface (Scheme 5.0 and 5.1).

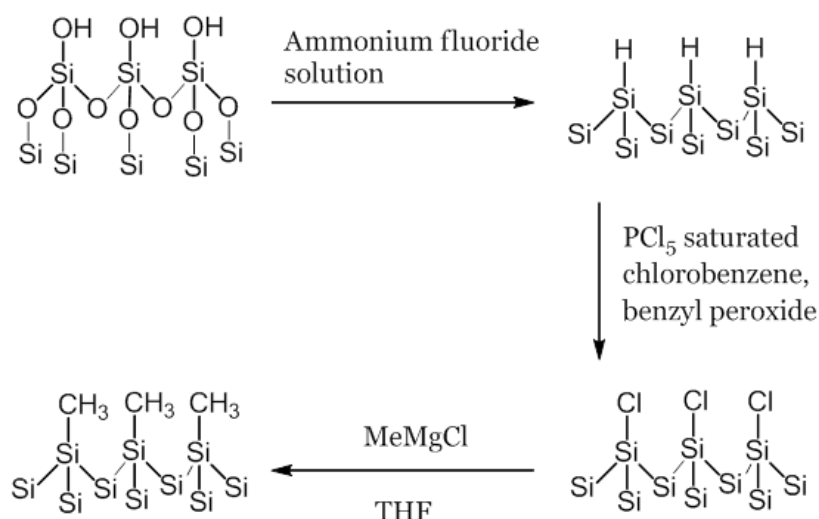


Scheme 5.0 - The wet-chemistry mechanism of surface chlorination



Scheme 5.1 - The chlorine gas mechanism of surface chlorination

The chlorine-terminated surfaces can then be alkylated through a reaction with a Grignard reagent. By using a Grignard reagent, different alkyl groups can be attached to the silicon surface affording greater flexibility than other silicon surface alkylation techniques (Scheme 5.2).



Scheme 5. 2 - Reaction scheme for the alkylation of silicon surfaces

5.2 Characterisation of Samples

5.2.1 Chlorine-terminated Surfaces

Chlorine-terminated surfaces were attempted by two literature methods; either (i) through the use of chlorine gas⁸⁷ or (ii) via a wet-chemistry route involving phosphorus pentachloride⁷⁰. The phosphorus pentachloride in chlorobenzene technique was preferred because of the greater literature knowledge of this process and the ease of transfer to the Grignard solution after chlorination. However both techniques were explored and X-ray photoelectron spectroscopy (XPS) was used to characterise the samples prepared.

The wet-chemistry chlorination method showed a clear peak in the XPS chlorine-binding region, confirming that the reaction had indeed been successful (Fig. 5.0). A small oxide peak was present in the silicon energy region, showing that partial oxidation of the silicon surface had also occurred during the chlorination reaction. A possible cause of the oxidation could be due to low concentrations of moisture in the solvent, although all of the solvents used were anhydrous.

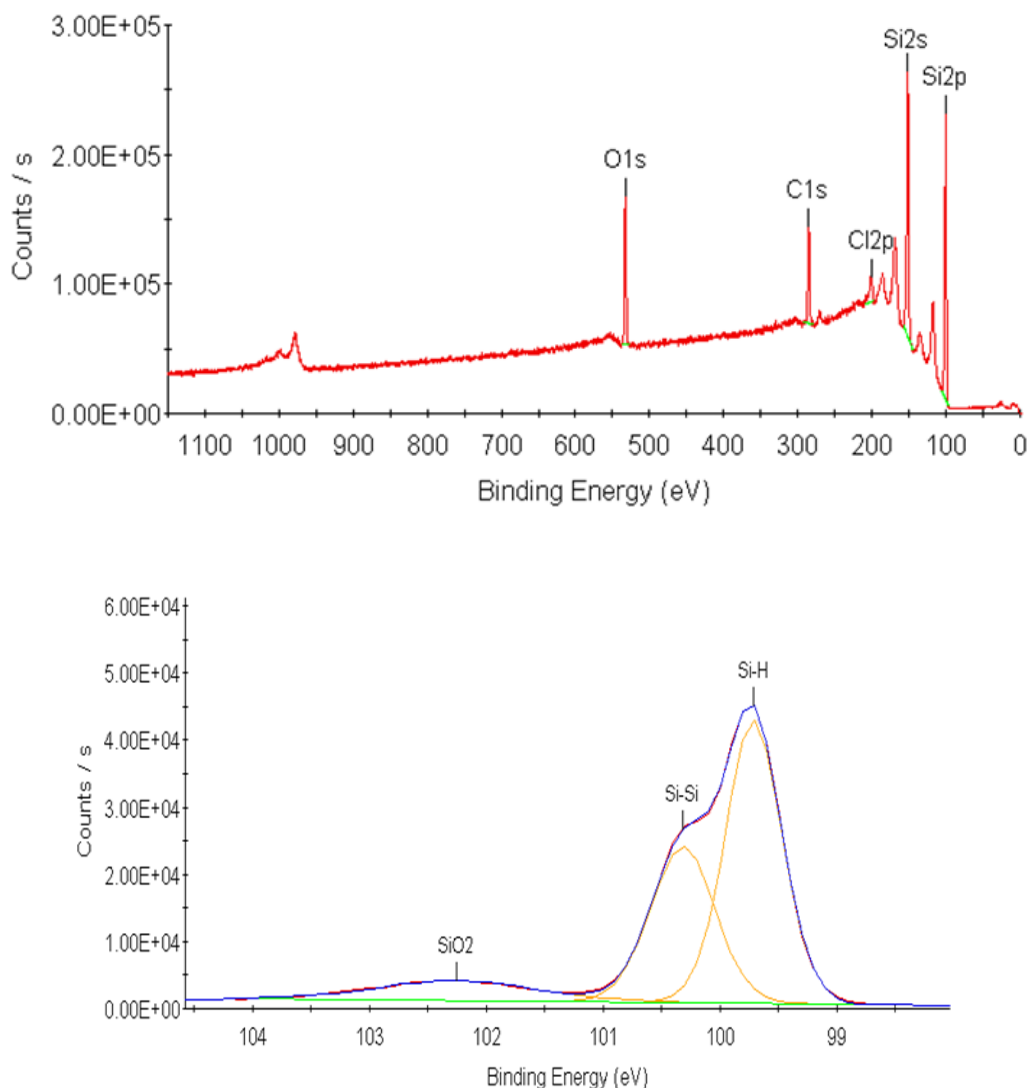


Fig. 5.0 - XPS spectra showing the overview (top) with a chlorine peak and the presence of silicon oxide in the silicon binding energy region (bottom) for surfaces produced by the wet-chemistry method

The chlorination of hydrogen-terminated surfaces with chlorine gas showed a marked reduction in silicon oxide formation (Fig. 5.1) when compared with the wet-chemistry technique (Fig. 5.0). A likely reason for this observation is because this is a solvent-free method, thereby reducing the trace oxygen and water levels in the reactor when compared to the wet-chemistry route. This is consistent with literature findings that the phosphorus pentachloride in chlorobenzene technique leads to a slight oxidation of the surface¹²³. Although it was found that a higher level of surface

oxide was present after chlorination, the wet-chemistry method was chosen as the preferable route. Literature findings suggest that this method has greater compatibility with the subsequent chemistry steps, with a shorter transfer time between the chlorination and alkylation steps, as well as achieving high lifetimes for alkylated surfaces⁷⁰. Through careful control of the conditions the oxide growth during the wet-chemistry chlorination route can also be reduced.

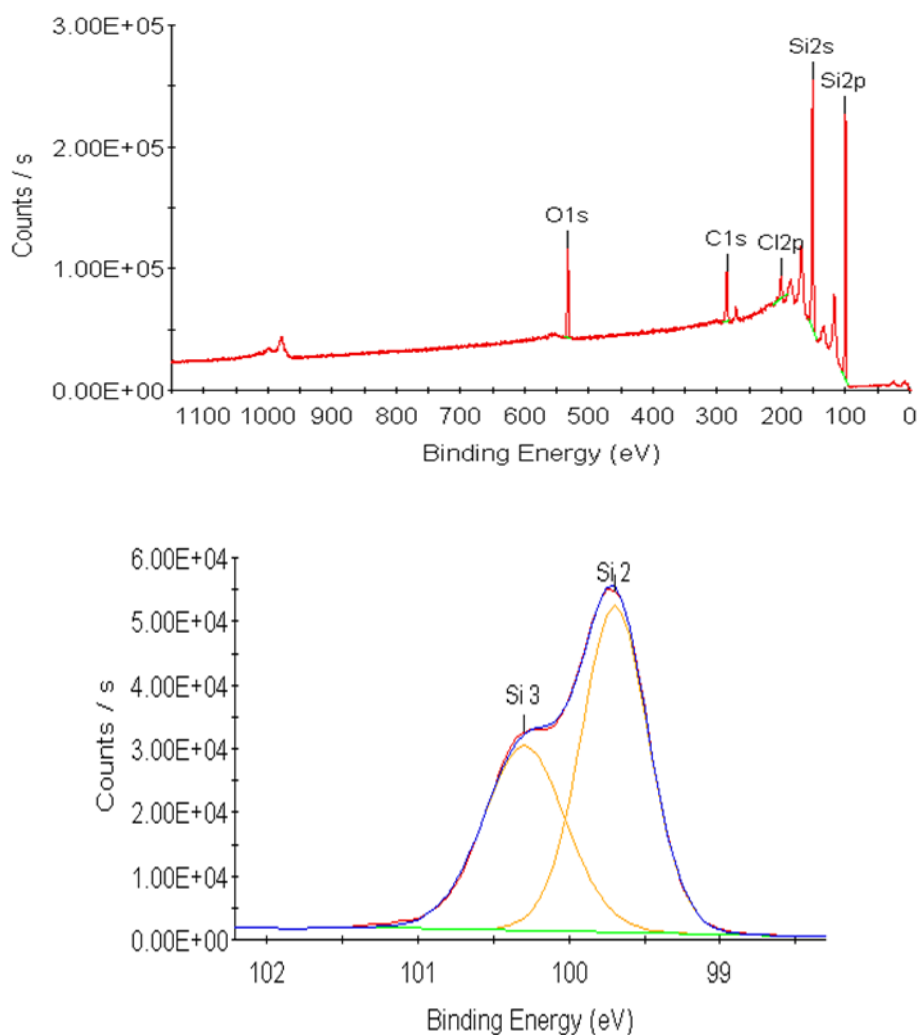


Fig. 5.1 - XPS spectra showing the chlorine peak in the overview spectrum (top) and the reduction of the silicon oxide peak in the silicon binding energy region (bottom) for samples produced by the chlorine gas method.

5.2.2 Alkylated Surfaces

After chlorination of the surfaces had been confirmed using XPS, alkylation of the surfaces was attempted using various Grignard reagents. The alkylated surfaces were firstly characterised using infrared spectroscopy (Fig. 5.2).

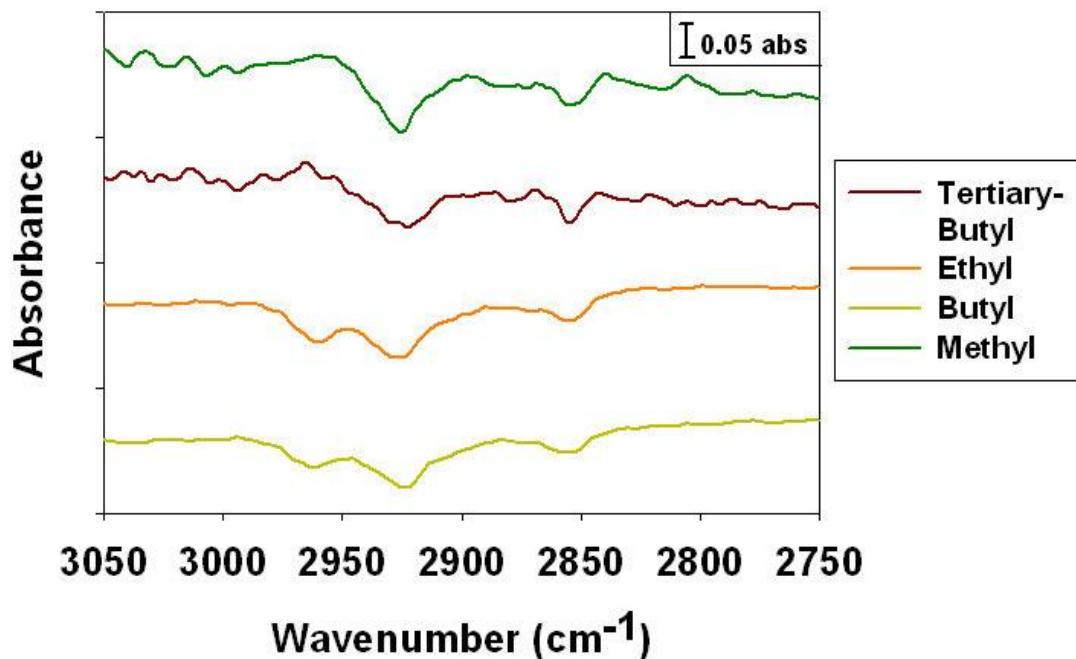


Fig. 5. 2 - Infrared spectrum of the C-H stretching region for Methyl, Ethyl, Butyl and Tertiary-Butyl terminated surfaces

The methyl- and tertiary butyl-terminated surfaces show two peaks at 2978.2 and 2889.3 cm⁻¹, corresponding to a symmetric and an asymmetric C-H stretch of a CH₃ unit respectively.

The ethyl- and butyl-terminated surfaces show three peaks at around 2960, 2925 and 2855 cm⁻¹, which correspond to a symmetric and asymmetric stretch of C-H from a CH₃ unit, and an asymmetric stretch from a CH₂ unit. A good correlation was observed with literature values^{122,124}.

The degree of surface coverage can be calculated by XPS, however the spectra must be compared with those from a reference sample (in this case the methyl terminated

sample)²⁹. This is because the X-ray interaction volume is different for different surfaces, as different heights from the detector to surface are used to achieve a maximum signal, and different surface roughness's leading to different surface areas. The carbon binding energy peak was chosen as this is the only single peak observed in the XPS spectrum that shows the C-Si bond. In the silicon binding energy, a peak for Si-C is not observed due to the similar binding energy of the lattice silicon and the silicon-carbon. Therefore the integral of the C-Si peak, which appears at a binding energy of around 284 eV²⁹, was used for coverage calculations. For ease of comparison between samples, the integral of the carbon-silicon peak was divided by the silicon integral to normalise the data.

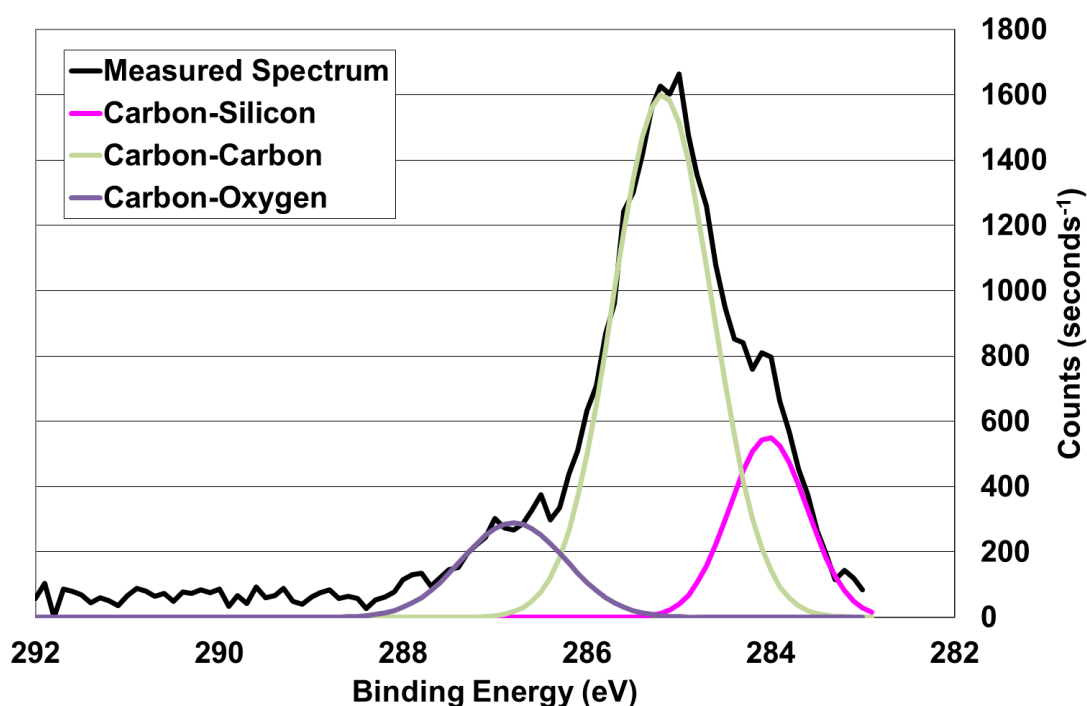


Fig. 5. 3 - XPS spectrum of the carbon 1s binding energy region for a butyl terminated surface showing peaks for carbon bonded to silicon, carbon and oxygen

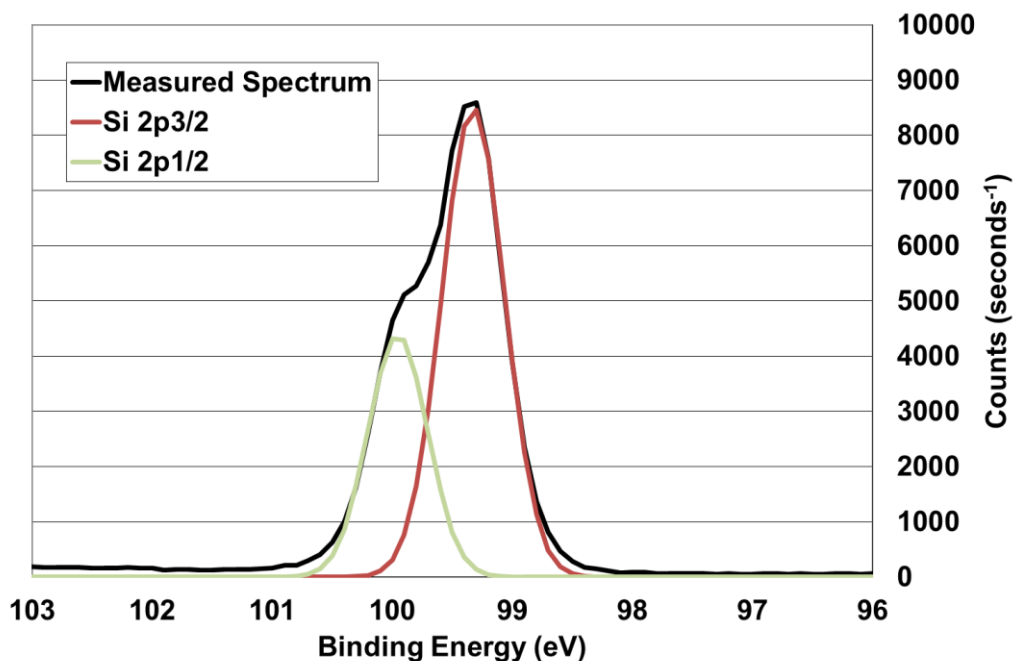


Fig. 5. 4 - XPS spectrum of the silicon binding energy region for a butyl terminated surface showing peaks for the Si 2p_{3/2} and 2p_{1/2}

By deconvoluting the XPS spectra and integrating the peaks for the carbon 1s (Fig. 5.3) and silicon 2p (Fig. 5.4) binding energy regions, the coverage of the different surfaces can be calculated. In the silicon 2p binding energy region, the binding energy difference between the silicon bonded to hydrogen and silicon bonded to carbon are too small to observe⁴⁷. The lattice silicon atoms have a similar binding energy, so that only 2 peaks are observed for silicon. These are assigned as Si 2p_{3/2} and Si 2p_{1/2}, in the expected 2:1 ratio. Interestingly, no peak for Si-O was observed (around 102-103 eV), indicating that relatively low levels of surface oxidation had occurred during the reaction.

	Integral of Si peaks	Integral of C-Si peak	Ratio of C-Si / Si	Fraction of CH ₃ coverage
Methyl	6343.0	812.7	0.1263	1
Ethyl	9019.1	637.8	0.0707	0.56
Butyl	8297.7	582.6	0.702	0.56
Iso-propyl	10071.1	492.4	0.0489	0.39
Tertiary-butyl	6200.0	350.2	0.0565	0.45

Table 5. 0 - The integrals of the Si peaks and C-Si peak as measured by XPS with implied surface coverage as compared to a methyl terminated surface

The integrals of the silicon and carbon-silicon peaks are shown in Table 5.0, along with the implied surface coverage as compared to a methyl-terminated surface. From the ratios of C-Si / Si, it can be seen that the methyl-terminated surface has the highest coverage. As the methyl group is the smallest alkyl chain, tight surface packing is observed. Straight-chain alkyl groups have the second highest coverage, with just over 50% of that of the methyl surface. The lower coverage is likely to arise as a result of the longer carbon chain, folding to some extent and restricting access to the surface for further groups to attach. Finally the lowest coverage is seen for the bulkier groups such as iso-propyl and tertiary-butyl. These groups sterically hinder the attachment of further alkyl groups, reducing the surface coverage to around 40% of that of the methyl group.

Contact angle measurements were performed on the surfaces to measure the effect of changing the surface functionality on the hydrophilicity / hydrophobicity of the surface. The contact angles for each surface are shown in Table 5.1, whilst the images for each surface are shown in Fig. 5.5.

	Contact Angle (°)
Native	<10
Ammonium Fluoride etched	101.9 ± 1.1
Chlorine	83.8 ± 4.9
Methyl	93.5 ± 4.2
Ethyl	86.7 ± 2.3
Butyl	73.7 ± 1.2
Iso-propyl	64.1 ± 1.3
Tertiary-butyl	54.1 ± 2.9

Table 5. 1 - The contact angles of the various functionalised surfaces

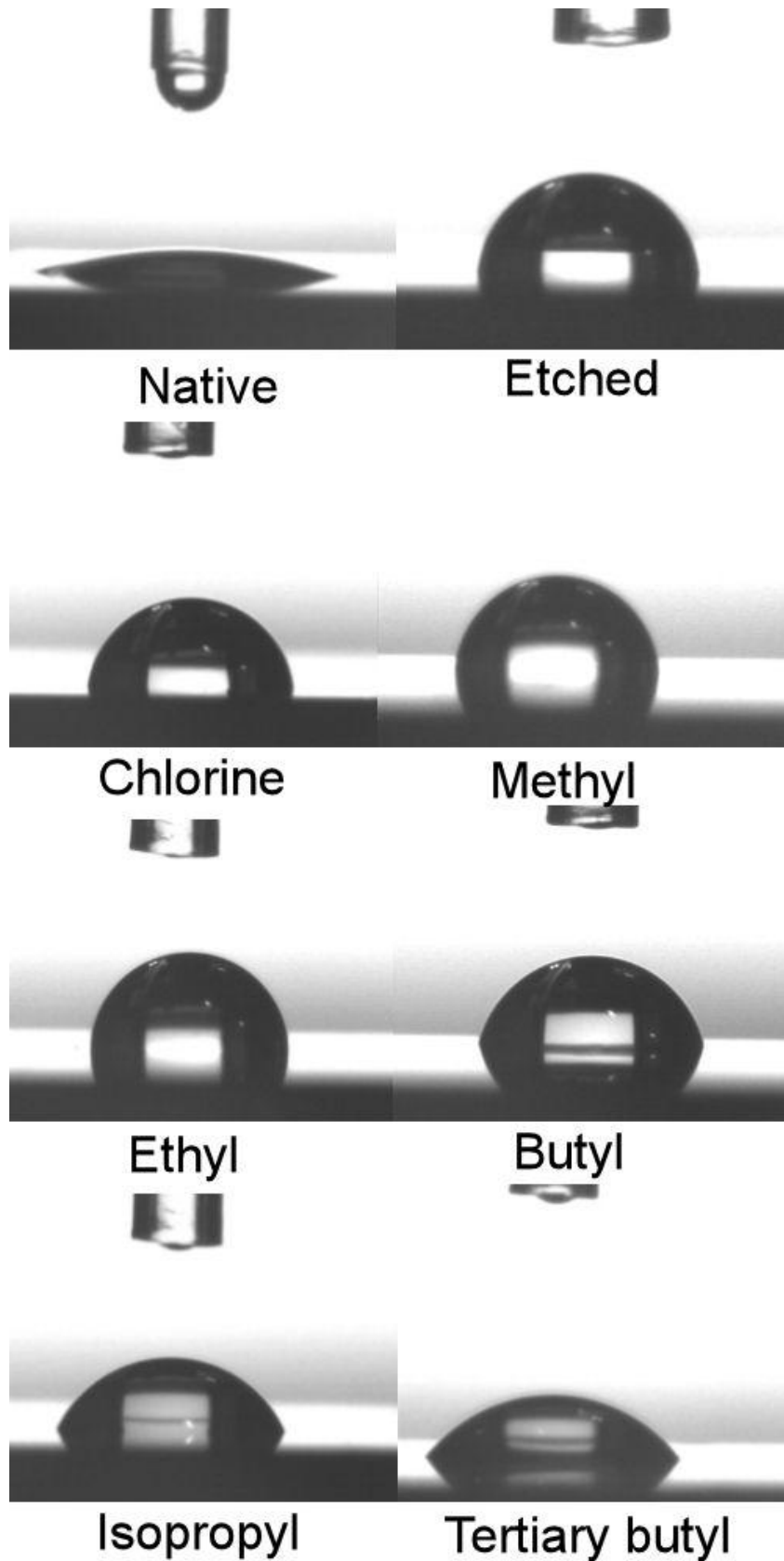


Fig. 5. 5 - The contact angle of water at each step of the reaction and for the various alkylated surfaces

The contact angles of native oxide samples were below 10° , signifying a high degree of hydrogen bonding between the water molecules and the oxide. Once the native oxide layer had been removed by etching in ammonium fluoride, an increase in contact angle was observed to around 102° .

Upon alkylation, the contact angle followed a similar trend to the surface coverage. The methyl-terminated surfaces show the highest contact angle, followed by the straight-chained alkyl groups, with the bulkier iso-propyl and tertiary-butyl surfaces giving the lowest contact angles. This corresponds to a higher degree of hydrogen bonding to the surface, possibly due to a larger degree of surface oxidation arising from lower surface coverage⁸⁴.

The surface roughness of the alkylated samples was investigated by Atomic Force Microscopy (AFM) and the result is shown in Fig. 5.6.

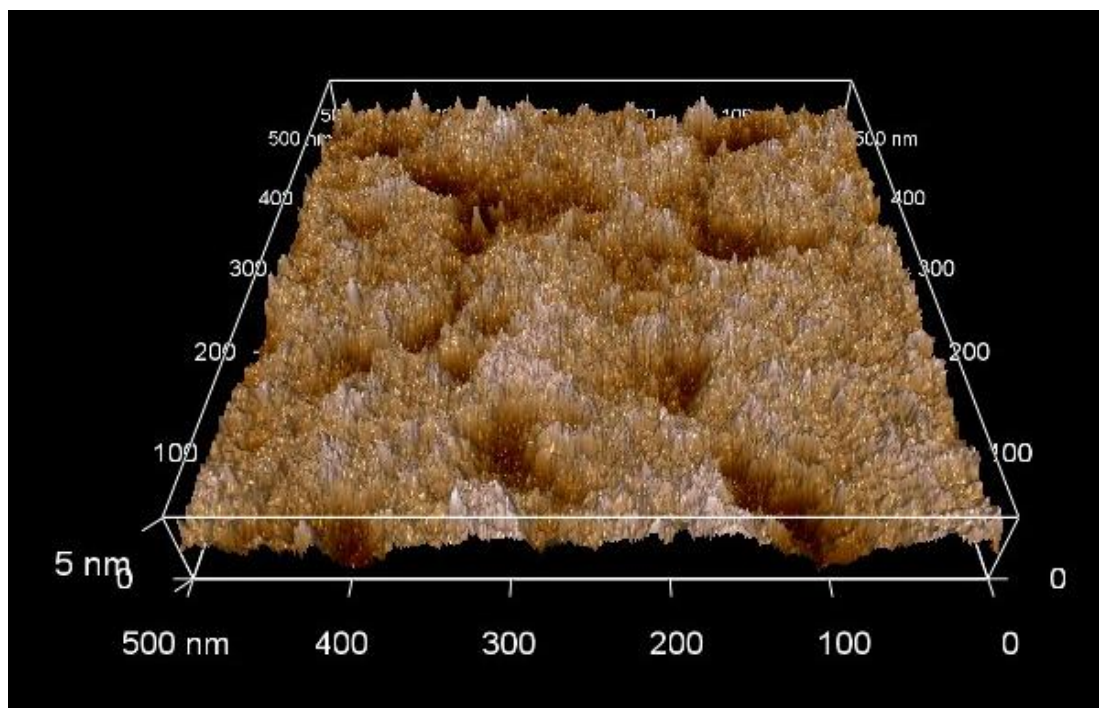


Fig. 5. 6 - Atomic force micrograph of a methyl-terminated surface

From the atomic force micrograph, it can be seen that the maximum difference between the lowest point and the highest point is around 3 nm, with large areas of almost atomically flat surface. Large indents are visible in the surface however, possibly introduced by the etching and cleaning steps.

5.3 Recombination Lifetime Studies

The minority-carrier recombination lifetimes were then measured by the Sinton lifetime tester. Minority-carrier recombination lifetimes measured on both hydrogen and chlorine-terminated surfaces were extremely low ($<10 \mu\text{s}$), consistent with the findings of other literature examples^{45,84}. This implies a surface recombination velocity of $>2700 \text{ cm s}^{-1}$, presuming that the majority of the recombination occurs at the surface. For comparison, the recombination lifetime of the native oxide wafer was $4.5 \mu\text{s}$ (6083 cm s^{-1}), indicating that the etching step has only a marginal effect on the recombination lifetime.

Upon alkylation of the samples, a substantial increase was observed in the charge-carrier recombination lifetime. Interestingly it was found that the highest lifetimes were achieved when the silicon samples were cleaned exclusively in piranha solution (1:3 hydrogen peroxide to sulphuric acid). If the samples were cleaned in solutions which should remove a greater proportion of surface metallic impurities such as the RCA-1¹²⁵ and RCA-2¹²⁶ technique, a lower lifetime was observed. Table 5.2 shows the recombination lifetime and surface recombination velocities obtained with the methyl, butyl and tertiary butyl functionalised surfaces showing the smallest surface recombination velocities.

	Recombination lifetime (μs)	Surface recombination velocity (cm s^{-1})
H-terminated	< 10	> 2700
Chlorine	< 10	> 2700
Methyl	200 \pm 30	110 \pm 24
Ethyl	100 \pm 30	247 \pm 118
Butyl	250 \pm 30	82 \pm 15.5
Iso-propyl	125 \pm 30	192 \pm 70
Tertiary-butyl	250 \pm 30	82 \pm 15.5

Table 5. 2 - Recombination lifetime and surface recombination velocities for the various steps of the alkylation process and for different alkyl-terminated surfaces

The recombination lifetimes of the alkylated samples should follow a similar trend to the surface coverage; that is that a high surface coverage should reduce the amount of surface states leading to an increase in the minority-carrier lifetime.

Other literature examples of the surface alkylation of silicon suggest that the lowest surface recombination velocity should be feasible with the methyl group, reflecting the lower steric bulk which allows higher surface coverage^{29,127}. This has not been observed in our work, probably as a result of the decomposition of the Grignard reagent, as even a two week storage of the reagent has been shown to dramatically decrease the surface coverage decreasing the recombination lifetime significantly⁶⁹. The recombination lifetime stability of the alkylated silicon samples during storage in air was then measured (Fig. 5.7).

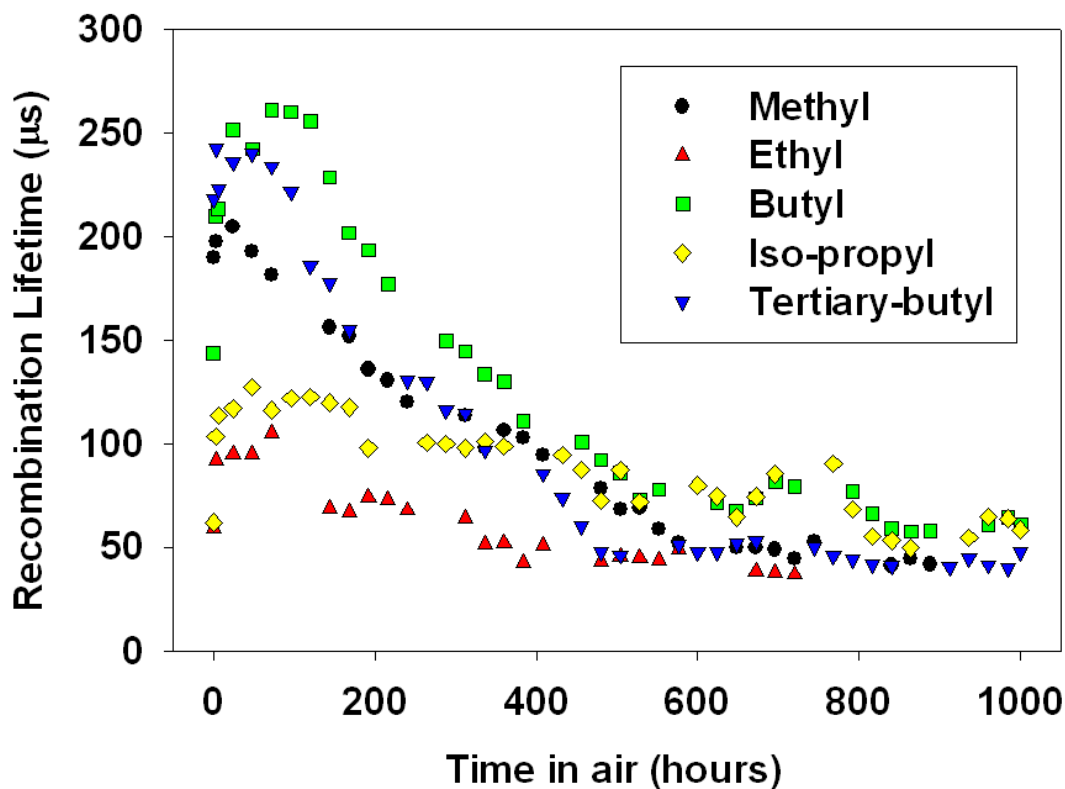


Fig. 5. 7 - The change in recombination lifetime of the alkylated samples during storage in air at ambient humidity and temperature

The recombination lifetimes of the alkylated samples decrease with storage time in air, stabilising at a value of around 50 μs after 600 hours in air. After further storage in air, the recombination lifetime values continue to decay with time, reaching a value of between 10 and 15 μs 500 days later. The decay in recombination lifetime can be attributed to the growth of oxide on the surface, decreasing the lifetime towards that of the starting native oxide samples. To enable facile comparison between synthesised and literature samples, the recombination lifetime was converted to surface recombination velocity (SRV) (Fig. 5.8).

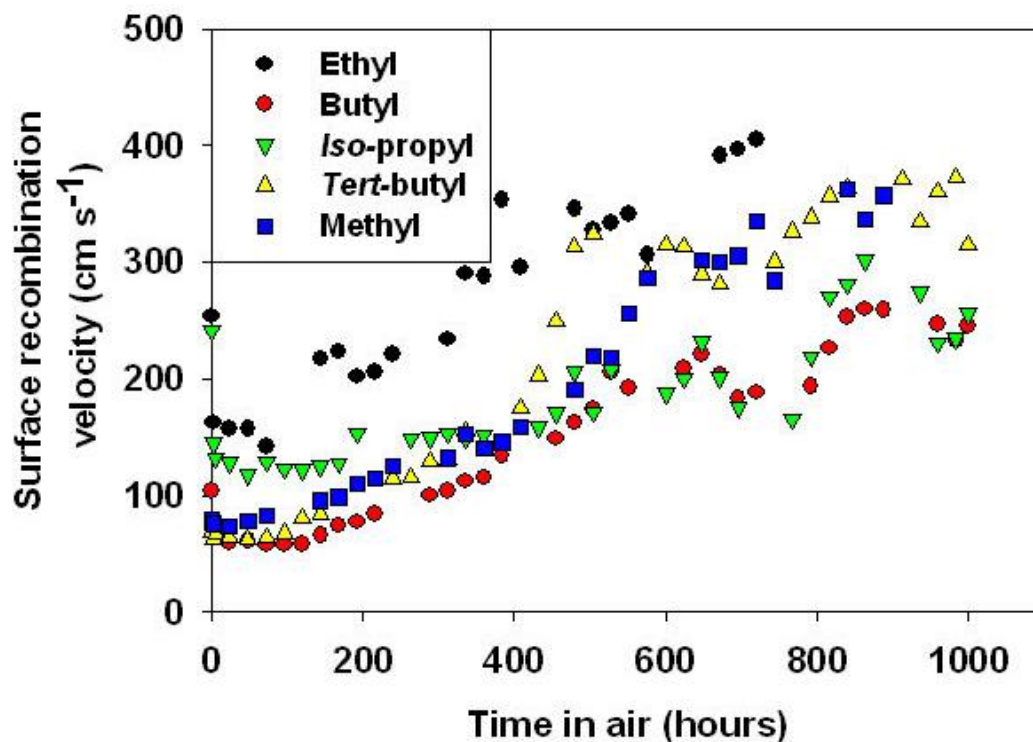


Fig. 5. 8 - The surface recombination velocity of alkylated samples stored in air

It can be seen that the surface recombination velocity remains under 400 cm s^{-1} , even after 1000 hours in air. The native oxide samples had a surface recombination velocity of $>2700 \text{ cm s}^{-1}$, showing that the alkyl layer retains some passivation even after extended periods of time in air. The increase in surface recombination velocity was also attributed to the growth of oxide on the surface, and was monitored by ellipsometry (Fig. 5.9).

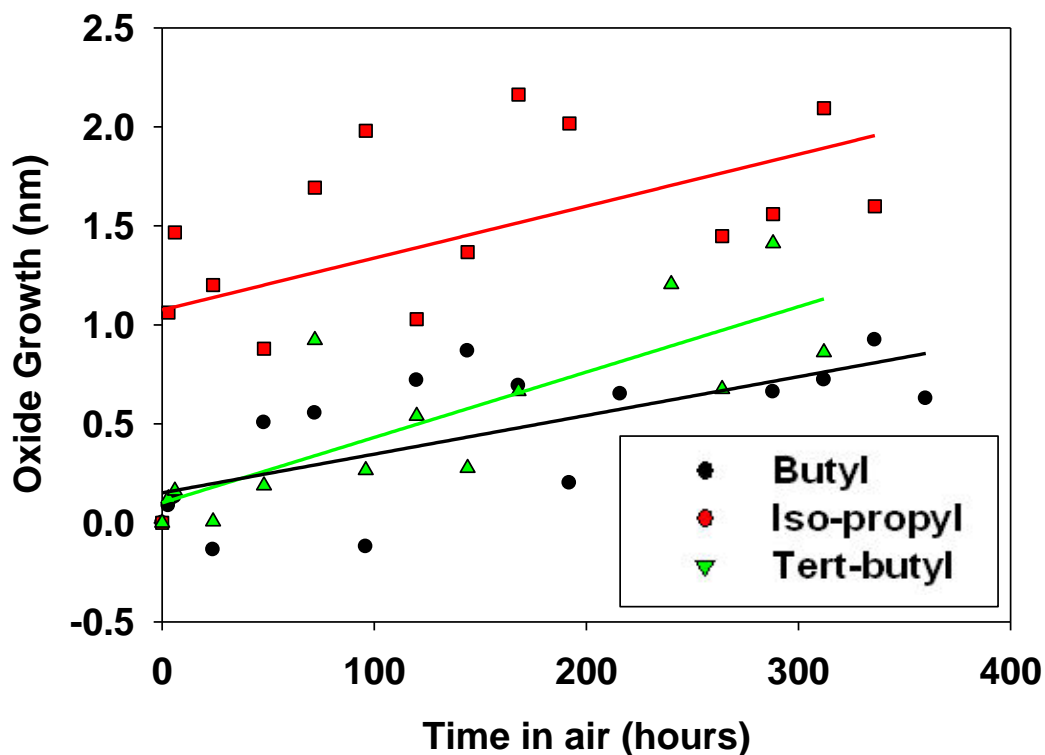


Fig. 5. 9 - Ellipsometry oxide thickness measured on various alkyl-terminated surfaces

As can be seen in the ellipsometry oxide thickness values, the straight chain butyl group affords the lowest oxide growth over 350 hours. The tertiary-butyl group gives the second lowest value of oxide growth, followed by the iso-propyl-terminated surface. By comparing the oxide growth to the XPS surface coverage, it is seen that they both follow a similar trend; the lower the surface coverage, the faster the oxide layer grows. Therefore to have the highest lifetime and the greatest resistance to oxidation, straight-chained alkyl groups should be used.

5.4 Electronic Characterisation of Samples

Kelvin Probe (SPV) measurements were recorded at each stage of the processing. Table 5.3 shows the results obtained from the SPV and recombination lifetime measurements at each stage of the alkyl group attachment to the silicon surfaces.

	Surface photovoltage (mV)	Recombination lifetime (μ s)
Native	141.7	4.5
Hydrogen	64.3	<10
Chlorine	<10	<10
Methyl	448.3	142
Ethyl	390.0	83
Butyl	339.9	63
Allyl	372.9	73
Iso-propyl	359.9	65
Tertiary-butyl	240.9	38

Table 5.3 - The surface photovoltage and recombination lifetimes of various functionalised surfaces

A decrease in the SPV signal was observed when moving from the native oxide samples to the hydrogen-terminated surface. This shows flattening of the electronic bands as a result of a reduction in surface states. The effective recombination lifetime, however, remains low.

Moving from the hydrogenated to the chlorinated surface, the SPV was diminished indicating a flat band state. A likely cause of this observation is the higher electronegativity of the chlorine atom when compared to that of silicon which allows charge neutralisation of the surface and a reduction in band bending. Once again, the effective lifetime remained low, indicating that the surface photovoltage measured is not directly correlated with the lifetime measured – therefore in these samples we

have both flat bands because of the electronegativity of chlorine atom removing surface charge, and the presence of surface states allowing recombination to occur.

Upon alkylation of the surface with a Grignard reagent, a substantial increase in the SPV to between 240-450 mV was observed. This is indicative of larger band bending than that present in the native oxide samples, showing a surface which is highly charged. Interestingly the effective recombination lifetime increases with the increase in SPV, probably due to the decrease in majority carrier concentration at the surface.

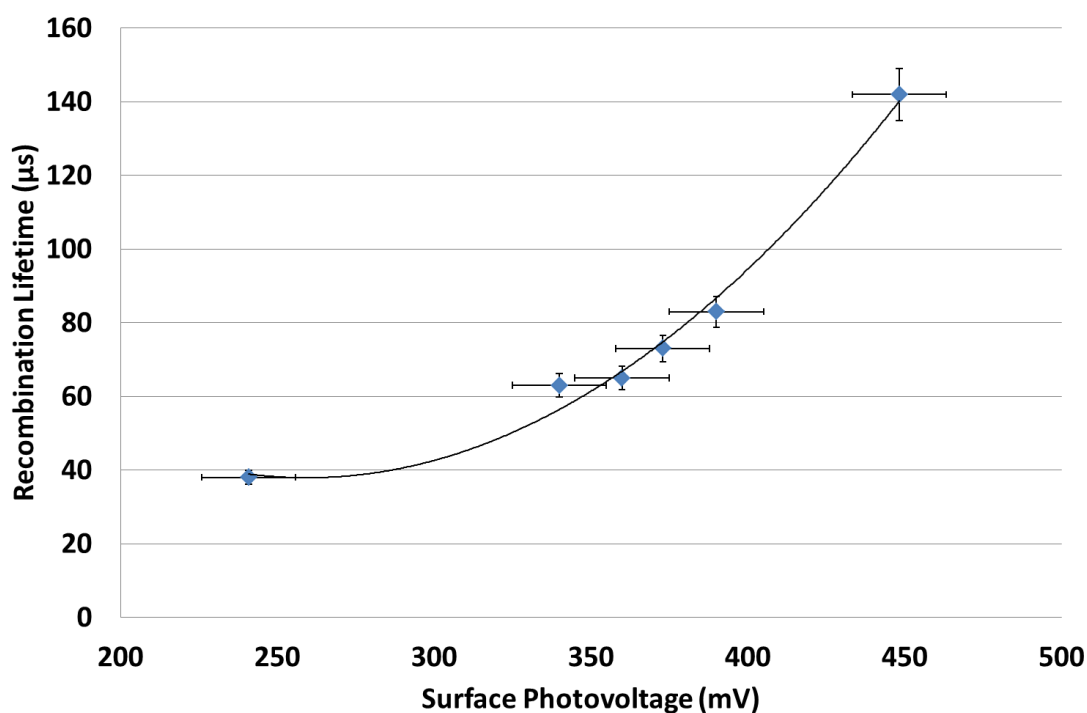


Fig. 5.10 - The surface photovoltage (SPV) of the different alkyl-terminated surfaces with the corresponding recombination lifetimes

The change in recombination lifetime with surface photovoltage is shown in Fig. 5.10. A similar trend is seen to that observed by Goossens *et al.*¹²⁸. As the surface photovoltage is increased, the recombination lifetime increases and can be fitted with a second order polynomial. The recombination lifetime initially increases slowly

with SPV, with a lifetime increase of around 20 μs when increasing the SPV from 250 mV to 350 mV. After a further increase from 350 mV to 450 mV, the recombination lifetime is significantly increased by approximately 80 μs . At even larger values of the SPV, the lifetime is expected to reach a maximum as observed by Goossens *et al.*¹²⁸ due to the depletion of majority carriers at the surface. A fully majority-carrier depleted surface will occur when the band bending is above the value the electron Fermi-level for the sample (810 mV in the present case).

Once more the SPV follows a similar trend to the XPS coverage data and recombination lifetime; that straight chain alkyl groups have a larger SPV (with the highest SPV being recorded for the methyl terminated surface), whilst a reduced value is observed for the bulkier, more sterically hindered groups.

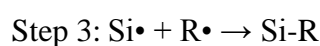
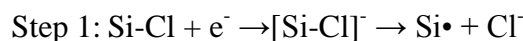
A high SPV and lifetime was observed on multiple samples. It was widely believed that samples with a high lifetime would be in an almost flat-band state when organically passivated – the surface states that promote recombination would not be present after passivation and no surface charge would be detected¹²⁹.

From this data, it appears that the amount of band-bending is the important factor when producing high-quality passivation layers. It appears that removal of the surface states through the covalent attachment of molecules on its own does not directly result in passivation, as the flat-band state of the low lifetime chlorine-terminated surfaces suggests. As the coverage of the alkyl groups will never reach 100% (and for bulky groups such as tertiary-butyl will be much lower), a complete removal of the surface states will not be observed, giving a greater backing to the theory that the majority of the passivation will occur due to band-bending. As even a

20 parts per trillion defect density can affect the recombination lifetime³⁹, the majority of the passivating effect is likely to be occurring due to band-bending.

The SPV remained high on the alkylated samples even after multiple washes in methanol / acetic acid, confirming that the band bending observed was not caused by adsorbed magnesium salts or any other ions present on the surface.

To further confirm that the observed increase in SPV was not due to the presence of magnesium in the surface depletion layer, a chlorinated surface was heated to the reaction temperature in a solution of magnesium chloride in tetrahydrofuran. Kelvin probe measurements on these samples still showed a low SPV of around 10 mV, combined with a low recombination lifetime (<10 μ s). Therefore evidence suggests that the increase in SPV is not due to the inclusion of charged magnesium salts on the surface. The observed large SPV signal is likely to be the result of the charging of the silicon surface during step 1 of the reaction scheme shown in Scheme 5.3²⁹.



Scheme 5.3 - The reaction scheme for the alkylation step of the reaction

During this step the negative charge could be incorporated into slow traps, which would give a high SPV for extended periods of time. Therefore the surface could become more charged than native oxide samples, increasing the band-bending observed and therefore the SPV obtained. This is a key difference in the alkylation reaction of the chlorinated surfaces with Grignard reagents, and could explain why the increase in SPV is not reported for organic monolayers on silicon synthesised by

differing routes. Repeating the measurements on samples that were stored in air for two weeks still showed a very high SPV (within 5% of SPV values from freshly made samples) (Fig 5.11).

An initial rise is observed in the surface photovoltage over the first 100 hours in air, due to the reaction of the remaining non-alkylated silicon sites with oxygen. This is the likely reason for the increase in recombination lifetime that is reported in other literature findings²⁹.

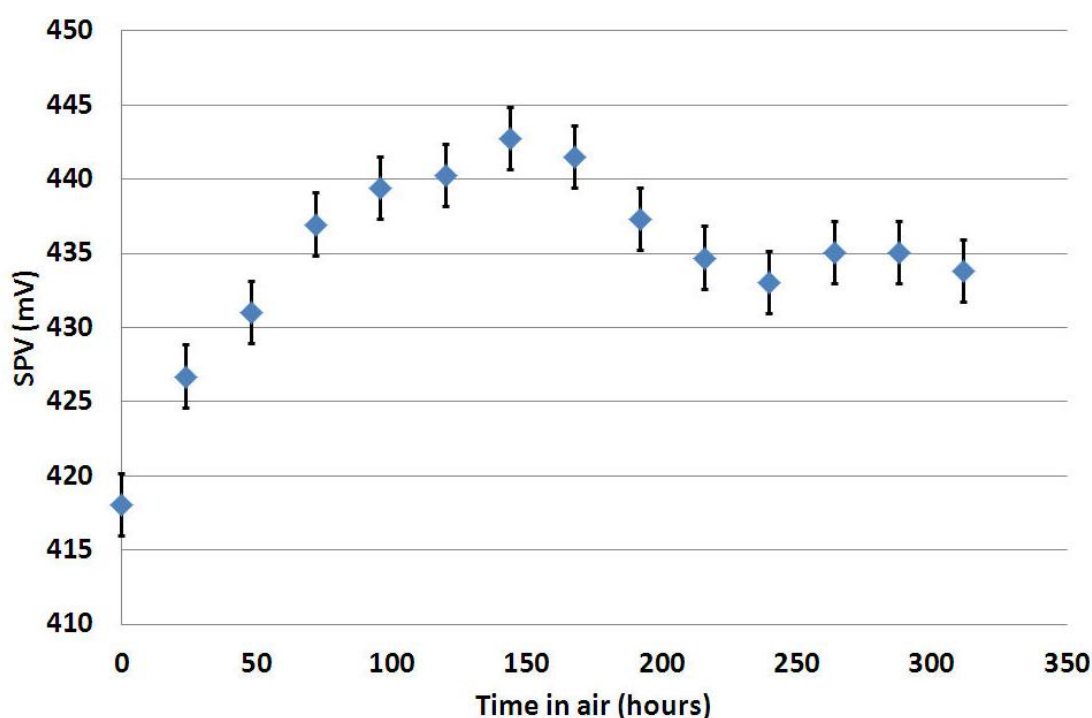


Fig. 5. 11 - The surface photovoltage of a methyl-terminated surface during storage in air

Interestingly, samples produced by the two-step chlorination-alkylation technique show excellent passivation properties when compared to other organic monolayers produced on silicon (for example, when we produced a methoxy-terminated surface by reaction of a chlorine-terminated surface with methanol, we obtained a lifetime of less than $10\mu\text{s}$ with an SPV of 10-20 mV). A likely explanation for this observation is that the band bending induced by the two-step chlorination-alkylation technique

reduces the concentration of the majority carriers (electrons) at the surface (Fig. 5.12), whilst little band-bending is observed with other alkylation techniques.

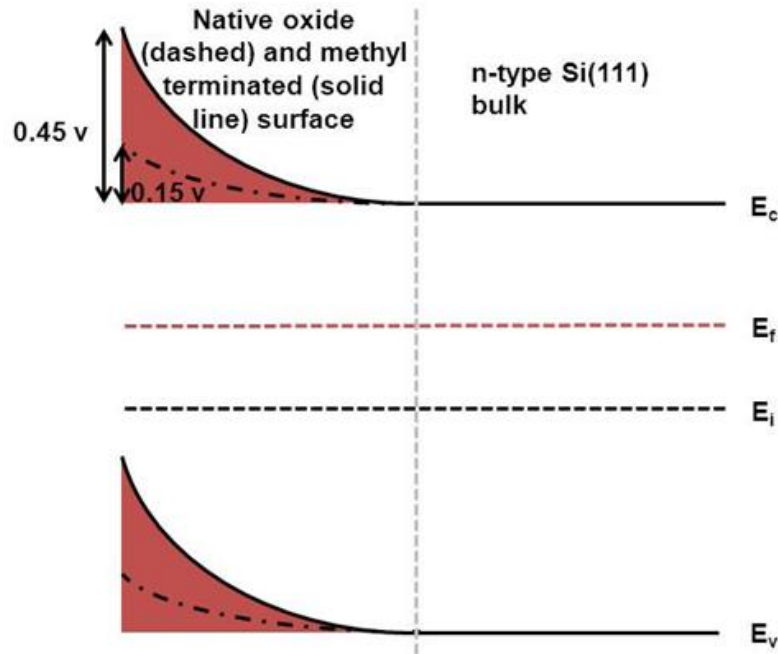


Fig. 5. 12 - The surface bands as measured by Kelvin probe for both the native oxide and methyl terminated surface

The passivation observed on the samples is different from the conventional picture which is that well passivated samples are in a flat band state due to the removal of surface states^{129,130}. In the samples produced by the two-step chlorination-alkylation method, however, both charging of the surface and removal of the surface states can combine to produce a sample with high effective recombination lifetimes. A likely explanation for this is that surface states are removed by the formation of silicon-carbon bonds, as well as fixed charge trapping which does not change with the Fermi-level. This results in band bending which repels majority carriers, increasing the recombination lifetime.

5.5 Conclusions

Two routes to chlorine-terminated surfaces have been investigated, a wet chemistry and a chlorine gas-based technique. Both methods produced a chlorine-terminated surface as shown by XPS, although the gas-based technique showed low surface oxide growth.

Alkyl-terminated silicon surfaces can be routinely and reproducibly synthesised through a two-step chlorination-alkylation method. This leads to the attachment of an alkyl monolayer on the surface possessing a high minority recombination lifetime and great stability in ambient conditions, retaining passivation effects for time periods of greater than 1000 hours. Straight-chain alkyl groups showed a higher surface coverage, with higher lifetimes and oxygen resistance than bulkier alkyl-terminated surfaces.

Samples were characterised using X-ray photoelectron spectroscopy and infra-red spectroscopy. These measurements confirmed the successful methylation of the surface, with C-H stretching bands visible in the infra-red spectrum and carbon-silicon binding energies visible in the XPS spectra.

Surface photovoltage measurements of the alkyl-terminated surfaces showed a substantial value along with an increase in the effective recombination lifetime. This can be attributed to an increase in surface band-bending, lowering the surface electron concentration and reducing recombination. The unusually large band bending observed is attributed to the accumulation of trapped charges during the alkylation procedure.

6. Determination of the Surface Recombination Velocity by Kelvin Probe

6.1 Introduction

The Kelvin probe has been shown to be a very powerful and versatile tool, allowing the extraction of data such as diffusion length^{131,132,133}, surface photovoltage^{134,135,101} and impurity concentrations^{132,133,136}. This chapter investigates the extraction of the surface recombination velocity (and by assuming a bulk lifetime, the recombination lifetime) from the I-V type dependence of the sample.

By using an X-Y stage, the recombination lifetime can be imaged for entire wafers, instead of obtaining an average value of lifetime similar to that obtained from the Sinton WCT-120 lifetime tool. The tip-size used in the experiments was 2 mm in diameter, but tips down to 50 μm area available if higher resolution is required. This is useful in determining where further improvements in the surface passivation can be obtained, by observing problem areas in the passivation layer. The Kelvin probe is a very surface-sensitive technique, allowing for accurate, fast and facile monitoring of the surface passivation layers¹³⁴.

6.2 Development of Theory

The surface band structure for an n-type silicon surface is shown below:

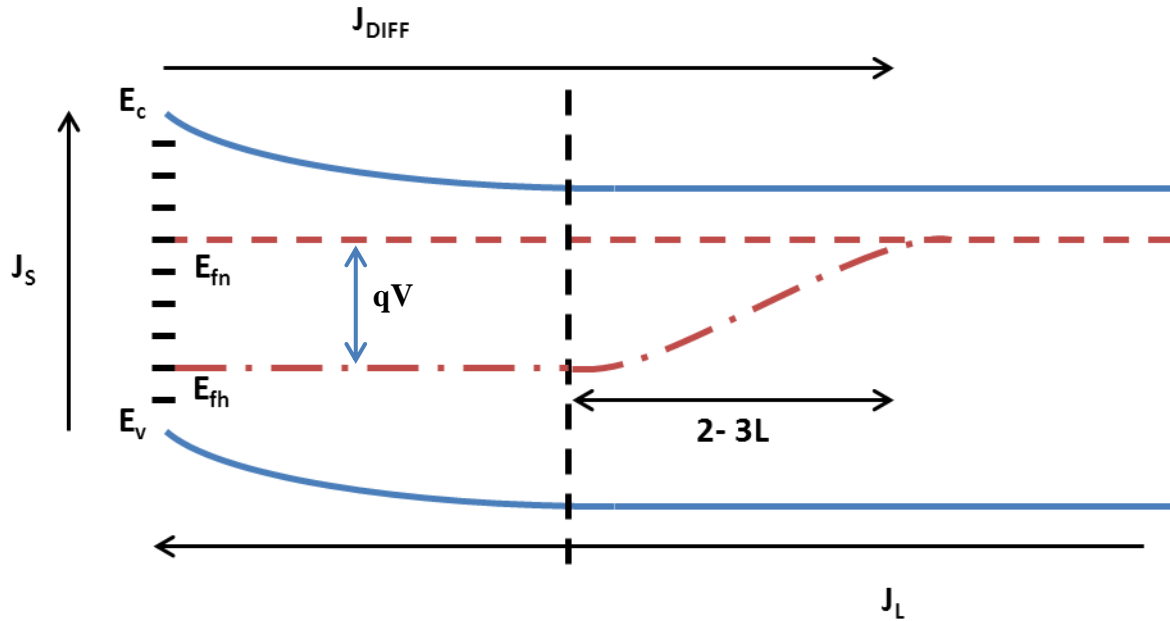


Fig. 6.0 - The surface band structure for n-type silicon showing the quasi-fermi-levels for electrons and holes (not to scale)

Where J_L is the photogenerated current, J_S is the surface recombination current, J_{DIFF} is the diffusion current of minority carriers away from the surface, qV is the internal voltage, L is the diffusion length and E_{fn} and E_{fh} are the electron and hole quasi-fermi-levels. Outside of the diffusion region, the minority carrier concentration returns to that of the bulk after 2-3 diffusion lengths.

Electron-hole pairs are generated in the bulk, where they diffuse towards the surface giving rise to the photogenerated current, denoted by J_L . If the diffusion length is sufficiently high (longer than the semiconductor thickness, as in this case – see below), it is safe to assume that all generated minority carriers will reach the surface and J_L will be given by the equation previously discussed in Chapter 3:

$$J_L = q\phi_0(1 - R) \quad (\text{eqn 3.19})$$

where R is the surface reflectivity⁵⁶. The net surface recombination current is given by a difference between the recombination rate and the (thermal) generation rate.

Assuming that the latter remains the same as in equilibrium we can write:

$$J_s = k_{eqs}(p_s n_s - p_0 n_0) \quad (\text{eqn 6.0})$$

where k_{eqs} is the equilibrium constant, p_s and n_s are the concentration of holes and electrons near the surface under illumination, and p_0 and n_0 are the concentration of holes and electrons in equilibrium. By the using the mass action law, we can simplify this expression to:

$$J_s = k_{eqs}(p_s n_s - n_i^2) \quad (\text{eqn 6.1})$$

where n_i is the intrinsic electron concentration. The electron and hole concentration under illumination can be calculated from the Fermi-level positions of the electrons and holes (as shown in Chapter 3). It has previously been shown (equation 3.3) that:

$$pn = n_i^2 e^{\frac{E_{fn} - E_{fp}}{k_B T}} \quad (\text{eqn 3.3})$$

By combining equations 6.1 and 3.3 and replacing $E_{fn} - E_{fp}$ by qV , we obtain the expression.

$$J_s = k_{eqs} n_i^2 (e^{qV/k_B T} - 1) \quad (\text{eqn 6.2})$$

By denoting $K_{eq} n_i^2$ by J_{0s} , we can write equation 6.2 in the form:

$$J_s = J_{0s} (e^{qV/K_B T} - 1) \quad (\text{eqn 6.3})$$

From equation 3.14, we observed that:

$$J_s = J_l - J_0 (e^{qV/K_B T} - 1) \quad (\text{equation 3.14})$$

By combining equations 6.3, 3.14 and 3.18, we can write:

$$(J_{0S} + J_0)(e^{qV/K_B T} - 1) = \phi_0(1 - R) \quad (\text{eqn 6.4})$$

To show the practical significance of this result we need to express J_{0S} in terms of more usual quantities. To this end, a comparison of equation 6.0 with the definition of the surface recombination velocity (equation 3.21 in Chapter 3) at low injections (n_0 remains constant) gives:

$$qS = k_{eqs}n_0 \quad (\text{eqn 6.5})$$

Using the definition of J_{0S} , we now obtain:

$$J_{0S} = k_{eqs}n_i^2 = qSp_0 \quad (\text{eqn 6.6})$$

linking equation 6.4 directly with the surface recombination velocity. To proceed further we need to determine the dark saturation current J_0 , given by equation 3.15 in Chapter 3:

$$J_0 = qp_0\left(\frac{D}{\tau}\right)^{0.5} \quad (\text{eqn 3.15})$$

Using the value of the hole diffusion constant $12.1 \text{ cm}^2 \text{ s}^{-1}$ and the minimum value of τ of $1000 \text{ } \mu\text{s}$ guaranteed by the manufacturer we find an upper bound on J_0 of $4.71 \times 10^{-14} \text{ A cm}^{-2}$.

This result shows that the dark saturation current is much smaller than J_{0S} , indicating that recombination is dominating by the surface. A similar calculation can also be used to determine the diffusion length from equation 3.30 in Chapter 3, giving a minority carrier diffusion length of $1100 \text{ } \mu\text{m}$, twice as large as the wafer thickness

(550 μm). Therefore we can assume that any minority carriers generated in the bulk reach the surface, and it is safe to set the collection efficiency equal to unity.

Neglecting J_0 in equation 6.4 we thus obtain that the surface recombination velocity can be determined by measuring the surface photovoltage at various values of photogenerated current (by changing the photon flux). It is important to note that as the intensity of photons changes, one would expect that the location of the Fermi-levels in the density of states may also change, as has been previously reported.

6.3 Calibration of Photon Source

The photon flux was calculated using a silicon diode, where we assumed that it has similar absorption and reflection properties as the silicon wafers used in the experiments. For our experiments, the photon flux can be change by changing the slit width on the monochromator, allowing more or less light into the optical fibre. The photon flux at the sample origin position is shown as a factor of slit width in Fig. 6.1.

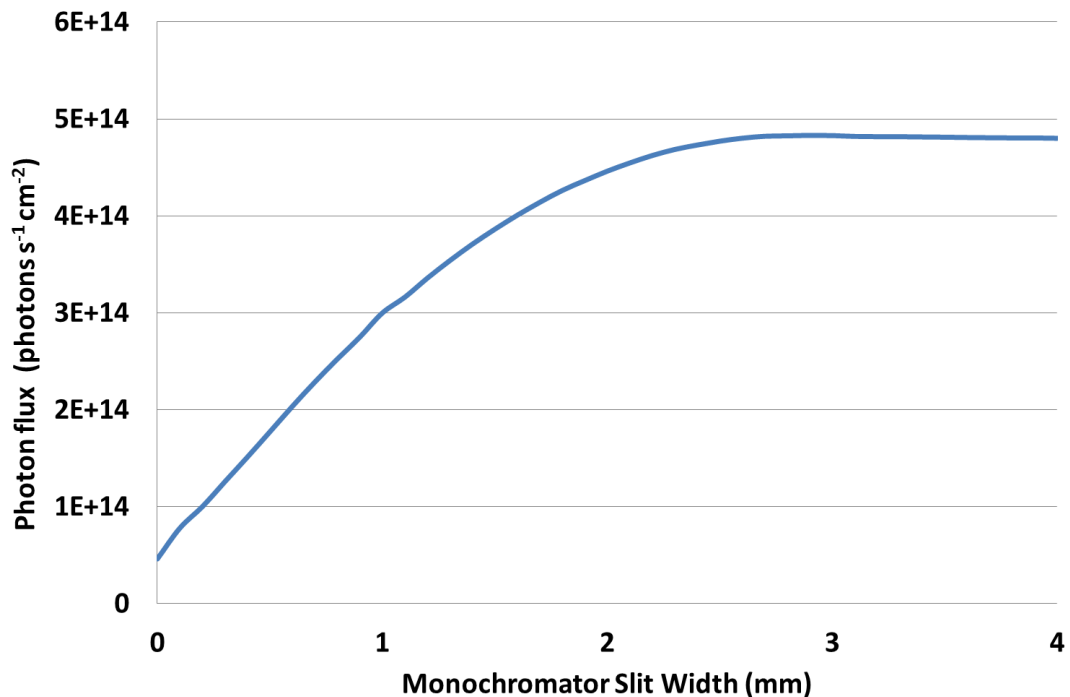


Fig. 6. 1 - The change in photon flux with monochromator slit width

It can be seen that the photon flux does not increase beyond a monochromator slit width of around 2.5 mm, limiting the maximum photon flux achievable. The photon flux does not reach zero at a slit width of 0 mm due to incomplete sealing of the monochromator slit. However, when necessary, this small flux can be eliminated by closing the monochromator shutter.

6.4 Surface Recombination Velocity Measurements

Measurements of the surface recombination velocity require a good back surface contact between the sample and stage. Following literature recommendations⁵⁶ we have found that repeatable method for obtaining a good contact was to apply a silver paste, to the rear surface following a heavy scratching of the rear of the sample to remove the back monolayer and any oxide present.

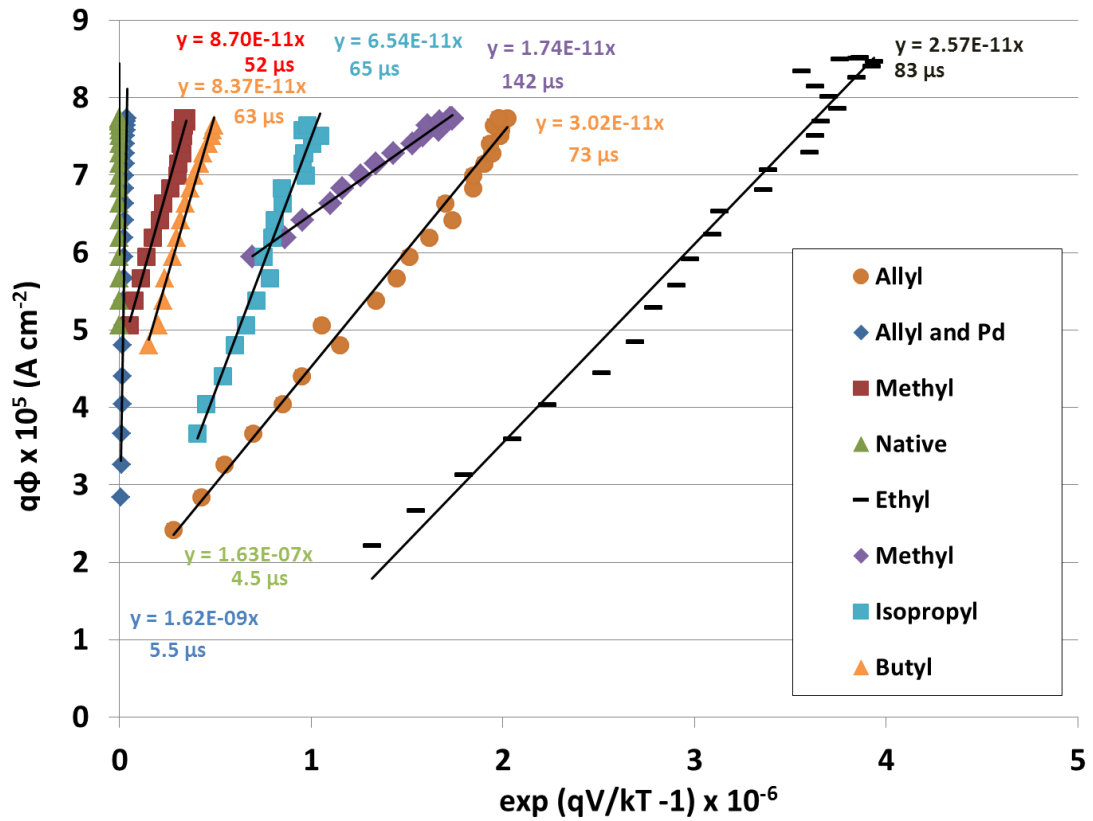


Fig. 6. 2 - The change in $\exp(qV/KT-1)$ for various functionalised surfaces, with the gradient of the linear trend and the recombination lifetime (measured by Sinton WCT-120)

Fig. 6.2 shows the results of measurements of the surface recombination velocity by the Kelvin probe and can be compared to those acquired from the Sinton (Table 6.0).

Sample	Sinton		Kelvin Probe		
	Measured Lifetime (μs)	Implied S (cm s^{-1})	J_{0S} Measured (A cm^{-2})	S Measured (cm s^{-1})	Lifetime Implied (μs)
Native	4.5	Very High (1E5 to 1E7)	5.47E-07	5.83E6	23
Methyl	142	185	1.74E-11	162	185
Methyl	52	501	8.62E-11	918	52
Ethyl	83	316	2.57E-11	239	133
Butyl	63	417	8.37E-11	776	53
Isopropyl	65	404	6.45E-11	601	67
Allyl	73	359	3.31E-11	308	108
Allyl / Pd	5.5	Very High (1E5 to 1E7)	1.96E-09	1.83E5	23

Table 6.0 - Comparison of recombination lifetime and surface recombination velocity for samples characterised by the Kelvin probe and Sinton WCT-120

A good fit is observed between the recombination lifetime values calculated from the Kelvin probe data and the Sinton lifetime tester, with higher lifetimes measured by the Sinton leading to a higher calculated value by the Kelvin probe. The difference between the two is likely to be due the Sinton giving an average lifetime value, which takes into account the full sample area. The Kelvin probe method looks at a smaller area, around 1 mm^2 (the size of the tip). Therefore this is more sensitive to small changes in the passivation layer, which can affect the recombination lifetime. This is useful as it allows us to map the lifetime changes over the sample area by moving the X-Y stage.

To make sure that the technique was correctly monitoring the surface recombination velocity, the allyl terminated surface was characterised by this method. Without removing the sample from the sample stage, the surface was contaminated by palladium which has been shown to reduce the recombination lifetime. The value of J_{0S} , and thus the value of recombination lifetime, decreased immediately. Both the value from the Kelvin probe data and Sinton WCT-120 were almost identical at around $6 \text{ }\mu\text{s}$, confirming that the difference in J_{0S} was due to the different sample lifetimes.

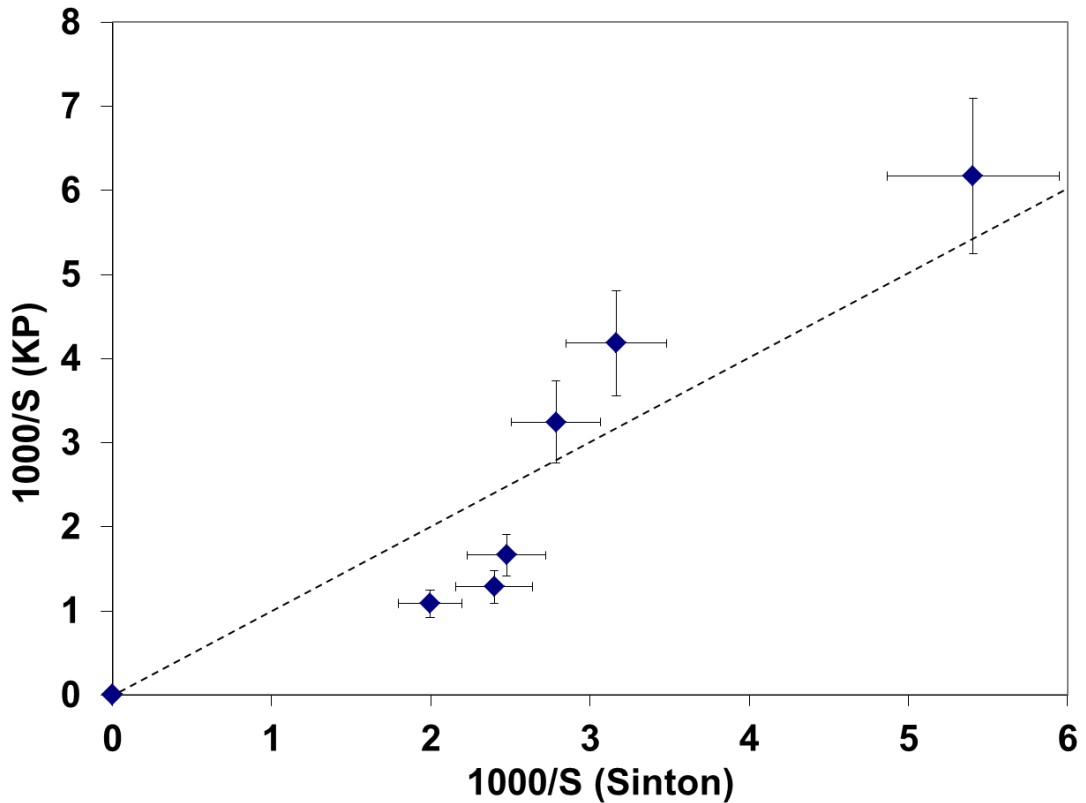


Fig. 6.3 - The surface recombination velocity as measured by the Kelvin probe against the surface recombination velocity as measured by the Sinton WCT-120

In Fig. 6.3, the correlation between the surface recombination velocity as measured by the Kelvin probe and Sinton WCT-120 method is shown. A linear trend would correspond to equal values obtained by the two measurement techniques and is marked with a dashed line. It is seen that the results for surface recombination velocity are similar, within experimental errors which are discussed below.

The Sinton WCT-120 measures the average lifetime over the sample, such that low-lifetime areas such as the edges (due to saw-damage) are included in the measured lifetime.

For the Kelvin probe technique, the data is obtained in the surface-probe tip interaction area, which is around 1 mm^2 . Therefore this is less sensitive to the low-lifetime areas, resulting in the difference in SRV between the two techniques.

6.5 2D Surface Lifetime Mapping

The new technique for measuring recombination lifetime could be used to map sample lifetime over a large area such as a complete wafer. This mapping technique can be easily automated by using two points on the linear part of the graph (at photon fluxes of 3.86×10^{14} and 4.77×10^{14} photons $\text{s}^{-1} \text{cm}^{-1}$), with the gradient calculated between these values. This was repeated for 784 points on the sample, giving the change in surface recombination velocity (and therefore recombination lifetime) over the whole sample. The surface recombination velocity map of the high-lifetime methyl sample from Fig. 6.2 is shown in Fig. 6.4.

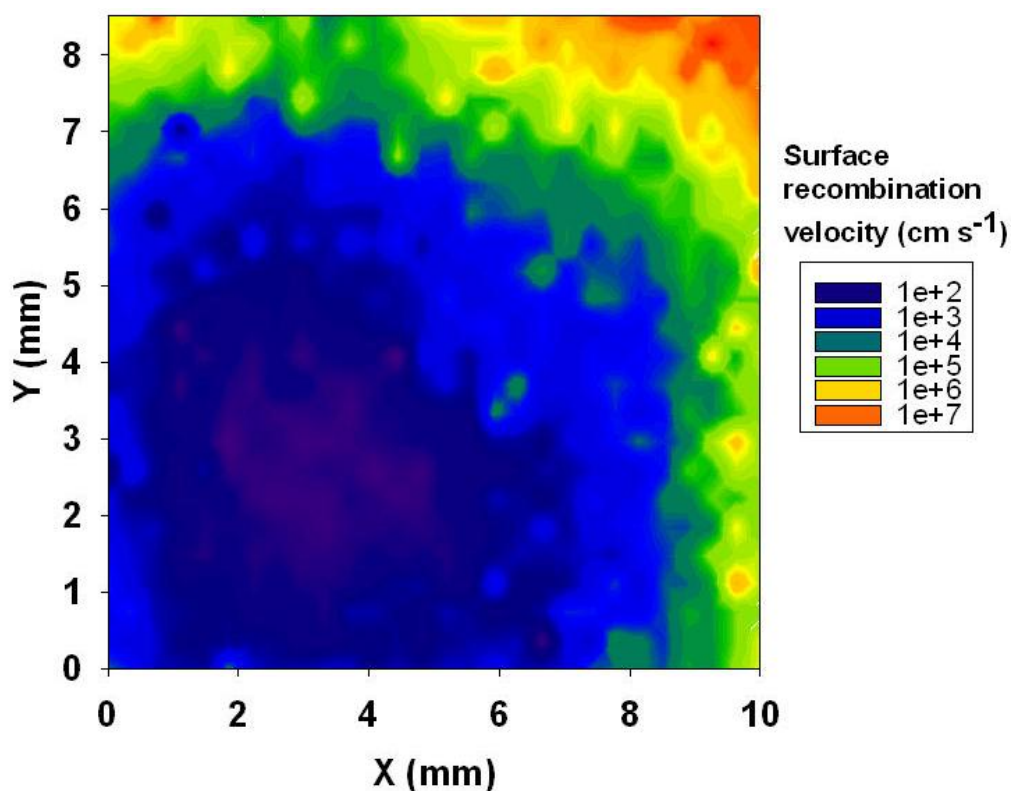


Fig. 6. 4 - Surface recombination velocity map of a high-lifetime methyl terminated surface

The edges of the passivated samples appear to have a reduced surface recombination velocity when compared to the centre. This is not surprising, as the edges have a higher area for recombination than the centre, as well as saw damage from wafer dicing^{27,137,138}, similar to other literature findings. The surface recombination

velocity values can then be used to calculate the surface recombination lifetime for each point using equation 3.25. These are shown in Fig. 6.5 to Fig. 6.7 for a native oxide, methyl- and ethyl-terminated surface.

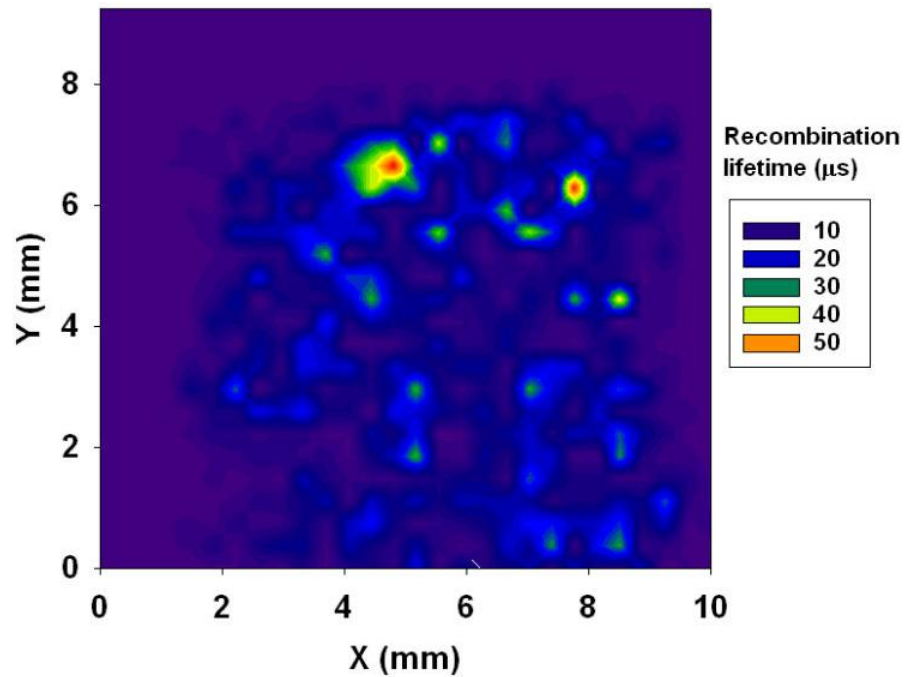


Fig. 6. 5 - Recombination lifetime map of native oxide samples acquired by Kelvin probe

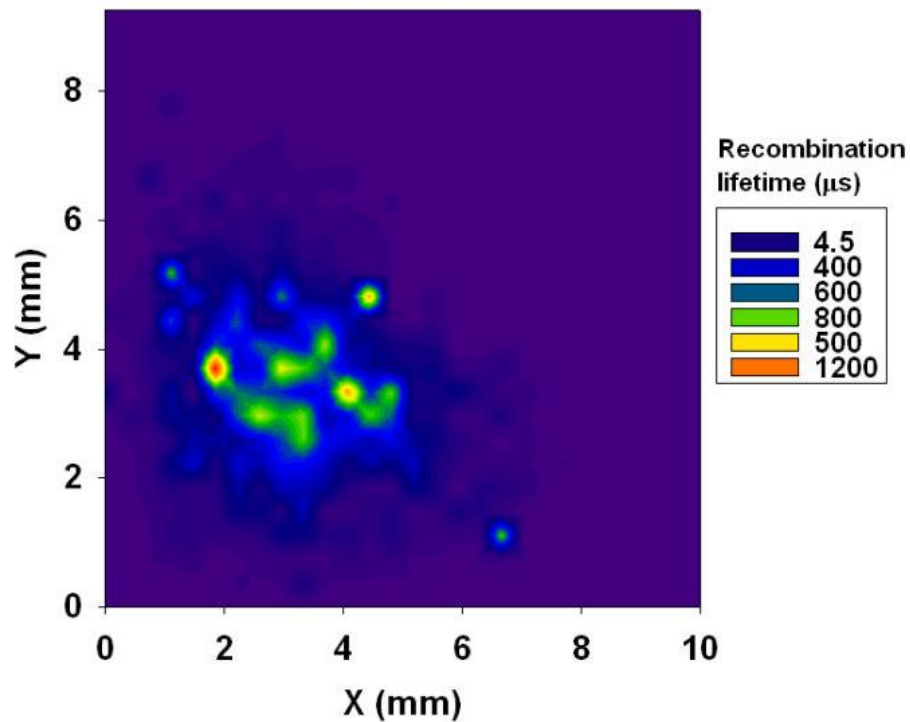


Fig. 6. 6 - Recombination lifetime map of methyl-terminated samples acquired by Kelvin probe

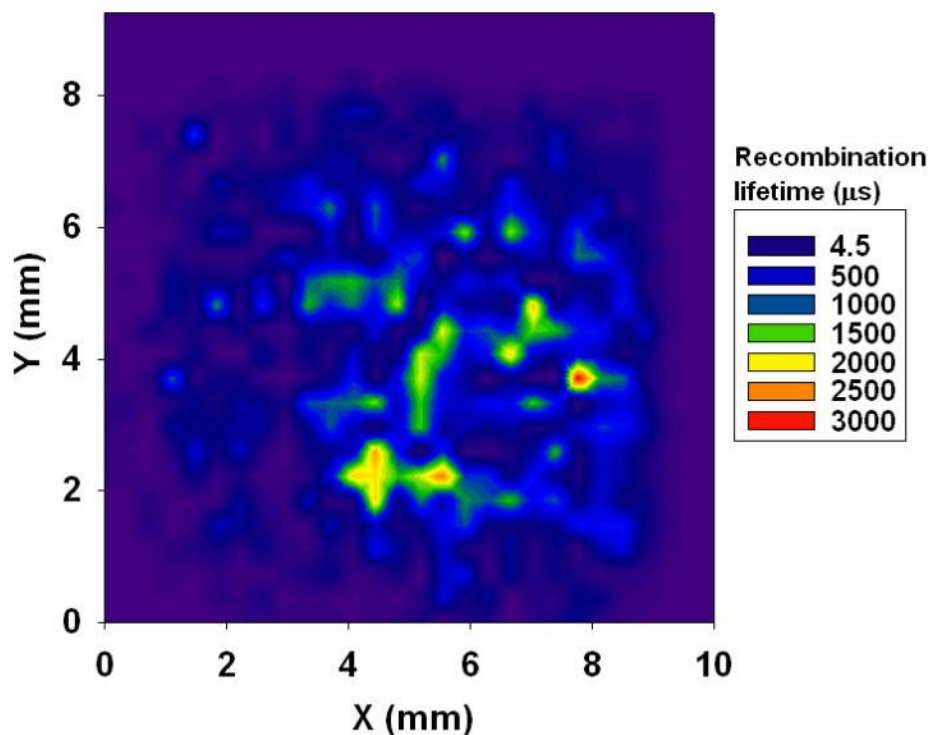


Fig. 6.7 - Recombination lifetime map of ethyl-terminated samples acquired by Kelvin probe

The native oxide samples showed a low lifetime throughout the sample, with the majority of the sample showing a lifetime of less than 20 μs . Several higher lifetime areas ($<50 \mu\text{s}$) are visible, which could be due to some surface contamination.

The high lifetime (142 μs) methyl terminated surface contained an area of high recombination lifetime in the lower left corner (Fig. 6.6). Compared to that of the ethyl terminated surface (Fig. 6.7), this area contains a more uniformly high lifetime section. Although containing areas with a higher maximum recombination lifetime, the ethyl-terminated surface exhibits a lower overall lifetime (83 μs) as measured by the Sinton WCT-120. This is likely due to the 'patchy' nature of the passivation in the high lifetime areas; the high lifetime sections are intersected by very low lifetime areas, which allow for fast recombination rates. Therefore the flow of electrons from the high lifetime areas to the low will be fast, as minimal distance (and less diffusion) is required to reach the recombination centres. In the methyl surface

however, large areas of the surface are well passivated, meaning that the minority carriers need to flow for a large distance before they reach recombination centres. This allows for a long recombination lifetime, and thus a low surface recombination velocity.

It should be noted that the new mapping technique for the recombination lifetime of wafers may find a ready application in industry as there are very few techniques available to do this task (infrared lifetime mapping^{139,140,141}, microwave reflectance^{142,143} and photoluminescence imaging^{111,144}), making this a valuable technique in the determination of passivation quality.

6.6 Conclusions

A novel technique has been developed to measure the surface recombination velocity and recombination lifetime of silicon samples. By changing the incident photon flux on the sample in a Kelvin probe, the photogenerated current can be calculated and the change in surface photovoltage measured. This allows the surface dark current (J_{0s}) to be extracted, from which the surface recombination velocity and recombination lifetime can be calculated. The results fit closely with those of the Sinton WCT-120, confirming the theory.

Accurate, reproducible results require a good contact to the rear surface, achieved by scratching the surface with sandpaper and the application of silver paste. This must be allowed to dry for at least 24 hours prior to obtaining measurements to allow for the evaporation of solvent in the silver paste.

By applying the same principal to a 2D scan of the wafer, the surface recombination velocity and recombination lifetime can be plotted over the sample area, allowing

defects in the surface passivation to be investigated. Few techniques are currently available that can map wafer lifetimes (infrared lifetime mapping, microwave reflectance and photoluminescence imaging) making this technique valuable in semiconductor quality analysis.

Thus the Kelvin probe has been shown to be a very sensitive technique for surface analysis, and an attractive method at characterising the passivation of semiconductor surfaces.

7. Passivation by Charge Anchorage

This chapter has been published in part as:

N. Alderman, L. Danos, M. Grossel and T. Markvart, 'Passivation of n-type silicon (111) surfaces by the attachment of charged molecules', *Proceedings of the 38th IEEE photovoltaics specialists conference (PVSC)*, 2012, 000992. (doi:10.1109/PVSC.2012.6317769)

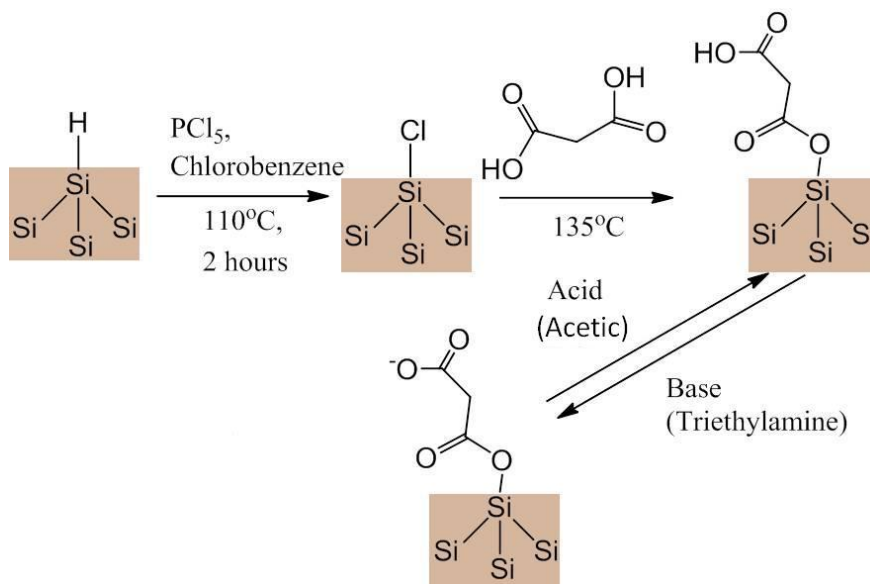
7.1 Introduction

Passivation layers have become ever more important with the drive towards smaller microelectronic and photovoltaic devices¹⁴⁵. An increasingly common technique for obtaining well-passivated samples is the charging of the semiconductor surface through the use of corona discharge^{50,74,146,147}, plasma-enhanced chemical vapour deposition (PECVD) of a charged film such as silicon nitride^{28,49,72,137,148} or immersion of the wafer in a chemical solution such as hydrofluoric acid^{56,149}, iodine in methanol^{71,75,116} or quinhydrone in ethanol^{66,68,150}.

This chapter investigates both the distance dependency of a charge from the silicon surface and the effect of the sign of the charge through the use of recombination lifetime and surface photovoltage measurements. By understanding the effect of the charged organic layers on these parameters, further improvements to low-temperature passivation techniques could be introduced.

Through anchoring of the charged species to the silicon surface, the magnitude of the charge can be measured, controlled and changed with the system requirements¹⁵¹

(Scheme 7.0). By incorporating reversibility of the attached charge (between neutral and charged) we can precisely understand its effect, by measuring samples during the charged state and the neutral state. This allows us to separate the degree of passivation due to the attachment of the organic monolayer (reduction of surface states) from the charging effect.



Scheme 7.0 - Reaction scheme for the attachment of dicarboxylic acids to silicon

7.2 Attachment of a Positive Charge to n-type Silicon

For the attachment of a positive charge to the silicon surface, choline iodide was chosen due to it containing a stable cation and its commercial availability. Choline iodide also contains an alcohol group which can be easily bonded to a chlorine terminated surface by literature routes^{152,153,154,155}. It is thought that a positive charge on n-type silicon should be preferable for passivation, due to an inversion of the surface bands which would repel minority carriers from the surface^{137,156}. As the concentration of the minority carriers is low, it is preferable to reduce the surface concentration to decrease recombination^{119,157}.

To confirm the attachment of the choline iodide group, infrared spectroscopy was performed on the sample. This showed peaks in the C-H stretching region at 2968 cm^{-1} and 2862 cm^{-1} corresponding to a symmetric and asymmetric C-H₃ stretch, and a peak at 2935 cm^{-1} corresponding to a C-H₂ stretch. In the C-N stretching region, a peak at 1074 cm^{-1} was observed (Fig. 7.0).

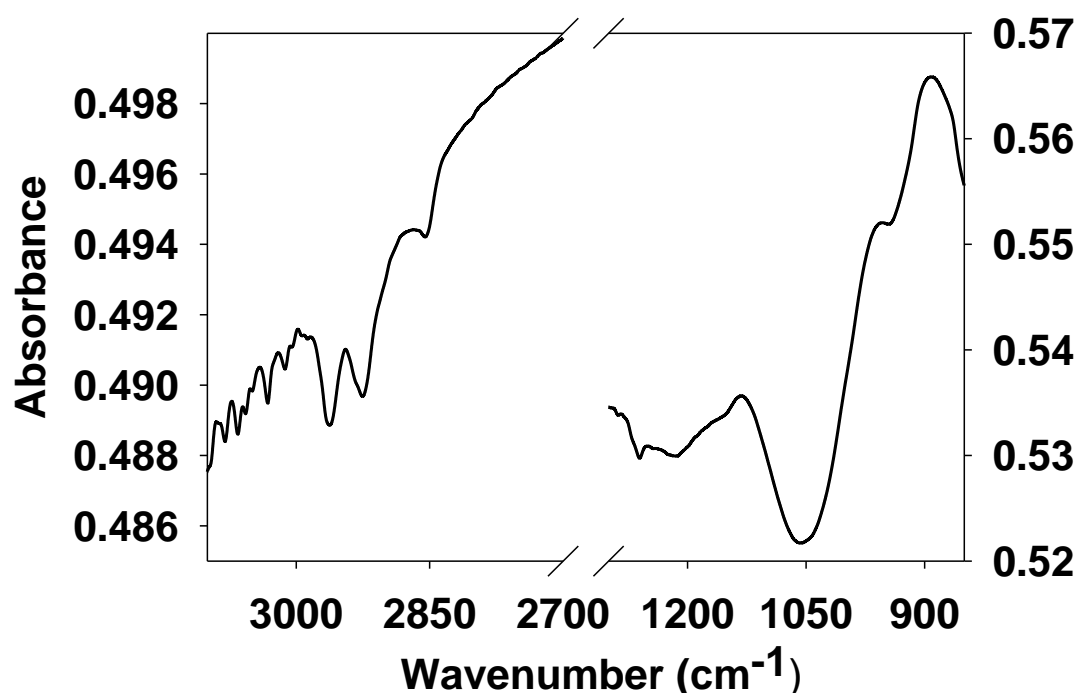


Fig. 7. 0 - Infrared spectrum showing the C-H and C-N stretching regions of a choline iodide terminated surface

Recombination lifetime studies showed a reduction in lifetime upon attachment of the organic group from the starting, native oxide value of 4.5 μs to 3.5 μs . The flat-band state was confirmed with Kelvin probe, with a low (<10 mV) surface photovoltage observed, confirming the reduction in the number of surface states through the attachment of the organic monolayer. This reduction, however, did not correspond to an improvement of the recombination lifetime as expected. A likely reason for this is due to the effect observed by Glunz *et al.*⁷⁶, where a negative

charge on p-type silicon initially increases the surface recombination velocity (decreases the recombination lifetime). After reaching a maximum surface recombination velocity (SRV), a reduction in the SRV is observed with further charging. Therefore with n-type silicon, this would be true for a positive charge on the surface. As the charge attached to our surface is small in comparison to the corona discharge method used in by Glunz *et al.*, we can presume that we are in the increasing surface recombination velocity area of surface potential.

The reason for the initial increase in the surface recombination velocity is due the ratio of electrons and holes at the surface. One could argue, on very general grounds, that recombination rate will reach a maximum when the rates of electron and hole capture are equal, in other words $\sigma_n n_s = \sigma_p p_s$, where n_s is the surface electron concentration, p_s is the surface hole concentration, σ_p is the hole capture cross section and σ_n is the electron capture cross section. Since our samples are n-type, the surface states are expected to be negatively charged, and therefore attractive for holes and repulsive for electrons. In this situation, one would expect the ratio of the hole and electron capture cross sections to be around 100-1000¹⁵⁸. Thus, we can:

$$n_s/p_s = \sigma_p/\sigma_n \approx 100 \quad (\text{eqn 7.0})$$

As we initially apply positive charge to the silicon surface, we reduce the hole concentration towards this ratio. As we apply a greater positive charge to the silicon, the hole concentration will decrease even further, away from this maximum value.

Therefore to achieve a highly passivated n-type sample with a positive charge, a much larger charge should be present on the surface. As the attachment of charge through our method forms a monolayer, this is not suitable for incorporation of a

large surface charge. Therefore we investigated the possibility of using a negative charge to move the mid-point away from a high concentration of surface states.

7.3 Attachment of a Negative Charge to n-type Silicon

Due to no improvement in the lifetime being observed with the attachment of a positive charge to silicon, the effect of attaching a negative charge was investigated. As there are very few stable and commercially available anions that can be bound to the surface, it was thought that the most promising technique would be charge generation in situ from a compound with a low pKa. A carboxylic acid group was judged to have the ideal properties, although a potential problem would be that the carboxylic acid O-H group could potentially bond with the silicon surface. To overcome this, a symmetrical dicarboxylic acid was used, with one end attaching to silicon whilst the other end would be free to generate the charge under basic conditions.

This method has also been shown to produce surfaces with a high degree of coverage, allowing the charge to be maximised⁸⁹. The distance of the charge from the surface can be calculated for alkyl siloxanes from an equation used in previous work by Aswal et al.¹⁵⁹:

$$d = 1.26 \times (n-1) \cos\Theta + 4.78 \quad (\text{eqn 7.1})$$

where Θ is the tilt angle of the chain, 1.26 Å is the carbon-carbon bond projection in the main molecule chain, n is the number of carbon atoms in the chain and 4.78 Å is the sum of the Si-O (1.33 Å), C-O (1.52 Å) and the length of the terminal C-H₃ group (1.93 Å).

Through a comparison of experimental literature data in the publication by Aswal et al., it was shown by spectroscopic ellipsometry that the most common tilt angle of siloxane chains on silicon surfaces is around 30° . Our calculations are based on an assumption that we have a similar tilt angle. We have assumed an error that is equal to the difference in the distance if the tilt angle is 30° and if the tilt angle is 45° , which is preferred as chain lengths decrease.

For deprotonation of the carboxylic acid group, triethylamine was chosen as it does not affect the underlying crystalline silicon^{89,160}. Triethylamine is also a non-coordinating base, which should allow the surface charge to be maximised. Acetic acid was chosen to regenerate the uncharged carboxylic acid due to the availability of the anhydrous form.

After removal of the samples from the glovebox and sonication in methanol, infrared spectroscopy was performed to confirm the functionalised surface (Fig. 7.1 and Fig. 7.2). This clearly shows peaks for C-H₂ at 2978 and 2927 cm^{-1} , adventitious C-H₃ and O-H at 3246 cm^{-1} , confirming both the attachment of the main chain and the attachment of a free carboxylic acid group which can be deprotonated, leading to surface-bound charge generation⁸⁹. In the C=O infrared stretching region, a peak was observed at 1698 cm^{-1} , corresponding to the carbonyl stretch of the carboxylic acid-functionalised surface.

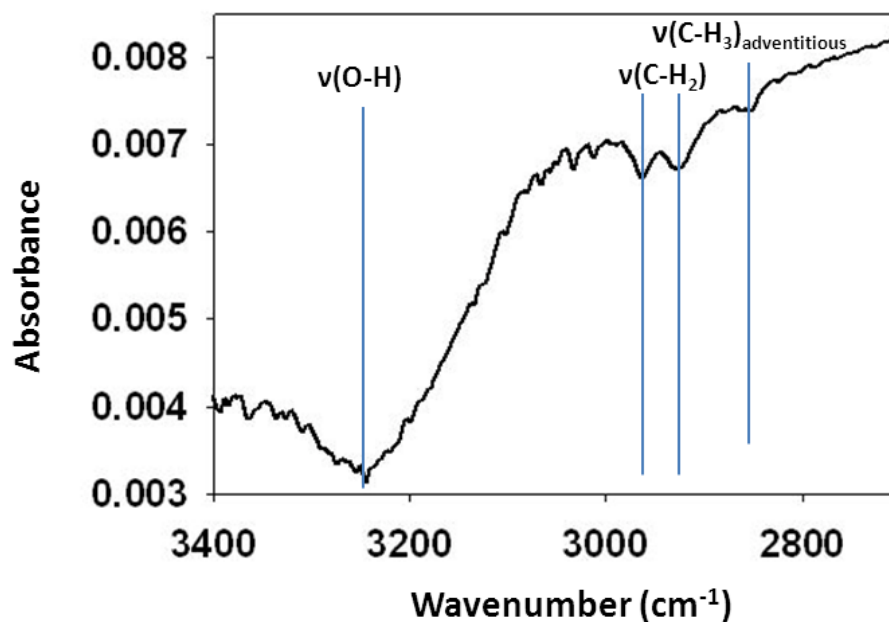


Fig. 7.1 - Infrared spectrum of the O-H and C-H stretching region of a Glutaric acid terminated surface

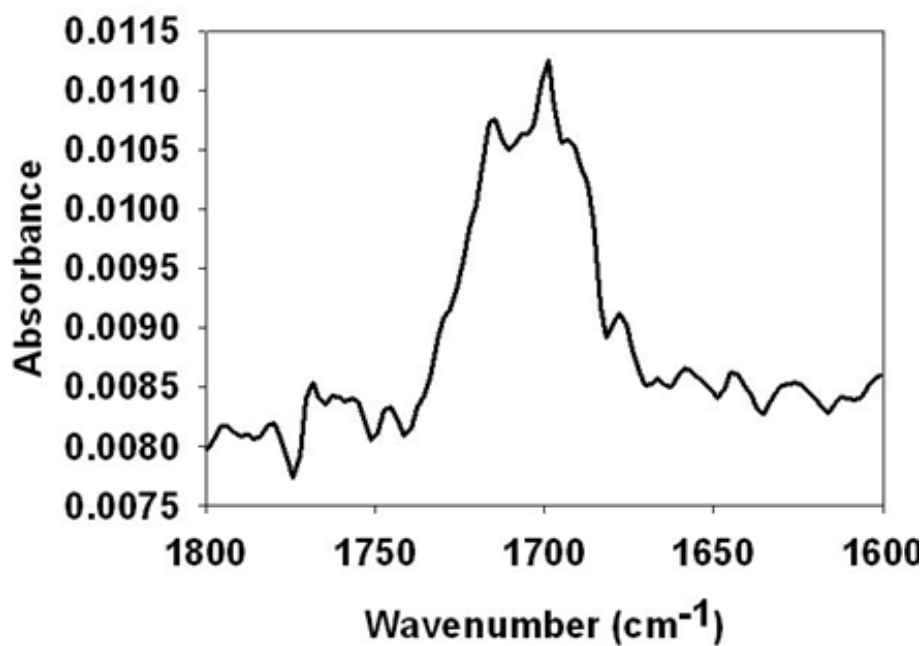


Fig. 7.2 - Infrared spectrum of the C=O stretching region of a succinic acid terminated surface

X-ray photoelectron spectroscopy further confirmed the attachment of the carboxylic acid functionality (Fig. 7.3, Fig. 7.4 and Fig. 7.5).

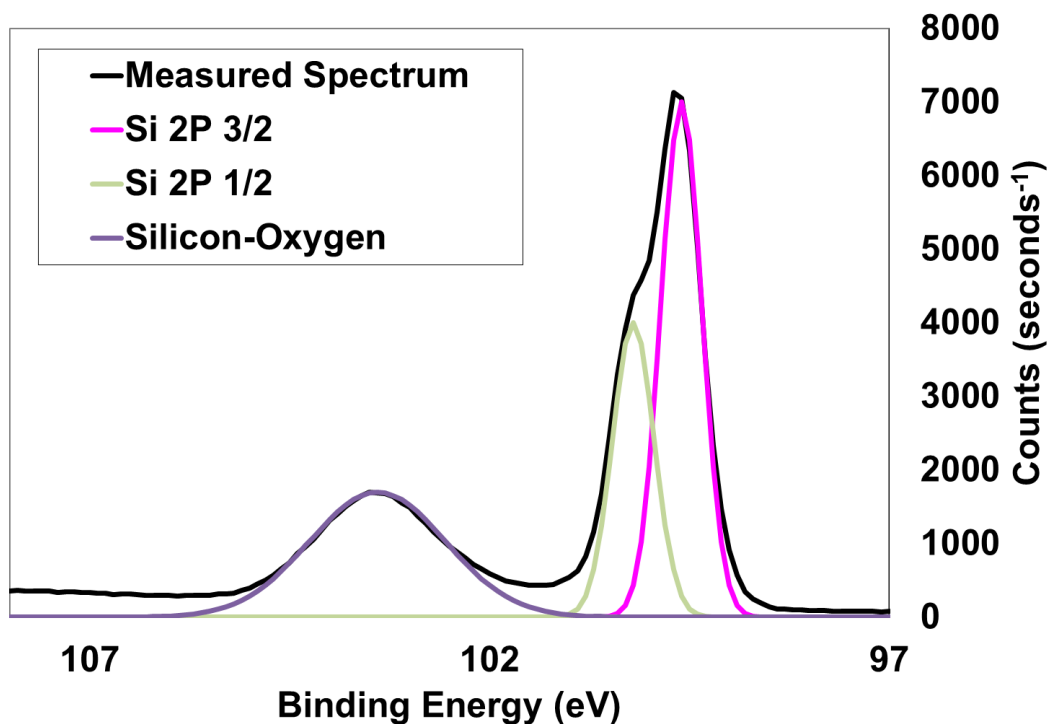


Fig. 7. 3 - The silicon 2p binding region for a Glutaric acid functionalised surface showing the presence of Si-O bonds

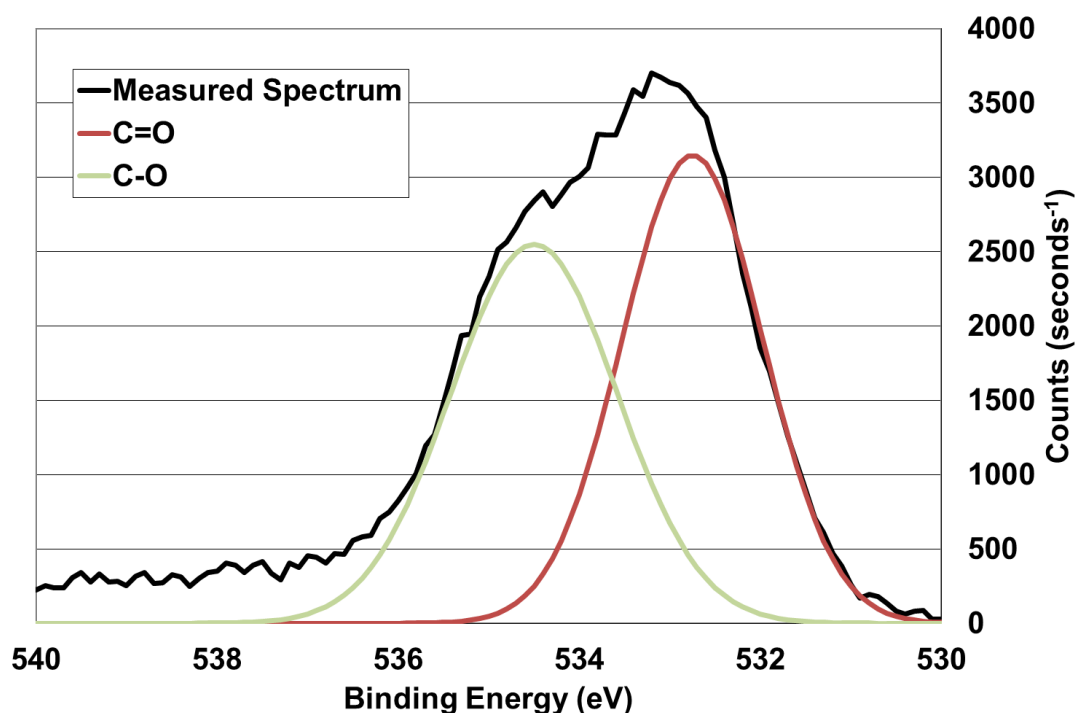


Fig. 7. 4 - The O 1s binding energy region for the Glutaric acid terminated surfaces showing two peaks for the two different oxygen environments (Quartz crystal microbalance in clinical application)

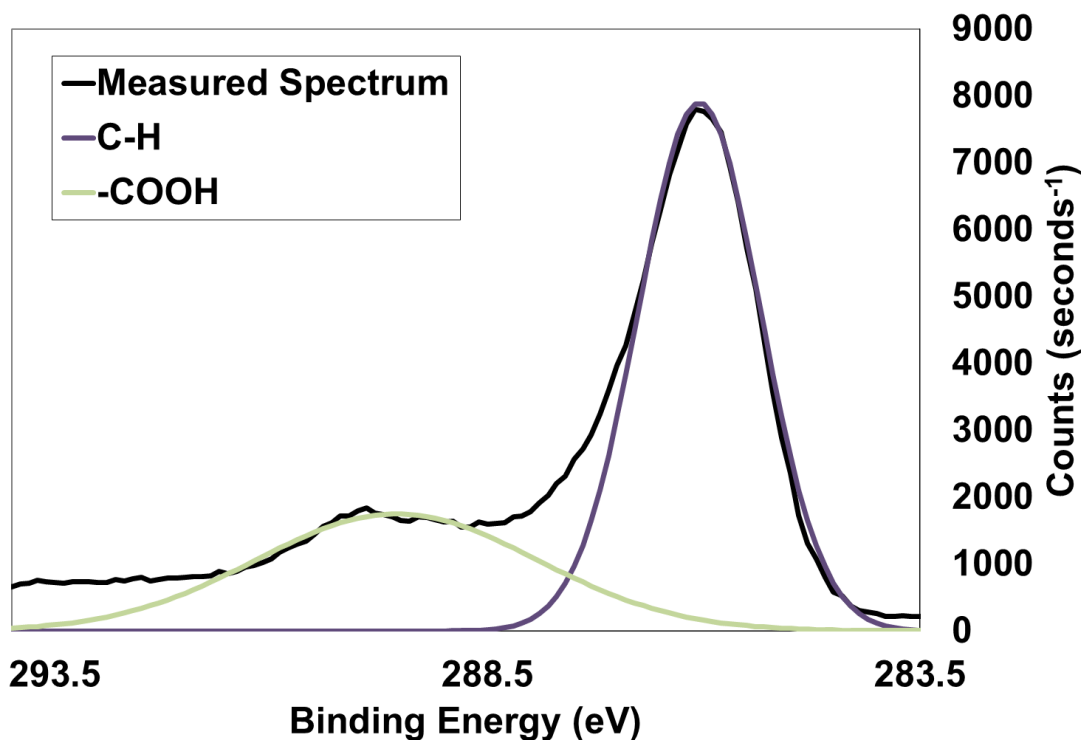


Fig. 7. 5 - The C 1s spectrum of the Glutaric acid terminated surface showing C-H binding energies and -COOH binding energies

The XPS spectra matched that of other carboxylic acid groups found in the literature, confirming successful attachment. A peak for Si-O was observed in the silicon binding energy region, whilst two peaks with an integral ratio of 1 : 0.98 were visible in the oxygen binding energy region corresponding to C=O and C-O of the carboxylic acid group respectively. In the carbon binding energy a side peak was clearly visible for -COOH, as well as carbon from the C-H chain^{89,161}.

The recombination lifetime of freshly synthesised carboxylic acid terminated surfaces was around 8 μ s. This is comparable with that of the native oxide samples, which had a lifetime of 4.5 μ s. Upon immersion in base, a substantial increase in recombination lifetime was observed due to the formation of a charge at a distance from the silicon surface dependent on the carboxylic acid chain length. After washing in acetic acid and water the lifetime returned to that of the initial sample. During multiple base and acid immersions, a reduction in recombination lifetime was

observed until the difference between the acid and base immersions was minimal (Fig. 7.6). For reference the lifetime of chlorinated silicon surfaces remained at around 7 μs during base immersions, confirming that the difference in lifetime was due to the attached carboxylic acid chain.

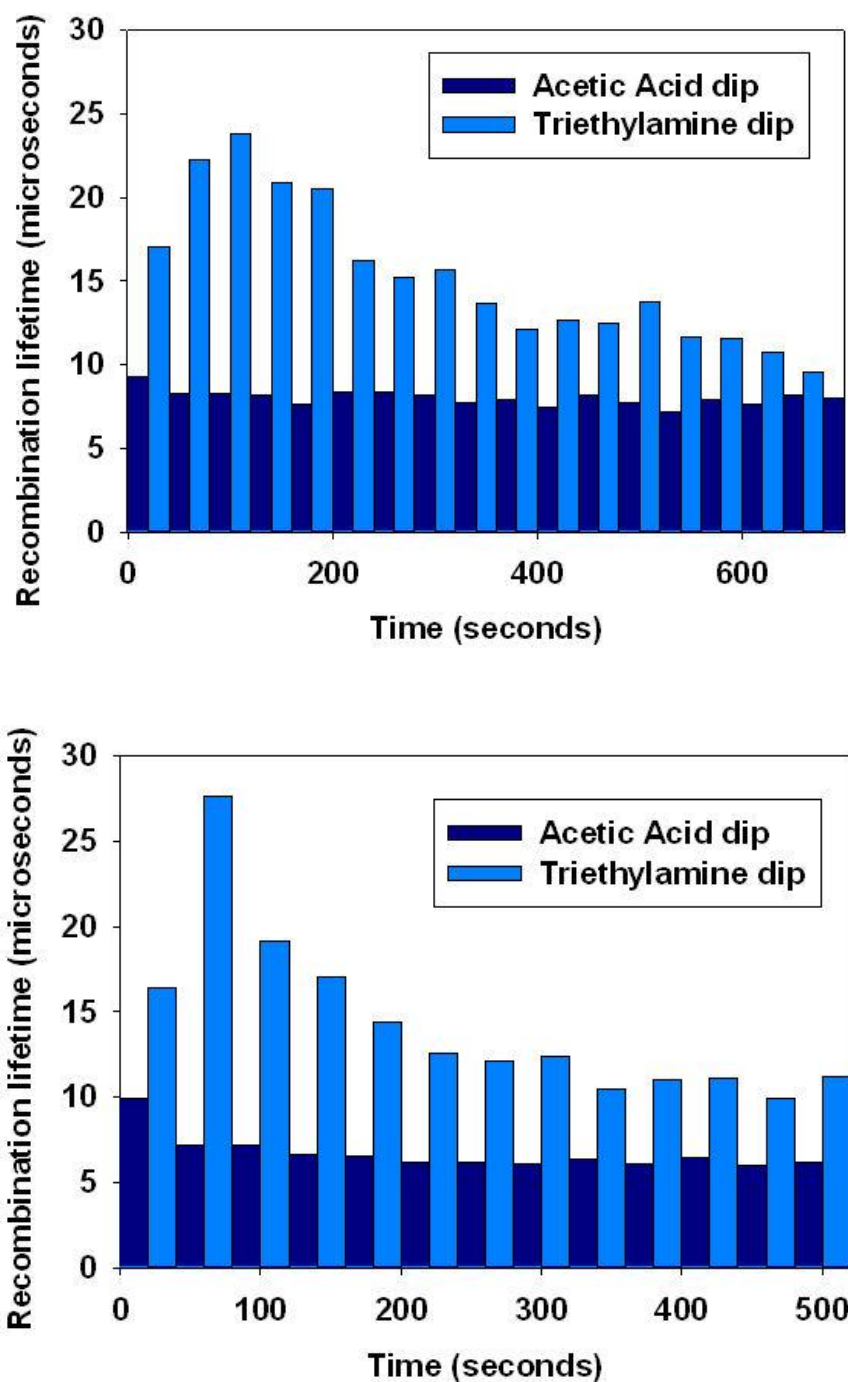


Fig. 7. 6 - The recombination lifetime of Succinic acid (top) and Malonic acid (bottom) terminated surfaces when immersed in acid and base

A plot of the maximum lifetime against the distance of the charge from the surface gave a linear correlation, with lower charge to surface distances giving a larger recombination lifetime (Fig. 7.7). The surface band structure was then investigated by Kelvin Probe measurements, where it was found that the surface photovoltage (SPV) increased in a similar manner to the recombination lifetime. This can be attributed to a reduction in surface electron concentration which, when combined with a reduction in the number of surface states (as shown by the almost flat-band state of the synthesised surface before base immersion), results in a substantially increased recombination lifetime.

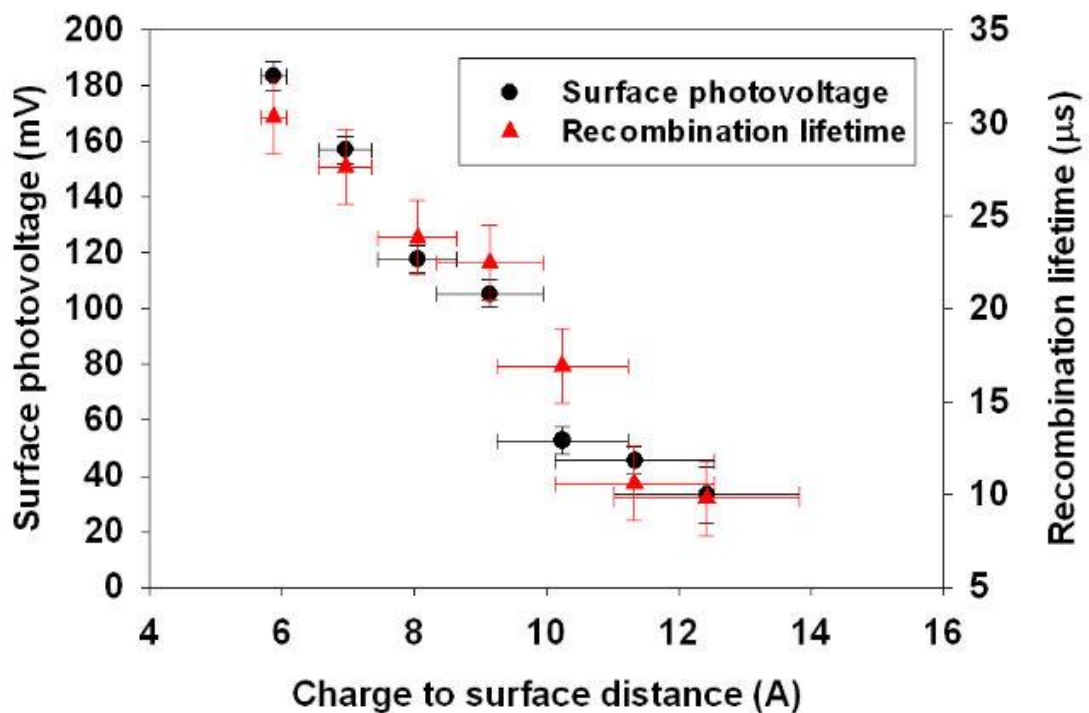


Fig. 7. 7 - The maximum recombination lifetime achieved for the carboxylic acid terminated surfaces and the change in surface photovoltage when immersed in base

This is similar to the passivation effect observed by Glunz *et al.*⁷⁶ through the use of corona discharge. It was observed that with a positively charged surface on p-type silicon, a strong accumulation of minority carriers at the surface was obtained, and

the surface recombination velocity decreases more and more with higher surface charging. As the experiments within this thesis use n-type silicon, the charge-type should be reversed (negative charge) to see this effect, resulting in a strong accumulation of holes at the surface. As this charge is increased (by moving the charge closer to the surface), the surface recombination velocity decreases with the accumulation of holes at the silicon surface. A similar effect has also been observed by Goossens *et al.*¹²⁸, where the recombination lifetime was investigated with surface band-bending. It was shown that the recombination lifetime increased with band-bending up to a value of around 400 mV. This is similar to the effect observed in our samples, except the samples used in this section have a smaller degree of band-bending, and thus a lower recombination lifetime.

The recombination lifetime of the carboxylic acid terminated surfaces degrades after multiple base / acid immersions. One several reactions was assumed to be responsible for the decrease, either the oxidation of the underlying silicon due to water or dissolved oxygen in the base and acid solutions, ester hydrolysis or due to the cyclization of two adjacent carboxylic acid groups in the base as observed by Perring *et al.*⁸⁹.

It was confirmed by infrared spectroscopy that the reduction in lifetime is due to the hydrolysis of the surface attached carboxylic acid group (Fig. 7.8). By deconvolution of the spectrum, it was shown that the surface remains partially functionalised even after multiple acid / base immersions. After multiple immersions in base and acid, the ratio of the surface hydroxyl peak to that of the Glutaric acid O-H increases, confirming that multiple immersions cause reduced carboxylic acid coverage (Scheme 7.1). This has the effect of reducing the charge magnitude, decreasing the recombination lifetime.

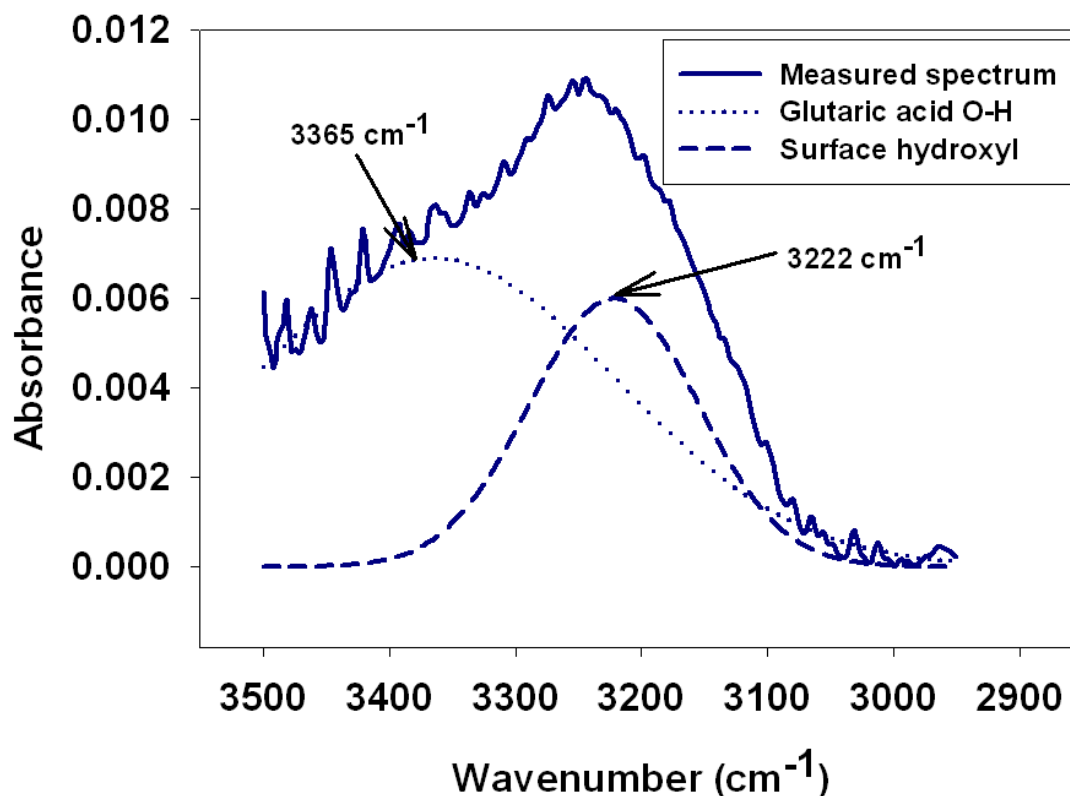
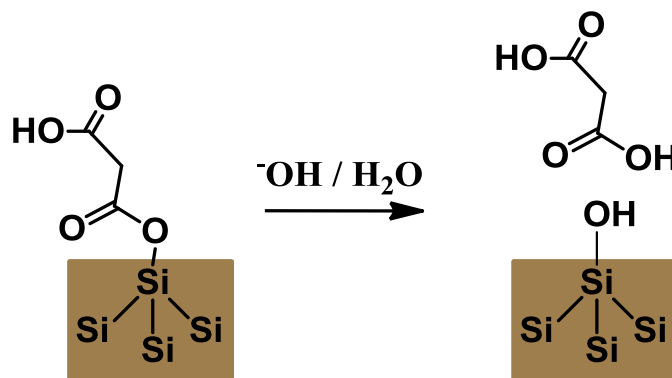


Fig. 7. 8 - Deconvoluted infrared spectrum of the O-H bonding region showing the contributions from the Glutaric acid O-H and silicon surface O-H after multiple immersions in acid and base



Scheme 7.1 - Likely oxidation mechanism for the oxalic acid terminated silicon surface upon immersion in water / base

To confirm the correct assignment of the silicon oxide peak (O-H), the experiment was performed on a chlorinated silicon surface. An increasing peak was observed at 3222 cm^{-1} after multiple base and acid immersions, corresponding to surface hydroxyl formation⁶⁴. Interestingly, this peak was broader than the surface hydroxyl

peak obtained on the carboxylic acid functionalised surfaces, possibly as a result of a reduction in the hydrogen bonding between hydroxyl groups on these surfaces due to the presence of the carboxylic acid groups.

The distance between the charge and the surface is an important factor in the degree of passivation imparted, with shorter distances having higher recombination lifetimes. This can be explained by a larger potential drop in the longer chain molecules, resulting in a reduced depletion region charge in the silicon with a lower SPV and recombination lifetime.

A linear correlation between the recombination lifetime and surface photovoltage was observed over the range of surface-charge distances. For very close distances (less than 8 Å) the observed SPV was higher than for native oxide samples (~130 mV), decreasing to below native oxide values for larger distances. All carboxylic acid terminated surfaces gave an increase in the recombination lifetime compared to native oxide samples. This indicates that the increase in lifetime is due to a combination of a reduction in surface states and a reduction in surface electron concentration away from the 100:1 ratio in equation 7.0.

The surface photovoltage measurements confirm that upon immersion in base, a negative charge is produced on the carboxylic acid group which is compensated by a positive charge in the space-charge region at the silicon surface (Fig. 7.9). This charge varies with the carboxylic acid charge distance, imparting surface passivation.

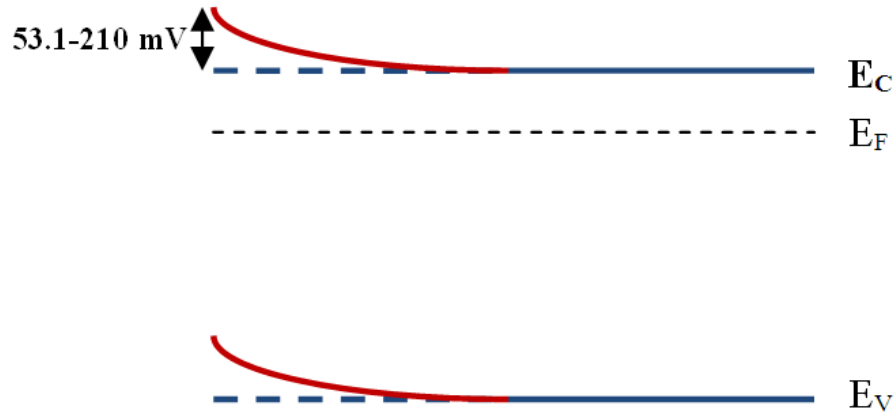


Fig. 7. 9 - The surface band structure after synthesis (blue dashed line) and after immersion of the carboxylic acid terminated surface in base (red line)

The surface potential measured can be converted to the surface charge atom density by the following equation:

$$\phi_s = (qN)^2 / 2K_s\epsilon_0qN_D \quad (\text{eqn 7.2})$$

where ϕ_s is the surface potential, N is the surface charge atom density (cm^{-2}), K_s is the dielectric constant of the semiconductor, q is the electron charge and N_D is the doping concentration of the semiconductor¹³². The surface charge atom density can then be calculated for each carboxylic acid terminated surface and is shown in Table 7.0. The results obtained from our studies show a surface charge density of between 2.17 and $1.09 \times 10^{10} \text{ cm}^{-2}$. For comparison, charging of the surface by the deposition of silicon nitride yields a value of around 6 to $7 \times 10^{11} \text{ cm}^{-2}$ for highly passivated samples^{72,137}. Therefore the charges produced at our surfaces are around 30 times lower than can be achieved through deposition of nitride films. A likely reason for this lower charge is a lower surface coverage of our carboxylic acid surfaces, as well as being a monolayer as opposed to thicker (around 50 - 100 nm) nitride layers.

The change in the surface recombination velocity with increasing depletion region charge atom density is shown in Fig. 7.10. A linear trend, which can be extrapolated

to the origin, is observed when plotting of the depletion region charge atom density with $10000/S$. We can therefore suggest that the surface recombination velocity is determined by the surface charge.

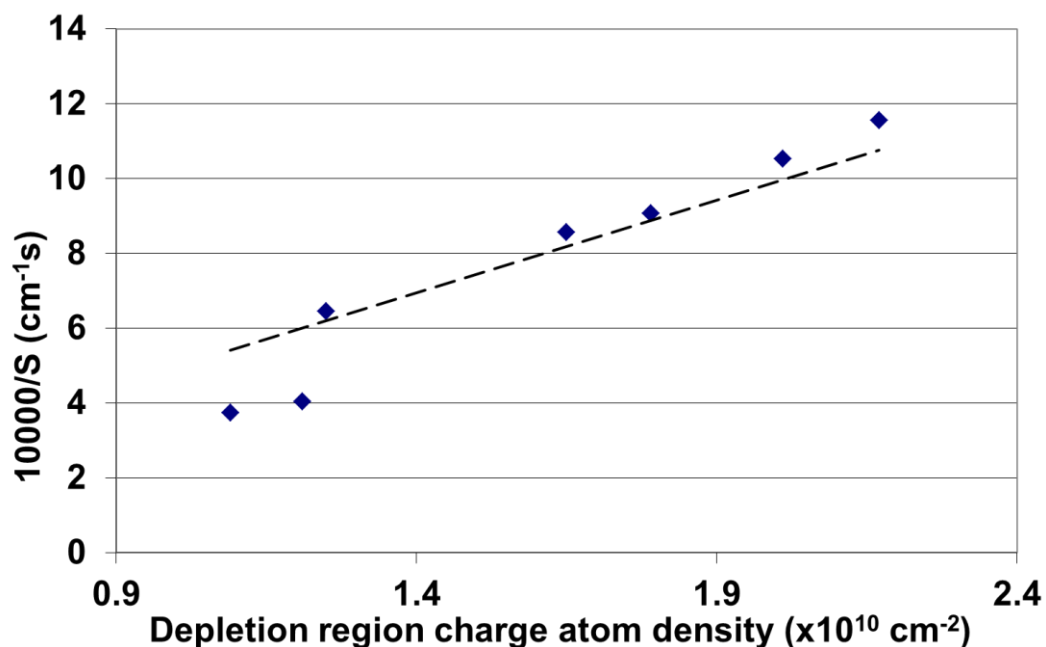


Fig. 7. 10 - The change in surface recombination velocity as a function of the depletion region charge atom density

For high-lifetime samples, it is important to maximise the charge within the surface depletion region. The charge should therefore be positioned as close to the surface as possible, giving a high surface coverage with a minimal amount of surface oxide. The reversible nature of our system makes it ideal for studying the effect of the surface charge, as we can easily separate the two main effects: the reduction in the number of surface states by the covalent attachment of the carboxylic acid and the effect of the generation of the surface charge on the SPV and recombination lifetime.

Carbon chain length	Surface-charge distance (Å)	SPV (mv)	Depletion charge atom density ($\times 10^{10} \text{ cm}^{-2}$)	region	Recombination lifetime (μs)	Surface recombination velocity (cm s^{-1})
2	5.87	210.0	2.17		30.32	866
3	6.96	180.2	2.01		27.63	950
4	8.05	142.2	1.79		23.83	1102
5	9.14	121.4	1.65		22.49	1167
6	10.24	69.3	1.25		16.92	1551
7	11.33	65.6	1.21		10.61	2474
8	12.42	53.1	1.09		9.81	2676

Table 7.0 - Summary of Kelvin probe and recombination lifetime results

7.4 Comparison of Surface Photovoltages

The barrier height (surface photovoltage) between the two different passivating monolayer attachment methods (through alkylation as in Chapter 5 and through the attachment of a charged carboxylic acid group as in Chapter 7) can be compared with the surface recombination velocity values obtained.

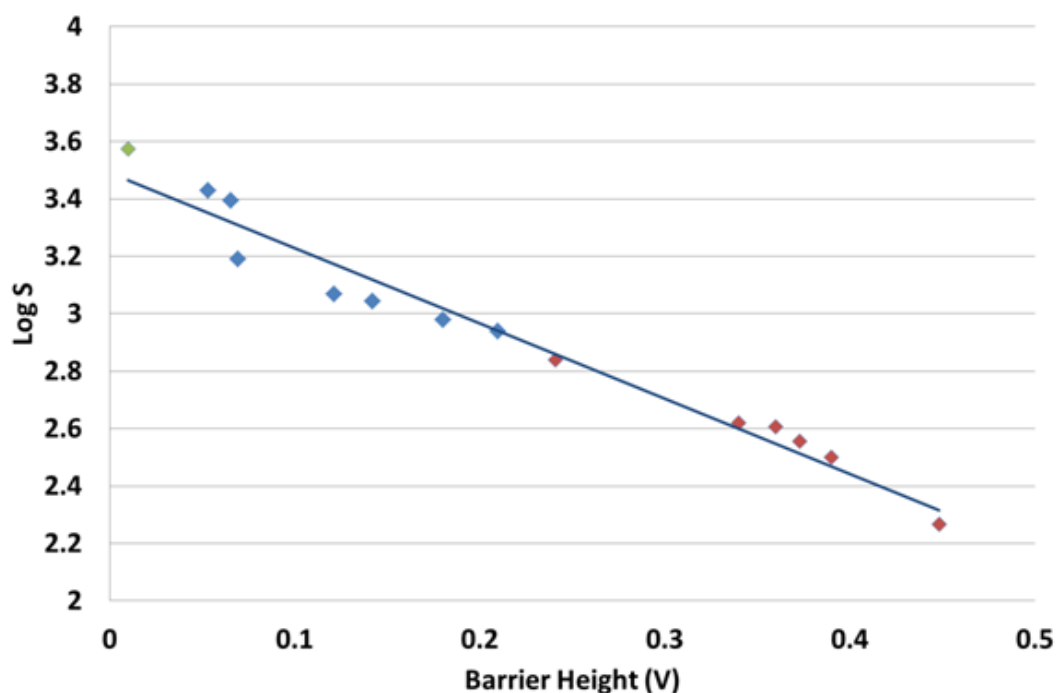


Fig. 7.11 – Comparison of barrier heights measured by Kelvin probe with the surface recombination velocity for chlorine terminated-surfaces (\diamond), carboxylic acid-terminated surfaces (\diamond) and alkyl-terminated surfaces (\diamond)

From Fig. 7.11 it can be seen that the barrier height as measured by the Kelvin probe and the surface recombination velocity are linked for all samples synthesised in this thesis. Our data suggests that this is independent to the synthesis method, as both Si-C and Si-O bonded monolayers have shown to induce passivation through charging. This suggests that the passivation effect observed within this thesis is due to the charging of the semiconductor surface and not due to a reduction in the surface states as suggested by previous work by Lewis *et al.*¹²⁹. In Chapter 2 it was stated that

upon passivation, the number of surface states reduces from around $10^{12} \text{ cm}^{-2} \text{ eV}^{-1}$ to around $10^{10} \text{ cm}^{-2} \text{ eV}^{-1}$. As a significant number of traps are present even in well passivated samples, and a trap density in the ppm range can be observed through recombination lifetime measurements, this is not likely to be the passivation route.

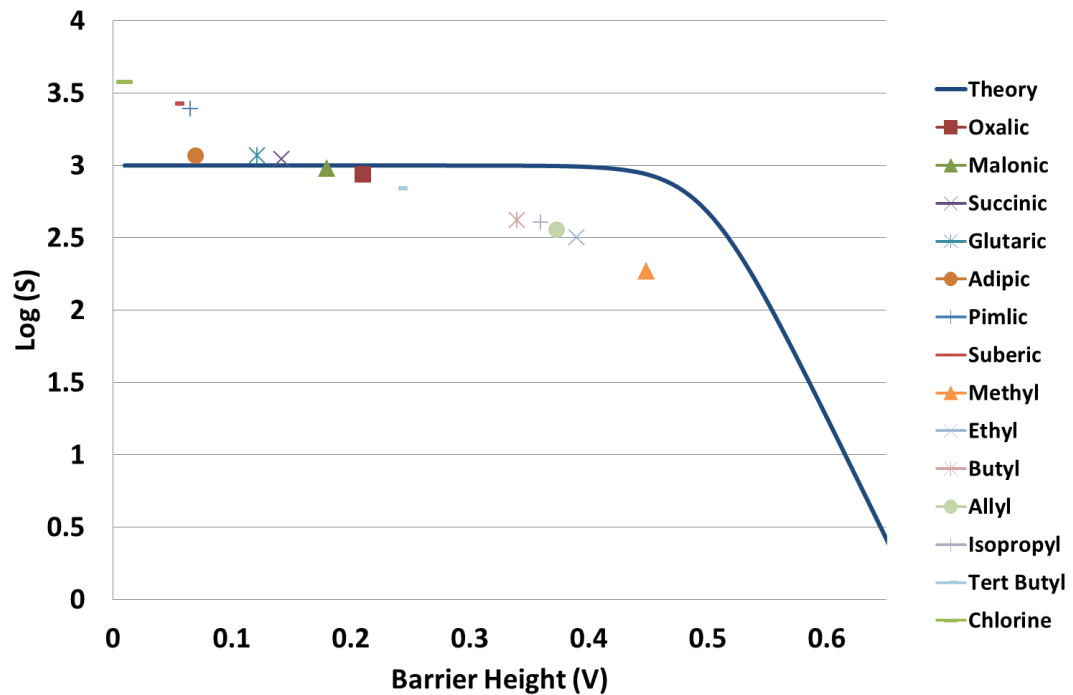


Fig. 7.12 – Comparison of the barrier height for synthesised samples with the Shockley-Read-Hall theory from Section 1.6.3

Fig. 7.12 shows the theoretical surface recombination velocity for the different barrier heights (from Chapter 3 [Fig. 3.9]) with the experimental values obtained. The values used to generate the model were taken from our samples, and are as follows:

The accepted value of N_t for well passivated samples is 10^{10} cm^{-2} ^{162,163}, whilst for v_{th} it is around $9 \times 10^6 \text{ cm s}^{-1}$ ¹⁶⁴. The capture cross sections for holes in n-type silicon will be around 10^{-13} cm^{-2} and for electrons will be around 10^{-15} cm^{-2} ⁷⁶. For our samples, p_0 is $6.7 \times 10^5 \text{ cm}^{-3}$ and n_0 is $1.74 \times 10^{14} \text{ cm}^{-3}$ ¹⁶⁵.

The model values and experimental values do not have a high degree of correlation as real samples have distribution of surface states as shown in Chapter 2 (Fig. 2.6), not a single trap state as the theory uses.

To achieve well passivated surfaces, the barrier height (or SPV) should be increased, reducing the charge-carrier concentration at the surface. This is similar to the effect that has been observed by charging of the surface with iodine in ethanol solutions or through corona discharging. Until now it was unclear as to the cause of the passivation effect due to the chlorination-alkylation method, especially as other alkyl monolayers do not report a high recombination lifetime. We can now suggest that the two-step chlorination-alkylation technique reported in this thesis produces well-passivated samples due to charging of the surface during the alkylation (Grignard) step. This is similar to the effect observed through the charged monolayer studies using the carboxylic acid, although a lower surface charge was reported resulting in a lower surface recombination velocity.

7.5 Conclusions

It has been shown that, through the attachment of charged monolayers, the lifetime of the silicon samples can be modified. Choline iodide has been used to attach a positive charge to the surface, although this results in a reduction in the recombination lifetime.

By functionalising the silicon surface with carboxylic acid groups, a negative charge can be generated upon immersion in base. This affords a significant improvement in the lifetime from around 8 μs to over 30 μs , due to a negative monolayer surface charge. This finding has been interpreted as resulting from a reduction in the surface

electron concentration away from the maximum recombination ratio of 100:1, as confirmed by surface photovoltage measurements.

By charging the surface and reduction of surface states by the attachment of organic molecules, the recombination lifetime can be increased. Once the surface charge is neutralised, both the recombination lifetime and surface photovoltage return to their initial value.

It has been shown that the reduction in surface states has a minimal effect on the passivation observed. The most important parameter for controlling the passivation effect is the barrier height, with the two different passivation methods (attachment of carboxylic acids and the two-step chlorination-alkylation technique) following a similar trend.

8. Attachment of Dyes to Silicon

8.1 Introduction

The covalent attachment of dyes to silicon is of great interest to the photovoltaic and sensing community, because of the ability for energy transfer to occur from the dye to silicon^{14,16,18}. By using a carefully chosen selection of dyes, photons of wavelengths which are poorly absorbed by silicon (>900 nm) could be absorbed by the dye and the energy then transferred to the silicon. Sensitisation of silicon (or light harvesting), in this way would allow the thickness of semiconductor required for a high efficiency solar cell to be reduced. Crystalline silicon represents large proportion of the cost of a solar cell, and considerable savings can be made through a reduction in the material thickness. Thin devices with around 70 nm of active silicon material have been reported although the efficiencies have so far been low¹⁶⁶.

Changing the distance from the dye to silicon, would allow the dependence of this energy transfer from chromophore to semiconductor to be investigated (Fig. 8.0). This can therefore help us to understand and improve upon the two principal functions of a solar cell (light capture and charge separation). By separating these functions, photovoltaic devices can be improved significantly. Concepts such as upconversion²³ and downconversion²² could also be included in future devices through this method, thereby enhancing their efficiency.

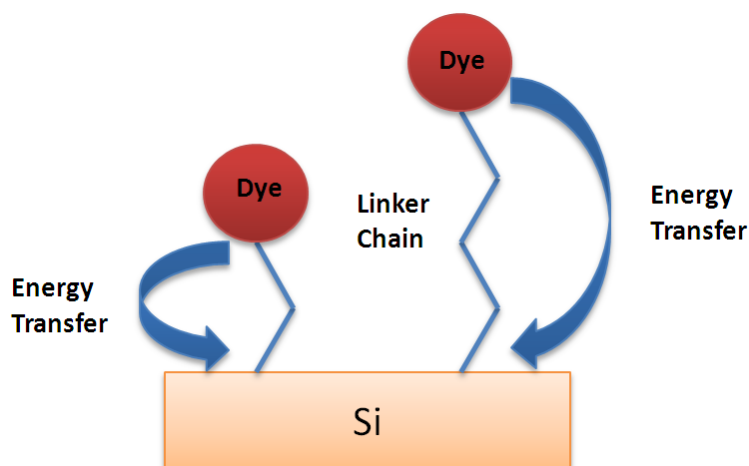


Fig. 8.0 - Two dye molecules covalently bonded to silicon at different silicon-dye distances

Although a detailed explanation of the energy transfer phenomenon is still unknown, investigations have shown that at small distances between the dye and silicon surface, more fluorescence quenching (and thus more energy transfer) is observed²⁰.

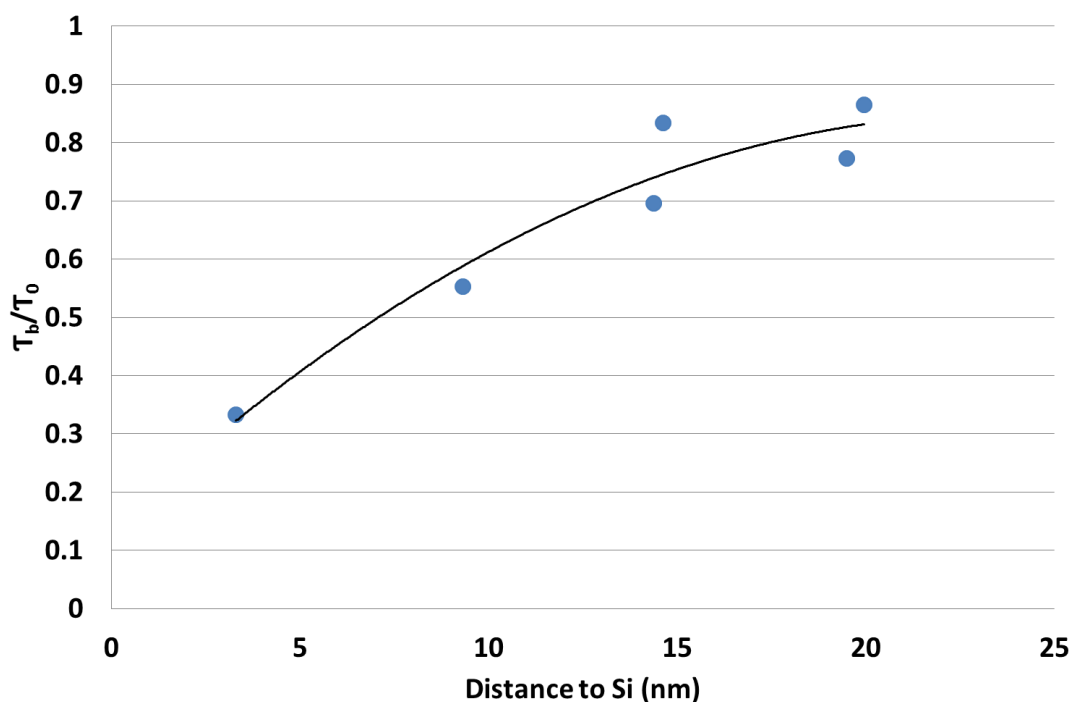


Fig. 8.1 - The fluorescence lifetime (τ_b/τ_0) of DiO with distance to the silicon (111) surface, where the lifetime has been divided by that of the dye on glass¹⁷

As can be seen in Fig. 8.1, it is preferable to attach the chromophore as close to the silicon surface as possible in order to maximise energy transfer. Therefore a thin,

stable passivation method suitable for attaching the chromophore to the surface is needed.

8.2 Protoporphyrin IX Functionalised Surfaces

The dye molecule protoporphyrin IX (as its disodium salt) was chosen as a suitable chromophore since it has an absorption maximum at around 426 nm, close to that of the excitation laser in the fluorescence lifetime spectrometer (445 nm). This particular porphyrin also incorporates functionalities which allow its attachment to a silicon surface, and can also be of interest to the sensing community because of the shift in absorption maxima produced by binding with metal ions¹⁶⁷.

In the present study, the absorption dependency of hematoporphyrin with different metal ions was investigated (Table 8.0) by reaction of the metal chloride with the porphyrin at room temperature. Hematoporphyrin was chosen for this investigation instead of protoporphyrin IX because of its increased stability under ambient conditions.

Metal	Absorption Maximum (nm)
None	395.5
Fe (II)	374.5
Mg (II)	385.5
Ni (II)	395.5
Mn (II)	396.0
Zn (II)	409.5
Co (II)	410.5

Table. 8. 0 - The absorption maximum of hematoporphyrin with various coordinated metal ions

The absorption maximum can be significantly shifted by coordination with metal ions, resulting in a maximum shift range of over 30 nm. Therefore the absorption properties of the porphyrin dye can be tuned to the requirements of the system. The

absorption and emission spectra were measured for protoporphyrin IX and after coordination with zinc (Fig. 8.2), as it was hoped that the absorption maximum would be closer to that of the excitation laser used in the fluorescence decay spectrometer.

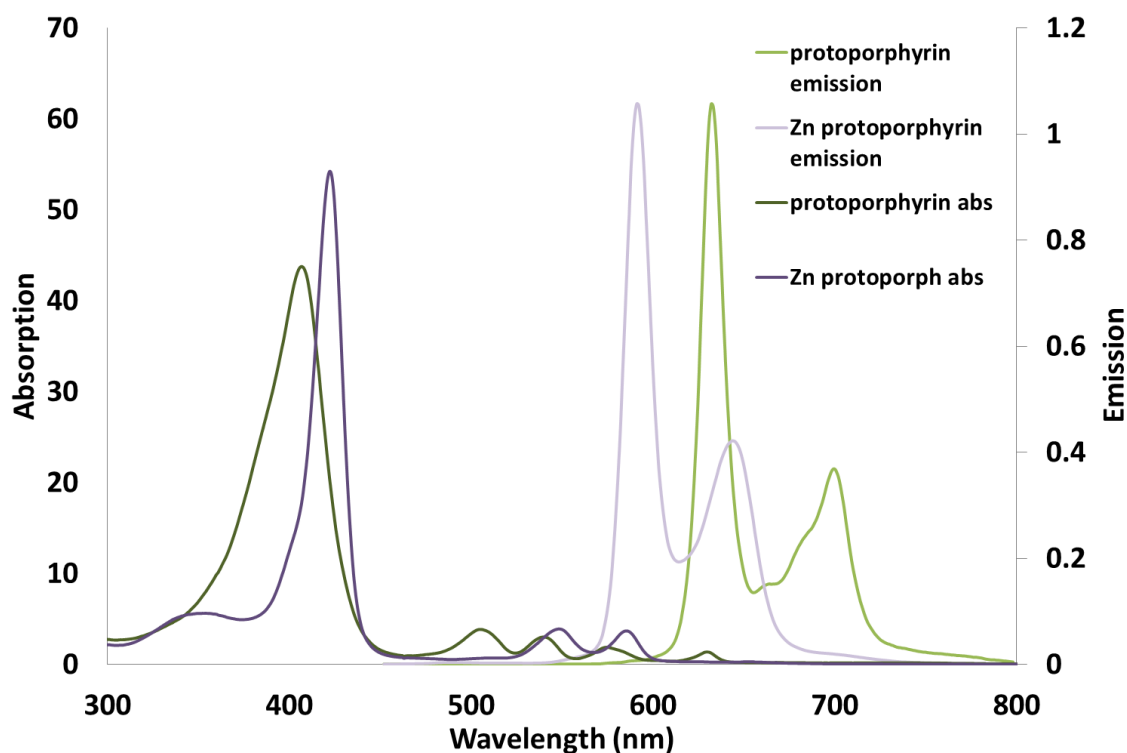
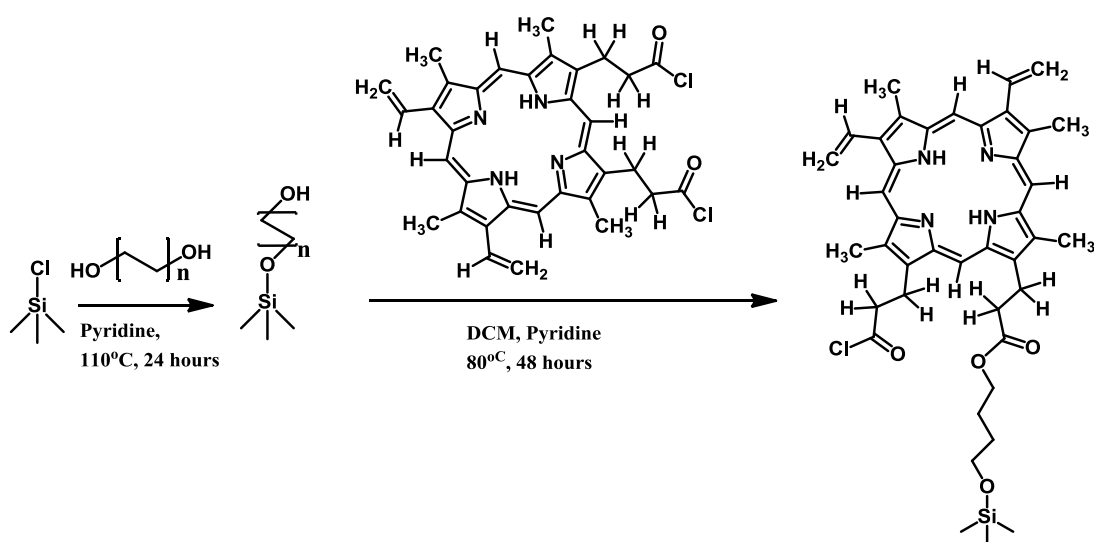


Fig. 8. 2 - The absorption and emission spectra of protoporphyrin IX before and after coordination with zinc

Upon coordination with zinc, the absorption maximum shifts from 409 nm to 423 nm, closer to the excitation laser. However, the absorption peak narrowed, giving a smaller range of absorption wavelengths. Although the absorption spectra were closer to the excitation laser, it was decided to use the uncoordinated porphyrin for spectroscopic studies on surfaces, because of a higher fluorescence yield. This should make detection of the fluorescent sub-monolayer easier.

To attach the porphyrin dye to silicon, a route via an acyl chloride porphyrin structure was attempted following various literature reporting of the synthesis of

such chromophores^{168,169,170,171}. Through the reaction of the acyl chloride porphyrin with an alcohol-terminated surface, the chromophore can be covalently bonded to the silicon surface. By using a 1,X diol (where X is the carbon chain length), one end should remain free to bond with the acyl chloride porphyrin. This method also allows the chain length to be changed easily, by simply changing the diol used (see Scheme 8.0). Indeed there are many literature reports which suggest that the reaction of an alcohol group with the silicon surface should result in siloxane formation^{152,172}.



Scheme 8.0 - Reaction scheme for the attachment of protoporphyrin IX

The first step towards attachment of the chromophore was the attachment of the appropriate diol (Scheme 8.0). Literature data suggests that by adding a small amount of base (such as pyridine), an increase in the uniformity of the siloxane monolayer is observed as well as a reduction in the required reaction temperature¹⁵⁴. The alcohol-terminated surfaces were characterised by infrared spectroscopy (Fig. 8.3).

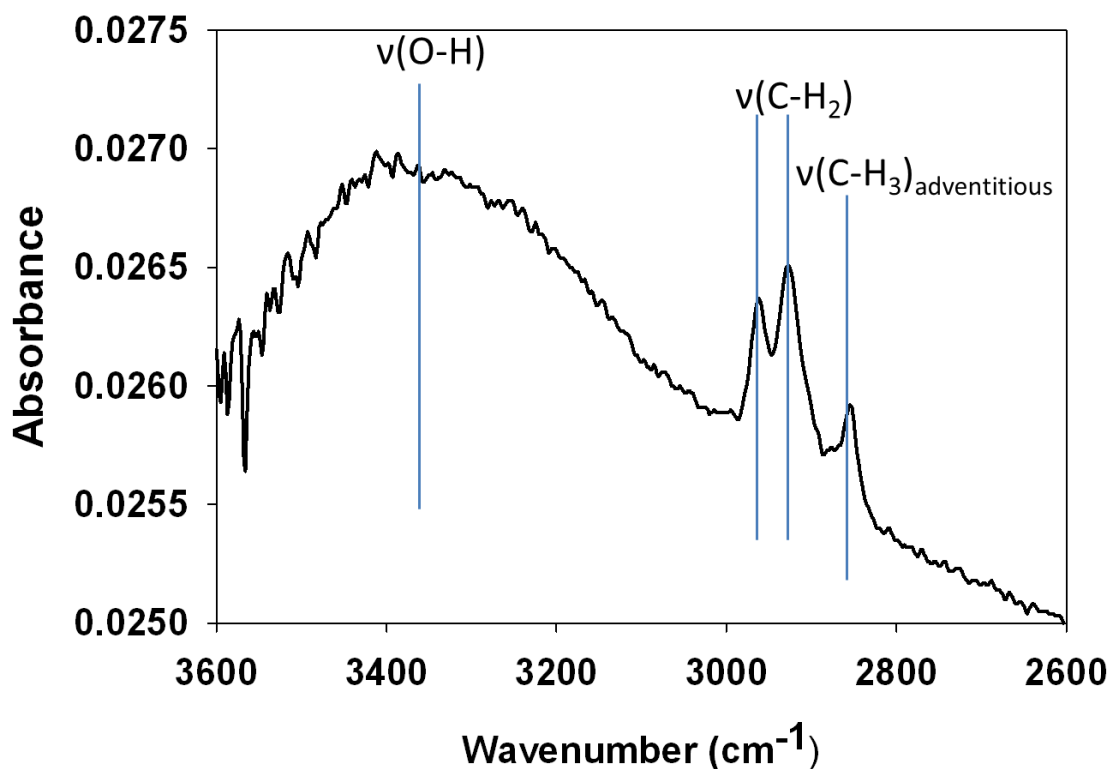


Fig. 8. 3 - Infrared spectrum of the C-H and O-H stretching region of a 1,4 butanediol terminated surface

Infrared spectroscopy confirmed the formation of the required monolayer, allowing subsequent functionalisation of the alcohol chain. XPS spectroscopy was also undertaken, showing one peak for oxygen in the oxygen 1S binding region and a peak for Si-O in the silicon 2P binding region. At lower temperatures, there was no evidence for alcohol or C-H groups being present on the surface by infrared spectroscopy, whilst the temperature had to be increased to $> 150^{\circ}\text{C}$ if pyridine was not added. This is consistent with other literature findings¹⁵².

Routes towards the synthesis of the acyl chloride porphyrin from the disodium salt were investigated through the use of either thionyl chloride or oxalyl chloride. Reactions with thionyl chloride gave a range of products in the mass spectrum, arising from chlorination of the alkene C-H groups as well as the carboxylic acid group of the porphyrin as observed by Mironov *et al.*¹⁷⁰. Therefore a more gentle

chlorination route was attempted using oxalyl chloride. By using only a low excess of the chlorinating agent, and by carrying out the reaction in a nitrogen environment, at room temperature and in darkness, the desired acyl chloride product could be obtained. As acyl chloride functionalities are unstable in ambient conditions, the product was reacted with methanol to give the methoxy ester porphyrin which could be analysed. This was confirmed by NMR (Fig. 8.4) and mass spectroscopy, showing that the required acyl chloride had been produced in the previous step.

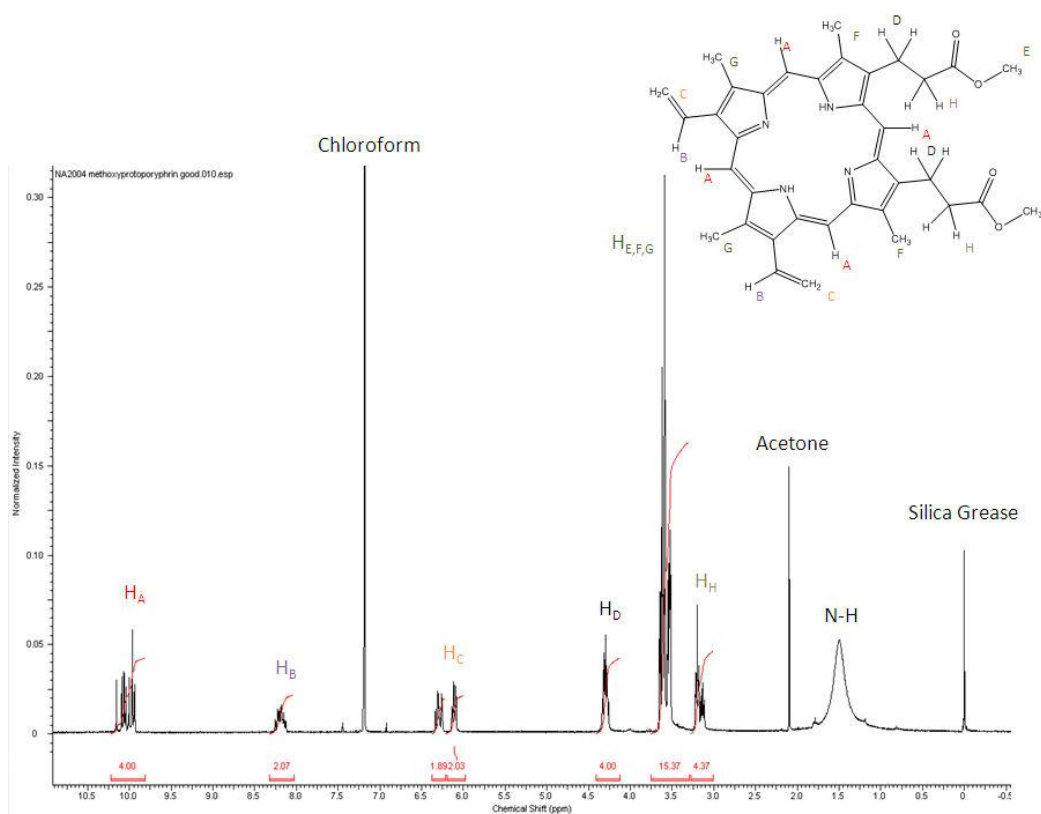


Fig. 8. 4 – ^1H NMR spectrum of the methoxy ester porphyrin synthesised via the acyl chloride protoporphyrin IX

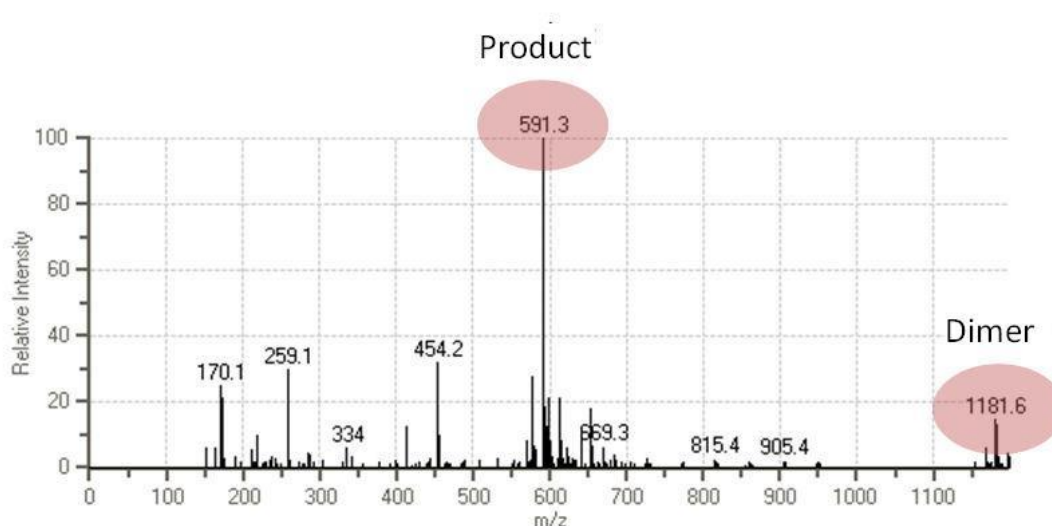


Fig. 8.5 - Mass spectrum of the methoxy ester porphyrin synthesised via the acyl chloride protoporphyrin IX, showing a parent ion peak for the product and a peak for the dimer of the product

Interestingly the mass spectrum of the compound showed two main ion peaks; one for the product and one for the dimer of the product (Fig. 8.5). The NMR spectrum also showed the expected proton peaks, confirming that the methoxy ester had been successfully synthesised. Therefore the reaction between the acyl chloride protoporphyrin and the alcohol terminated silicon surface was attempted.

It was found that to attach the porphyrin to the surface successfully, pyridine should be added to reduce the reaction temperature between the porphyrin and alcohol surface. This allowed a more gentle heating temperature of 80°C, reducing the chance of porphyrin decomposition. These surfaces were then washed with 10 x 5 mL of DCM to remove any physisorbed porphyrin, and infrared, XPS and fluorescence data were obtained.

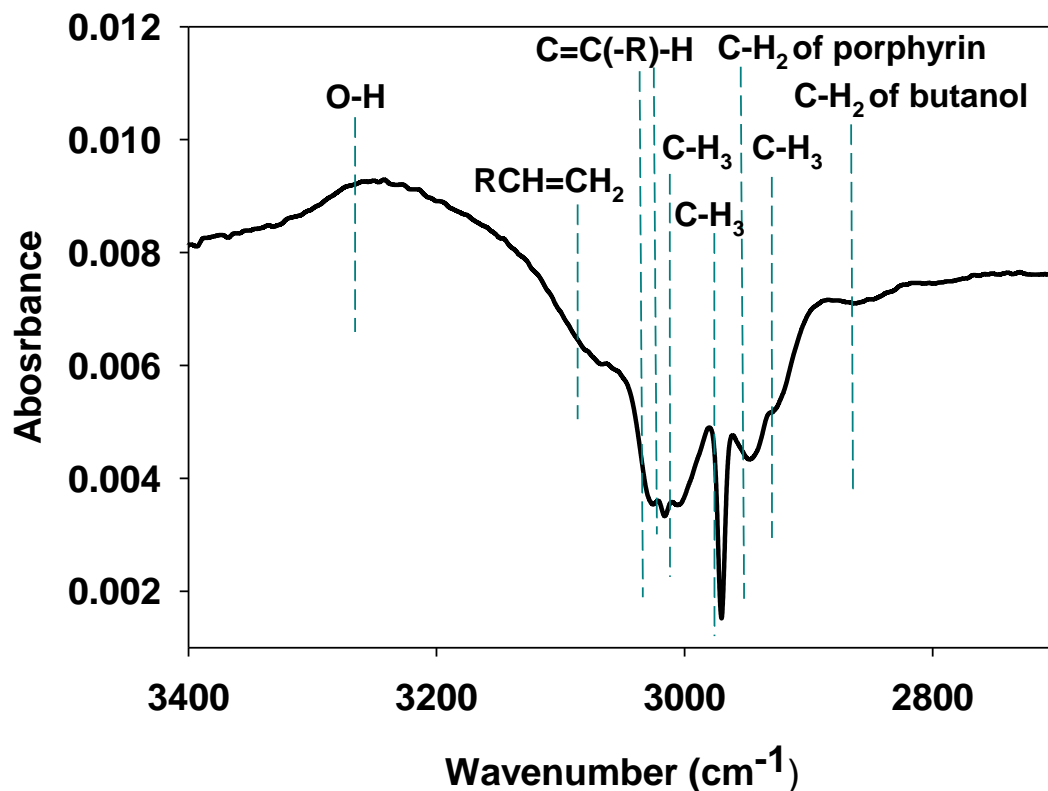


Fig. 8. 6 - The infrared spectrum in the C-H and O-H stretching region of a 1,4 butanediol silicon surface with attached protoporphyrin IX

The infrared spectrum of a 1,4 butanediol treated silicon surface after functionalisation with protoporphyrin IX is shown in Fig. 8.6. The O-H peak of the functionalised surface is clearly visible, showing that unreacted alcohol groups remain. This is due to the much larger porphyrin group blocking unreacted surface sites. The various C-H groups of the porphyrin are clearly visible in the spectrum, as well as the C-H₂ peak of the butanol-terminated surface.

To further confirm the presence of the porphyrin, XPS data was obtained. The nitrogen 1s binding region showed three distinct nitrogen binding energies; one for physisorbed nitrogen, another for iminic nitrogen, and finally a peak for pyrrolic nitrogen (Fig. 8.7 and Fig. 8.8).

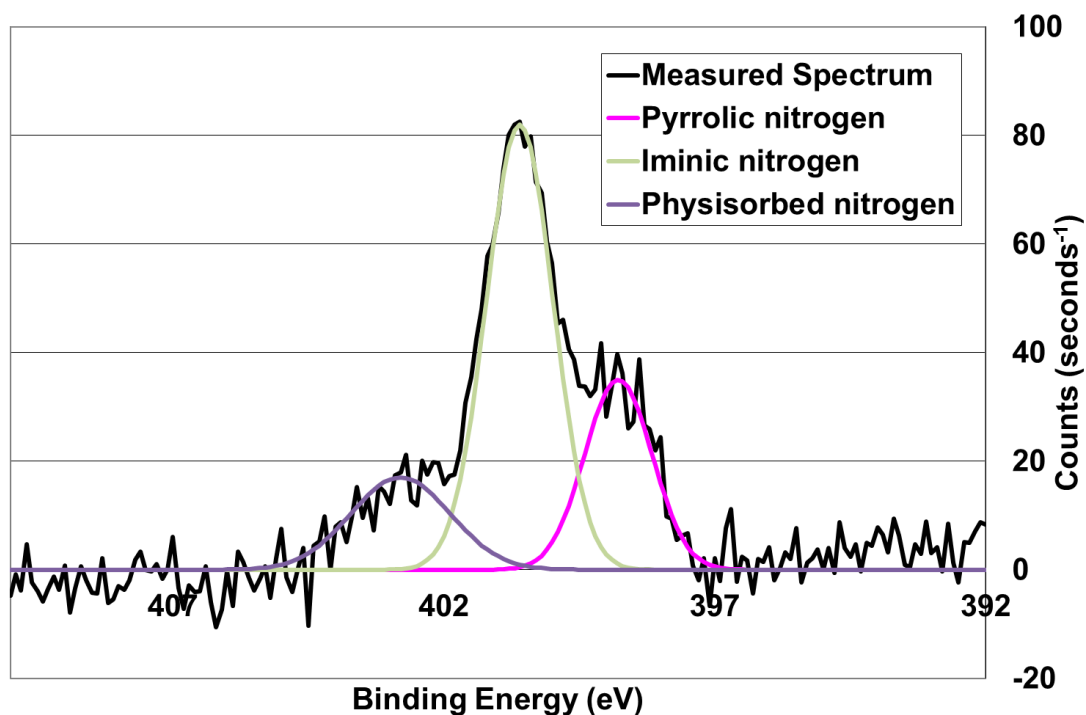


Fig. 8. 7 - XPS spectrum in the nitrogen 1s binding region for a 1,4 butanediol surface with protoporphyrin IX

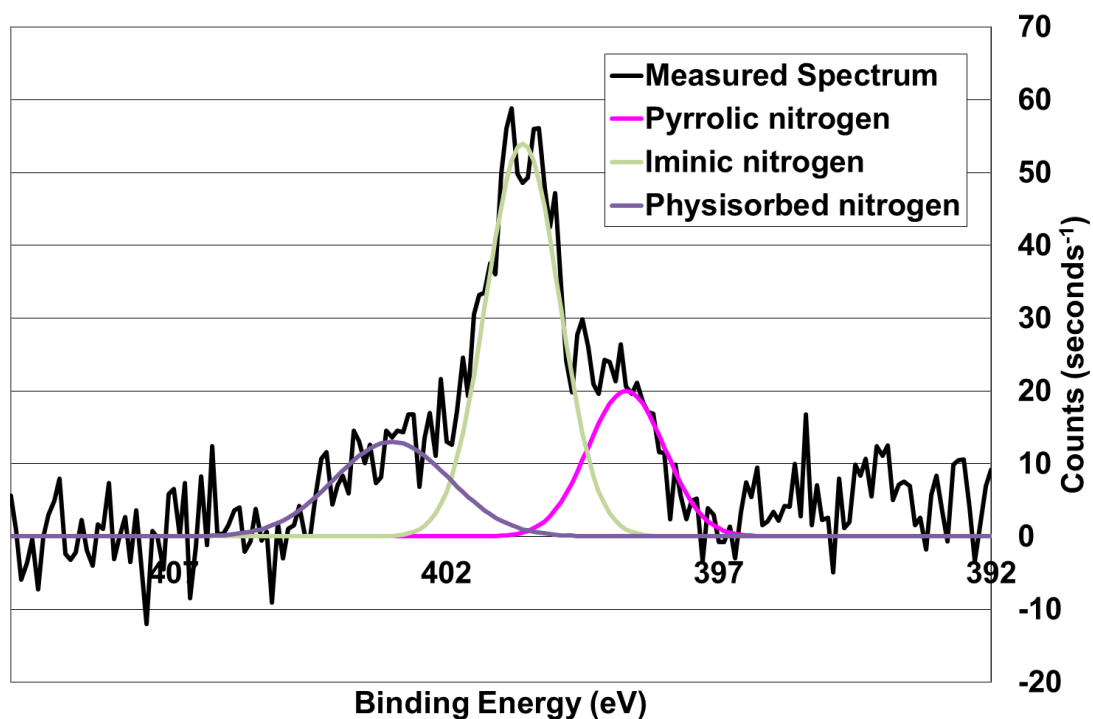


Fig. 8. 8 - XPS spectrum in the nitrogen 1s binding region for a 1,10 decanediol surface with protoporphyrin IX

The two peaks in the nitrogen 1s binding energy matched other literature data for porphyrins^{88,173}. Interestingly, a 1:1 ratio of the integrals of the pyrrolic and iminic nitrogen peaks is not obtained as would be expected. This suggests that a proportion of the surface-attached porphyrin has bound a transition metal ion within the porphyrin ring, reducing the number of pyrrolic nitrogen atoms observed. This metal could be incorporated during the porphyrin processing steps, arising from trace metal impurities found in all solvents.

To confirm the correct assignment of the physisorbed nitrogen, a nitrogen 1s XPS spectrum was obtained for a 1,4-butanediol surface. This should only contain physisorbed nitrogen, and is shown in Fig. 8.9.

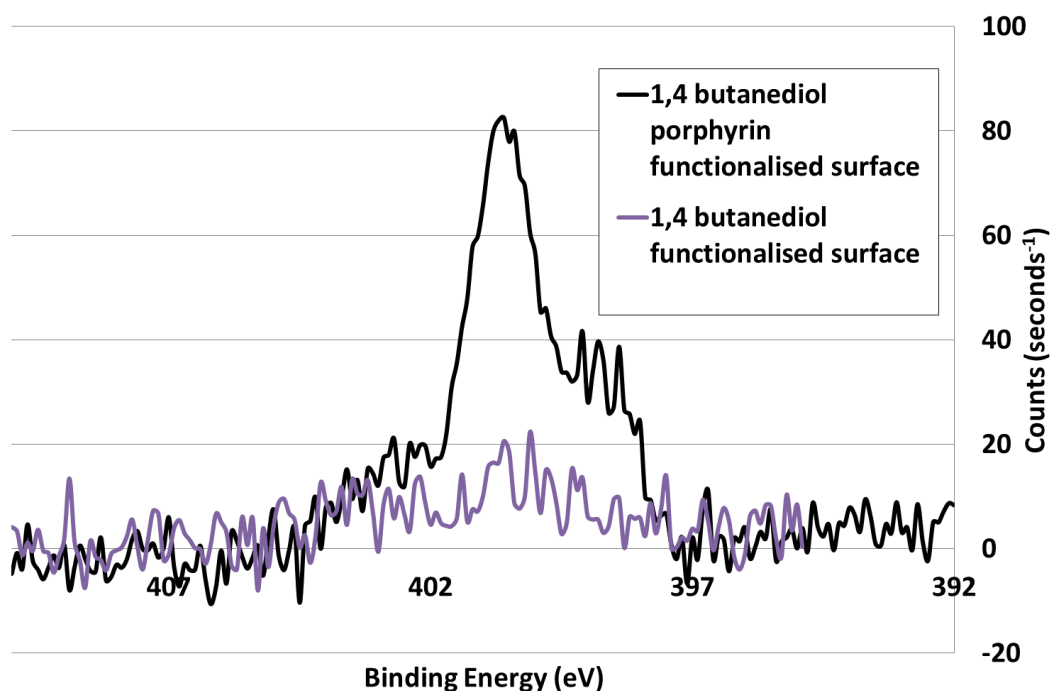


Fig. 8.9 - XPS spectrum in the nitrogen 1s binding region for a 1,4-butanediol terminated surface and 1,4 butanediol porphyrin terminated surface

The fluorescence spectra for each porphyrin-functionalised surface were then obtained (Fig. 8.10). To confirm that the spectrum was indeed due to the attachment

of the porphyrin, a fluorescence spectrum of a 1,4-butanediol terminated surface was also obtained.

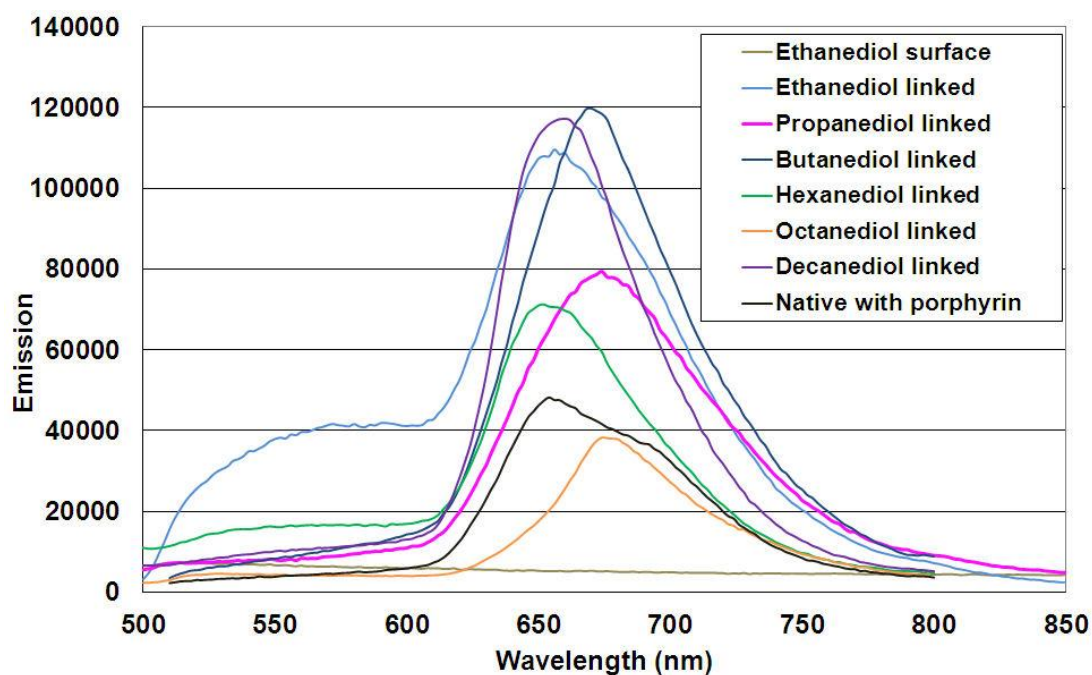


Fig. 8. 10 – Fluorescence spectra of various porphyrin functionalised surfaces, with an alcohol terminated surface for comparison

In the solution-phase fluorescence spectrum of the protoporphyrin IX dye (Fig. 8.2), two fluorescence emission peaks were clearly visible. In Fig. 8.10 only 1 emission peak is visible for the covalently bound porphyrin in the fluorescence spectrum. The likely reason for this is due to the signal from the sub-monolayer of porphyrin dye being very low, such that a large monochromator slit width (2 mm) had to be used. This gives a large band-width, such that the two peaks visible in the solution phase fluorescence spectrum could not be separated in the solid-phase spectrum. Therefore we obtain one peak with a maximum at a wavelength approximately mid-way between the two fluorescence peaks. It was noted that the maximum emission wavelength changes slightly between samples, possibly due to the porphyrin binding different amounts of transition metals as shown by the XPS in Fig. 8.7 and Fig. 8.8.

The fluorescence decay spectra of the various porphyrin-linked surfaces, normalised to a maximum fluorescence intensity of 1, are shown in Fig. 8.11.

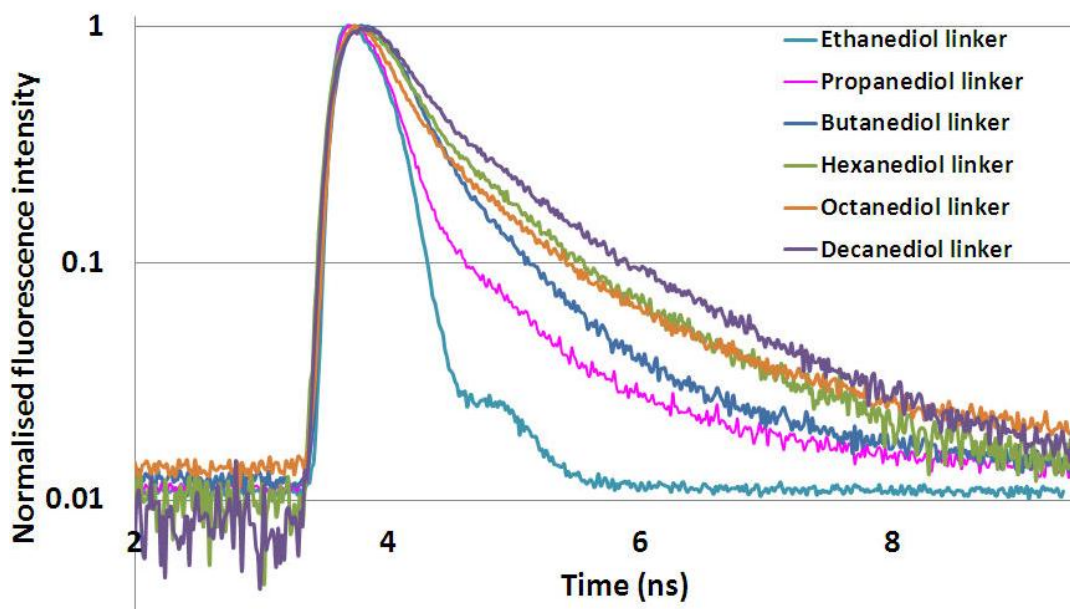


Fig. 8. 11 - The fluorescence decay spectra of various chain-length terminated surfaces functionalised with protoporphyrin IX

The fluorescence decay spectra show that as the fluorophore is moved closer to the silicon surface, the fluorescence decay becomes shorter. The reason for the quenching of the fluorescence is likely to arise from energy transfer from the porphyrin dye to the silicon^{14,18}. As the distance between the dye and surface is reduced, the energy transfer becomes greater and the decay shorter. When the chromophore-surface distance becomes very small (such as for the ethanediol-linked porphyrin), the decay almost matches the decay of the laser pulse, with an extra peak observed in the decay spectrum. As the linker chain-length is increased, the fluorescence decay time increases, although the largest differences in decay rates were for shorter linker groups. Therefore, to have the greatest amount of energy transfer from dye to silicon, the shortest possible chain-length linker groups should be used.

By measuring the time taken for the fluorescence to decay to 10% of the original value, the decay times can be compared between different linker chain-lengths (and for porphyrin-silicon distances using equation 7.1 with similar assumptions).

Carbon chain length	Distance from surface (Å)	Time for fluorescence to decay to 10% (ns)
2	5.87	0.624
3	6.96	0.864
4	8.05	1.296
6	10.24	2.016
8	12.42	1.712
10	14.60	2.339

Table 8.1 - The time taken for the fluorescence to decay to 10% for various porphyrin-linker silicon surfaces

As can be seen in Table 8.1, the fluorescence lifetime increases with distance to the surface. The value for the octanediol porphyrin-terminated surface falls slightly outside this trend because of experimental error. The fluorescence lifetime change is considerable, changing by almost a factor of 4 when moving from ethanediol to decanediol-terminated surfaces. Therefore the porphyrin-silicon distance must be carefully controlled for the production of future, high efficiency devices such as light harvesting solar cells.

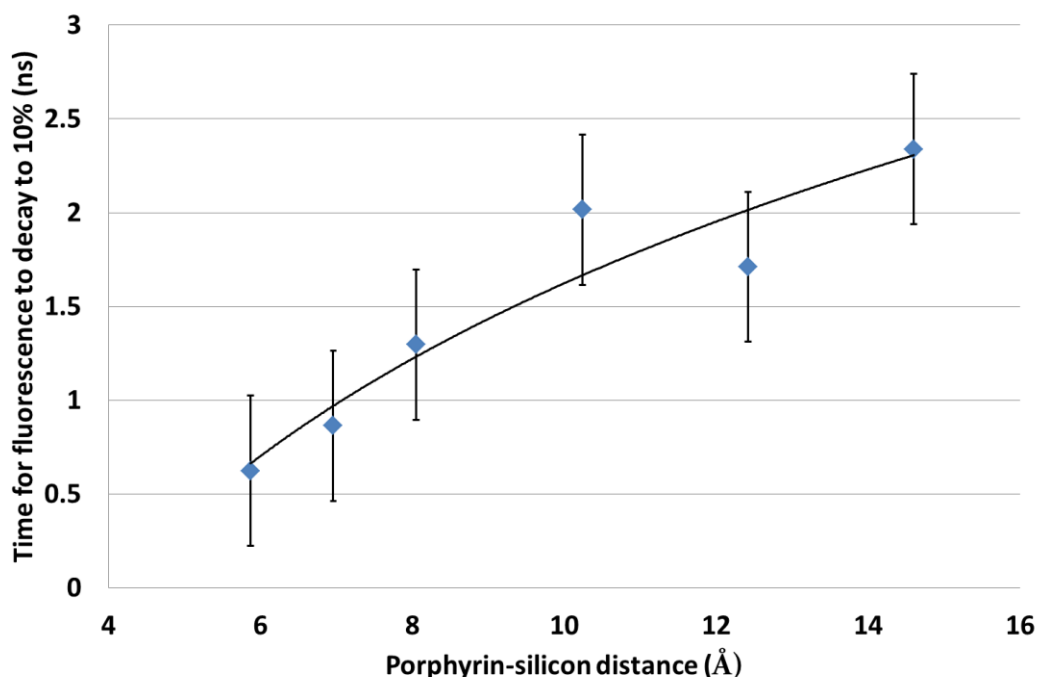


Fig. 8.12 - The fluorescence decay time for various diol linked porphyrin surfaces

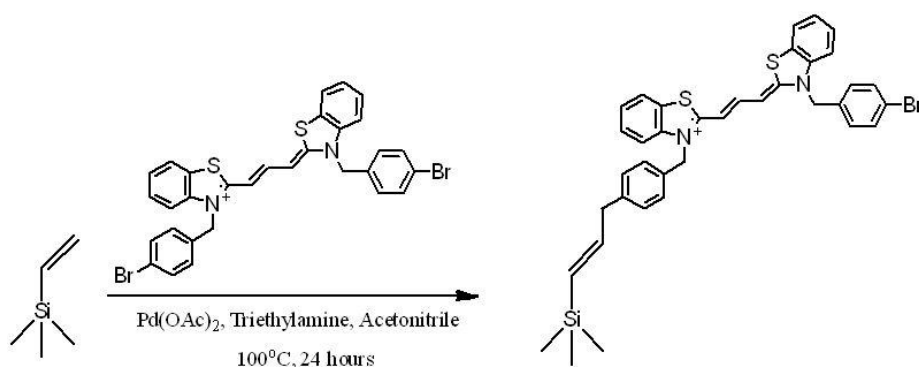
The time for the fluorescence to reach 10% of the initial value is shown for the diol-linked porphyrin-terminated surfaces in Fig. 8.12. It is expected that at distances even greater than the porphyrin-silicon interaction distance that the fluorescence decay should reach a maximum. Therefore the decay time should plateau at high linker chain lengths. By fitting a logarithmic curve to the data, we could obtain the plateau effect whilst passing through each error bar. The error bars were obtained by multiple repeats of the data collection at different spots on the functionalised wafer, and taking the maximum difference between those and the data point obtained for the centre of the wafer.

A downside of this dye attachment method is that no passivating effect is observed on the samples, with recombination lifetime remaining low at around 5-10 μ s. Therefore a route for attaching dyes that could incorporate a passivation layer would be of interest, as this could be used in solar cells for light harvesting / passivation layer hybrid surfaces.

8.3 Attachment of 3,3'-di(4-bromobenzyl)thiadibenzocyanine bromide

To form a passivating layer / light harvesting hybrid monolayer, the alkyl monolayers from Chapter 5 were used as a starting point, since these imparted high levels of passivation. This technique also allows the functionalisation of the silicon surface with alkyl groups, which can be further functionalised by many routes. By palladium cross coupling of terminal alkene surfaces with a halogen-terminated chromophore, the formation of a new carbon-carbon bond between the linker group and the dye can occur³⁰.

It was decided to use the Heck reaction, as this has been shown to work for bromine and chlorine-halogenated chromophores, and is a low temperature process widely investigated in the literature^{93,160,174}. Only trace amounts of the metal catalyst are required, making this a very attractive method for future scale-up (Scheme 8.1).



Scheme 8.1 - The attachment of the cyanine dye through palladium cross coupling

To confirm the successful reaction between the allyl-functionalised surface and the cyanine dye, infrared spectroscopy was undertaken (Fig. 8.13 and Fig. 8.14).

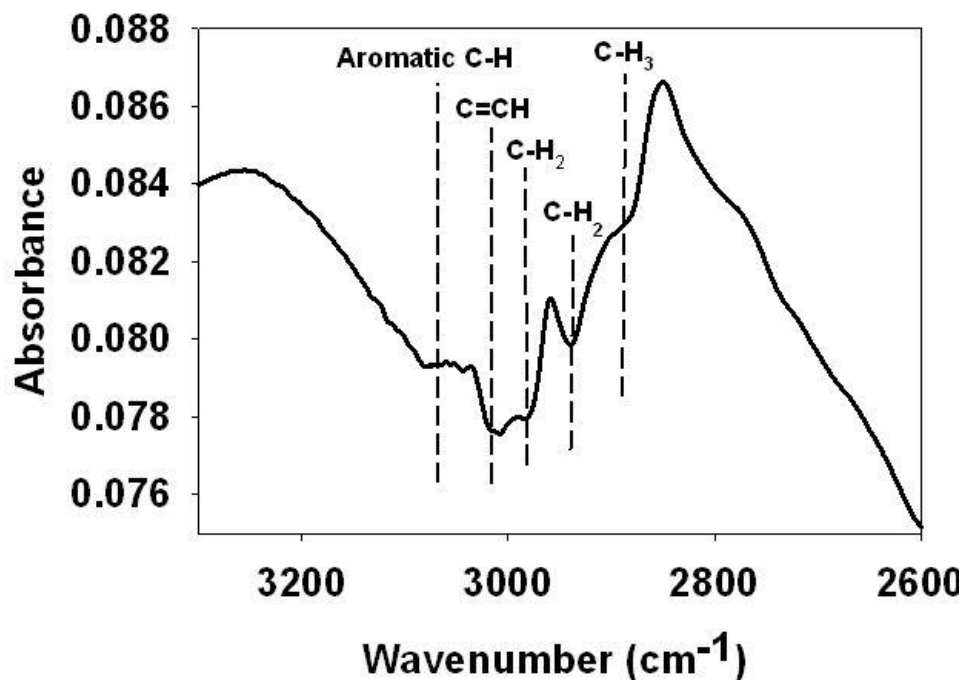


Fig. 8. 13 - Infrared spectrum for the C-H stretching region of the cyanine dye terminated surface

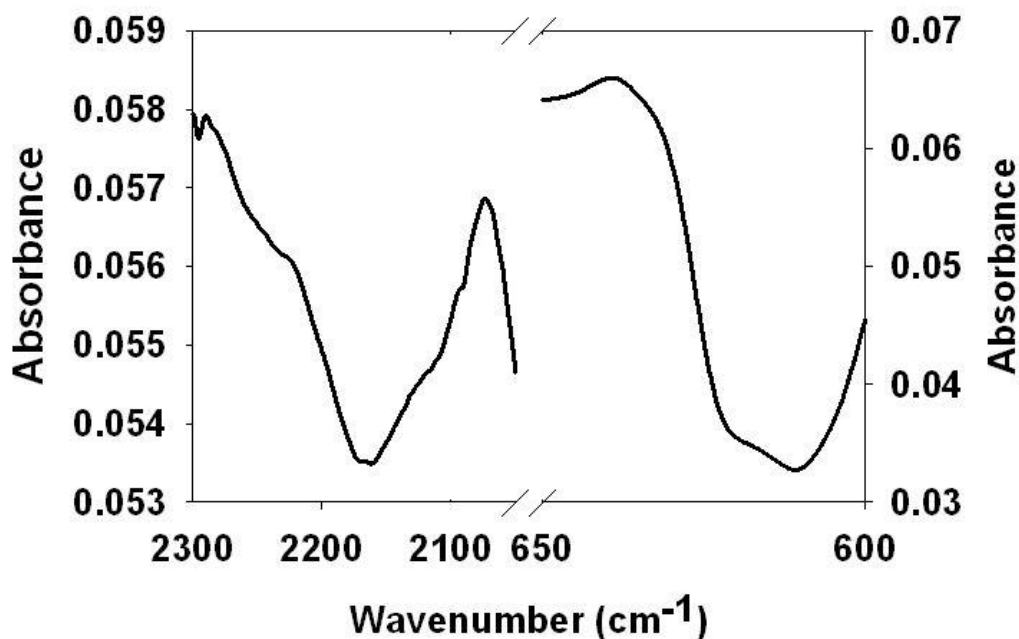


Fig. 8. 14 - Infrared spectrum for the Si-H stretching region (left) and C-Br (right) of the cyanine dye terminated surface

In the C-H stretching region peaks are clearly visible from the surface for aromatic C-H of the cyanine dye, C=C-H of the dye and linker chain, as well as other alkane

C-H stretches within the dye. A Si-H stretching peak was observed at 2169 cm^{-1} , confirming that, after the alkylation and the Heck reaction step, the chlorinated surface had become hydrogen terminated. A peak for the carbon-bromine bond from the cyanine dye was also observed, confirming the presence of the dye.

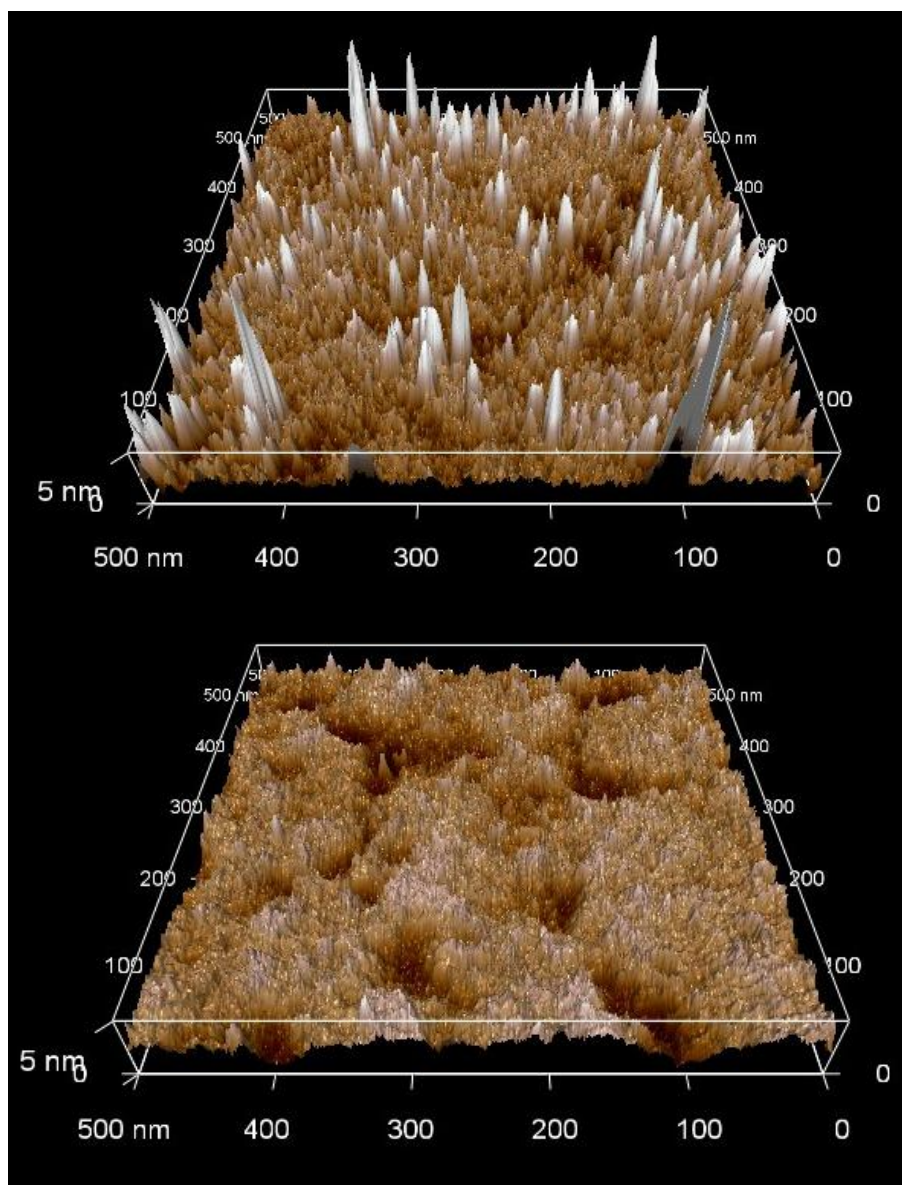


Fig. 8. 15 - Atomic force micrograph of a cyanine dye functionalised surface (top) and the alkyl terminated surfaces (bottom)

Atomic force microscopy was undertaken on the cyanine dye functionalised surface (Fig. 8.15). When compared with a micrograph of an alkyl-terminated surface, many

pronounced features can be seen at a greater height than the surface roughness. These are likely to be dye directly bonded to the allyl terminated surface, with the taller features aggregates of dye forming on top of the initial monolayer.

Once the direct attachment of the cyanine dye to the semiconductor surface had been confirmed, recombination lifetime measurements were undertaken. Before attachment of the cyanine dye, the allyl-functionalised surface showed a recombination lifetime of 74 μs . Upon reaction with the cyanine dye, this had reduced to around 6 μs . The reason for this decrease is likely to be two-fold; the positive charge on the cyanine dye reducing the recombination lifetime by band-bending as of Section 7.2, and the incorporation of palladium metal onto the surface. Heavy metal contamination has been shown to dramatically reduce recombination lifetimes due to the incorporation of surface states close to the centre of the band energies^{175,103}. The recombination lifetime did not change after multiple washes in acetonitrile, confirming that the metal contamination could not be removed by washing.

To see if the recombination lifetime could be increased by the use of a longer carbon-chain linker, 1-decene-10-magnesium chloride was reacted with the chlorinated wafer. This results in a decene-terminated surface, allowing the alkene group to be further functionalised. After reacting with the cyanine dye as with the allyl surface, the recombination lifetime was 9 μs . Although the recombination lifetime was higher as the charge and heavy metal centres are moved away from the surface, this was not suitable for our studies as we wish to try to get the chromophore as close to the surface as possible, as shown in the porphyrin attachment studies. The

absorption spectrum of the cyanine dye used for the attachment is shown in Fig. 8.16.

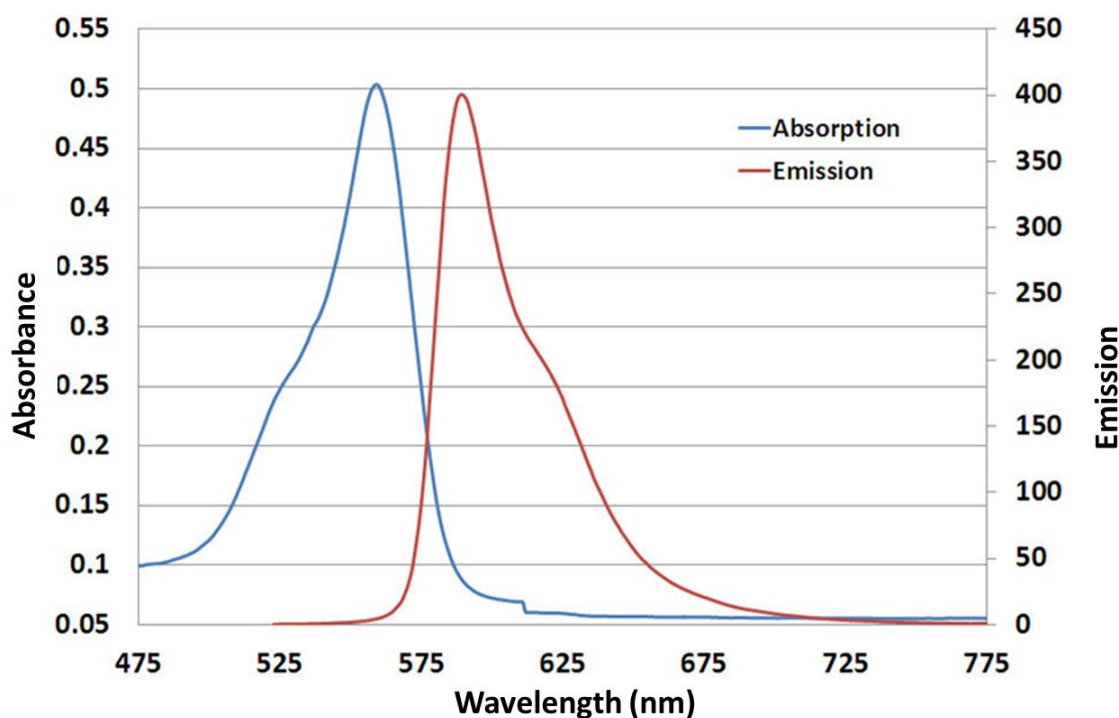


Fig. 8. 16 - Absorption spectra of the cyanine dye

No fluorescence measurements (spectra or decays) could be performed of the cyanine dye attached to the silicon surface due to the lack of availability of a laser at the correct wavelength for excitation. In the future a new technique which does not involve heavy metals with a dye that absorbs at around 445 nm (the wavelength of the excitation laser) should be investigated.

8.4 Conclusions

The successful attachment of two different types of dye (cyanine dye and porphyrin dye) have been attached by two different methods (siloxane/alcohol technique and via an alkene-terminated surface using palladium cross coupling). These were characterised by infrared spectroscopy, with further analysis (XPS, fluorescence spectroscopy) on the more successful porphyrin-functionalised surface.

On the porphyrin-functionalised surfaces, it was found that the closer the chromophore was moved to the surface, the shorter the fluorescence lifetime. By using ethanediol as the linker chain, the decay was around 0.6 ns. At these close distances the contributions for the laser decay became visible, indicating that the fluorescence lifetime was in the region of the laser decay timeframe. To have the highest energy transfer between the dye and the silicon substrate, the shortest possible organic linker chain should be used.

X-ray photoelectron spectroscopy (XPS) confirmed the presence of porphyrin on our surface. From the integrals for the pyrrolic and iminic nitrogen peaks, it appears that some porphyrin groups have bound a metal atom. This is likely to have come from trace metal impurities present in the solvents used.

As the porphyrin attachment route showed no surface passivation, a secondary route was attempted involving an allyl-functionalised surface which showed good passivation properties. Upon addition of the cyanine dye and palladium acetate, the chromophore was attached to the functionalised surface and the recombination lifetime decreased from around 74 μ s to 6 μ s. This was attributed to the incorporation of recombination centres are roughly half band-gap caused by the heavy metal contamination. Another reason could be due to the positive charge on

the cyanine dye, which could reduce the recombination lifetime as observed in Chapter 7.

To build high efficiency devices, both a well-passivated linker layer and high dye-to-silicon energy transfer are required (a small chromophore-to-semiconductor distance). Therefore a different technique would need to be found to functionalise the organic alkyl layers that produce passivation and which does not involve heavy metal catalysis which reduces the recombination lifetime significantly.

9. Conclusions and Further Work

9.1 Conclusions

The work described in this thesis aims to improve the efficiency of thin crystalline silicon solar cells by attachment of organic molecules to the silicon surface, leading to two principal aims:

- Passivation of the silicon surface, reducing surface recombination
- Enhancement of silicon photoexcitation via light harvesting in terms of Förster-like energy transfer between dye molecules and silicon

Two main methods of passivation were investigated; a two-step chlorination-alkylation technique and the attachment of charged monolayers. The first step towards passivation for both techniques is the removal of surface oxide. It was found to achieve atomically smooth, hydrogen terminated surfaces degassed ammonium fluoride should be used^{35,57,81}. Attempts to remove the oxide layer with hydrofluoric acid lead to surface roughness, with a reduction in recombination lifetime.

It was found that the two-step chlorination-alkylation technique incorporates charge into the surface, causing band-bending. This has the effect of reducing the majority carrier concentration at the surface which, when coupled with a reduction in surface states, leads to well passivated surfaces. The lifetime increased from around 4.5 μs up to 250 μs . It has been shown that a reduction in surface states on its own does not

directly lead to long lifetimes – both the hydrogen and chlorine-terminated surfaces were in an almost flat-band state but did not show a considerable increase in recombination lifetime.

The surface coverage (and passivation imparted) on the silicon surface reduces with chain length due to steric interactions between the alkyl groups. As the steric bulk of the alkyl group is increased (for example isopropyl and tertiary butyl), the coverage, resistance to oxidation and recombination lifetime decrease. This was in the range of literature values obtained²⁹. Therefore to achieve well passivated samples, small alkyl groups such as methyl are preferential.

Charged monolayers were bound to the silicon surface through the use of a siloxane bond. It was found that a negative charge had a passivation effect on the n-type silicon surface, whilst a positive charge reduced the recombination lifetime observed. The observed lifetime increase was lower than for other passivation techniques, giving a maximum lifetime of around 30 μ s. This was attributed to low monolayer charge, forming a low charge at the silicon surface. As the negative charge was moved closer to the silicon surface, an increase in the recombination lifetime was observed, as well as an increase in the surface photovoltage (band bending). This decreases the majority carrier concentration at the surface, increasing the recombination lifetime. The as-synthesised sample was in an almost flat-band state, confirming the reduction in surface states. Therefore the contributions from the surface states and charging could be separated by generation of the charge in situ (by immersion in base).

After multiple immersions in acid and base, the recombination lifetime decreased. This was due to surface oxidation and a reduction in the monolayer coverage,

reducing the magnitude of the charge and moving the charge further from the silicon surface.

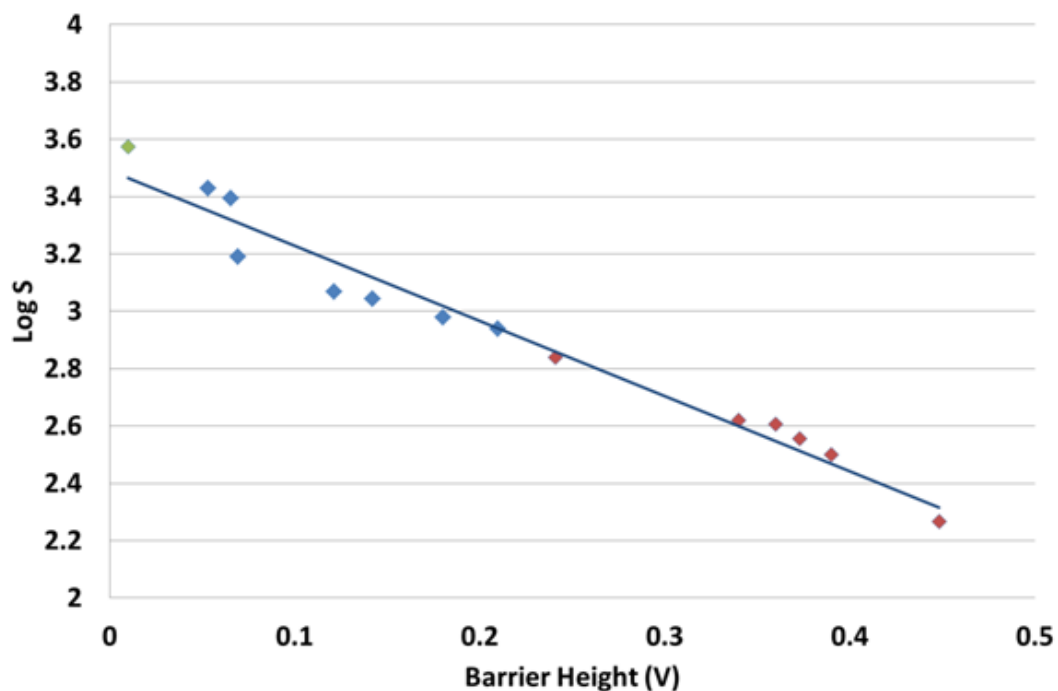


Fig. 9. 0 – Comparison of barrier heights measured by Kelvin probe with the surface recombination velocity for chlorine terminated-surfaces (\diamond), carboxylic acid-terminated surfaces (\diamond) and alkyl-terminated surfaces (\diamond)

It has been shown in Chapter 7 (Fig. 9.0, above) that the barrier height as measured by the Kelvin probe and the surface recombination velocity are linked for all samples synthesised in this thesis. The surface recombination velocity is dependant only upon surface charge and not on the attached functionality, as both Si-C and Si-O bonded monolayers have shown to induce passivation through charging. This is contradictory to the previous work by Lewis *et al.*¹²⁹ where it was stated that the passivation is due to the reduction in surface states, resulting in flat surface bands. In Chapter 2 it was stated that upon passivation, the number of surface states reduces from around $10^{12} \text{ cm}^{-2} \text{ eV}^{-1}$ to around $10^{10} \text{ cm}^{-2} \text{ eV}^{-1}$. As a significant number of traps are present even in well passivated samples, and a trap density in the ppm range can

be observed through recombination lifetime measurements, this is not likely to be the passivation route.

For the synthesis of well passivated surfaces, the barrier height (or SPV) should be increased, reducing the charge-carrier concentration at the surface. A similar effect is observed through charging of the surface with iodine in ethanol solutions or corona discharging. Until now it was unclear as to the cause of the passivation effect due to the chlorination-alkylation method, especially as other alkyl monolayers do not report a high recombination lifetime. Through the detailed studies of the surfaces synthesised in this report, it can now be suggested that the two-step chlorination-alkylation technique reported in this thesis produces well-passivated samples due to charging of the surface during the alkylation (Grignard) step.

A novel method for the determination of the surface recombination velocity was investigated using the Kelvin probe. By modification of the ideal diode equation and measuring the surface voltage at different photogenerated currents (from the photon flux value), the surface dark current density can be extracted. This can be linked to the surface recombination velocity and recombination lifetime through equations found in the literature. The obtained values for surface recombination velocity correlated well with the values obtained through more traditional methods (Sinton WCT-120).

By measuring the surface voltage change over the sample area, a 2D map of the lifetime can be obtained. Very few recombination lifetime characterisation methods can perform this function, making this a useful technique in surface characterisation^{50,103,141}.

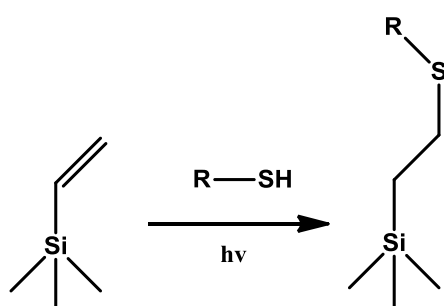
To investigate possible energy transfer between a dye and silicon, porphyrin chromophores were attached to the silicon surface through a variable chain-length linker. By varying this single parameter, we could study the energy transfer rate by monitoring the distance dependence of the fluorescence decay. The existence of energy transfer is supported by an observed reduction of fluorescence lifetime with a decreasing chromophore-silicon distance. We have observed a logarithmic relationship between the fluorescence decay and distance from the silicon surface. We have also found that to achieve efficient energy transfer, the distance between the chromophore and silicon should be less than 6 Å.

Observation of electron-hole pair generation in silicon, however, was hampered by a lack of surface passivation associated with the porphyrin attachment. To overcome this, a secondary route was attempted using an allyl terminated surface achieved through the two-step chlorination-alkylation technique. This monolayer was subsequently functionalised with a cyanine dye by palladium cross coupling. Although successful, the lifetime decreased significantly from 70 μs to 4μs after secondary functionalisation due to the incorporation of palladium on the silicon surface.

9.2 Future Work

Future work on this project would focus on the incorporation of passivating layers with the chromophore attachment. This would bring us a step nearer to achieving the goal of manufacturing a thin-silicon solar cell device with high efficiencies. The passivating linker chain can be incorporated using the two-step chlorination-alkylation technique explored in this thesis. Many different groups can be attached

via this technique, but for secondary functionalisation the route with the chance of greatest success would be via a terminal alkene linker which shows a high degree of passivation^{30,78,176}. Further functionalisation of the alkene-terminated surfaces should then be possible through either isothiocyanate, carbene or thiol click chemistry^{96,177}. Multilaminar systems can then be made possible through the formation of Langmuir-Blodgett layers on top of the chromophore functionalised silicon surface^{20,178,179}. This should allow the absorption and energy transfer of a wide range of the incident spectrum.



Scheme 9.0 - The thiol-ene reaction for the synthesis of secondary functionalised passivating monolayers

The method shown in Scheme 9.0 has been shown to work for tetravinylsilanes¹⁷⁷, so should be able to produce the functionalised monolayers. The R group allows for added flexibility, such that the dye can be changed with the requirements of the system (for example to emit close to the silicon bandgap energy). This also gives high yields, so should be able to achieve the desired high surface coverage. A small amount of photoinitiator can be added (1 mol % of benzophenone) to aid the reaction, which should complete within 2-4 hours.

A suitable dye might be a Ru(II) pyridine complex as reported by Ohlsson *et al.* (Fig.9.1)¹⁸⁰

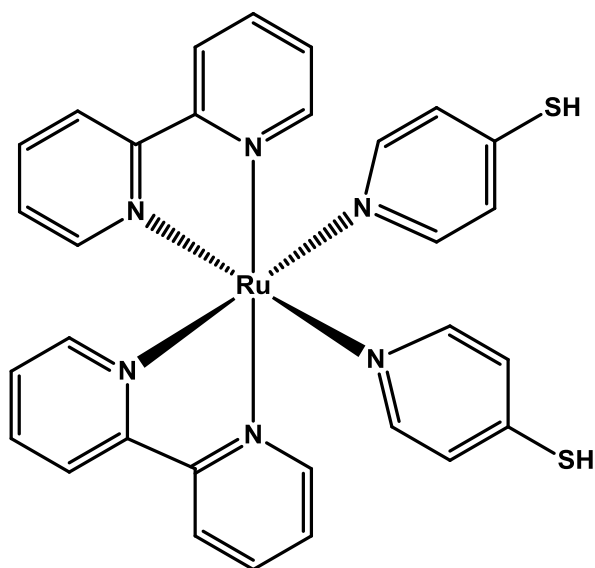


Fig. 9. 1 - The Ru(II) pyridine complex prepared by Ohlsson *et al.*

This complex has an absorption maximum at 460 nm, and was prepared from $\text{Ru}(\text{bpy})_2\text{Cl}_2 \cdot 2\text{H}_2\text{O}$ and pySH. Refluxing in a 1:1 mixture of ethanol and water for 16 hours, followed by addition of NH_4PF_6 affording the solid of cis-Ruthenium-bis[2,2'-bipyridine]-bis[4-thiopyridine]-bis[hexafluorophosphate].

Singh *et al.* subsequently used the ruthenium-based dye on zinc oxide nanoparticles for use in dye-sensitized solar cells¹⁸¹. Therefore the dyes should be stable enough to be used in subsequent reactions.

10. Experimental

10.1 Etching and Bulk Lifetime

10.1.1 Etching Experiments

All chemicals used were purchased anhydrous from Sigma-Aldrich and used as received. Silicon wafers (10.5x10.5mm squares, n type, $25 \Omega \text{ cm}^{-1}$, 500 μm thickness, double side polished) were cleaned by immersion in the following solutions; hydrogen peroxide in sulphuric acid (1:3, 30 minutes)⁹⁴, ammonium hydroxide and hydrogen peroxide in de-ionised water (1:1:5, 30 minutes)¹²⁵ and hydrochloric acid and hydrogen peroxide in de-ionised water (1:1:6, 30 minutes)¹²⁶ with a thorough rinse in de-ionised water between each step. These cleaning steps remove both organic and inorganic contaminants from the surface of the wafer.

The freshly cleaned sample was then immersed in a solution of hydrofluoric acid (2-48%, diluted from 48% solution with de-ionised water). Wafers were then dried under a flow of argon and briefly transported under an argon atmosphere for ellipsometry and recombination lifetime measurements.

10.1.2 Bulk Lifetime Measurements

The silicon wafers (either 10.5 x 10.5 mm squares, n-type, $25 \Omega \text{ cm}^{-1}$, 500 μm thickness, Siltronics or 10 x 10 mm squares, n-type, $2500 \Omega \text{ cm}^{-1}$, 300 μm thickness, University Wafers, both with a guaranteed lifetime $>1000 \mu\text{s}$) were cleaned as above.

A specially constructed glass sample holder (Fig. 10.0) was placed on the recombination lifetime tester, and calibrated such that when the sample was in the holder a similar value of the lifetime was achieved as when the sample was measured normally. The specially constructed sample holder allowed the passivating solution to completely surround the sample, whilst adding minimal distance from the sample to the lifetime tester sensor.

Once calibrated, either the HF solution (1-48%), iodine in methanol solution (0.09 mol/L)⁷⁵ or quinhydrone in methanol solution (0.01 mol/L)⁶⁶ was added to the sample holder until the wafer was only just submersed. Lifetimes were then measured for times between 5 and 1000 seconds at 5 second intervals using the transient mode on the Sinton WCT-120 wafer lifetime tool.

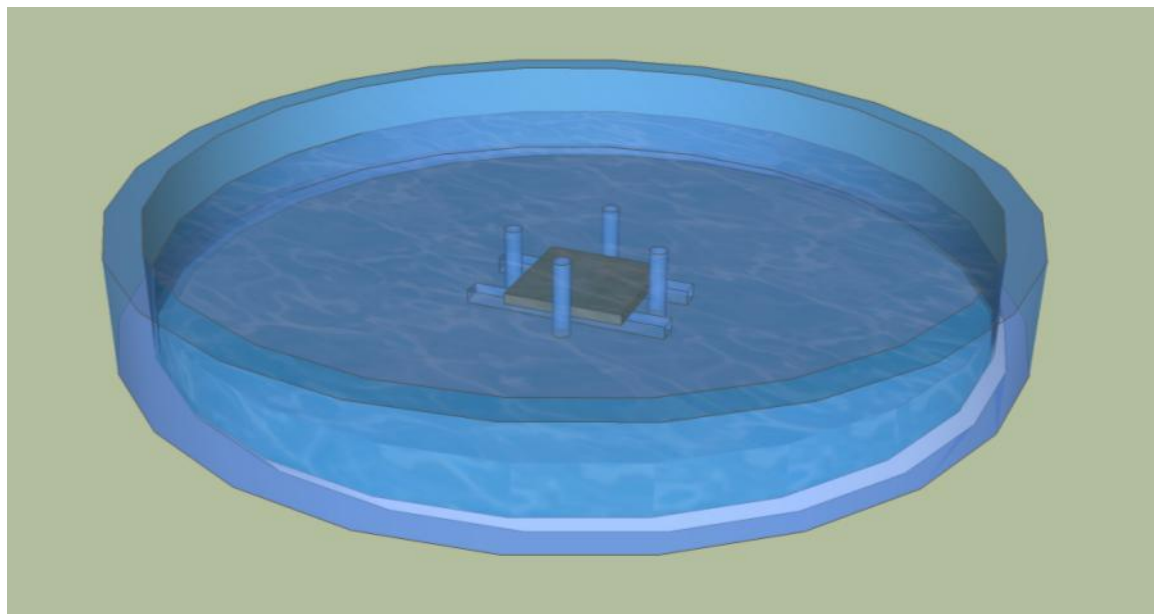


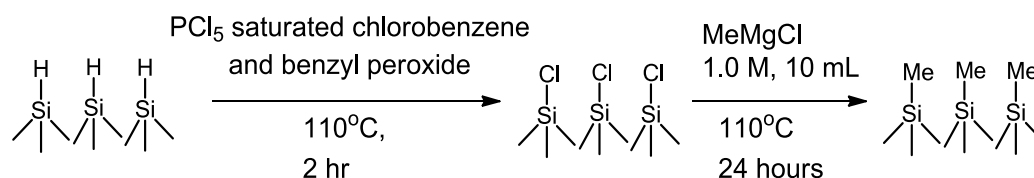
Fig. 10. 0 - Sample holder for measurements of bulk lifetimes

10.2 Alkylation of Silicon Wafers

The silicon sample (10.5 x 10.5mm squares, n-type, $25 \Omega \text{ cm}^{-1}$, 500 μm) was cleaned in a hydrogen peroxide in sulphuric acid (1:3, 45 minutes) solution, followed by a thorough rinse in de-ionised water.

Once the sample had been thoroughly cleaned, the surface of the silicon was etched in semiconductor grade ammonium fluoride (40% in water, degassed with N₂, 15 minutes) to remove the native oxide layer and hydrogen-terminate the surface. After drying under flowing nitrogen, the sample was passed into a nitrogen filled glovebox for functionalisation.

The hydrogen-terminated silicon was immersed in a saturated solution of phosphorus pentachloride in chlorobenzene (110°C, 1.5 hours) to which a few grains (<1mg) of benzyl peroxide were added as a radical initiator. The sample was then washed in chlorobenzene and tetrahydrofuran (THF), followed by immersion in a 1M Grignard solution (XMgCl where X= Me, Et, Bu, ⁱPr, ^tBu or allyl) in THF (110°C, 20 hours). After washing in THF, methanol and sonication in a methanol / acetic acid (10:1) solution, spectroscopic measurements were taken (Scheme 10.0).



Scheme 10.0 - Reaction scheme for the alkylation of silicon surfaces

To produce chlorine-terminated surfaces by the chlorine gas method, the samples were cleaned and hydrogen-terminated as above. After transfer to a purged stainless steel reactor, a 10% chlorine gas in nitrogen mixture was passed over the sample, and heated such that the gas outlet temperature was 90°C. After allowing to cool for 30 minutes whilst purging with nitrogen, the sample was transferred to a nitrogen-purged container and spectroscopic data obtained.

10.3 Passivation by Charge Anchorage

10.3.1 Choline Iodide Terminated Surfaces

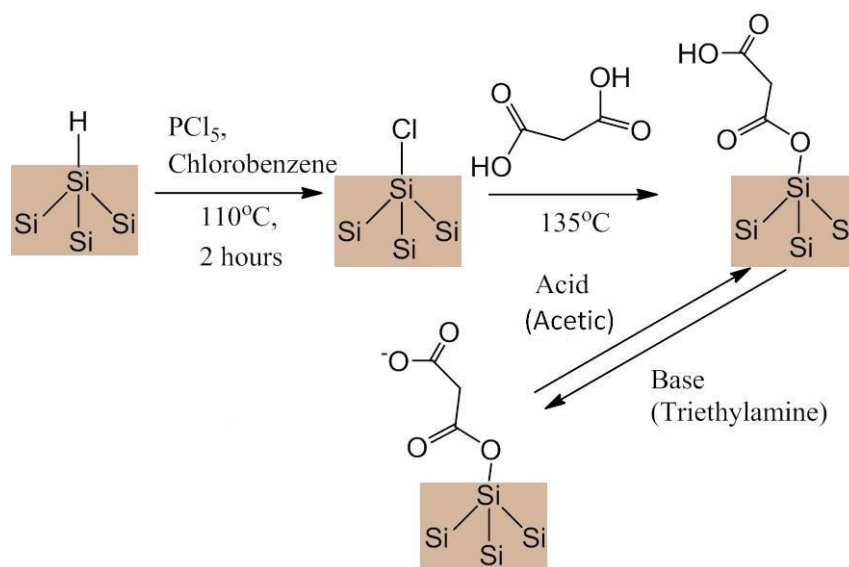
Silicon samples were cleaned, etched and chlorinated as of Section 10.2. After washing the sample in chlorobenzene and tetrahydrofuran, the wafer was allowed to dry. Solid choline iodide was added to the sample, which was heated to 260°C for 24 hours. After cooling and washing in THF and methanol, spectroscopic measurements were taken.

10.3.2 Carboxylic Acid Terminated Surfaces

Silicon samples were cleaned, etched and chlorinated as of Section 10.2. After a chlorobenzene and tetrahydrofuran wash, the appropriate solid dicarboxylic acid was added and the sample heated to either 190°C or 5°C below the decomposition temperature, whichever was lower (Care should be taken for the shorter carbon chain length carboxylic acids, as the decomposition temperature is low. At or above this temperature, carbon dioxide can be given off resulting in trapped pressure and a potential explosion. To minimise this risk, the minimum amount of the acid to completely cover the wafer when melted was used). Once the dicarboxylic acid had melted, the sample was left for 48 hours after which the molten acid was decanted. After cooling, the wafer was removed from the nitrogen filled glovebox and sonicated in methanol.

The functionalised surface was then placed on the calibrated Sinton lifetime tester and measured in quasi steady-state mode prior to charge studies. The sample was then immersed in triethylamine for 10 seconds to deprotonate the acid group, after which the lifetime was measured. After a brief water wash, the sample was immersed in glacial acetic acid for 10 seconds, and dried with a nitrogen stream to

return the sample to the protonated state. After measuring the lifetime, the immersion steps were repeated (Scheme 10.1).



Scheme 10.1 - Functionalisation of the silicon surface with Malonic acid, including the charge generation step

10.4 Attachment of Dyes to Silicon

10.4.1 Attachment of 3,3'-di(4-bromobenzyl)thiadibenzocarbocyanine bromide

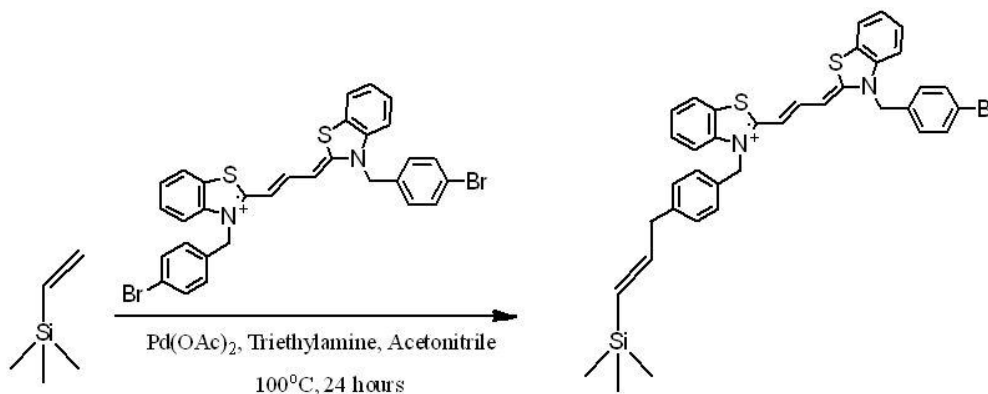
Silicon samples were cleaned, etched and chlorinated as of Section 10.2. After a chlorobenzene and tetrahydrofuran wash, either allyl magnesium chloride (1M in THF, from Sigma-Aldrich) or 1-decene-10-magnesium chloride (synthesised) was added and heated at 110°C for 24 hours.

To synthesise 1-decene-10-magnesium chloride, 1,10-dichlorodecane (10g, 10mL, 0.047 moles) was taken and added dropwise to a potassium tertbutoxide solution (6.86g, 0.0611 moles) in THF⁹⁴. After stirring at room temperature for 3 hours, the solvent was removed under vacuum. Water was added to the resulting residue, and the aqueous phase extracted with ether (3 x 50 mL) before removing the ether under vacuum. The resulting mixture was separated by distillation, and the resulting liquid

characterised by NMR and mass spectrometry, showing a 1:15 ratio of the 1-chloro-10-decene : 1,10-dichlorodecane.

After transferring the 1-chloro-10-decene to a nitrogen purged glovebox, magnesium metal (1g) and THF (10 mL) were added. To this a small amount of iodine (0.1g) was added and the resulting mixture heated to 90°C for 20 hours. The resulting light-yellow solution was filtered to remove any unreacted magnesium before using in the alkylation of the wafers¹⁸². The wafer was then alkylated through the previous experimental method (See Section 10.2).

After washing in THF and acetonitrile, the 10x10 mm wafer was taken and immersed in a solution of 3,3'-di(4-bromobenzyl)thiadibenzocyanine bromide (0.01 g, 0.0142 mmoles, synthesised by Georgie Halloworth) in 1:10 triethylamine : acetonitrile (5 mL total). To this, palladium acetate (<0.01g) was added and the resulting solution heated to 100°C for 24 hours in a pressure vessel (Scheme 10.2). The wafer was then removed from the glovebox, and sonicated in acetonitrile (10 x 5 mL, 5 minutes per cycle) followed by methanol (2 x 5 mL, 5 minutes per cycle). After drying under nitrogen, infrared spectrometry, atomic force microscopy and recombination lifetime measurements were performed on the samples.

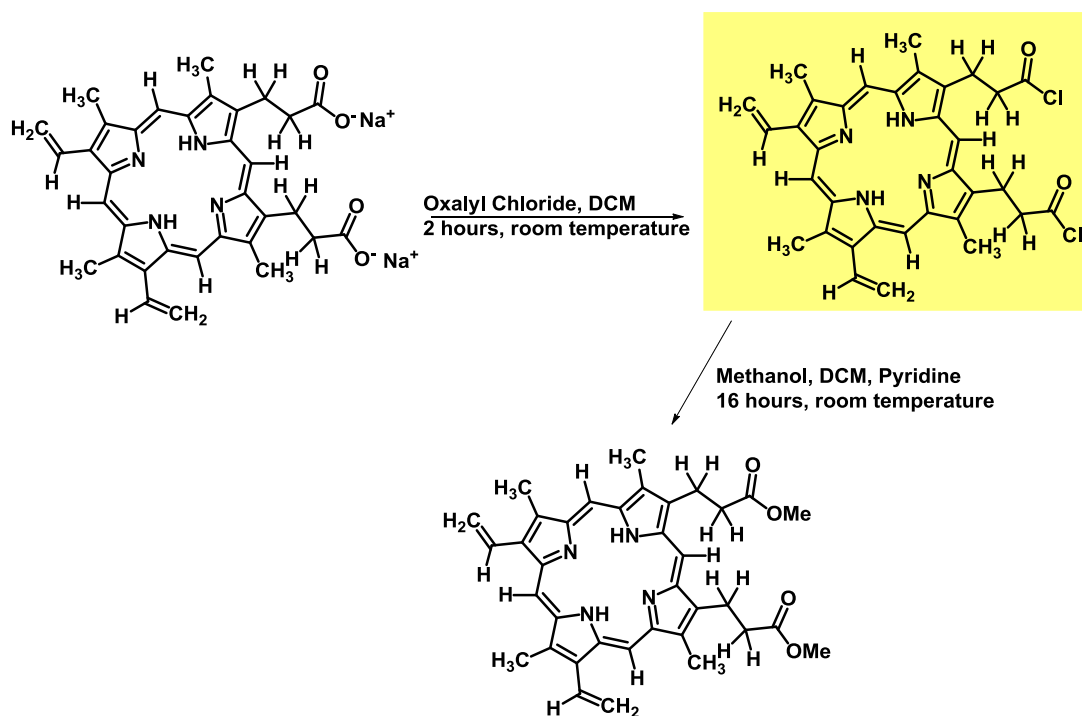


Scheme 10.2 - Reaction scheme for the attachment of cyanine dyes to silicon

10.4.1 Synthesis of Acyl Chloride Protoporphyrin IX

All porphyrin containing solutions were kept in darkness and under nitrogen. To a solution of protoporphyrin IX disodium salt (250 mg) in dry DCM (20 mL), 2.5 mL of a 2M solution of oxalyl chloride (0.7616 moles) was added and the solution stirred for 2 hours. After removal of the solvent under vacuum, the green powder was transferred to a glovebox for subsequent reactions.

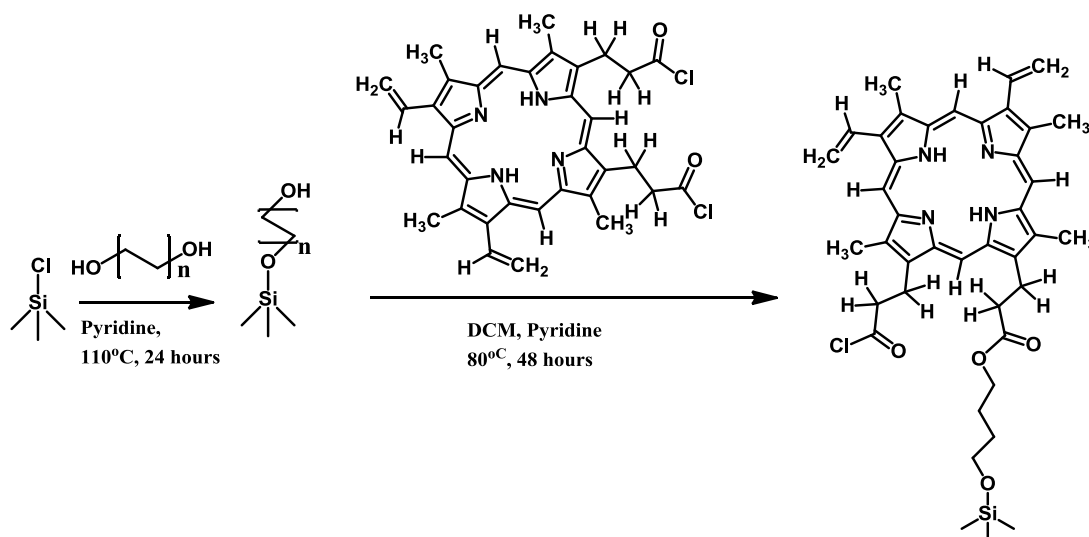
To confirm the presence of the acyl chloride porphyrin, the product was reacted with methanol (5 mL) in DCM (10 mL), with the addition of pyridine (1 mL) for 16 hours at room temperature (Scheme 10.3). After removal of the solvent under vacuum, the red / purple solid was purified by column chromatography using a 1:10 methanol : DCM eluent. Two red compounds were obtained; the starting material and the dimethoxy porphyrin which was analysed. MS(ES⁻) m/z: 1181.6 (Dimer of product), 591.3 (Product), 454.2, 259.1, 170.1. ¹H NMR (300 MHz, CDCl₃) δ ppm: 3.11-3.24 (4.37 H, 2xT), 3.50-3.67 (15.37 H, M), 4.25-4.35 (4.00 H, QN), 6.07-6.15 (2.03 H, T), 6.25-6.35 (1.89 H, T), 8.11-8.27 (2.07 H, M), 9.91-10.18 (4.00 H, M)



Scheme 10.3 - Synthesis of acyl chloride protoporphyrin IX

10.4.2 Attachment of Protoporphyrin IX

Silicon samples were cleaned, etched and chlorinated as of Section 10.2 and washed with chlorobenzene and the appropriate 1,X diol (where X = carbon chain length). The chlorinated wafer was then immersed in the appropriate diol (10 mL) with 1 mL of pyridine and heated to 110°C for 24 hours. After allowing the solution to cool and washing with methanol, the acyl chloride protoporphyrin IX (100 mg) in DCM (10 mL) was added in darkness with a few drops of pyridine at 80°C for 48 hours (Scheme 10.4). The sample was then sonicated with acetonitrile (10 x 5 mL) and dried under nitrogen, yielding the required surface.



Scheme 10.4 - Attachment of the acyl chloride porphyrin to the silicon surface

10.5 Characterisation Techniques

10.5.1 Ellipsometry

Ellipsometry measurements were taken using a spectroscopic phase modulated ellipsometer (UVISEL, HORIBA Jobin Yvon). The data obtained was then analysed using a model of silicon oxide on silicon developed from the DeltaPsi2 software package. The incident angle was fixed at 70° , with measurements of Δ and Ψ made in the range 270-500 nm.

10.5.2 Infra-red Spectroscopy

Measurements were taken using a Bruker Tensor 27 spectrometer fitted with a mercury-cadmium-telluride (MCT) detector and a variable angle reflection accessory with polariser (VEEMAX II, PIKE technologies). For functionalised silicon samples, the reflection angle for the measurements was set to 37° with S-polarisation of the reflected beam, the scan count set to 500 scans, with a resolution of 4 cm^{-1} in the scan region $500 - 4000\text{ cm}^{-1}$ ¹⁸³. For all samples, a background of the native oxide was subtracted from the spectrum.

Our spectrometer uses an external reflection infrared spectroscopy (ERIRS) technique, which is more sensitive to thin layers¹⁸³. By reflection from the functionalised surface, less bulk material is observed because of the low penetration depth of the beam. By looking at one polarisation of the reflected beam (such that we observe only the wave perpendicular to the bond dielectric field) we can further increase the sensitivity towards our monolayers. The angle of incidence to the sample has been investigated in the literature for silicon substrates, and depends upon the polarisation. For S-polarised light (which has the lowest investigated signal to noise ratio for silicon), the optimum incidence angle was found to be 0-50°. The reflectivity difference between a clean substrate (R_0) and a substrate with a thin (10 Å) absorbate layer (R_S) at 3000 cm^{-1} with different angles of incidence and polarisation is shown in Fig. 10.1¹⁸³.

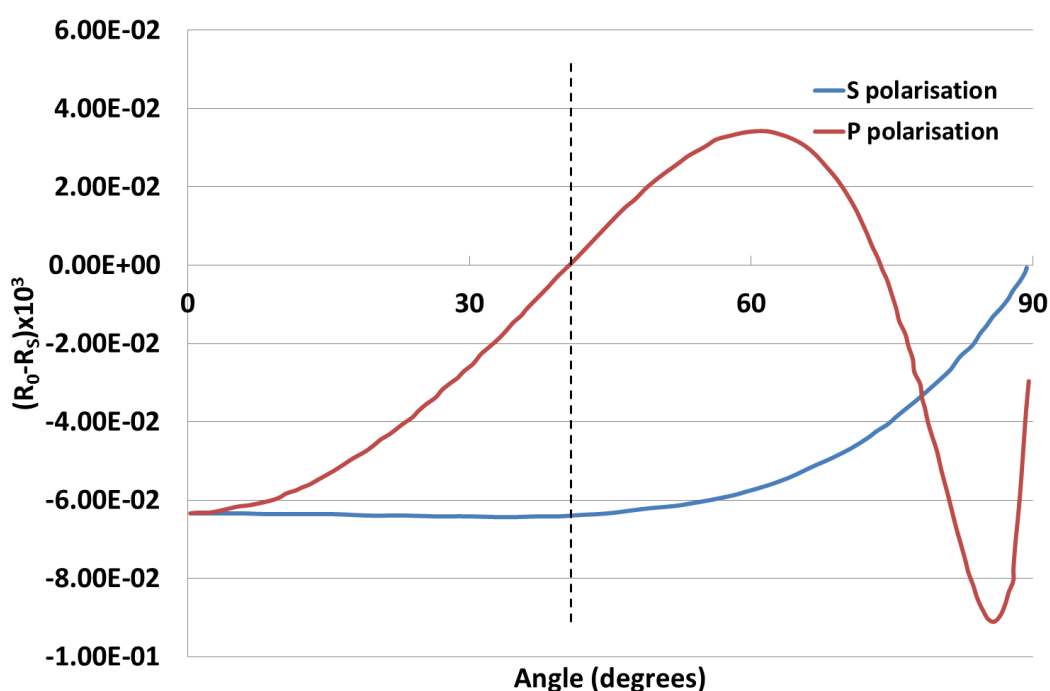


Fig. 10.1 - Calculated difference in reflectivity between a clean substrate (R_0) and absorbate covered substrate (R_S) for S and P polarised light at various angles of incidence.

As can be seen above, when the angle of incidence is 37° (dashed line) there is no change in reflectivity of the p-polarised light from the clean substrate and the functionalised substrate. However with the s-polarised light there is a difference in reflectivity. At this point, if a background of the clean substrate is used, the sensitivity in the s-polarised plane should be increased with little absorption of p-polarised light.

10.5.3 Recombination Lifetime Measurements

Recombination lifetimes of samples were measured on a Sinton instruments WCT-120 offline wafer-lifetime tool set to quasi-steady state (QSS) mode for samples with a recombination lifetime below 200 μs , and to transient mode for samples with lifetimes above 200 μs . For QSS mode, the X5D flash head was set to 400Ws, Man4 and 1/1 whilst for transient measurements the head was set to 400Ws, Man4 and 1/64.

The Sinton WCT-120 lifetime tester measures the decay of carriers after illumination conductively, using an RF coil¹⁰². This is known as the Eddy-current method, where the instrument stage sensor coil sends electromagnetic waves into the silicon sample. The light source is then flashed, creating electron-hole pairs in the silicon. The increase in conductivity arising from the generated carriers is then sensed by the coil, allowing the carrier concentration (which is proportional to the conductivity) to be calculated¹⁸⁴.

By measuring the minority carrier concentration decay after a short flash of light, the lifetime can be calculated. For short lifetime samples, this is not possible as the decay would be too fast. A different technique called “quasi-steady-state” is used

where the lifetime is calculated from the generation rate and the carrier concentration, as shown previously in equation 3.15.

As the minority carrier density increases, the recombination lifetime decreases. Therefore it is very important to state the minority carrier concentration that the lifetime is measured at, to allow comparison between samples. The most common literature value to measure the lifetime at is $5 \times 10^{14} \text{ cm}^{-3}$, which will be used throughout this thesis^{67,73,102}.

10.5.4 X-ray Photoelectron Spectroscopy (XPS)

Experiments on the chlorinated silicon surfaces were performed by Midlands Surface Analysis at Aston University, Birmingham using a Thermo Fisher ESCALAB 250 imaging XPS instrument with a monochromatic Al X-ray source. The scan count was set to 5 scans for the overview and 20 scans for the elemental binding energy spectra.

Experiments on the alkylated and porphyrin terminated samples were performed on a Thermo Fisher ME17 Thetraprobe XPS system with a monochromatic Al X-ray source, set to a 400 μm spot size. For alkylated samples the scan count was 5 scans for overview spectra, and 50 scans for the elemental binding energy spectra. For porphyrin samples the scan count was set to 5 scans for the overview spectra, 50 scans for carbon, oxygen, chlorine and silicon, with 500 scans for the nitrogen spectra. Deconvolution of the spectra were performed in excel by fitting the data to multiple Gaussian bands, reducing the residual square to a minimum.

XPS is a very surface sensitive technique, characterising the top 1-10 nm of the sample(Nemanick, Hurley, Webb, et al., 2006). This is therefore an excellent method

for monolayer composition determination, as both the functionalities present and surface coverage can be investigated.

In XPS, the binding energies of electrons from the atomic orbitals probed are recorded. Once X-ray photons (of energy 1.49 keV) are focussed onto a sample, electrons escape from the energy levels of the material. By measuring the kinetic energy of these electrons, both the material and bonding state of the atoms can be determined by:

$$E_{binding} = E_{photon} - E_{kinetic} \quad (\text{eqn. 10.0})$$

where $E_{binding}$ is the binding energy of the electron, E_{photon} is the energy of the X-ray beam and $E_{kinetic}$ is the kinetic energy of the emitted photon.

By observing the chemical state of the surface silicon atoms, we can confirm the attachment of organic groups, observe the removal of surface oxide and gain quantitative analysis of the degree of surface coverage.

10.5.5 Contact Angle Goniometry

Contact angle measurements were taken on a Kruss DSA 100 using ultra-pure de-ionised water with a 1 μl drop size, with the contact angle measurements obtained by fitting of the image using the supplied software (SMARTDROP).

10.5.6 Nuclear Magnetic Resonance (NMR)

Spectra were collected on a Bruker 300 MHz NMR spectrometer and analysed using the ACD labs 12.0 NMR manager program.

10.5.7 Mass Spectroscopy

Data was obtained on a Micromass ZMD electrospray MS and analysed using the Remote Analyser system.

10.5.8 Kelvin Probe (Surface Photovoltage) Measurements

Kelvin probe measurements were performed on a scanning Kelvin Probe system (SKP5050) from KP Technology. This was fitted with a X-Y-Z sample holder, allowing 2D scans of samples to be undertaken (Fig. 10.2).

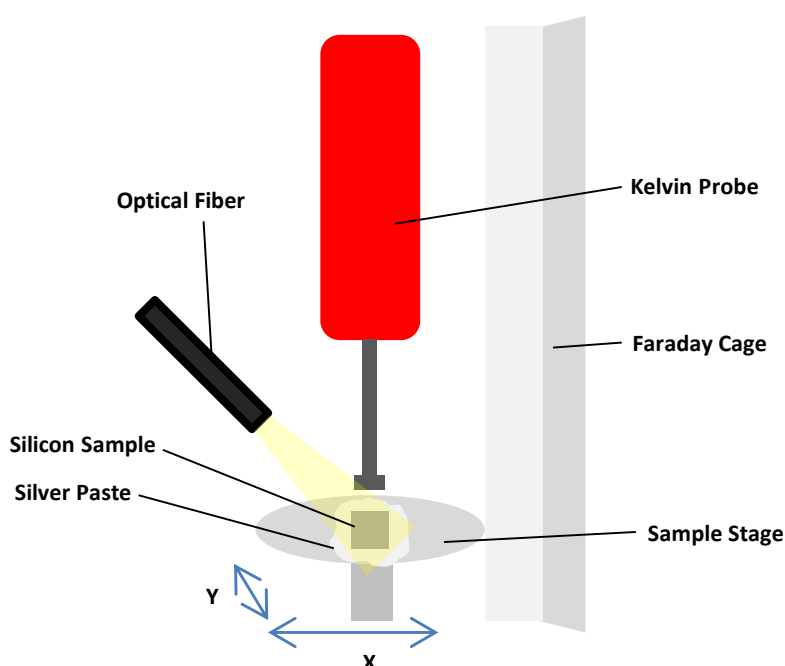


Fig. 10. 2 - Kelvin probe experimental set-up

The Kelvin probe measures the work function of the surface, and by taking measurements in dark and illuminated conditions both the bent and flat-band conditions can be measured. The difference between the two measurements is known as the surface photovoltage (SPV) and is directly related to the amount of band-bending at the surface.

To achieve a good contact between the wafer and sample stage, the rear side of the wafer was scratched with sand paper to remove any insulating oxide, and silver paste

applied. After placing the wafer on the sample stage, the paste was allowed to dry for 24 hours prior to measurements being undertaken.

The samples were illuminated by optical fibre whilst in the Kelvin Probe with a xenon lamp as the source. This was passed through a monochromator (Bentham Instruments) before reaching the sample, such that the intensity and wavelength of light could be altered as desired. For surface photovoltage measurements the illumination intensity was varied until the surface photovoltage reached saturation.

For surface recombination velocity measurements it is important to know the photon flux at each monochromator slit width, such that the current flow in the sample can be calculated. To calculate the photon flux at each monochromator slit width, a diode was used as this has similar area to our samples, and does not contain an anti-reflection coating or contacts so should have similar absorption to our samples.

By measuring the current at each slit width, the number of photons absorbed in our sample can be calculated by dividing the current (in amps) by the charge of an electron. By dividing the calculated value by the area of the diode, the photons absorbed per cm^2 of the sample is measured. The surface photovoltage was then measured at various photon flux values, and applied to our theory in Section 6.2.

10.5.9 Fluorescence Spectra

Fluorescence spectra were performed on liquid samples (using methanol solvent) on a Cary Eclipse Fluorescence spectrometer. The source intensity was changed for each sample such that a maximum signal was obtained that did not flood the detector. Excitation-emission spectra were obtained by measuring the fluorescence of the dye using the spectrometer, then setting the maximum emission wavelength in

the software. By scanning the excitation wavelength and measuring the fluorescence intensity, the excitation spectrum can be obtained.

10.5.10 Fluorescence Lifetime Measurements

Fluorescence lifetime measurements were performed using a PicoQuant FluoTime 200 system fitted with a 445 nm laser with a frequency of 20 MHz, allowing a time domain of 50 ns for the fluorescence decay. The laser intensity was set to 4.0, with the iris and lens set such that a maximum output signal was obtained at the desired wavelength. A slit width of 2 mm was used before the monochromator and detector to maximise the signal output. By setting the laser pulse as a reference, the effect of the laser decay (~5 picoseconds) can be removed from the measurements, allowing the fluorescence decay to be observed. The data was analysed using the supplied FluoFit program, giving the fluorescence decay curves.

To obtain the fluorescence spectra of the surfaces, the fluorescence decay was measured at 2 nm intervals from 480 to 750 nm. After measuring the decay at each point for 15 seconds, the emission spectrum can be obtained by plotting the maximum intensity at each wavelength.

11. References

1. *UK Energy in Brief*, United Kingdom Statistics Authority, 2012.
2. K. Branker, M. J. M. Pathak, and J. M. Pearce, *Renewable and Sustainable Energy Reviews*, 2011, **15**, 4470–4482.
3. *Quarterly Energy Prices*, United Kingdom Statistics Authority, 2012.
4. D. M. Chapin, C. S. Fuller, and G. L. Pearson, *Journal of Applied Physics*, 1954, **25**, 676.
5. H. Yuen, in *Proceedings of the 3rd International Solar Energy Technology Conference*, 2011.
6. M. A. Green, *Progress in Photovoltaics: Research and Applications*, 2009, **17**, 183–189.
7. *Taken from Photon Magazine, 04-2010*.
8. D. K. Schroder, *IEEE Transactions on Electron Devices*, 1997, **44**, 160–170.
9. X. X. Liu and J. R. Sites, *Journal of Applied Physics*, 1994, **75**, 577–581.
10. K. L. Chopra, P. D. Paulson, and V. Dutta, *Progress in Photovoltaics: Research and Applications*, 2004, **12**, 69–92.
11. A. Boukai, *SPIE Newsroom*, 2010, **5**, 2–3.
12. L. Danos, G. Jones, R. Greef, and T. Markvart, *Physica Status Solidi (C)*, 2008, **5**, 1407–1410.
13. P. V. Kamat, *Journal of Physical Chemistry C*, 2008, **112**, 18737–18753.
14. I. Nabiev, A. Rakovich, A. Sukhanova, E. Lukashev, V. Zagidullin, V. Pachenko, Y. P. Rakovich, J. F. Donegan, A. B. Rubin, and A. O. Govorov, *Angewandte Chemie (International ed. in English)*, 2010, **49**, 7217–21.
15. J. Kim and J. Cao, *The journal of physical chemistry. B*, 2010, **114**, 16189–97.
16. Y. Ishida, T. Shimada, D. Masui, H. Tachibana, H. Inoue, and S. Takagi, *Journal of the American Chemical Society*, 2011, **133**, 14280–6.
17. L. Danos and T. Markvart, *quantsol.org white paper*.

18. H. M. Nguyen, O. Seitz, D. Aureau, A. Sra, N. Nijem, Y. N. Gartstein, Y. J. Chabal, and A. V. Malko, *Applied Physics Letters*, 2011, **98**, 161904.
19. D. L. Dexter, *Journal of Luminescence*, 1979, **18–19**, 779–784.
20. L. Danos, R. Greef, and T. Markvart, *Thin Solid Films*, 2008, **516**, 7251–7255.
21. G. Shao and C. Lou, *Photovoltaic Specialists Conference (PVSC)*, 2012, 2596–2600.
22. J. Liu, Q. Yao, and Y. Li, *Applied Physics Letters*, 2006, **88**, 173119.
23. P. Gerner, C. Fuhrer, C. Reinhard, and H. U. Güdel, *Journal of Alloys and Compounds*, 2010, **132**, 14203–14211.
24. J. C. Boyer, C. J. Carling, B. D. Gates, and N. R. Branda, *Journal of the American Chemical Society*, 2010, **132**, 15766–72.
25. G. F. Brown and J. Wu, *Laser & Photonics Review*, 2009, **3**, 394–405.
26. F. Varsanyi and G. Dieke, *Physical Review Letters*, 1961, **7**, 442–443.
27. A. Elamrani, I. Menous, L. Mahiou, R. Tadjine, A. Touati, and A. Lefgoum, *Renewable Energy*, 2008, **33**, 2289–2293.
28. B. Sopori, *Silicon nitride coatings for Si solar cells: Control of optical reflection and surface/bulk passivation*, *National Renewable Energy Laboratory White Paper*, .
29. E. J. Nemanick, P. T. Hurley, B. S. Brunshwig, and N. S. Lewis, *The Journal of Physical Chemistry. B*, 2006, **110**, 14800–8.
30. K. E. Plass, X. Liu, B. S. Brunshwig, and N. S. Lewis, *Chemistry of Materials*, 2008, **20**, 2228–2233.
31. P. Yu and M. Cardona, *Fundamentals of Semiconductors Physics and Materials Properties*, 2010.
32. M. A. Green and M. J. Keevers, *Progress in Photovoltaics: Research and Applications*, 1995, **3**, 189–192.
33. E. Kasper and M. Oehme, *Physica Status Solidi (C)*, 2008, **5**, 3144–3149.
34. M. Copel, R. J. Culbertson, and R. M. Tromp, *Applied Physics Letters*, 1994, **65**, 2344.
35. P. Allongue, V. Kieling, and H. Gerischer, *Electrochimica Acta*, 1995, **40**, 1353–1360.

36. G. Trucks, K. Raghavachari, G. Higashi, and Y. Chabal, *Physical Review Letters*, 1990, **65**, 504–507.
37. G. Higashi, R. Becker, Y. Chabal, and A. Becker, *Applied Physics Letters*, 1991, **58**, 1656–1658.
38. S. S. S. Vegunta, J. N. Ngunjiri, and J. C. Flake, *Langmuir: the ACS journal of surfaces and colloids*, 2009, **118**, 7225–7226.
39. A. J. Reddy, J. V. Chan, T. A. Burr, R. Mo, C. P. Wade, C. E. D. Chidsey, J. Michel, and L. C. Kimerling, *Physica B: Condensed Matter*, 1999, **273-274**, 468–472.
40. J. M. Langer and W. Walukiewicz, in *Materials Science Forum*, 1995, vol. 196-201, pp. 1389–1394.
41. I. W. Moran and K. R. Carter, *Langmuir: the ACS journal of surfaces and colloids*, 2009, **25**, 9232–9.
42. A. Edwards, *Physical Review B*, 1991, **44**, 1832–1838.
43. C. Helms and E. Poindexter, *Reports on Progress in Physics*, 1994, **57**, 791–852.
44. L. A. Ragnarsson and P. Lundgren, *Journal of Applied Physics*, 2000, **88**, 938.
45. E. J. Nemanick, P. T. Hurley, L. J. Webb, D. W. Knapp, D. J. Michalak, B. S. Brunschwig, and N. S. Lewis, *The Journal of Physical Chemistry. B*, 2006, **110**, 14770–8.
46. L. J. Webb and N. S. Lewis, *The Journal of Physical Chemistry B*, 2003, **107**, 5404–5412.
47. A. Bansal, X. Li, I. Lauermaann, N. S. Lewis, S. I. Yi, and W. H. Weinberg, *Journal of the American Chemical Society*, 1996, **118**, 7225–7226.
48. B. Hoex and J. Schmidt, *Proceedings of the 33rd Photovoltaic Specialists Conference*, 2008, 7–10.
49. K. J. Weber and H. Jin, *Applied Physics Letters*, 2009, **94**, 063509.
50. M. Schofthaler and R. Brendel, *Conference Record of the First WCPEC*, 1994, 1509–1512.
51. E. Yablonovitch, D. Allara, C. Chang, T. Gmitter, and T. Bright, *Physical review letters*, 1986, **57**, 249–252.
52. I. Magid, L. Burstein, O. Seitz, L. Segev, L. Kronik, and Y. Rosenwaks, *Journal of Physical Chemistry C*, 2008, **112**, 7145–7150.

53. S. Vegunta, S. J. Ngunjiri, and J. C. Flake, *Electrochemical Passivation of (100) Silicon in Alkyl Grignard Solution*, 2002, vol. 2565.
54. S. Mack, U. Jaiger, and G. Kastner, *35th PVSC Conference Proceedings*, 2010, 34–38.
55. G. Willeke and K. Kellermann, *Semiconductor Science and Technology*, 1996, **11**, 415–421.
56. D. Watanabe, a. En, S. Nakamura, M. Suhara, and T. Okumura, *Applied Surface Science*, 2003, **216**, 24–29.
57. M. Ramonda and P. Dumas, *Surface Science*, 1998, **411**, 839–843.
58. S. J. Fang, W. Chen, T. Yamanaka, and C. R. Helms, *Applied Physics Letters*, 1996, **68**, 2837–2839.
59. M. Niwano, J. Kageyama, K. Kurita, K. Kinashi, I. Takahashi, and N. Miyamoto, *Journal of Applied Physics*, 1994, **76**, 2157–2163.
60. S. Ye, T. Saito, S. Nihonyanagi, K. Uosaki, P. B. Miranda, D. Kim, and Y. Shen, *Surface Science*, 2001, **476**, 121–128.
61. M. Kolíbal, J. Čechal, M. Bartošik, J. Mach, and T. Šikola, *Applied Surface Science*, 2010, **256**, 3423–3426.
62. T. Miura, M. Niwano, D. Shoji, and N. Miyamoto, *Applied Surface Science*, 1996, **100**, 454–459.
63. S. Takami and Y. Egashira, *Japanese Journal of Applied Physics*, 1997, **36**, 2288–2291.
64. E. Boonekamp and J. Kelly, *Journal of Applied Physics*, 1994, **75**, 8121–8127.
65. G. J. Kluth and R. Maboudian, *Journal of Applied Physics*, 1996, **80**, 5408–5414.
66. B. Chhabra, S. Bowden, R. L. Opila, and C. B. Honsberg, *Applied Physics Letters*, 2010, **96**, 063502.
67. B. Chhabra, S. Suzer, R. L. Opila, and C. B. Honsberg, in *33rd IEEE Photovoltaic Specialists Conference*, IEEE, 2008, pp. 1–4.
68. H. Takato, I. Sakata, and R. Shimokawa, *Japanese Journal of Applied Physics*, 2002, **41**, 870–872.
69. S. Rivillon Amy, D. Michalak, Y. Chabal, L. Wielunski, P. Hurley, and N. Lewis, *Journal of Physical Chemistry C*, 2007, **111**, 13053–13061.

70. E. J. Nemanick, P. T. Hurley, L. J. Webb, D. W. Knapp, D. J. Michalak, B. S. Brunschwig, and N. S. Lewis, *The Journal of Physical Chemistry. B*, 2006, **110**, 14770–8.
71. A. Stephens, *Solar Energy Materials and Solar Cells*, 1997, **45**, 255–265.
72. C. Li, B. Sopori, P. Rupnowski, A. Fiory, and N. Ravindra, *National Renewable Energy Laboratory White Paper*.
73. B. Hoex, J. Schmidt, R. Bock, P. P. Altermatt, M. C. M. van de Sanden, and W. M. M. Kessels, *Applied Physics Letters*, 2007, **91**, 112107.
74. J. Mizsei, *Applied Surface Science*, 2006, **252**, 7691–7699.
75. B. Sopori, P. Rupnowski, J. Appel, V. Mehta, C. Li, and S. Johnston, in *2008 33rd IEEE Photovoltaic Specialists Conference*, IEEE, 2008, pp. 1–4.
76. S. W. Glunz, D. Biro, S. Rein, and W. Warta, *Journal of Applied Physics*, 1999, **86**, 683.
77. B. Chhabra, C. B. Honsberg, and R. L. Opila, *34th IEEE Photovoltaic Specialists Conference (PVSC)*, 2009, 2187–2190.
78. L. E. O’Leary, E. Johansson, B. S. Brunschwig, and N. S. Lewis, *The Journal of Physical Chemistry B*, 2010, **114**, 14298–302.
79. T. K. Mischki, R. L. Donkers, B. J. Eves, G. P. Lopinski, and D. D. M. Wayner, *Langmuir: the ACS journal of surfaces and colloids*, 2006, **22**, 8359–65.
80. T. K. Mischki, G. P. Lopinski, and D. D. M. Wayner, *Langmuir: the ACS journal of surfaces and colloids*, 2009, **25**, 5626–30.
81. P. Allongue, C. Henry de Villeneuve, S. Morin, R. Boukherroub, and D. D. M. Wayner, *Electrochimica Acta*, 2000, **45**, 4591–4598.
82. S. Ciampi, J. B. Harper, and J. J. Gooding, *Chemical Society reviews*, 2010, **39**, 2158–83.
83. B. Eves and G. Lopinski, *Surface Science*, 2005, **579**, 89–96.
84. A. Bansal, X. Li, S. I. Yi, W. H. Weinberg, and N. S. Lewis, *The Journal of Physical Chemistry B*, 2001, **105**, 10266–10277.
85. S. Rivillon, Y. J. Chabal, L. J. Webb, D. J. Michalak, N. S. Lewis, M. D. Halls, and K. Raghavachari, *Journal of Vacuum Science & Technology A: Vacuum, Surfaces, and Films*, 2005, **23**, 1100–1106.
86. S. D. Solares, D. J. Michalak, W. A. Goddard, and N. S. Lewis, *The Journal of Physical Chemistry. B*, 2006, **110**, 8171–5.

87. S. Rivillon, F. Amy, Y. J. Chabal, and M. M. Frank, *Applied Physics Letters*, 2004, **85**, 2583.
88. H. Liu, F. Duclairoir, B. Fleury, L. Dubois, Y. Chenavier, and J. Marchon, *Dalton transactions*, 2009, **19**, 3793–9.
89. M. Perring, S. Dutta, S. Arafat, M. Mitchell, P. J. a Kenis, and N. B. Bowden, *Langmuir: the ACS journal of surfaces and colloids*, 2005, **21**, 10537–44.
90. R. Voicu, R. Boukherroub, V. Bartzoka, T. Ward, J. T. C. Wojtyk, and D. D. M. Wayner, *Langmuir: the ACS journal of surfaces and colloids*, 2004, **20**, 11713–20.
91. P. Wagner, S. Nock, J. A. Spudich, W. D. Volkmuth, S. Chu, R. L. Cicero, C. P. Wade, M. R. Linford, and C. E. Chidsey, *Journal of Structural Biology*, 1997, **119**, 189–201.
92. S. R. Puniredd, O. Assad, and H. Haick, *Journal of the American Chemical Society*, 2008, **130**, 13727–34.
93. S. R. Puniredd, O. Assad, T. Stelzner, S. Christiansen, and H. Haick, *Langmuir: the ACS journal of surfaces and colloids*, 2011, **27**, 4764–71.
94. S. Dutta, M. Perring, S. Barrett, M. Mitchell, P. J. A. Kenis, and N. B. Bowden, *Langmuir: the ACS journal of surfaces and colloids*, 2006, **22**, 2146–55.
95. A. Juang, O. A. Scherman, R. H. Grubbs, and N. S. Lewis, *Langmuir*, 2001, **17**, 1321–1323.
96. M. A. C. Campos, J. M. J. Paulusse, and H. Zuilhof, *Chemical communications*, 2010, **46**, 5512–4.
97. P. Cao, K. Xu, and J. R. Heath, *Journal of the American Chemical Society*, 2008, **130**, 14910–14911.
98. G. Shambat, A. Deberardinis, B. Chen, P. Reinke, B. J. Venton, L. Pu, J. Tour, and J. Bean, *Applied Surface Science*, 2009, **255**, 8533–8538.
99. G. Parker, *Introductory semiconductor device physics*, 2004.
100. D. Cahen and A. Kahn, *Advanced Materials*, 2003, **15**, 271–277.
101. L. Kronik and Y. Shapira, *Surface Science Reports*, 1999, **37**, 1–206.
102. R. A. Sinton and A. Cuevas, *Applied Physics Letters*, 1996, **69**, 2510.
103. R. A. Sinton, in *SEMI standards meeting, Hamburg*, 2009, pp. 1–47.
104. F. Werner, A. Cosceev, and J. Schmidt, *Energy Procedia*, 2012, **27**, 319–324.

105. W. Shockley and W. Read, *Physical Review*, 1952, **87**, 835–842.
106. C.-T. Sah and W. Shockley, *Physical Review*, 1958, **109**, 1103–1115.
107. S. Olibet, E. Vallat-Sauvain, L. Fesquet, C. Monachon, A. Hessler-Wyser, J. Damon-Lacoste, S. De Wolf, and C. Ballif, *Physica Status Solidi (a)*, 2010, **207**, 651–656.
108. M. R. Houston and R. Maboudian, *Journal of Applied Physics*, 1995, **78**, 3801–3808.
109. N. Araki, *Japanese Journal of Applied Physics*, 2009, **48**, 011201.
110. X. Wang, R. E. Ruther, J. A. Streifer, and R. J. Hamers, *Journal of the American Chemical Society*, 2010, **132**, 4048–9.
111. H. Angermann, J. Rappich, I. Sieber, K. Hübener, and J. Hauschild, *Analytical and Bioanalytical Chemistry*, 2008, **390**, 1463–70.
112. H. Angermann, *Solar Energy Materials and Solar Cells*, 2004, **83**, 331–346.
113. M. Shao, L. Cheng, X. Zhang, D. D. D. Ma, and S. Lee, *Journal of the American Chemical Society*, 2009, **131**, 17738–9.
114. M. Morita, T. Ohmi, E. Hasegawa, M. Kawakami, and M. Ohwada, *Journal of Applied Physics*, 1990, **68**, 1272–1281.
115. A. Kovalgin, A. Zinine, R. Bankras, H. Wormeester, B. Poelsema, and J. Schmitz, *Microelectronic Engineering*, 2006, 1017–1017.
116. B. Chhabra, C. Weiland, R. L. Opila, and C. B. Honsberg, *Physica Status Solidi (a)*, 2011, **208**, 86–90.
117. F. Wu, Modeling for control of an etch process in semiconductor fabrication, 1986.
118. L. Wagner and W. Spicer, *Physical Review Letters*, 1972, **28**, 1381–1384.
119. A. Aberle and S. Glunz, *Journal of Applied Physics*, 1992, **71**, 4422–4431.
120. C. Leguijt, P. Lölgen, J. A. Eikelboom, A. W. Weeber, F. M. Schuurmans, W. C. Sinke, P. F. A. Alkemade, P. M. Sarro, C. H. M. Marée, and L. A. Verhoef, *Solar Energy Materials and Solar Cells*, 1996, **40**, 297–345.
121. D. Biro and W. Warta, *Solar Energy Materials and Solar Cells*, 2002, **71**, 369–374.
122. E. Johansson, P. T. Hurley, B. S. Brunschwig, and N. S. Lewis, *The Journal of Physical Chemistry C*, 2009, **113**, 15239–15245.

123. S. Rivillon, Y. J. Chabal, L. J. Webb, D. J. Michalak, N. S. Lewis, M. D. Halls, and K. Raghavachari, *Journal of Vacuum Science & Technology A: Vacuum, Surfaces, and Films*, 2005, **23**, 1100–1106.
124. L. J. Webb, S. Rivillon, D. J. Michalak, Y. J. Chabal, and N. S. Lewis, *The Journal of Physical Chemistry. B*, 2006, **110**, 7349–56.
125. M. Bachman, *INRF application note, UCI Integrated Nanosystems Research Facility*, 1999, 1–3.
126. M. Bachman, *UCI Integrated Nanosystems Research Facility*, 2002, 1–3.
127. W. J. Royea, A. Juang, and N. S. Lewis, *Applied Physics Letters*, 2000, **77**, 1988–1990.
128. A. Goossens and J. Schoonman, *Journal of Electroanalytical Chemistry*, 1990, **289**, 11–27.
129. R. Hunger, R. Fritsche, B. Jaeckel, W. Jaegermann, L. Webb, and N. Lewis, *Physical Review B*, 2005, **72**, 045317.
130. S. A. Kulkarni and K. P. Vijayamohanan, *Surface Science*, 2007, **601**, 2983–2993.
131. M. Takihara, T. Takahashi, and T. Ujihara, *Applied Physics Letters*, 2009, **95**, 191908.
132. D. K. Schroder, *Materials Science and Engineering: B*, 2002, **91-92**, 196–210.
133. M. Dukic, *Vibrating Kelvin Probe Measurements of a Silicon Surface with the Underside Exposed to Light*, 2007.
134. L. Kronik and Y. Shapira, *Surface and Interface Analysis*, 2001, **31**, 954–965.
135. J. Clabes and M. Henzler, *Physical Review B*, 1980, **21**, 625–631.
136. D. Cavalcoli, A. Cavallini, and M. Rossi, *Journal of The Electrochemical Society*, 2004, **151**, 248–251.
137. N. M. Nursam, Y. Ren, and K. J. Weber, *Advances in OptoElectronics*, 2010, **2010**, 1–8.
138. M. J. Kerr and A. Cuevas, *Semiconductor Science and Technology*, 2002, **17**, 35–38.
139. J. Muller, K. Bothe, S. Gatz, F. Haase, C. Mader, and R. Brendel, *Journal of Applied Physics*, 2010, **108**, 124513.
140. P. Pohl, J. Schmidt, K. Bothe, and R. Brendel, *Applied Physics Letters*, 2005, **87**, 142104.

141. M. Bail, J. Kentsch, R. Brendel, and M. Schulz, *Conference Record of the Twenty-Eighth IEEE Photovoltaic Specialists Conference*, 2000, 99–103.
142. R. K. Ahrenkiel and S. W. Johnston, *Solar Energy Materials and Solar Cells*, 2008, **92**, 830–835.
143. N. Ikeda and F. Shimura, *Applied Physics Letters*, 1993, **63**, 2914–2916.
144. H. Sugimoto and M. Tajima, *Japanese Journal of Applied Physics*, 2007, **46**, 339–341.
145. J. M. Buriak, *Chem. Commun.*, 1999, 1051–1060.
146. D. K. Schroder, *Measurement Science and Technology*, 2001, **12**, 16–31.
147. D. K. Schroder, *Materials Science and Engineering: B*, 2002, **91-92**, 196–210.
148. M. S. Jeon, M. Dhamrin, T. Saitoh, and K. Kamisako, *2006 IEEE 4th World Conference on Photovoltaic Energy*, 2006, 1425–1428.
149. T. Nammori, K. Okamoto, T. Nunoi, and Y. Hayashi, *Japanese Journal of Applied Physics*, 1990, **29**, 166–168.
150. B. Chhabra, C. B. Honsberg, and R. L. Opila, in *24th European Photovoltaic Solar Energy Conference*, IEEE, 2009, pp. 1645–1648.
151. R. Cohen, N. Zenou, D. Cahen, and S. Yitzchaik, *Chemical Physics Letters*, 1997, **279**, 270–274.
152. R. Boukherroub, S. Morin, P. Sharpe, D. D. M. Wayner, and P. Allongue, *Langmuir*, 2000, **16**, 7429–7434.
153. V. T. Joy and D. Mandler, *ChemPhysChem*, 2002, **3**, 973–5.
154. X. Y. Zhu, V. Boiadjev, J. A. Mulder, R. P. Hsung, and R. C. Major, *Langmuir*, 2000, **16**, 6766–6772.
155. R. Boukherroub, *Current Opinion in Solid State and Materials Science*, 2005, **9**, 66–72.
156. F. Yahyaoui, T. Dittrich, T. Burke, M. Aggour, S. Lust, C. Lévy-Clément, and J. Rappich, *Journal of The Electrochemical Society*, 2002, **149**, 472–478.
157. R. B. M. Girisch, R. F. Mertens, and R. F. De Keersmaecker, *IEEE Transactions on Electron Devices*, 1988, **35**, 203–222.
158. P. Landsberg, *Recombination in semiconductors*, 1991.
159. D. K. Aswal, S. Lenfant, D. Guerin, J. V. Yakhmi, and D. Vuillaume, *Analytica Chimica Acta*, 2006, **568**, 84–108.

160. H. Mizuno and J. M. Buriak, *ACS applied materials & interfaces*, 2010, **2**, 2301–7.
161. J. Lee, F. Serna, J. Nickels, and C. E. Schmidt, *Biomacromolecules*, 2006, **7**, 1692–5.
162. P. Gorostiza, C. Henry De Villeneuve, Q. Y. Sun, F. Sanz, X. Wallart, R. Boukherroub, and P. Allongue, *The Journal of Physical Chemistry. B*, 2006, **110**, 5576–85.
163. W. Eades and R. Swanson, *Journal of Applied Physics*, 1985, **58**, 4267–4276.
164. X. Fan, L. F. Register, B. Winstead, M. C. Foisy, W. Chen, X. Zheng, B. Ghosh, and S. K. Banerjee, *IEEE Transactions on Electron Devices*, 2007, **54**, 291–296.
165. W. R. Thurber, *Journal of The Electrochemical Society*, 1980, **127**, 1807.
166. Y. Yu, V. E. Ferry, A. P. Alivisatos, and L. Cao, *Nano letters*, 2012, **12**, 3674–81.
167. K. Smith, *Accounts of Chemical Research*, 1979, **12**, 374–381.
168. M. Nango, T. Dannhauser, D. Huang, K. Spears, L. Morrison, and P. A. Loach, *Macromolecules*, 1984, **17**, 1898–1902.
169. E. Samuels, R. Shuttleworth, and T. S. Stevens, *Journal of the Chemical Society C: Organic*, 1968, 145.
170. A. Mironov, V. Rumyantseva, and O. Ponamoreva, *Mendeleev Communications*, 1998, **71**, 205–206.
171. A. N. Kozyrev, A. N. Nizhnik, and A. F. Mironov, *Journal of the Chemical Society, Perkin Transactions 1*, 1990, **7**, 1945–1949.
172. J. Bateman and B. Horrocks, *Journal of the Chemical Society*, 1997, **93**, 2427–2431.
173. R. González-Moreno, C. Sánchez-Sánchez, M. Trelka, R. Otero, A. Cossaro, A. Verdini, L. Floreano, M. Ruiz-Bermejo, A. García-Lekue, J. A. Martín-Gago, and C. Rogero, *The Journal of Physical Chemistry C*, 2011, **115**, 6849–6854.
174. X. F. Wu, P. Anbarasan, H. Neumann, and M. Beller, *Angewandte Chemie (International ed. in English)*, 2010, **49**, 9047–50.
175. K. Watanabe and C. Munakata, *Semiconductor Science and Technology*, 1993, **8**, 230–235.

176. E. Johansson, S. W. Boettcher, L. E. O'Leary, A. D. Poletayev, S. Maldonado, B. S. Brunschwig, and N. S. Lewis, *The Journal of Physical Chemistry C*, 2011, **115**, 8594–8601.
177. C. Rissing and D. Y. Son, *Organometallics*, 2008, **27**, 5394–5397.
178. K. Naito, A. Miura, and M. Azuma, *Langmuir*, 1991, **7**, 627–629.
179. C. Li and T. Imae, *Langmuir*, 2003, **19**, 779–784.
180. J. Ohlsson, H. Wolpher, A. Hagfeldt, and H. Grennberg, *Journal of Photochemistry and Photobiology A: Chemistry*, 2002, **148**, 41–48.
181. J. Singh, J. Im, J. E. Whitten, J. W. Soares, and D. M. Steeves, *Chemical Physics Letters*, 2010, **497**, 196–199.
182. B. Arkles, G. Silverman, and P. Rakita, *Handbook of Grignard Reagents*, Gelest, 1996.
183. H. Brunner, U. Mayer, and H. Hoffmann, *Applied Spectroscopy*, 1997, **51**, 209–217.
184. R. A. Sinton, A. Cuevas, and M. Stuckings, in *Conference Record of the Twenty Fifth IEEE Photovoltaic Specialists Conference*, IEEE, 1996, pp. 457–460.
185. G. Higashi, Y. Chabal, G. Trucks, and K. Raghavachari, *Applied Physics Letters*, 1990, **56**, 656–658.
186. H. Yin, *Microelectronic Engineering*, 2004, **73-74**, 830–836.
187. A. Moraillon, A. C. Gouget-Laemmel, F. Ozanam, and J. N. Chazalviel, *Journal of Physical Chemistry C*, 2008, **112**, 7158–7167.